Durham E-Theses

Magma genesis in the northern Lau Basin, S.W. Pacific

A. Sarah Acland

How to cite:

Acland, A. Sarah (1996) Magma genesis in the northern Lau Basin, S.W. Pacific. Doctoral thesis, Durham University.

Use policy

Magma genesis in the northern Lau Basin, S.W. Pacific

by

A. Sarah Acland M.A.
Cambridge University,
England.

**A thesis submitted in partial fulfilment of
the requirements for the degree of
Doctor of Philosophy**

**Department of Geological Sciences,
Durham University, U.K.
July 1996**

To my parents

GLOSSARY

NTB, east:	North Tongan boninites from the western ophiolite section dredged on the 'Kallisto' 1982 cruise.
NTB, west:	North Tongan boninites from site 26, dredged on the 'Kallisto' 1982 cruise.
NTB, St21:	North Tongan boninites dredged from Station 21 on the 'Natsushima' 1984 cruise.
Taf:	Tafahi.
Niua:	Niuatoputapu.
NF:	Niuafo'ou.
Tofua arc:	Active-arc associated with the Tongan supra-subduction zone, including the islands of Fonualei (F), Hunga Haapa'ai (HH), Late (L) and Ata (A).
Lau Ridge:	Remnant-arc.
NLSC:	Northern Lau Spreading Centre, the northeastern limb of the King's Triple Junction (KTJ).
CLSC:	Central Lau Spreading Centre.
ELSC:	Eastern Lau Spreading Centre.
NWLSC:	Northwestern Lau Spreading Centre.
PR:	Peggy Ridge
NTTh:	north Tongan tholeiites from the eastern ophiolite section dredged on the 'Kallisto' 1982 cruise.
SSh:	Samaon shield volcanics.
SPE:	Samoan post-erosional volcanics.
SS:	Samoan seamount.
PVS:	Pacific volcanogenic sediments (with distinct isotopic compositions from volcanogenic sediements derived from Samoa).
PPS:	Pacific pelagic sediments.
IMM:	Indian MORB mantle
PMM:	Pacific MORB mantle
FMM:	Fertile MORB mantle of *Pearce & Parkinson (1993)*.
DMM:	Depleted MORB mantle
R_A:	The atmospheric $^3He/^4He$ ratio ~ 1.4×10^{-6}
LILE:	Large-ion-lithophile elements.
LREE:	Light-rare-earth-elements.
MREE:	Middle-rare-earth-elements.
HREE:	Heavy-rare-earth-elements.
HFSE:	High-field-strength-elements.

Frontispiece: Aerial view of Niuatoputapu, and the volcanic cone of Tafahi in the distance.

Abstract

The northern Lau Basin contains the northeastern-most part of the Tonga arc-basin system. Volcanic rocks associated with the recent-arc have been sampled from Tafahi and Niuatoputapu, and young basalts (<1.5Ma) have been dredged from Northern Lau Spreading Centre (NLSC), the northeastern limb of the King's Triple Junction. The 1982 'Kallisto' cruise dredged two ophiolite sections, one containing boninitic, and the other tholeiitic, lavas, from the inner wall of the northern Tonga trench. The magma genesis of these lava suites is related to the structural and geochemical controls imposed during the tectonic evolution of the region. The geochemical controls result from processes related to the mantle dynamics in the northern Lau Basin, and to along-trench variations and the degree of influence of the subduction component.

The lavas associated with the Central Lau Spreading Centre are derived from the Lau Basin mantle reservoir, which has Indian MORB mantle (IMM) isotopic characteristics. This reservoir has been present under the region since early-arc magmatism, as indicated by the trace elements and IMM isotopic signatures of the tholeiitic lavas from the eastern ophiolite section, and Eocene lavas from 'Eua.

A reservoir with the geochemical characteristics of residual Samoan plume mantle underlies the northern Lau Basin. This mantle has been influxing through the rip in the Pacific plate, at the northern termination of the Tonga trench, since the Lau Basin began to open (< 6Ma), as a result of processes relating to subduction roll-back. The north Tongan boninites, the lavas from Tafahi and Niuatoputapu have residual plume mantle sources. However, prior to the opening of the Lau Basin, the proto-Tonga trench formed a barrier to this influx, and therefore, the influence of the plume cannot be detected in lavas associated with the early-arc, such as the tholeiites from one of the ophiolite sections and the Eocene lavas from 'Eua. The variations in the trace element and Pb isotopic compositions of the lavas from the Northern Lau Spreading Centre indicate that mixing has occurred between Lau Basin and residual plume mantle end-members in the central northern Lau Basin.

The residual plume mantle sources of the north Tongan boninites and the lavas from Tafahi, Niuatoputapu and the Tofua arc have been enriched by a subduction component, the characteristics of which are enrichment in LILE, Pb ± LREE. In the south, the subduction component is made up of fluids derived from subducted Pacific altered oceanic crust and pelagic sediments. However, in the north, it is comprised predominantly of fluids derived from Pacific volcanogenic sediments, with a contribution from altered oceanic crust and possibly subducted plume crust.

Declaration

I declare that this thesis, which I submit for the degree of Doctor of Philosophy at the University of Durham, is my own work and not substantially the same as any which has previously been submitted at this or another university.

Sarah Acland

A. Sarah Acland
University of Durham
July 1996

A thesis is a mirror:
if an ass peers into it,
you can't expect an
apostle to look out.

G.C. LICHENBERG

ACKNOWLEDGEMENTS

CHAPTER 1

Introduction

1.1 Tectonism and magma genesis at a supra-subduction zone setting

The Tonga arc-basin system, S.W. Pacific, is a type-locality for the study of processes associated with supra-subduction zones. The Lau Basin, the young back-arc basin (<6 Ma) associated with the Tongan supra-subduction zone, is shallow (2-3km), and separates the Lau Ridge remnant arc in the west from the active Tofua arc and the older, inactive Tongatapu arc (Tonga Ridge) in the east (Figure 1.1). It has been the focus for multi-disciplinary research since the 1970s aimed at better understanding the geochemical and tectonic evolution of intra-oceanic arc-backarc systems. However, the northern Lau Basin, defined by the Tonga trench in the east, an east-west transform zone in the north, the Northwestern Lau Spreading Centre in the west and the Peggy Ridge in the south-west, has remained elusive to detailed study (Figure 1.1) due to its tectonic and magmatic complexity. This thesis describes the petrology and geochemistry of suites of lavas from the northern Lau Basin. These are from: (i) the young volcanic-arc islands of Tafahi and Niuatoputapu; (ii) the Northern Lau Spreading Centre, which is the northeastern limb of the King's Triple Junction, and (iii) two ophiolite sections, one containing boninitic lavas and the other tholeiitic, which were dredged from the inner wall of the northern Tonga trench.

A transect of the Ocean Drilling Program (Leg 135) was carried out in 1990, in the central part of the basin (Figure 1.1; sites 834-9; *ODP Leg 135 Scientific Results*). Important synthesis papers documented the geochemical (*Hergt & Hawkesworth, 1994; Ewart et al., 1994a, b; Hergt & Farley, 1994; Hawkins, 1995*), and the tectonic processes occurring during the evolution of the Lau Basin (*Parson & Hawkins, 1994*). Gloria sidescan surveys led to the identification of propagating spreading centres in the central Lau Basin, at which extension is concentrated (*Parson et al., 1990*). However, the discontinuous magnetic anomalies in the older parts of the basin suggested that extension was taken up on small pull-apart basins before the back-arc spreading centres were fully established (*Parson & Hawkins, 1994*).

Limited GLORIA sidescan imagery of the northern Lau Basin shows that extension has been taken up on pull-apart basins, similar to those in the central part of
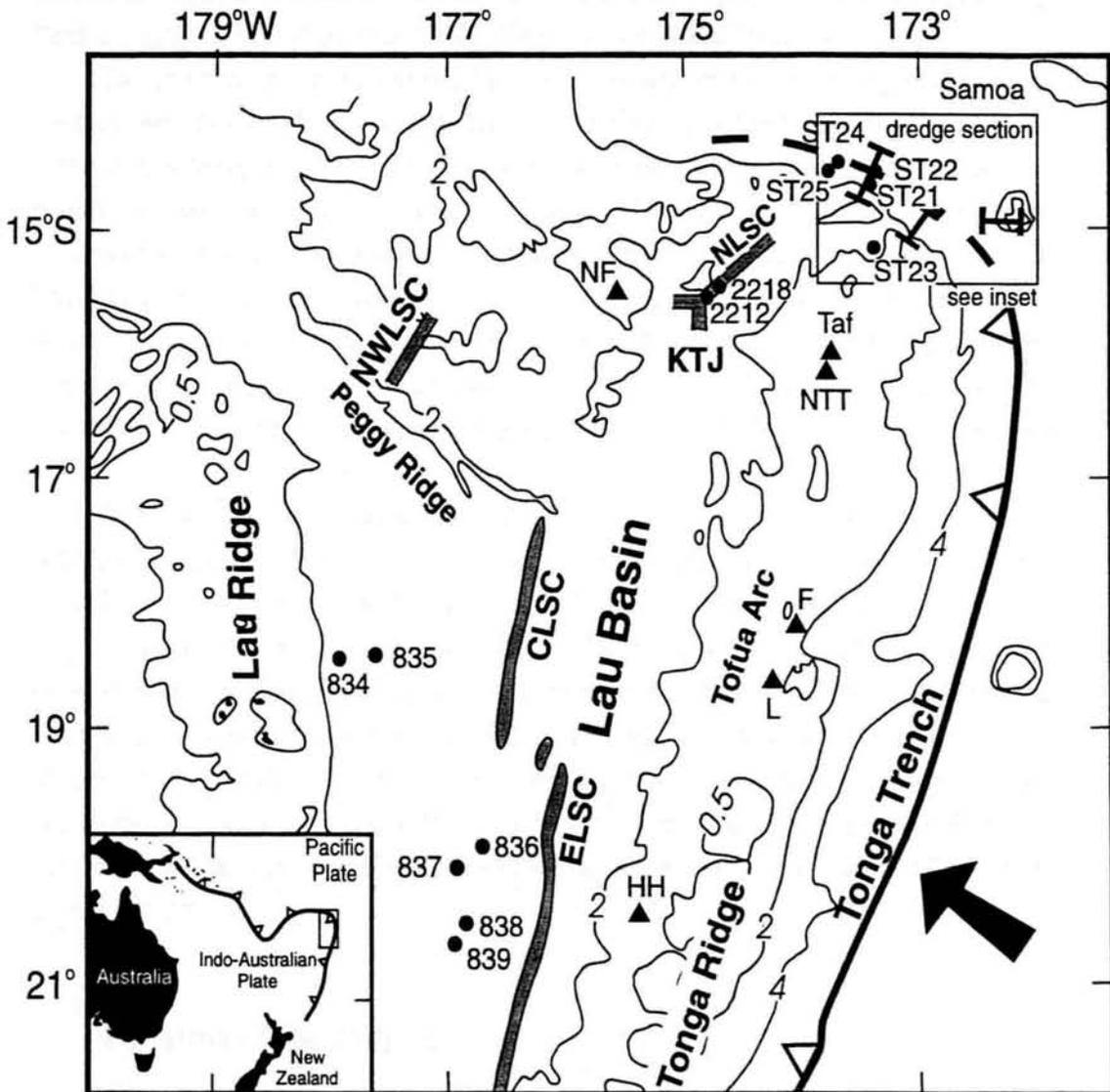
Figure 1.1: Map of the Lau Basin showing the locations of samples used in this thesis from the Northern Lau Spreading Centre (NLSC; 2212, 2218), and of the dredge sections of the 'Kallisto' 1982 cruise, and the islands of Tafahi (Taf) and Niuatoputapu (NTT), and drill sites from ODP Leg 135 in the central part of the basin. The location of sites in the northern Lau Basin where boninites were dredged on the 'Natsushima' 1984 cruise are also shown (ST 21-25). The main tectonic features of the basin are labelled and have been described in Chapter 2. Other islands from the Tofua arc are Hunga Haa'pai (HH), Late (L), and Fonualei (F). The back-arc spreading centres are the Central and Eastern Lau Spreading Centres (CLSC and ELSC) in the central Lau Basin, and in the north, the Northwestern Lau Spreading Centre (NWLSC), and the Northern Lau Spreading Centre (NLSC) which is the northeastern limb of the King's Triple Junction (KTJ).

the basin, but is now concentrated on the Northwestern and Northern Lau Spreading Centres since ~3 Ma (*Parson & Tiffin, 1993; Parson & Hawkins, 1994*).

The process of subduction roll-back is a mechanism for generating extension in the back-arc region, which may lead to the formation and evolution of back-arc basins (*Uyeda & Kanamori, 1979*). This process also plays a major role in controlling the mantle dynamics under these basins (e.g. *Hergt & Hawkesworth, 1994*), as it can lead to a passive influx of aesthenospheric mantle which replenishes the mantle wedge. This has been particularly important in the northern Lau Basin, as the direct influence of a plume has been detected in lavas from this area. This plume signature originates from residual mantle from the Samoan plume, which has influxed into the northern Lau Basin from the northeast, through the rip in the Pacific plate at the northern termination of the Tonga trench.

Boninites are associated with many SSZ tectonic settings in the western Pacific (Izu-Bonin fore-arc, *Pearce et al., 1992a, b*; the Marianas, *Beccaluva & Serri, 1988*; Chichijima, *Taylor et al., 1994; Hickey & Frey, 1982*) and also SSZ-related ophiolites (e.g. Troodos, Cyprus, *Rogers et al., 1989; Cameron, 1985*). These boninites have been interpreted to be contemporaneous with early stages of subduction, having formed as a result of either subduction of a ridge, or subduction beneath a ridge (*Pearce et al., 1992b; Crawford et al., 1989*). However, the boninites dredged from the northern Lau Basin, are more likely to be related to the recent development (<3.5Ma) of back-arc spreading at the Northern Lau Spreading Centre (*Falloon & Crawford, 1991*).

1.2 Aims of the project

Figure 1.2 is a schematic diagram summarising the main physical and chemical processes which may have an important role in controlling the compositions of lavas associated with a supra-subduction zone tectonic setting (*Pearce & Peate, 1995*). These can be grouped into: (1) derivation of the subduction component; (2) transport of the subduction component to the melting column; (3) depletion and enrichment of the mantle wedge, and (4) processes in the melting column. Information about these processes can be gained from the compositions of SSZ-related lavas (along with experimental data on element behaviour). In this thesis, compositional evidence for these processes is acquired from a detailed geochemical study of suites of lavas from the northern Lau Basin. The major aims of this project are three-fold:
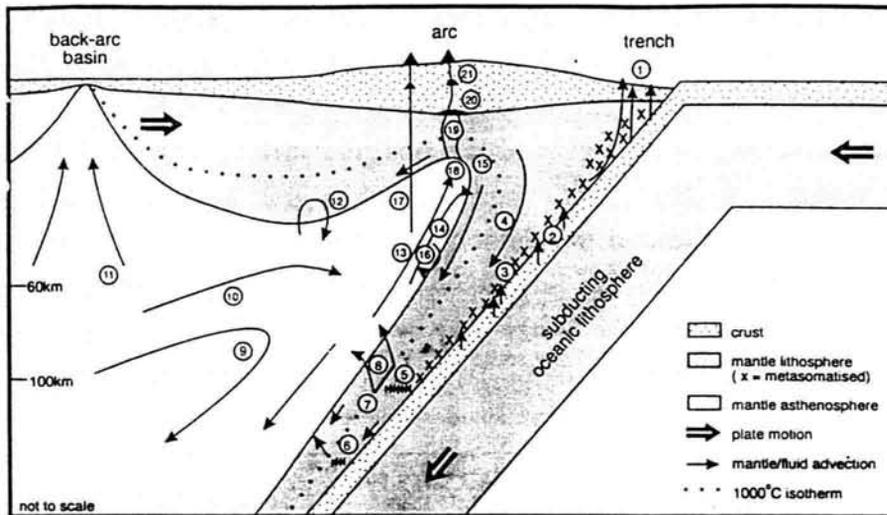
Figure 1.2: Schematic summary of the processes affecting arc magma composition from Pearce & Peate (1995).

Slab dehydration and melting: 1. fluid loss via accretionary prisms and serpentinite seamounts; 2. dehydration ± partial melting of subducting oceanic crust and sediment.

Transport of subduction component: 3. hybridization of subduction component and down-dragged mantle lithosphere; 4. slab-induced downward drag of hybridized mantle; 5. rerelease and lateral migration of aqueous fluids by amphibole breakdown at about 100 km depth; 6. rerelease of aqueous fluids by breakdown of other hydrous phases at greater depth; 7. initiation of hydrous melting of mantle at about 1000°C; 8. migration of small-volume hydrous melts through cross-fed mantle to the base of the melting column.

Mantle source processes: 9. slab-driven "corner flow" of mantle into the mantle wedge; 10. replenishment of the melting column by mantle advection; 11. mantle source depletion by small-volume melt loss in back-arc region; 12. mantle source enrichment by delamination of sub-continental lithosphere.

Melting column processes: 13. buoyancy-driven mantle counterflow; 14. decompression-melting of the mantle from about 60 km depth; 15. separation of residual mantle from the melting column aided by slab-induced downward drag; 16. column depletion by imperfect separation or reincorporation of residual mantle; 17. selective tapping of the melting column.

Lithosphere-melt interactions: 18. melt segregation at the base of the lithosphere; 19. interaction with, and crystallisation within, mantle lithosphere; 20. magma-assimilation-storage-homogenisation at the base of the crust; 21. assimilation-fractional crystallisation at shallower crustal levels.

♦ to collect a complete major, trace element and Sr, Nd and Pb isotope dataset of suites of lavas from the northern Lau Basin. This geochemical database is then used to study the extent to which (a) the Samoan plume, (b) along-trench variations in the composition of the subduction component, and (c) localised mantle dynamics, have influenced the magma genesis of these lavas;

♦ to carry out sampling and mapping of the lava flows on Tafahi and Niuatoputapu, north Tonga, in order to investigate the origins of any differences in the

geochemistry between lavas from the two islands and between individual ones on Tafahi. Their geochemical characteristics are compared with those of the other lavas from north Tonga and the central Tofua arc (*Ewart & Hawkesworth, 1987*);

♦ to investigate any relationship between the compositions of the lavas from the northern Lau Basin, the timing of their eruptions and the tectonic evolution of the region. Some of the lavas have ages close to that of the initiation of subduction, and therefore give an insight into processes occurring during early-arc magmatism. However, the younger lavas (<6 Ma), which erupted after the opening of the Lau Basin, give an insight into more recent processes during the evolution of this basin.

1.3 Description of the thesis

Chapter 2 outlines the tectonic setting and evolution of the Lau Basin and describes the geology of each of the north Tongan terranes. The dating of the ophiolite sections and lavas from Tafahi and Niuatoputapu is used to constrain their relationship to the tectonic evolution of the northern Lau Basin.

Chapter 3 documents the petrography and mineral chemistry of the dredged samples and those from Tafahi and Niuatoputapu. Two-pyroxene thermometry is used to determine their temperatures of crystallisation, from which the temperatures of their primary magmas, and hence the nature of their mantle sources are inferred.

Chapter 4 describes the major and trace element geochemistry of the lavas from north Tonga in order to identify some of the geochemical characteristics of their mantle sources and any slab-fluxes.

Chapter 5 outlines the isotopic characteristics of possible isotopic end-member components. The isotope systematics of the lavas from north Tonga are described, and a three-component model is then proposed for their magma genesis.

Chapter 6 develops the model for the magma genesis of the lavas from north Tonga, using combinations of trace elements and isotopes.

Chapter 7 discusses the magma genesis of the tholeiitic ophiolite section, which is then used as an insight into the petrogenetic processes of the early-arc system.

Chapter 8 summarises the major conclusions of the thesis and discusses the implications of the magma genesis of the lavas from north Tongan in terms of the Tongan arc-basin system.

CHAPTER 2

Geology of the North Tongan Terranes

2.1 Introduction and general geology

This chapter describes fieldwork carried out on the islands of Niuatoputapu and Tafahi, Kingdom of Tonga, S.W. Pacific, and the location of samples on the islands. In 1982 the Russian 'Kallisto' vessel sampled from the inner wall of the Tonga trench at its northern termination in the northern Lau Basin. The geology and locations of samples from two of the dredge sections carried out on this cruise are described in this chapter. The locations of dredge sites from previous cruises to the Northern Lau Spreading Centre (NLSC) in the northern Lau Basin (NLB) are also described. The lavas from the northern Lau Basin and the Tofua arc, reported in the literature (*Falloon et al., 1992; Ewart & Hawkesworth, 1987; Ewart et al., 1973, 1977*), are used as a comparison. K-Ar dating of the samples from the dredge sections and lavas from Tafahi and Niuatoputapu are reported and used to understand the tectonic evolution of the northern Lau Basin.

Figure 2.1 shows a map of the Tonga arc-basin system with the locations of samples. The Pacific plate is being subducted westwards beneath the Indo-Australian plate at the Tonga trench. The Lau back-arc basin lies between the Lau Ridge remnant arc and the active Tofua arc. It began to open at about 7-6 Ma when the Lau Ridge remnant arc split from the then-active arc, along an irregular zone of rifting (*Karig, 1971; Uyeda & Kanamori, 1979*). Extension, accompanied by localised magmatism, was taken up on small pull-apart basins until 5.5 Ma. This extension has given the older parts of the Central Lau Basin (CLB) to the west, a horst and graben topography. At this time the Eastern Lau Spreading Centre (ELSC) and the North-western Lau Spreading Centre (NWLSC) initiated at either end of the Peggy Ridge (*Parson & Hawkins, 1994; Parson & Tiffin, 1993*). By 1.5 Ma the Central Lau Spreading Centre (CLSC) had begun to propagate southwards from the Peggy Ridge, at the expense of the ELSC (*Parson et al., 1990; Parson & Hawkins, 1994*). There is a small intermediate spreading centre between the southerly propagating CLSC and the receding ELSC, which lies in a highly tectonised zone (*Parson et al., 1990*). The southerly tip of the ELSC, the Valu Fa Ridge is propagating southwards. The Valu Fa
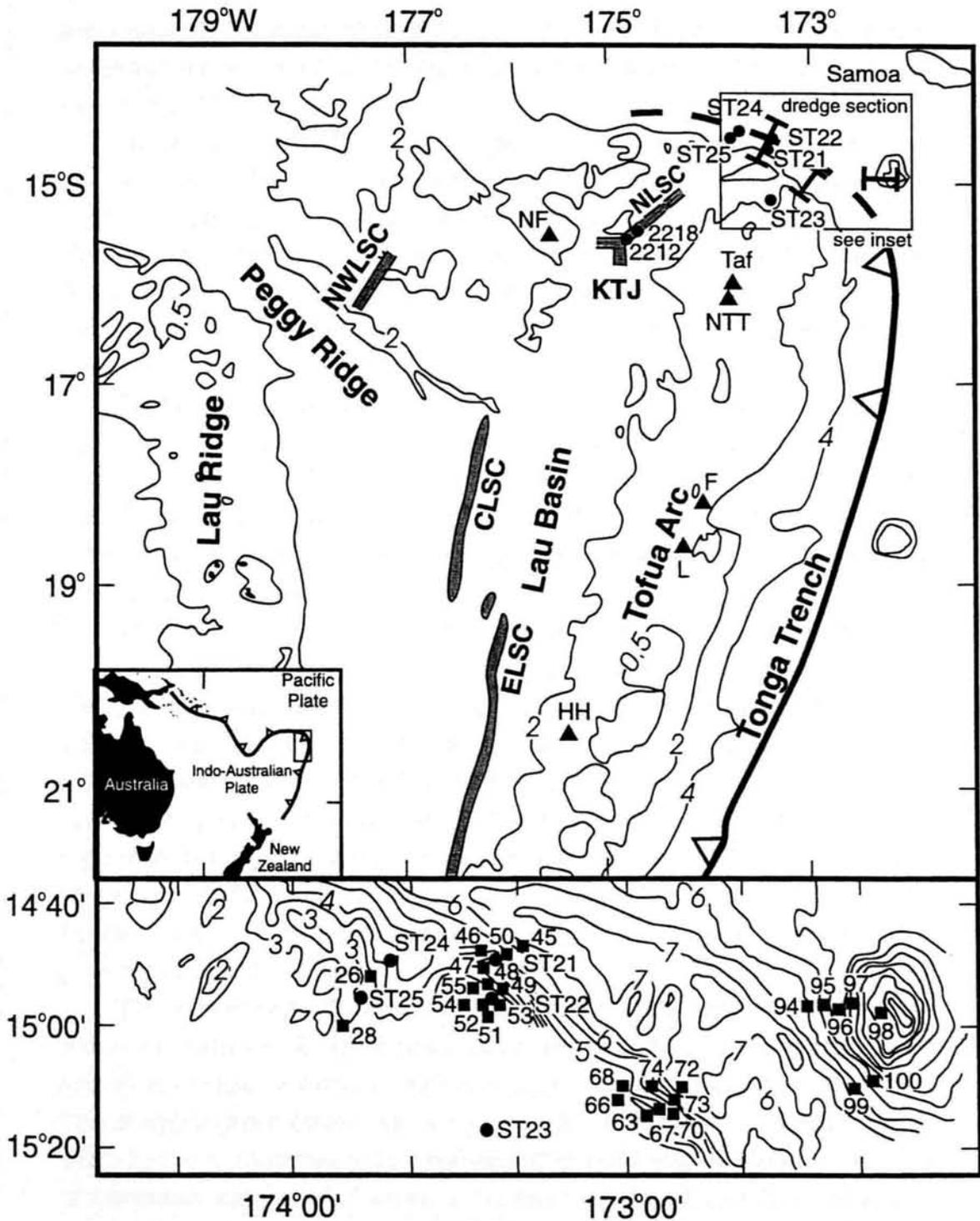
Figure 2.1: Map of the Lau Basin showing the locations of samples used in this thesis from (a) the Northern Lau Spreading Centre (NLSC; 2212, 2218), and the islands of Tafahi (Taf) and Niuatoputapu (NTT), and (b) from two ophiolite sections (sites 45-53 and 63-74) from the inner wall of the northern Tonga trench, a Samoan seamount (sites 94-100) and boninites (from sites 26 and 28) were dredged on the 'Kallisto' 1982 cruise. The location of other sites in the northern Lau Basin at which boninites were also dredged, on the 'Natsushima' 1984 cruise, are shown (ST 21-25). The main tectonic features of the basin are labelled, and have been described in this chapter. Other islands from the Tofua arc are Hunga Haa'pai (HH), Late (L), and Fonualei (F). The back-arc spreading centres are the Central and Eastern Lau Spreading Centres (CLSC and ELSC) in the central Lau Basin. In the north, the Northwestern Lau Spreading Centre (NWLSC), and the Northern Lau Spreading Centre (NLSC), which is the northeastern limb of the King's Triple Junction (KTJ).

Ridge presently lies within 30km of the active Tofua arc. A more detailed description of the tectonic history of the Lau Basin is given in *Parson & Hawkins (1994)* and *Parson et al. (1990)*.

Figure 2.2 is a GLORIA image of the NLB with an interpretation taken from *Parson & Tiffin (1993)*. *Parson & Tiffin* divided the area into five morphotectonic regimes (Figure 2.2), (i) the basement ridge and sedimented inter-ridge area, (ii) the King's Triple Junction, (iii) the sedimented block terrain in the central north Lau Basin, (iv) the North-western Lau Spreading Centre, and (v) the northern Peggy Ridge. These are fully described in their paper. A summary of the main features is given here.

The basement ridge and sedimented inter-ridge area lies in the central northern Lau Basin. It is dominated by N-S trending steep-sided basement ridges which are separated by flat-floored, deeply-sedimented basins, some being more than 2800m deep. There are four ridges (A-D on Figure 2.2), the descriptions of which are given in *Parson & Tiffin (1993)*. The eastern-most ridge (A) is identified as the western side of the northern Tonga Ridge.

The King's Triple Junction (KTJ) has developed since 1.5 Ma. Its north-eastern limb, the Northern Lau Spreading Centre (NLSC), is propagating to the northeast into a highly tectonised zone which extends towards the trench-transform intersection. This region is characterised by myriads of fine, parallel and closely-spaced linear reflectors which are interpreted as normal fault scarps, and areas of intensely backscattering sea-floor on the GLORIA image which represent the neovolcanic regions of the KTJ. The western limb is propagating westwards along a fracture zone where some shallow earthquakes have been detected (*Hamburger & Isaacs, 1988; Parson & Tiffin, 1993*). A more detailed description of the King's Triple Junction is given in Section 2.8.

The sedimented block terrain is bounded to the south-west by the Peggy Ridge and to the north-west by the brightly backscattering linear zone, interpreted as the neovolcanic spreading centre of the North-western Lau Spreading Centre (NWLSC). This morphotectonic domain has a uniform back scatter on the GLORIA image, which has been interpreted to be a sedimented basin. In addition there are two areas of hummocky and pinnacled terrain in the east (ridge E in Figure 2.2), and a small area extending east-west from the NWLSC, including the Zephyr Shoal which is a seamount rising to 15 m below sea-level. There are few linear fault scarps to be observed in the hummocky ridge areas, but within the sedimented basin there are complex intersecting sets of faults. The most obvious of these are arcuate and concaved northwards, with north-facing scarps, in the west central part of this basin.

(a)

(b)
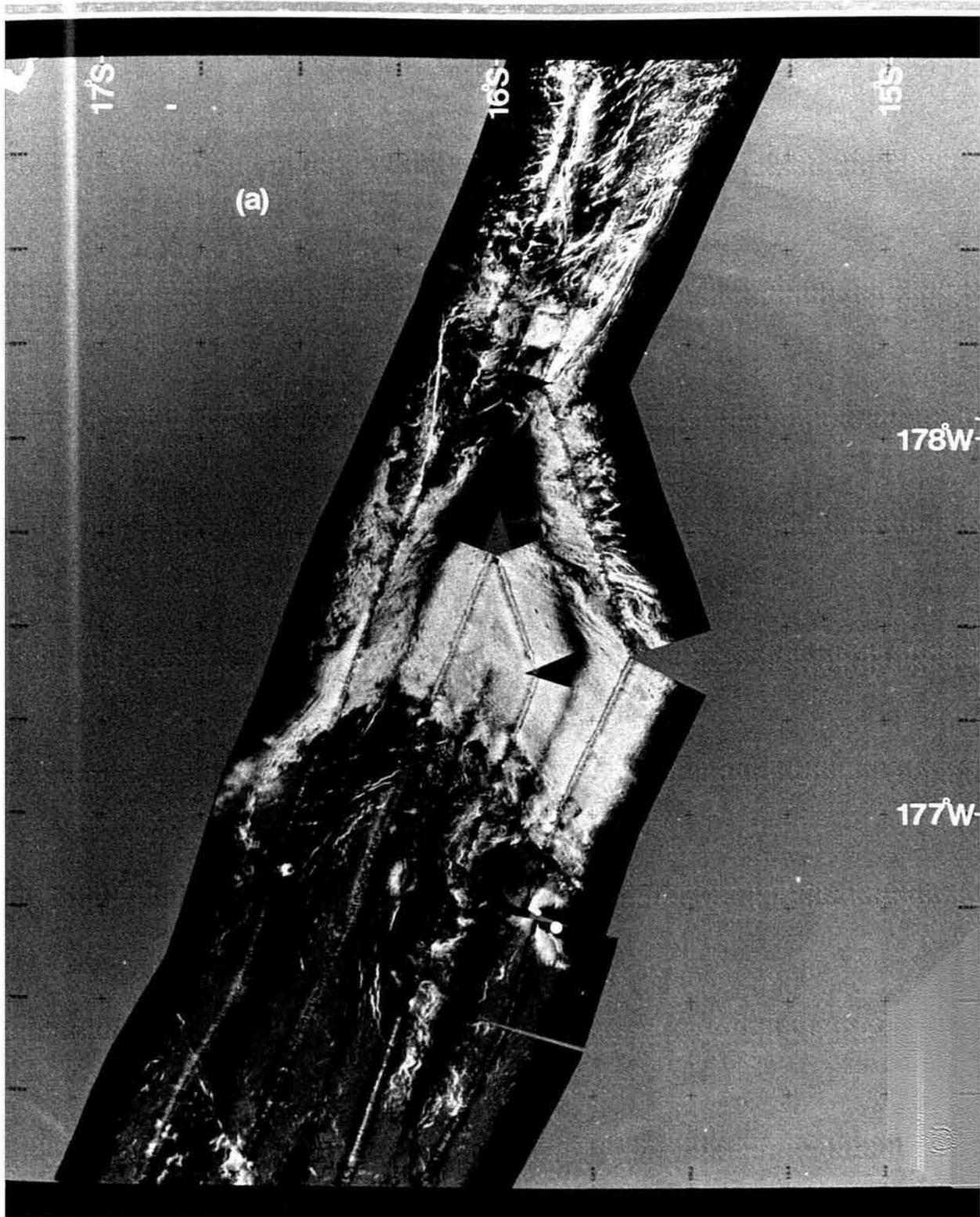
Gloria Mosaic

(c)
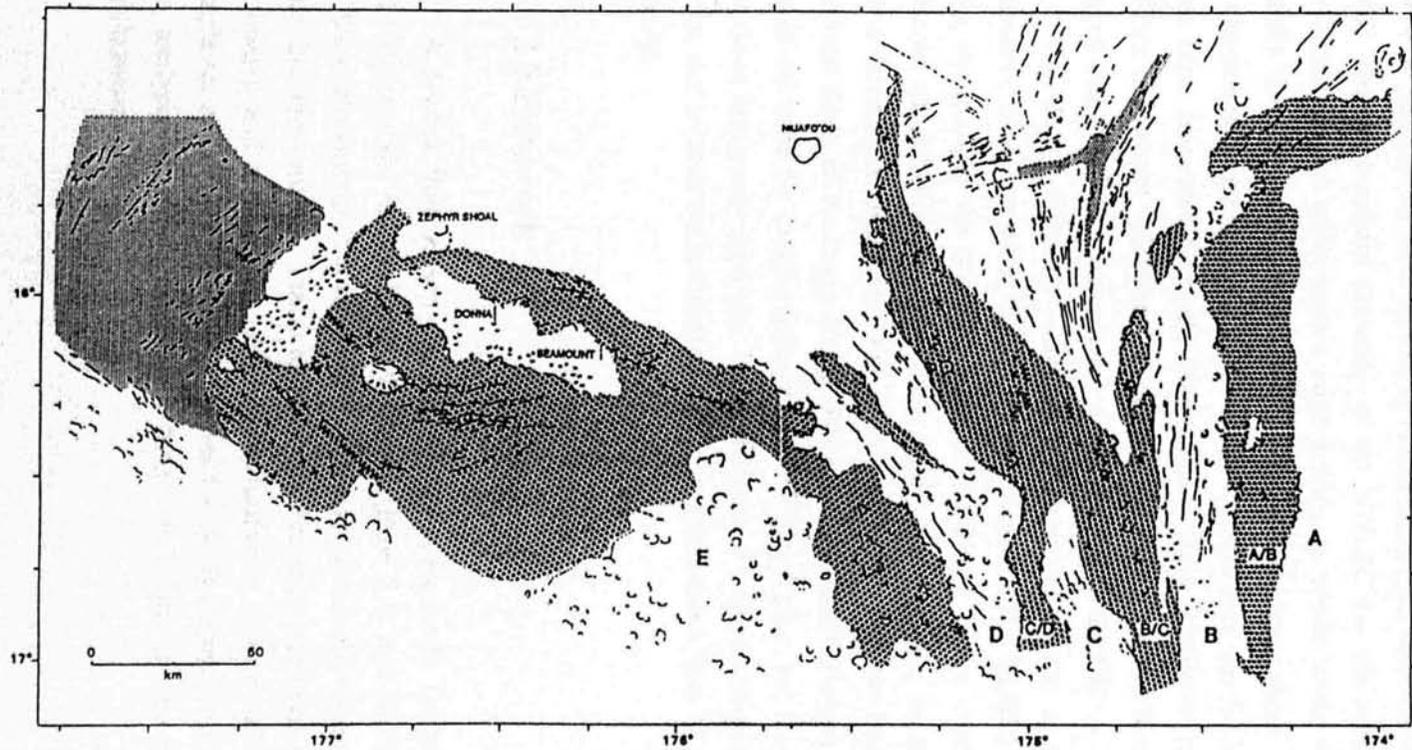
Figure 2.2(a) and (b): GLORIA images of the northern Lau Basin (NLB) taken in 1989 (Tiffin, 1993). Neovolcanic regions of the ocean-floor are highly backscattering and therefore appear bright on these images. Regions of the ocean-floor that are covered by sediment are weakly backscattering and are therefore are of darker tones on these images. Other features have been identified on these images such as a hummocky and pinnacled terrain, lineations which can be interpreted as fault scarps and volcanoes. A full interpretation of these GLORIA images has been made by Parson & Tiffin (1993). (a) a GLORIA image of the central and northeast of the northern Lau Basin, showing the highly backscattering, tectonised region associated with the King's Triple Junction, the basement ridge and sedimented inter-ridge area of the central NLB and the more blocky terrain to the west, (b) a GLORIA image of the neovolcanic zone of the Northwestern Lau Spreading Centre, trending at 040°, and the northern Peggy Ridge. Highly backscattering areas on the northern flanks of the Peggy Ridge can be interpreted as sheet flows (c) A structural interpretation of the GLORIA data from Parson & Tiffin (1993) showing the sedimented basin areas (coarse stipple), neovolcanic zones (fine stipple), ridges and basement outcrop (no pattern). Letters refer to ridges (single letter) and inter-ridge basins (double letter). (d) a map showing the five morphotectonic domains. A description of these domains is given in the text.
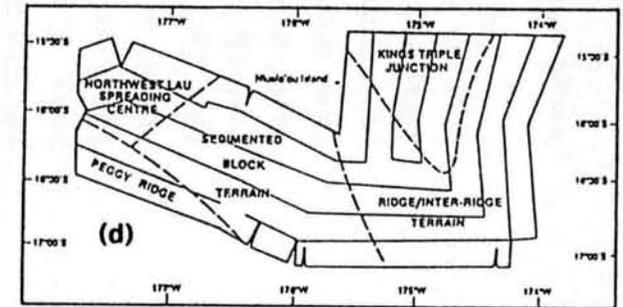
The North-western Lau Spreading Centre (NWLSC) has been the main spreading centre in the NLB since 5.5 Ma. It is offset from the CLSC by the Peggy Ridge and is marked on the GLORIA image by a broad zone of highly backscattered data which is finely lineated (Figure 2.2). This image is typical of the axial valley floors of medium to slow spreading ridges described elsewhere (*Parson & Searle, 1986*). The north-eastern extremity of the NWLSC has not been imaged. However, the fabric and the south-eastern edge, having an approximate strike of 040°, trend directly towards Rochambeau Bank, a large shoal area about 75 km to the NE. Evidence has been found of a high heat flow in this area and fresh basalts and glasses have been recovered from the Rochambeau Bank (*Schlater et al., 1972*). These indicate that recent volcanism has occurred in the area of the Rochambeau Bank and suggest that the NWLSC may reach at least that far to the NE.

The Peggy Ridge is a dextral transform fault with a component of E-W extension. There are some highly reflective areas on the GLORIA image of the flat-lying sea-floor of the northern flank of the Peggy Ridge, which are likely to be volcanic sheet flows. Small volcanic ridges and irregular seamounts or 'haystack' pillow constructs intersperse the sheet flows, which have been observed on the southeast flank of the Peggy Ridge (*Parson et al., 1990*). *Parson & Tiffin (1993)* use this as evidence for magma-leakage on the Peggy Ridge, but *Hawkins (1995)* argues that these lavas may represent some of the first magmas erupted as the Lau Basin opens, due to their unfractionated compositions derived from high degrees of partial melting.

2.2 Fieldwork

A 3-week field season was carried out on the north Tongan islands of Tafahi and Niuatoputapu in October 1992. Tafahi (Plate 2.1) and Niuatoputapu (Plate 2.2) are the northernmost islands of the Tofua arc, located above the Tongan subduction zone, but they are now inactive. These islands have not been extensively sampled previously and so the main aim of the fieldwork was to collect a representative sample set of the lavas of both volcanoes for detailed geochemical analysis. There is one analysis of Niuatoputapu and three of Tafahi in the literature (*Ewart & Hawkesworth, 1987*).

2.2.1 Access and exposure

Tafahi island lies 9 km north-northeast of Niuatoputapu and 60km east of the King's Triple Junction. It is steep sided, and cone-shaped with a summit of 656m (Plate 2.1). It can be reached by an hour's boat journey from Niuatoputapu. Landing on to the island can be done through a gap in the reef close to the village on the northern end of the island. The island is mostly covered with dense tropical woodland, but there is good exposure of lavas in three steep gullies on the western side of the island, along the coast and along the paths which network the island, all of which are within a day's walk of the village. Figure 2.3 is a map of Tafahi showing the outcrop of the lavas, sample locations and the situation of the village on the northern end of the island.

Niuatoputapu island is 5 km long and up to 4km wide and has a lagoon on the northern side (Figure 2.4). There are three villages, Hihifo, Vaipoa and Falehau on Niuatoputapu, which are situated on the northern shore of the island. The land around these villages is farmed. Most of the island is formed from flat-lying limestone that lies between 0 and 10 m above sea-level, but the north of the island is dominated by a ridge which is 2km long and rises to 165m (Plate 2.2). The sample locations of the volcanic lavas, flows and agglomerates along the ridge are shown in Figure 2.4. There are tracks up onto the ridge from all the villages and along the top of it, and a traverse of the ridge can be done in a day. However, the ridge is covered by dense tropical bush, so exposure of the lavas is not extensive. The south of the island is covered with dense tropical woodland and the beaches are only accessible by three tracks.

2.2.2 Sampling

The main aim of the fieldwork was to sample the lava flows of Tafahi and Niuatoputapu as systematically as possible and to sample successive flows in a sequence, in order to determine any temporal changes in lava geochemistry. This was difficult, especially on Niuatoputapu, because of the dense vegetation covering the volcanic areas. Alteration of samples is potentially a problem in tropical climates but most of the samples from both of the islands had only surficial alteration and therefore fresh samples could be obtained. However, many of the lavas from the coastal areas of Tafahi have undergone intense seawater alteration, so as much as possible of the alteration zone was removed during sampling.

Tafahi village

TAFAHI
ISLAND

Cloud
obscured
area

•46 Sample location
→ 45 Sample section
Rock outcrop

Scale

0   0.5   1 km
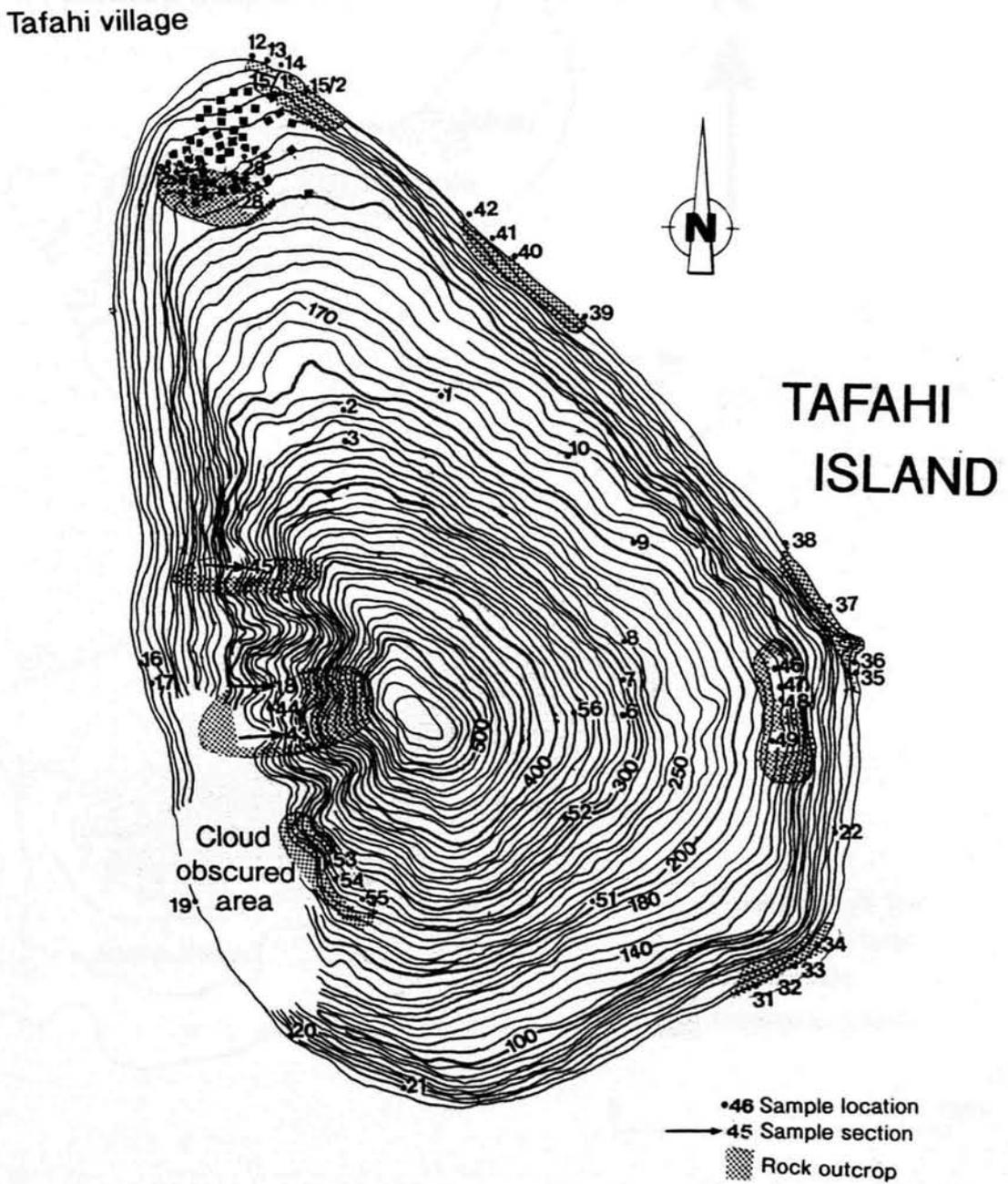
Figure 2.3: A topographic map of Tafahi showing the location of samples and the rock outcrop. The only village on the island is shown on the northwestern shore.
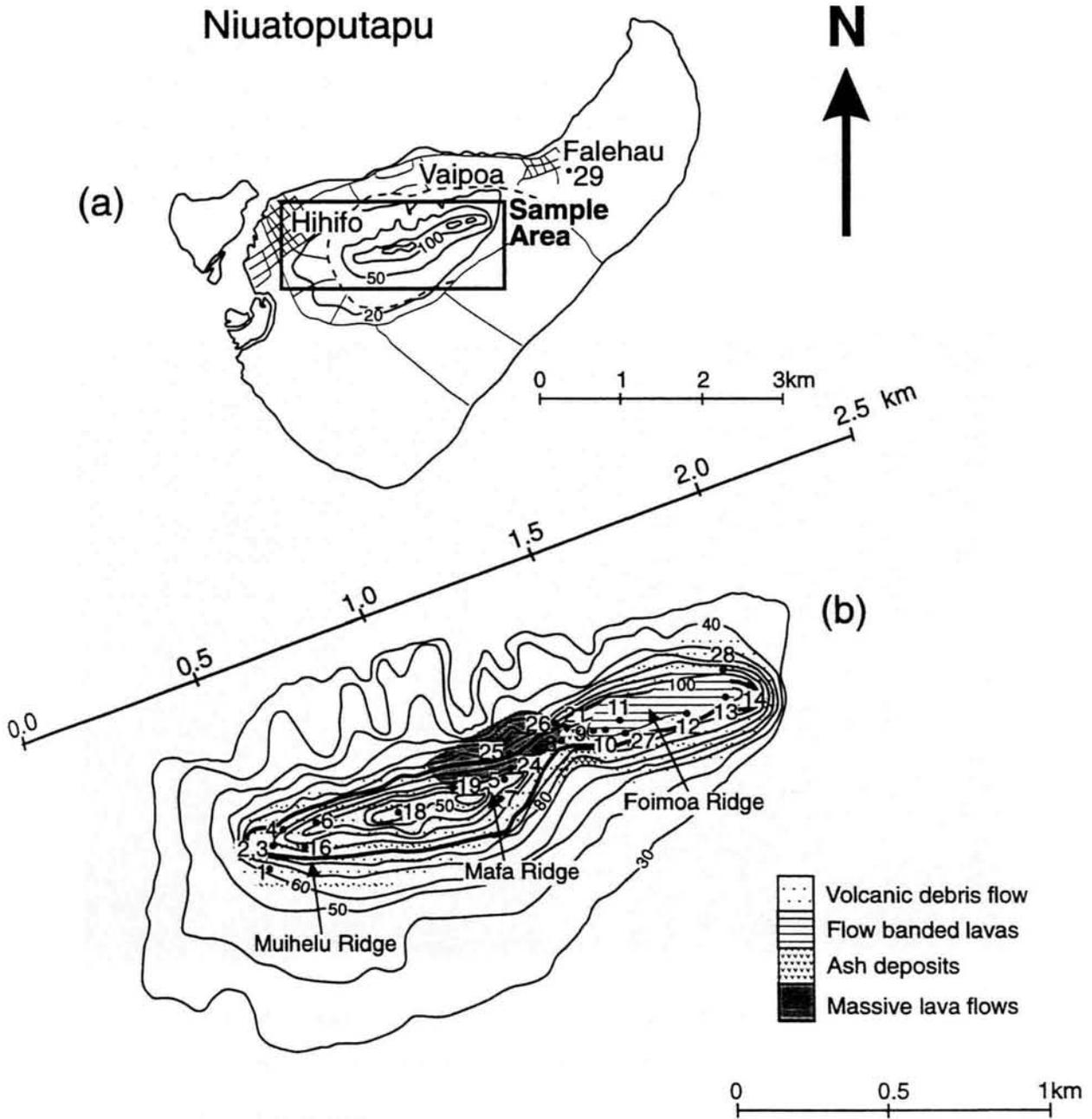
Figure 2.4: (a) A map of Niuatoputapu showing the three villages of Hihifo, Vaipoa and Falehau. A lagoon lies to the north of these villages. The 3km long volcanic ridge on the northern side of the island is outlined by the box; (b) A detailed geographical map of the volcanic ridge on Niuatoputapu showing the location of samples. The line used to reconstruct the volcanic stratigraphy of the island (Figure 2.5) is also shown.

16

2.3 Tafahi

Tafahi is covered with tropical bush, but outcrops of lavas occur along the coastline, up some steep gullies on the western side of the island, in the paths that network the island and in the village on the northern part of the island. Samples were taken from all these localities and special care was taken to sample successive lava flows where they are exposed in the gully sections. The basal lava flow is broken up into a blocky flow along parts of the coastline. Figure 2.3 shows the sample locations and the outcrop of lavas on the island.
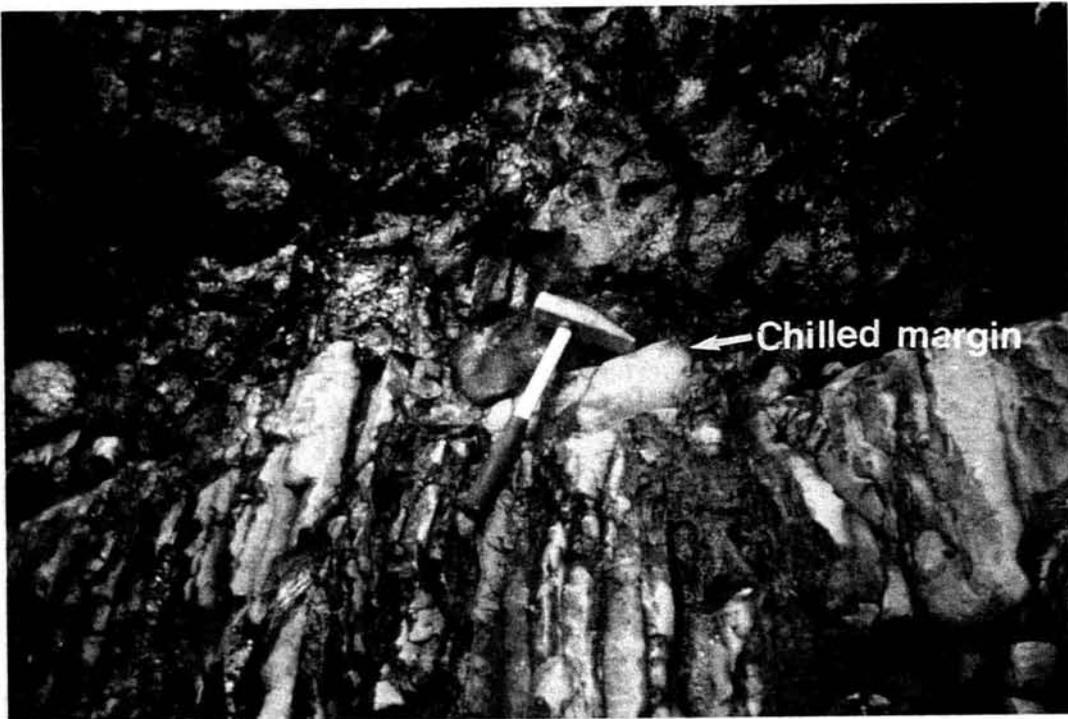
Plate 2.3 The irregular contact between successive lava flows showing a chilled margin.

2.3.1 Gully sections

The western side of the volcano is very steep sided, which has led to deep gullies being eroded into the volcano flanks during storms or the wet season. Excellent sections of lavas are exposed in the gully floor and sides, from sea level to close to the summit of the volcano. The torrential flow of water has removed any covering vegetation and soil from the lavas and smoothed the lava surface.

The lava flows are between 30 cm and 2 m thick and are distinguishable by their different weathering, the amount of phenocrysts and vesicularity. The lavas contain

plagioclase and pyroxéne phenocrysts in varying proportions, with up to 25% plagioclase phenocrysts and up to 15% pyroxene phenocrysts. The lavas containing a higher proportion of plagioclase phenocrysts have a paler weathering colour. The majority of the lavas from the gully sections are avesicular but occasionally there is a vesicular lava flow within the sequence. The contacts between lavas are irregular with a thin chilled margin (Plate 2.3). They are angular, with the upper lava flowing over the angular surface of the lower flows, suggesting that the lavas had enough time to cool before the next lava flowed on top.

2.3.2 Coastal sections

There is good exposure of the lower lava flows along the coast. Much of the basal lava flow is brecciated into blocks and clasts, from 2cm up to 1m in diameter, which are surrounded by a fine-grained matrix which has a similar composition to the blocks themselves (Plate 2.4). These blocks and clasts are sub-angular and have experienced some surficial weathering, giving a pitted appearance to the surface of the unit. The clasts and blocks are chaotically sorted and are welded into the matrix suggesting the breccia formed whilst the whole unit was still hot.

The contact between the basal lava flow and the underlying reefal limestone is especially well-exposed along the coast. This contact is very irregular but, unlike the contacts of successive lava flows which are angular, it is more rounded with dykelets of lava intruding into the limestone (Plate 2.5). Pockets of breccia are sometimes caught up between the bulk of the lava flow and the underlying limestone (Plate 2.5). In places, the basal lava flow has almost completely eroded away leaving isolated blocks of lava on top of the limestone on the beach (Plate 2.6). The reefal limestone was therefore older than the lava succession but their relative ages could not be constrained.

2.3.3 Causes of vesicularity

The lavas exposed around the coast are more vesicular than the lavas exposed higher up the volcano. Most of the lavas from the gully sections are avesicular. This suggests that the cause of the vesicularity of the coastal lavas is incorporation of sea water into the lava at the lava-sea water contact, which has then vaporised and formed vesicles. Although some of the lavas from higher up the volcano are also vesicular, which can be explained by the exsolution of volatiles from the magma before and during eruption, incorporation of sea water into the lava may more convincingly explain the intense vesicularity of the coastal lavas.

phenocryst contents, vesicularity and weathering similar to the main lava flows, suggesting that they were once part of a similar flow before it broke up.

2.4 Niuatoputapu

The main rock-types which outcrop on the Niuatoputapu Ridge are volcanic debris-flows, massive, aphyric lavas and flow-banded lavas. Plate 2.7 is a view along Foimoa Ridge from Mafa Ridge, showing the dense tropical bush that covers the ridge. Figure 2.4 shows a geological map of the units. Samples were taken of clasts from the volcanic debris-flows, the massive aphyric lavas and the flow-banded lavas. Figure 2.5 shows the reconstructed volcanic stratigraphy of the Niuatoputapu lava field. The sections were constructed by projecting the sample sites onto the horizontal line marked on Figure 2.4 and then plotting this value against the vertical height above sea-level of the site. The flow banded lavas are stratigraphically above the volcanic debris-flows, which in turn overlie the massive lava flows.

2.4.1 Volcanic debris-flows

The volcanic debris-flows outcrop on the western Muihelu Ridge and on the lower slopes of Mafa Ridge, forming normally-graded layers, 10-50cm thick. These layers contain clasts which are between 5mm and 20cm in diameter, and are sub-angular to rounded. There is a large variety of clast types which all have a volcanic origin. Plate 2.8 shows an outcrop of normally-graded debris-flows on the westerly end of Muihelu ridge. Table 2.1 shows the clast types found in the volcanic debris-flows and the location of samples. Samples of clasts were taken from single debris-flows to study the variety of clasts. The main clast types are fine-grained avesicular aphyric basalts, which have a similar field appearance to the massive lava flows, and avesicular plagioclase-rich basalts. The aphyric basaltic clasts contain up to 5% plagioclase and 2% clinopyroxene microphenocrysts which can only be observed in thin-sections of the samples. The plagioclase-rich basalts contain up to 25% plagioclase phenocrysts in a fine-grained basaltic groundmass. The plagioclase phenocrysts have compositions between An_{55} and An_{70}, which are similar in composition to those in the Tafahi lavas (Appendix 3). The debris-flow deposits are likely to have formed when material settled out from debris-flows, which were initiated during eruptions and flowed down the flanks of the volcano (former) on Niuatoputapu.
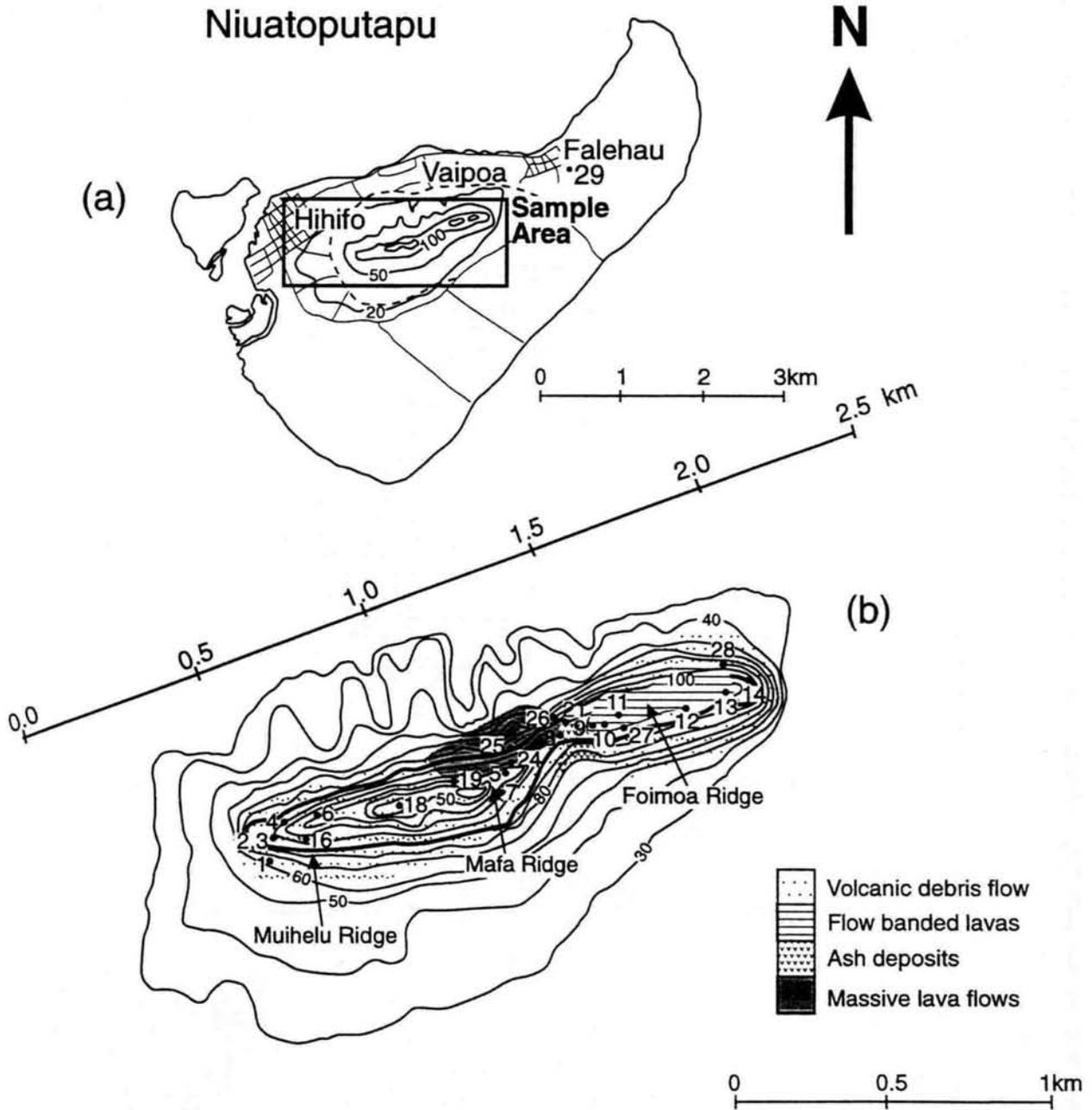
21

Figure 2.4: (a) A map of Niuatoputapu showing the three villages of Hihifo, Vaipoa and Falehau. A lagoon lies to the north of these villages. The 3km long volcanic ridge on the northern side of the island is outlined by the box; (b) A detailed geographical map of the volcanic ridge on Niuatoputapu showing the location of samples. The line used to reconstruct the volcanic stratigraphy of the island (Figure 2.5) is also shown.
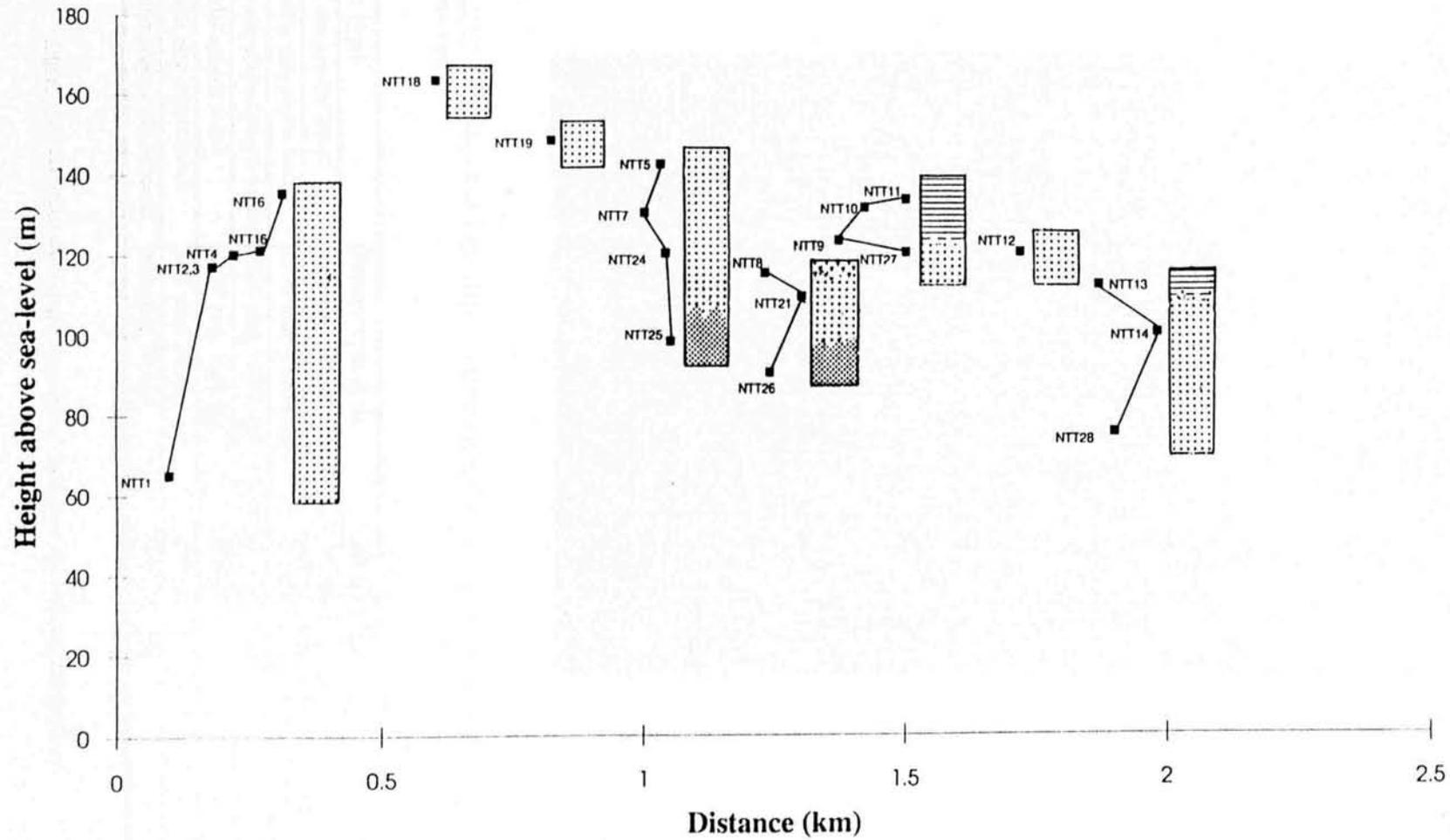
Figure 2.5: *The reconstructed stratigraphy of the volcanic ridge of Niuatoputapu, using the baseline on the geological map (Figure 2.4). The key for rock-types is the same as in Figure 2.4.*

plagioclase and clinopyroxene. They contain fewer microphenocrysts than the 'aphyric' basaltic clasts from the volcanic debris-flows. Samples were taken systematically through the thickness of the exposed massive lava flows, so that any geochemical changes within and between flows could be detected.

2.4.3 Flow-banded lavas

The flow-banded lavas are exposed on the central part of Foimoa Ridge and also close to the saddle point between Foimoa and Mafa Ridge. The lavas are banded on a mm scale and contain 1-2% lithic clasts which have a volcanic origin. These lavas contain vesicles, which are elongated parallel to the direction of flow. The size of the vesicles varies from less than 1mm in diameter to 0.5cm in length. Samples were taken of the flow-banded lavas where they are exposed.

2.5 Inner trench wall ('Kallisto' western section) and Stations 21 and 22 of the 'Natsushima' 1984 cruise

The 1982 Russian 'Kallisto' cruise dredged an ophiolite section from the inner wall of the northern Tongan Trench, close to the trench-transform intersection. A more detailed map of the locations of dredge samples from the ophiolite sections is shown in Figure 2.1(b), and a sketch section of the inner trench-wall and rock-types dredged at the sites is shown in Figure 2.6.

15 dredges were recovered from 7km of vertical relief on the inner wall of the Tonga trench. All components of a supra-subduction zone ophiolite are present and have been described by Vysotsky *et al.* (in press). Tectonised, variably serpentinised harzburgites which contain olivine (70%) and orthopyroxene (30%), but very little clinopyroxene (<5%) are found towards the base of the dredge section. The plutonic rocks are made up of cumulate ultramafics and gabbros of the 'layered sequence', and gabbro norites, tonalites and trondhjemites of the 'high level plutonic suite'. The ultrabasic cumulates are dunites and pyroxenites which have undergone serpentinisation and clay alteration. The gabbros have cumulate textures and mainly contain clinopyroxene (up to 40%) and plagioclase (up to 60%) but some contain primary and secondary amphibole. Sheeted dykes may be present but sheet flows and dykes are hard to distinguish in the dredged samples as evidence of chilled margins is required to confirm their presence. Porphyritic boninitic lavas were recovered towards the top of the section at Sites 51, 53, 54, 55, 56, and 57 (Figure 2.6). These boninites contain orthopyroxene (up to 20%), clinopyroxene (10%) and plagioclase (up to 15%) as phenocryst phases.

Western ophiolite section

(a)
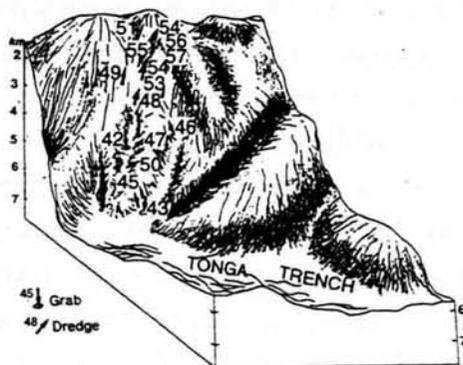
Dredge sections of the 'Kallisto' 1982 cruise

Rock Type	Dredge Site
Boninitic lavas + tuffs	51,53,54,55,56,57
Diabase	43,45,49
Cumulate gabbros	43,45,48,49,50,52,53
Plagiogranite, dacite	42,48
Cumulate ultramafics	48,49,50,52,53
Serpentinised harzburgites	43,45,46,47,50

Eastern ophiolite section

(b)
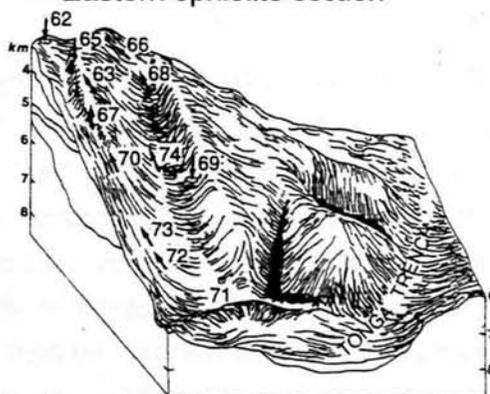
Rock Type	Dredge Site
Basalts + tuffs	65,66,67,69,72 62,63,70,71,73,74
Diabase	66,67,69,70,72,73
Cumulate gabbros	68,72,73
Plagiogranites, diorites	73
Cumulate ultramafics	73

Figure 2.6: Sketches of the inner wall of the northern Tonga trench showing the location of samples from two ophiolite sections dredged on the 'Kallisto' 1982 cruise. (a) the western ophiolite section, contained boninitic lavas, whereas (b), the eastern ophiolite section, contained tholeiitic lavas. The rock-types dredged at each site are shown in the tables below the sketches.

A detailed study of the petrography and mineral chemistry of the western ophiolite section is given in Section 3.5, and the major and trace element and isotopic data of the boninitic lavas is presented in Chapters 4, 5 and 6.

Station 21 and 22 dredge sites from the 'Natsushima' 1984 cruise have a similar location to the western ophiolite section (Figure 2.1(b)). Boninites from these stations are used as a comparison to the boninites, dredged on the 'Kallisto' cruise, from this study. *Falloon et al. (1987)* and *Falloon & Crawford (1991)* present the detailed petrography, mineralogy and geochemistry of the boninitic lavas from Station 21 and 22. These lavas contain modal proportions of up to 10% olivine, up to 21% orthopyroxene and up to 15% clinopyroxene. Some of the lavas contain up to 17% plagioclase phenocrysts. These lavas contain olivine as an assessory phase rather than as a main phenocryst phase. The plagioclase is very calcic (An_{90}). The olivines are very magnesian (up to Fo_{93}) reflecting very MgO-rich magmas and a very refractory peridotite source. Glomeroporphyritic clusters of pyroxenes are common. The phenocrysts are in a quench matrix of microlitic pyroxenes and plagioclases or in some lavas the matrix is glassy.

2.6 Inner trench wall ('Kallisto' eastern section)

A second section was dredged up the inner trench wall of the Tonga trench, on the 'Kallisto' 1982 cruise, 60km east of the 'western' section (Figure 2.1(b)). This contained cumulate ultramafics and gabbros, diorites, plagiogranites, diabases, tholeiitic basalts and tuffs, which forms part of a suite of rocks from another supra-subduction zone ophiolite. Figure 2.6(b) shows a sketch of the dredge section up the inner trench wall with a table of the rock-types found at each dredge site.

No tectonised harzburgites from the mantle sequence were recovered from this ophiolite section, but pyroxenites and gabbros from the cumulate sequence were successfully recovered. The gabbros have cumulate textures with phenocrysts of olivine (1-3%), clinopyroxene (30%) and plagioclase (67%). In some samples the plagioclase is altered to sericite, and secondary chlorite or amphibole is present. The rocks contain Fe-Ti oxides, which have possibly grown during hydrothermal alteration. Plagiogranites and diorites from the 'high-level plutonic sequence' were recovered. The plagiogranites contain sericitically-altered plagioclase intergrown with quartz, secondary epidote and chlorite. The tholeiitic basalts are aphyric and are altered to clay minerals, but some of the original quench textures are retained after alteration (Section 3.6; Plate 3.17). Full petrographic and mineralogic descriptions are given in Section 3.6. The major, trace element and isotopic data of the tholeiitic lavas,

and a discussion of their relationship to the underlying cumulates and diabases, are presented in Chapter 7.

2.7 Sites 26 and 28, 'Kallisto' cruise, Stations 23, 24 and 25, 'Natsushima' 1984 cruise

Boninitic lavas were also dredged at sites 26 and 28 from 40km to the west of the western ophiolite section (Figure 2.1(b)), closer to the Northern Lau Spreading Centre. Preliminary geochemical data on these boninites have been reported by *Sharaskin et al. (1983a, b)*. Full major, trace element and isotopic analysis of the boninites is presented in this thesis (Chapters 4-6). These boninites contain modal proportions of up to 15% olivine, 6% orthopyroxene and between 1-5% clinopyroxene, in a matrix composed of clinopyroxene microlites.

Boninites were also dredged at Station 23 of the 'Natsushima' 1984 cruise, south of the western ophiolite section, and at Stations 24 and 25 which lie further to the west, at locations similar to sites 26 and 28 of the 'Kallisto' 1982 cruise. Petrographic, mineralogic and geochemical data for Stations 23, 24 and 25 is presented in *Falloon et al. (1987, 1989)*. The boninitic lavas contain a high proportion of phenocrysts of olivine (up to 16%) and orthopyroxene (up to 18%), but only small amounts of clinopyroxene (1-2%) and Cr spinel (<1%). The matrix of the lavas is glassy with some quench pyroxene microlites, which have a composition range from augite to subcalcic augite. Some of the lavas from Station 23 have a basaltic andesitic composition and contain 3-14% plagioclase as a phenocryst phase. The plagioclase is extremely calcic (An_{89-93}), which is a characteristic of the Tongan arc lavas (*Ewart et al., 1973; Falloon et al., 1987*).

2.8 King's Triple Junction

To the west of the ophiolite sections, the Northern Lau Spreading Centre, the north-east limb of the King's Triple Junction, which trends at 025°, intersects the trench in a highly tectonised zone (*Falloon et al., 1992*). Close to the triple junction, at 15°37' 174°50', the axial zone is highly backscattering on the GLORIA image (Figure 2.2). It is composed of bright lineations and is about 18km wide close to the triple junction, but narrows to the northeast and tapers to a narrow slot at 15°07'. In the region of the triple junction, the fault lineations vary from being closely spaced, less than 100m apart, to major continuous fault scarps, downthrown up to 500m towards the adjacent axes.

South of 15°40', an acuate array of fanning lineaments, which are interpreted to represent normal extensional fault scarps, strike at 195° and converge to the south. This area is defined by a narrow, southerly tapering tongue of uniformly high backscatter. Bathymetric and seismic data show that these lineaments are derived from many small faults with a maximum of about 50m throw. This region is an axial rift region of the southerly limb of the King's Triple Junction.

Close to the core area, around 153°7'S 174°52'W, an orthogonal set of lineaments, trending at 250°, crosscuts the southerly trending fabric, and can be traced for 30km to the west. This limb of the KTJ continues westwards as a tectonic lineament as far as a point located at 15°00'S 176°W, near to the Rochambeau Bank, along which shallow earthquakes have been detected (*Hamburger & Isaacs, 1988*).

Five dives were carried out in the northern Lau Basin by the submersible 'Mir' during the 1990 cruise of the research vessel 'Akademik Mstislav Keldysh'. Three of the dives, 2212, 2218 and 2226 were carried out on the NLSC at 15°S (Figure 2.1). The rocks recovered from dives 2212 and 2218 are vesicular and contain stellate clusters of microcrystalline plagioclase (10-12%) and clinopyroxene (3-5%). They have a fine-grained matrix that has devitrified to opaque minerals such as iron-titanium oxides. Major and trace element data and Sr, Nd and Pb isotopic data for these lavas are presented in *Falloon et al. (1992)* and in Chapters 4, 5 and 6.

2.9 Comparative data: Tofua arc, 'Eua, Samoa, the Central Lau Spreading Centre, Pacific MORB mantle and Pacific sediments

The comprehensive geochemical data set in the literature for the islands of Fonualei, Late, Hunga Ha'apai and Ata (Figure 2.1) from the Tofua arc in *Ewart & Hawkesworth (1987)*, *Ewart et al. (1977)* and *Ewart et al. (1973)* has been used in comparison with that of the north Tongan boninites and the lavas from Tafahi and Niuatoputapu. The Eocene volcanics from 'Eua and the north Tongan tholeiites are likely to have similar ages, and therefore their geochemical data have been compared (*Ewart & Bryan, 1972; Cunningham & Anscombe, 1985*).

The lavas from north Tonga may have either MORB-, or plume-mantle sources (Chapters 4, 5, 6; *Loock et al., 1990; Volpe et al., 1988; Falloon & Crawford, 1991; Hergt & Hawkesworth, 1994; Ewart et al., 1994*). The compositions of the sources of the lavas from the Central Lau Spreading Centre (CLSC) are likely to be similar to those of the MORB-mantle that may be present in the source regions of the lavas from north Tonga. Therefore, the isotopic compositions of the CLSC lavas are used

Plume athenospheric mantle has influxed into the northern Lau Basin through the rip in the Pacific plate (Figure 5.4). The lavas from north Tonga may be derived from either this mantle, or from a mixture of this and MORB-mantle. Data for post-erosional lavas and shield volcanics of Samoa (*Wright & White, 1986/87; Palacz & Saunders, 1986*) are used as possible end-member isotopic compositions for this mantle.

The shield volcanics are the earlier eruptions of the Samoan plume, the deepest accessible levels of which have transitional compositions between tholeiitic and alkalic lavas, whereas the caldera fill are alkali olivine basalts, hawaiites and trachytes. A second post-erosional series of lavas was erupted after a period of quiescence and erosion from the Pleistocene to Historic. These lavas consist of alkali olivine basalts, basanites, and olivine nephelinites which are rich in incompatible elements such as Rb, Sr, Ba, and Nb. It has been proposed that these later lavas were produced in response to the flexure of the Pacific plate southward along the east-west portion of the Tongan Trench (*Hawkins & Natland, 1975; Natland, 1980*). The flexure of the plate produces a region where melts can concentrate. The post-erosional lavas are found on Tutuila, Upolu and Savai'i, but not Manu'a, which is the most easterly island of Samoa, suggesting that the fracturing and volcanism resulting from flexure only takes place in the vicinity of the Tonga trench, and does not extend as far eastwards as Manu'a. *Farley et al. (1992)'s* additional use of He, as well as Sr, Nd and Pb isotopes show that the variations in the compositions of the shield volcanics from Tutuila, Western Samoa are a result of mixing between two isotopically extreme mantle end-members: one derived from recycled crustal material and the other originating from a largely undegassed and highly primitive mantle (primitive helium mantle: PHEM). The former has very high $^{87}Sr/^{86}Sr$ and low $^{3}He/^{4}He$ ratios, and high $\Delta8/4$ and $\Delta7/4$ values (see *Hart (1984)* and Section 6.2.2 for definitions), whereas the latter has high $^{3}He/^{4}He$ ratios (>24R$_A$) and intermediate Sr, Nd and Pb isotopic ratios.

The post-erosional lavas have isotopic compositions which are distinct from those of the shield volcanics, implying that they have been derived from different mantle sources (*Wright & White, 1986*). The post-erosional isotopic compositions are produced by the mixing of the shield end-member with an 'enriched' post-erosional end member. The 'enriched' end-member may have originated from ancient recycled sediment, which has broadly similar isotopic characteristics to the post-erosional lavas: low $^{143}Nd/^{144}Nd$ and $^{206}Pb/^{204}Pb$, and high $^{207}Pb/^{204}Pb$ and $^{87}Sr/^{86}Sr$. A post-erosional source can be modelled as a mixture of about 1% recycled sediment with 99% depleted mantle. The compositional variation in the post-erosional lavas can be explained by varying the proportions of recycled sediment and depleted mantle end-

members. However, some of the variation may be due to heterogeneity of the recycled sediment. The post-erosional magmas originate by melting of a mixture of the shield source and up to 60% of the post-erosional source (*Wright & White, 1986*).

The subduction component may be hydrous or siliceous fluids that have been derived from the subducting slab and any sediments that have been carried down as the slab subducts. This component will therefore have the isotopic composition of a mixture between that of altered oceanic crust and Pacific sediments (Section 5.3.2). Isotopic data for Pacific pelagic and volcanogenic sediments (*Ben Othman et al., 1989; Pearce & Hergt unpubl. data*) are used as approximations of end-member isotopic compositions of this component. The Pb, Sr and Nd isotopic data (*Pearce and Hergt unpubl.*) are from DSDP sites 204 and 595, which are located approximately 100 and 1000km east of the Tonga trench respectively, in the western Pacific. These contain sediments which are likely to have similar composition to those of sediments that have been, or are being, subducted along the Tonga trench. Sediments from DSDP site 595 are zeolitic metalliferous pelagic clay of Mesozoic to Miocene age (Table 2.2). The sediment samples taken from the DSDP site 204 core are iron oxide-rich glass-shard silty clays, tuffaceous coarse sandstones of Quaternary to Oligocene-Early Miocene age, conglomerates of possibly Cretaceous age, and vitric tuffs of unknown age (Figure 2.7). Figure 2.7 shows a stratigraphic section of the DSDP site 204 core, giving the location of the samples in the core, the stratigraphy and age of the core.

The isotopic composition of altered oceanic crust is assumed to be similar to that of average Pacific MORB from the East Pacific Rise (*Hamelin et al., 1984; White et al., 1987; Ito et al., 1987*), but with an adjustment for the 87/86 ratio of Sr due to the interaction of this crust with seawater (*Hart & Staudigel, 1989;* Section 5.3.2). The trace element composition of the subduction component is estimated from those of the lavas from north Tonga, using the method of *Pearce et al. (1995a)* on Figure 4.12.

2.10 Radiometric dating of the ophiolite sections

Radiometric dating of the boninites from the 'Kallisto' 1982 cruise was carried out in collaboration with Prof. J.G. Mitchell at the University of Newcastle. The samples exhibit varying degrees of secondary alteration with zeolites, chlorite and smectite as the main alteration phases. It has been assumed that the samples chosen
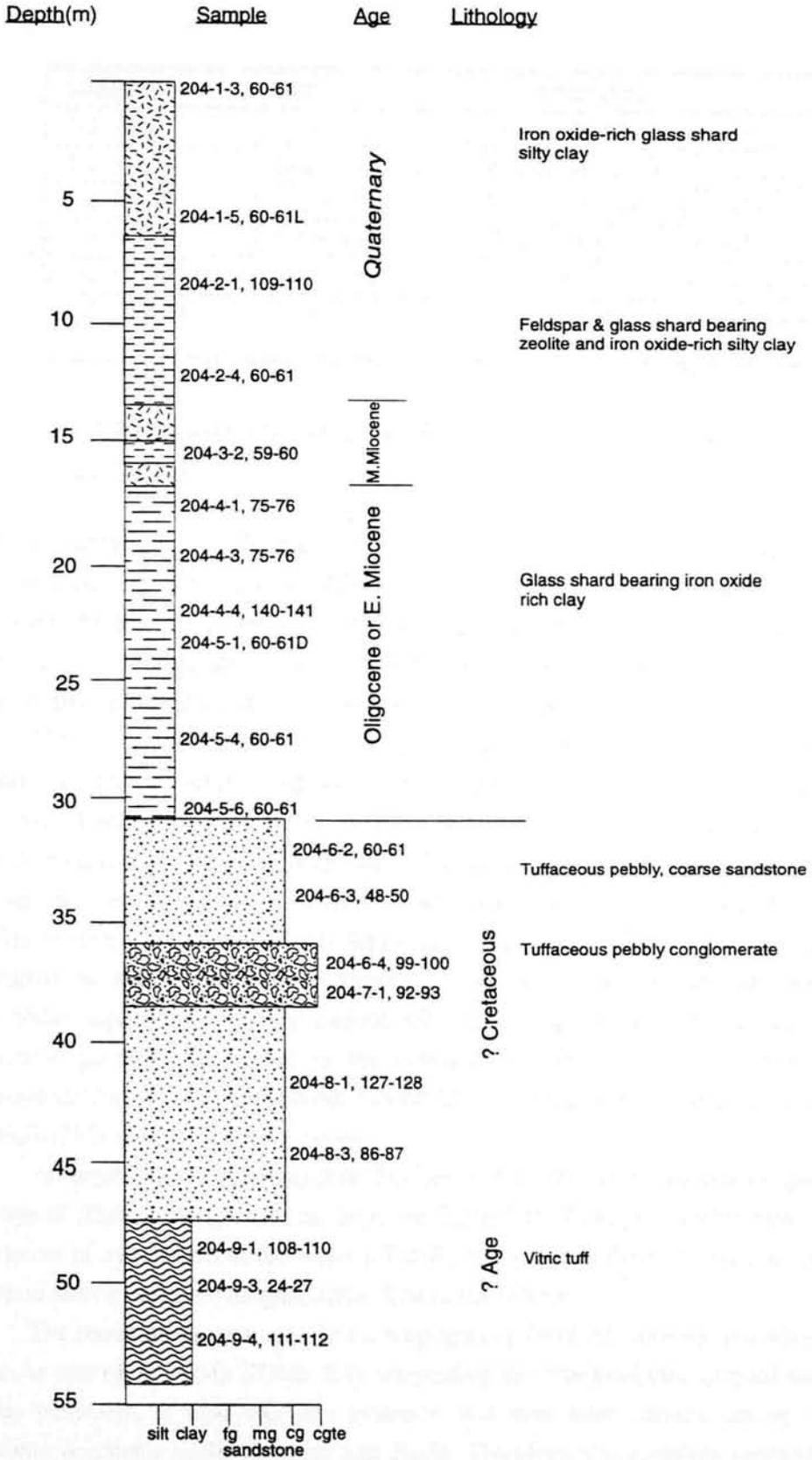
Figure 2.7: Stratigraphic log of the DSDP Site 204 core from the western Pacific, showing the depth and location of sediment samples, the age and the lithology.

33

Sample	Age	Sediment type
1-2, 42-47	Miocene	Zeolitic metalliferous pelagic clay
2-2, 47-53	Eocene/Oligocene	Zeolitic metalliferous pelagic clay
2-4, 36-41	Eocene/Oligocene	Zeolitic metalliferous pelagic clay
3-2, 94-100	Palaeocene	Zeolitic metalliferous pelagic clay
4-3, 90-96	Mesozoic	Zeolitic metalliferous pelagic clay
8-1, 110-115	Mesozoic	Zeolitic metalliferous pelagic clay with porcellanite

Table 2.2: Sediment samples from DSDP site 595 used for isotopic analysis.

have experienced a single alteration and vesicle-filling event only, following the methodology of *Mitchell et al. (1992).* The assumption is that the alteration was produced by the same heat source as the magmatic event and therefore that the two are almost contemporaneous. It is therefore likely that the K-Ar date of the samples has not been reset by a post-magmatic metamorphic event.

The K-Ar ages of the north Tongan boninites are shown in Table 2.3. The boninites from the 'western' ophiolite section (16-51/9 and 16-51/16) are older than the other boninites (16-26/1 and 16-26/2). A boninite from Station 21 (3-23) has a whole-rock K-Ar age of 1.40 ± 0.03 Ma (*T. Falloon pers. comm.*; Table 2.4). This may suggest that the older boninites erupted when the crust of the northern Lau Basin was under extension, before the development of the King's Triple Junction, which occurred at about 1.5Ma. The boninites from west of the section are younger ($<$1.5Ma) suggesting that they erupted after the development of the King's Triple Junction, possibly as a result of the northeast propagation of the Northern Lau Spreading Centre. A boninite from Station 23 (5-27) has a whole rock K-Ar age of 2.03 ± 0.11 Ma (*T. Falloon pers. comm.*).

An amphibole in a gabbro (Site 73) from the 'eastern' ophiolite section has a K-Ar age of 50 ± 9 Ma (*Vysotsky et al., in press*; Table 2.4). This age is within error of the initiation of subduction in the western Pacific and suggests the tholeiitic section was formed during early-arc magmatism in Tonga (Chapter 7).

The boninites are younger than a plagiogranite from the same section which has a K-Ar age of 13 ± 3 Ma (Table 2.4), suggesting that the boninites erupted onto an older basement. It also supports evidence that they were formed during recent tectonic processes in the northern Lau Basin. Therefore, the cumulate sequences of eastern and western sections are likely to form part of an older basement which has been present above the Tonga trench since the Miocene and Eocene, respectively.

This evidence assumes that the K-Ar ages of the gabbro and the plagiogranite from the eastern and western sections are representative of the ages of the ophiolite sequences excluding the lavas.

2.11 Dating of the lavas from Tafahi and Niuatoputapu

K-Ar ages of one lava from Tafahi and three lavas from Niuatoputapu are shown in Table 2.3. These ages suggest that Tafahi is older than Niuatoputapu. However, the Tafahi lavas show significant U-Th disequilibria, which indicates that they have ages of less than 350Ka (*S. Turner pers. comm.*). This is the time required for U-Th equilibrium to be reattained, after disequilibrium occurs as a result of addition of a slab-flux (high Th/U ratio). The estimated age of these lavas is 10-20Ka from the degree of this disequilibria. The lavas from Niuatoputapu show a much smaller degree of U-Th disequilibria, which indicates that the lower limit of their age is around 350Ka, whereas the upper limit is 2.10Ma from the K-Ar dating. The contrast in topography between Tafahi and Niuatoputapu may also be evidence for the differences in their ages: Tafahi has maintained its perfect volcanic cone (Plate 2.1), whereas the volcanic rocks of Niuatoputapu are only preserved along a narrow ridge (Figure 2.4), suggesting that much of its original topography may have eroded away. However, if much of the original volcano of Niuatoputapu was volcanic agglomerates, which are more favourably eroded than massive lava flows, then this may be more likely to be the reason why the volcanic deposits are not extensive on this island.

Sample	K_2O wt%	$^{40}Ar*$ $(10^{-5}mm^3g^{-1})$	Atmospheric content (%)	Age $(Ma\pm 1\sigma)$
North Tongan boninites				
Western dredge section				
16-51/9	0.281±0.002	2.40±0.67	97.5	2.54±0.74
16-51/16	0.273±0.002	2.80±0.60	96.0	3.09±0.48
West				
16-26/1	0.295±0.002	0.61±0.56	97.6	0.58±0.20
16-26/2	0.316±0.002	0.95±0.41	97.4	0.89±0.04
Tafahi				
TAF31/1	0.246±0.004	5.62±0.60	95.0	7.10±0.80
Niuatoputapu				
NTT9	0.424±0.003	2.85±0.58	95.9	2.10±0.40
NTT25/2	0.592±0.005	5.30±0.72	94.6	2.80±0.40
NTT26/1	0.528±0.009	2.78±0.63	96.1	1.60±0.40

Table 2.3: K-Ar radiometric ages of the north Tongan boninites and lavas from Tafahi and Niuatoputapu. Data from J. Mitchell (pers. comm.).

Sample	K-Ar Age Ma	Whole rock/mineral	Source of data
'Kallisto' 1982 cruise **Western section** Plagiogranite site48	13±3	Biotite	Vysotsky *et al.*
Eastern section Gabbro site73	50±9	Amphibole	Vysotsky *et al.*
'Natsushima' 1984 Boninite Stn 21, 3-23 Boninite Stn 23, 5-27	1.40±0.03 2.03±0.11	whole rock whole rock	T. Falloon T. Falloon

Table 2.4: K-Ar radiometric ages of the ophiolite sections from the 'Kallisto' 1982 cruise and boninites from the 'Natsushima' 1984 cruise.

CHAPTER 3

Petrography and mineral chemistry

3.1 Introduction

The petrography of the north Tongan boninites and tholeiites, lavas from
Tafahi, Niuatoputapu and the Northern Lau Spreading Centre are described in this
chapter. The temperatures of crystallisation from two-pyroxene thermometry of
pyroxenes from the north Tongan boninites and the lavas from Tafahi are also
estimated. The temperatures of the primary magmas are then estimated by
extrapolating from the crystallisation temperatures of the pyroxenes from the most
primitive lavas. Evidence for the nature of their sources is then derived from the
estimated temperatures of their primary magmas.

3.2 Primary igneous textures

Cox *et al.* (*1979*) recognise two main stages of crystallisation in lavas, the
intratelluric stage and the *quench* stage. Phenocrysts from the intratelluric stage form
as the magma slowly cools in either a magma chamber, or a conduit, prior to eruption
at the surface. These phenocrysts are typically larger than those of the quench stage.
In the quench stage, phenocrysts form during and after eruption of the lava, as it
rapidly cools at the surface. The north Tongan boninites and the lavas from Tafahi
contain phenocrysts that formed in both stages of crystallisation, but the north Tongan
tholeiites, the lavas from Niuatoputapu and the Northern Lau Spreading Centre only
contain quench stage phenocrysts.

3.3 Tafahi

The high-Mg basaltic-andesitic lavas from Tafahi have *porphyritic* or
glomeroporphyrytic textures, with large phenocrysts of plagioclase and two
pyroxenes, in a fine- to moderately coarse-grained 'quench' felsitic groundmass (Plate

sample locality mineral	TAF6 rim plag1	TAF6 core plag1	TAF6 rim plag3	TAF6 core plag3	TAF6 rim plag5	TAF6 core plag5	TAF44/3 rim plag2	TAF44/3 core plag2	TAF18/12 rim plag2	TAF18/12 core plag2
SiO_2	45.37	44.74	47.14	45.09	44.48	45.25	46.49	46.17	45.85	45.37
TiO_2	0.00	0.00	0.00	0.00	0.00	0.00	0.00	0.00	0.00	0.00
Cr_2O_3	0.06	0.00	0.00	0.00	0.00	0.10	0.00	0.00	0.14	0.00
Al_2O_3	32.93	33.66	33.19	34.58	34.92	34.80	33.37	34.02	33.05	33.80
FeO	0.76	0.68	1.10	0.86	0.65	0.76	0.97	1.00	0.83	0.72
MnO	0.00	0.00	0.00	0.00	0.00	0.00	0.00	0.00	0.00	0.00
MgO	0.34	0.43	0.43	0.34	0.39	0.41	0.48	0.33	0.19	0.20
CaO	17.69	18.26	17.69	18.82	19.33	18.96	17.84	18.63	17.86	18.57
Na_2O	1.32	0.95	1.62	0.81	0.54	0.89	1.56	1.13	1.20	0.93
K_2O	0.00	0.00	0.00	0.00	0.00	0.00	0.00	0.00	0.00	0.00
Total	98.50	98.73	101.16	100.50	100.31	101.17	100.70	101.27	99.11	99.60
An%	88.2	91.4	85.8	92.8	95.2	92.2	86.3	90.1	89.2	91.7

sample locality mineral	TAF43/6 core plag3	TAF43/6 rim plag3	TAF43/6 core plag4	TAF43/6 rim plag4	TAF43/6 core plag5	TAF43/6 rim plag5	TAF45/7 core plag1	TAF45/7 rim plag1	TAF45/7 core plag3	TAF45/7 rim plag3
SiO_2	45.77	45.04	46.84	45.70	45.74	45.30	44.56	46.65	44.81	45.89
TiO_2	0.00	0.00	0.09	0.00	0.00	0.00	0.00	0.12	0.00	0.00
Cr_2O_3	0.00	0.00	0.09	0.10	0.00	0.00	0.00	0.00	0.11	0.00
Al_2O_3	33.34	34.28	31.50	32.97	33.05	33.55	33.46	31.52	33.80	33.41
FeO	0.80	0.76	2.00	1.09	0.82	0.87	0.83	1.73	0.74	1.03
MnO	0.00	0.00	0.00	0.00	0.10	0.00	0.00	0.00	0.00	0.00
MgO	0.25	0.21	0.63	0.27	0.22	0.27	0.24	0.58	0.39	0.21
CaO	18.07	18.72	17.18	18.06	17.72	18.35	18.27	16.96	18.19	18.07
Na_2O	1.13	0.92	1.40	1.21	1.09	1.00	1.08	1.41	1.04	1.28
K_2O	0.00	0.00	0.05	0.00	0.00	0.00	0.00	0.03	0.00	0.00
Total	99.35	99.93	99.80	99.39	98.73	99.34	98.44	99.03	99.09	99.89
An%	89.9	91.8	87.2	89.2	90.0	91.0	90.4	86.9	90.6	88.7

Table 3.1: *Representative data set from the microprobe analyses of the plagioclase phenocrysts of the Tafahi lavas.*
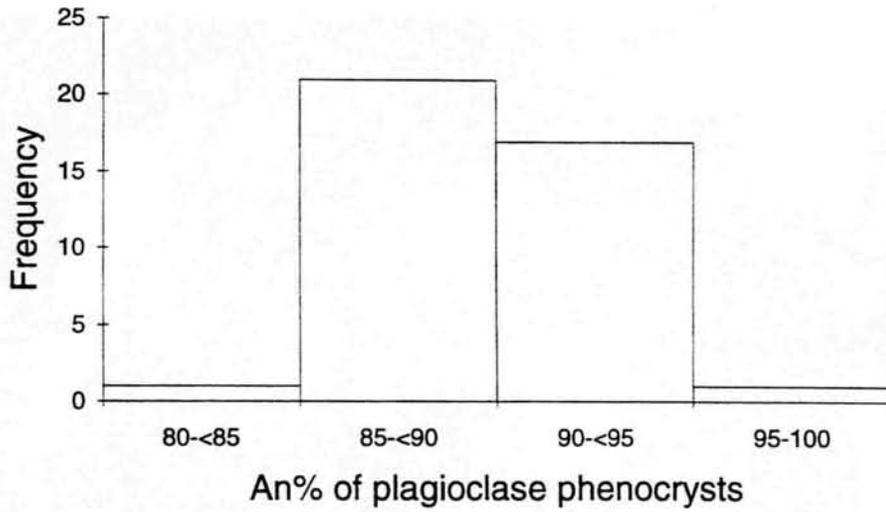
Figure 3.1: Histogram showing the frequency distribution of the compositions of the plagioclase phenocrysts where An % = Ca/(Ca+Na)*100.
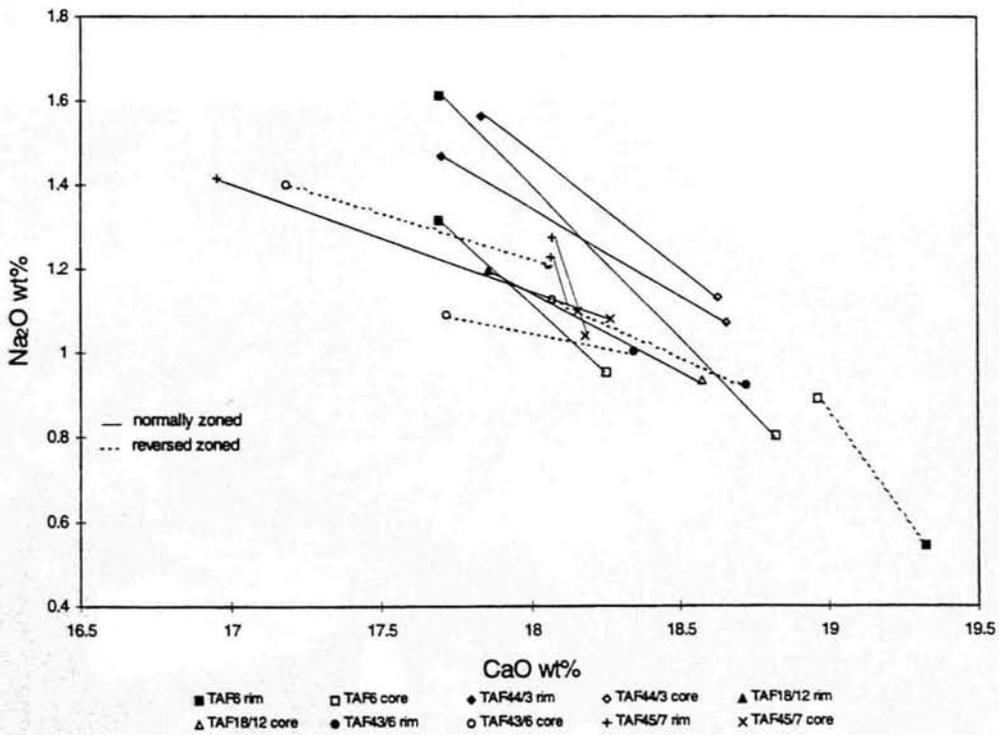
Figure 3.2: Plot of CaO against Na$_2$O contents of the cores and rims of the plagioclase phenocrysts of the Tafahi lavas, showing that most of the rims are more sodic than the corresponding cores.

3.3.1.2 Olivine

Olivine occurs as a minor intratelluric phase in two of the Tafahi lavas. The phenocrysts are subhedral to resorbed and are altered to iddingsite. The olivines have forsterite contents between Fo_{76} and Fo_{85} which are less magnesian than those in the north Tongan boninites (Fo_{78} to Fo_{91}). Plates 3.5 and Plate 3.6 show a subhedral phenocryst of olivine in a vesicular plagioclase rich lava in plane- and cross-polarised light. Plate 3.6 highlights its subhedral crystal habit and alteration to iddingsite along cracks and around the rim. Table 3.2 contains microprobe analyses of olivine phenocrysts from the Tafahi lavas.

sample	TAF6	TAF23	TAF23	TAF23	TAF43/6	TAF43/6	TAF43/6	TAF43/6
locality	core	core	core	core	core	core	core	core
mineral	ol1	ol1	ol2	ol3	ol1	ol2	ol3	ol4
SiO_2	39.70	38.96	39.72	38.87	39.67	40.27	39.93	39.20
TiO_2	0.00	0.00	0.00	0.00	0.00	0.00	0.00	0.00
Cr_2O_3	0.00	0.00	0.00	0.00	0.00	0.19	0.11	0.00
Al_2O_3	0.00	0.00	0.00	0.00	0.00	0.00	0.00	0.00
FeO	16.18	20.47	20.61	22.08	14.22	13.87	17.56	20.20
MnO	0.25	0.00	0.00	0.00	0.00	0.00	0.00	0.00
MgO	43.93	40.82	40.96	39.04	44.75	45.11	42.54	40.29
CaO	0.20	0.26	0.24	0.24	0.22	0.28	0.21	0.25
Na_2O	0.59	0.46	0.34	0.54	0.36	0.38	0.35	0.46
K_2O	0.00	0.00	0.00	0.00	0.00	0.00	0.00	0.00
Total	100.84	100.97	101.87	100.76	99.21	100.10	100.70	100.40
Fo%	82.9	78.0	78.0	75.3	84.9	85.3	81.2	78.1

Table 3.2: Microprobe analyses of olivine phenocrysts in the Tafahi lavas.

3.3.1.3 Pyroxene

Both clinopyroxene and orthopyroxene are present as intratelluric phases, but only clinopyroxene is present as a quench phase. The lavas may contain up to 10% clinopyroxene or orthopyroxene, but some of them may only be present as a minor phenocryst phase. Clinopyroxene occurs either as a megacryst or as tabular (Plate 3.7) or resorbed phenocrysts, or as part of large resorbed glomerocrysts with orthopyroxenes and plagioclases (Plate 3.8). Orthopyroxene is a minor phenocryst

phase in the lavas compared with clinopyroxene and plagioclase, occurring either in glomerocrysts, or as singular subhedral phenocrysts (Plate 3.7), or occasionally in radiating stellate clusters (Plate 3.9). Some of the orthopyroxenes have alteration rims of clinopyroxene (Plate 3.10) suggesting that a reaction has taken place with the host groundmass.

Table 3.3 is a representative selection of microprobe data of the cores and rims of pyroxene phenocrysts from the Tafahi lavas, taken from Appendix 2.

sample	TAF23	TAF23	TAF23	TAF23	TAF18/12	TAF18/12	TAF18/12	TAF18/12	TAF45/7	TAF45/7
locality	rim	core	rim	core	core	rim	core	rim	core	rim
mineral	opx1	opx1	opx4	opx4	opx1	opx1	opx2	opx2	opx4	opx4
SiO₂	54.45	54.88	53.76	54.58	53.63	54.02	54.39	54.83	53.59	53.76
TiO₂	0.18	0.08	0.12	0.08	0.23	0.14	0.00	0.18	0.16	0.10
Cr₂O₃	0.14	0.16	0.15	0.11	0.00	0.00	0.00	0.00	0.00	0.00
Al₂O₃	1.75	1.88	1.82	1.79	1.44	1.56	1.26	1.46	1.52	1.39
FeO	15.34	13.75	14.85	13.56	15.62	14.37	15.77	15.58	17.95	17.48
MnO	0.00	0.00	0.14	0.00	0.34	0.34	0.42	0.38	0.49	0.43
MgO	26.90	28.11	26.64	27.80	25.69	26.76	26.61	26.73	24.44	25.08
CaO	2.11	2.12	2.26	2.00	2.22	2.16	2.26	2.29	2.13	2.08
Na₂O	0.14	0.29	0.31	0.39	0.30	0.37	0.27	0.20	0.41	0.43
K₂O	0.05	0.06	0.00	0.00	0.00	0.00	0.00	0.00	0.00	0.00
total	101.25	101.34	100.03	100.31	99.47	99.72	100.97	101.65	100.69	100.74
Mg#	0.76	0.78	0.76	0.79	0.75	0.77	0.75	0.75	0.71	0.72

sample	TAF6	TAF6	TAF31/1	TAF31/1	TAF44/3	TAF44/3	TAF43/6	TAF43/6	TAF45/7	TAF45/7
locality	core	rim	core	rim	core	rim	core	rim	core	rim
mineral	cpx4	cpx4	cpx1	cpx1	cpx2	cpx2	cpx3	cpx3	cpx1	cpx1
SiO₂	52.50	53.03	52.13	52.69	53.62	52.97	52.63	52.63	51.32	52.59
TiO₂	0.10	0.00	0.26	0.20	0.16	0.12	0.25	0.11	0.16	0.23
Cr₂O₃	0.09	0.00	0.10	0.13	0.27	0.25	0.16	0.15	0.32	0.21
Al₂O₃	2.37	1.75	2.12	1.68	1.91	2.46	2.19	1.75	2.94	2.41
FeO	8.67	10.45	10.69	11.01	8.47	10.08	9.07	9.74	7.31	10.21
MnO	0.15	0.15	0.35	0.47	0.00	0.00	0.00	0.10	0.16	0.20
MgO	16.81	17.14	16.13	15.95	17.54	17.91	17.59	17.46	16.34	16.19
CaO	19.26	17.60	18.23	18.43	19.18	16.59	17.81	17.41	20.67	18.90
Na₂O	0.46	0.40	0.55	0.50	0.30	0.36	0.37	0.33	0.39	0.42
K₂O	0.00	0.00	0.00	0.00	0.00	0.00	0.00	0.00	0.00	0.00
total	100.40	100.52	100.57	101.06	101.45	100.74	100.08	99.67	99.63	101.38
Mg#	0.78	0.75	0.73	0.72	0.79	0.76	0.78	0.76	0.80	0.74

Table 3.3: Microprobe analyses of pyroxene phenocrysts of the Tafahi lavas.

Figure 3.3 is a diagram of the CaO and FeO* contents against Mg# of clinopyroxene phenocrysts, where FeO* is the total iron as Fe^{II} and Mg# is Mg/(Mg+Fe) at the point of microprobe analysis. Figure 3.3(b) shows that the rims of the clinopyroxene phenocrysts have higher iron contents and lower magnesium contents than the cores. However, the CaO contents of the cores are more variable compared to those of the rims (Figure 3.3(a)). Some cores have a higher CaO content than their corresponding rims, whereas others have a lower CaO content.

The variation in the FeO* and CaO contents between the cores and rims of the clinopyroxene phenocrysts suggests that there is some zoning. Zoning occurs when the phenocrysts do not equilibrate with their host liquid during cooling. The central core compositions of the phenocrysts correspond to the compositions at the initial temperature of crystallisation. As the phenocryst grows, these compositions are progressively overgrown with lower-temperature compositions due to the cooling of the host magma (*Cox et al., 1979*). The decrease in temperature of the host liquid also causes a decrease in FeO* content from core to rim of the clinopyroxene phenocrysts, and is similarly a result of disequilibrium between the phenocrysts and the host liquid. The resorbed nature of the some of the clinopyroxene phenocrysts also suggests that they are not in equilibrium.

Figure 3.4 is a plot of the FeO* content against Mg# of the orthopyroxene phenocrysts at the point of microprobe analysis. This plot shows that the cores of the phenocrysts from all the samples, except three from TAF23, have lower Mg#'s and higher FeO* contents than their corresponding rims. This suggests that the orthopyroxene phenocrysts have some zoning. The subhedral crystal habit and the nature of the reaction rims of the orthopyroxene phenocrysts, along with the zoning, all suggest that they are not in equilibrium with their host liquid.

3.3.1.4 Agglutinated agglomerophyric clusters

The glomerocrysts consist of euhedral to subhedral micro- to macro-phenocrysts of clinopyroxene and orthopyroxene with some plagioclase, which have grown together as part of larger clusters, that may be up to 3mm in diameter. In some lavas, orthopyroxene forms the core to a glomerocryst of the predominantly clinopyroxene phenocrysts (Plate 3.8). These clusters are rounded and the outer surface is resorbed. Glomerocrysts have been noted in other high-Mg lavas from north Tonga (*Falloon et al., 1989*; Section 3.5). The glomerocrysts are likely to have originated from the sides of the magma chamber from where they were ripped off as the magma ascended towards the earth's surface.

Clinopyroxene core-rim compositions of the Tafahi lavas

■TAF6 rim □TAF6 core ◆TAF44/3 rim ◇TAF44/3 core ▲TAF35/3 rim △TAF35/3 core ●TAF18/12 rim
○TAF18/12 core ✕TAF31/1 rim ✕TAF31/1 core +TAF43/6 rim −TAF43/6 core ▤TAF45/7 rim ✕TAF45/7 core
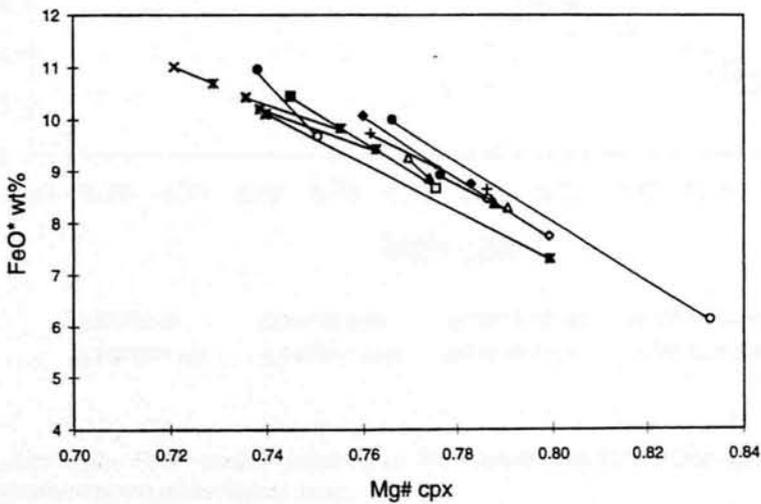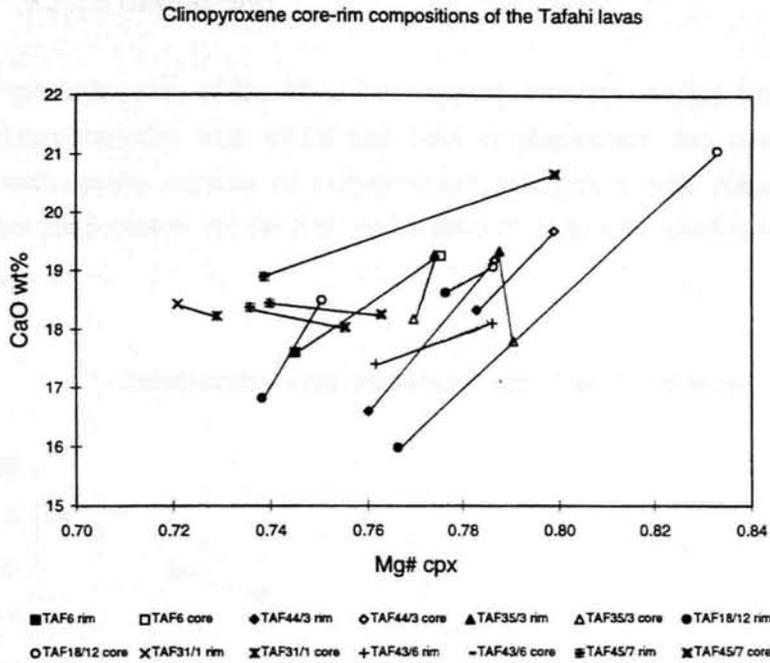
Figure 3.3 : CaO and FeO* vs Mg# of the clinopyroxenes of the lavas from Tafahi. (a) the rims of the clino-pyroxenes have variable CaO contents compared with their corresponding cores. (b) the rims of the clino-pyroxenes have higher iron contents and lower magnesian contents than the cores. FeO* is the total iron as Fe^II and Mg# is Mg/(Mg+Fe). This variation suggests that zoning has occurred in the clinopyroxene phenocrysts, and that they were, therefore, not in equilibrium with their host liquids during growth.

3.3.1.5 Groundmass

The groundmasses of the lavas have quench textures varying between finer-grained glassy varieties with <0.05 mm laths of plagioclase, and coarser-grained varieties with stubby crystals of clinopyroxene intergrown with plagioclase. The groundmass plagioclases and the rims of intratelluric ones have similar compositions (An_{85}-An_{95}).

Orthopyroxene core-rim compositions of the Tafahi lavas
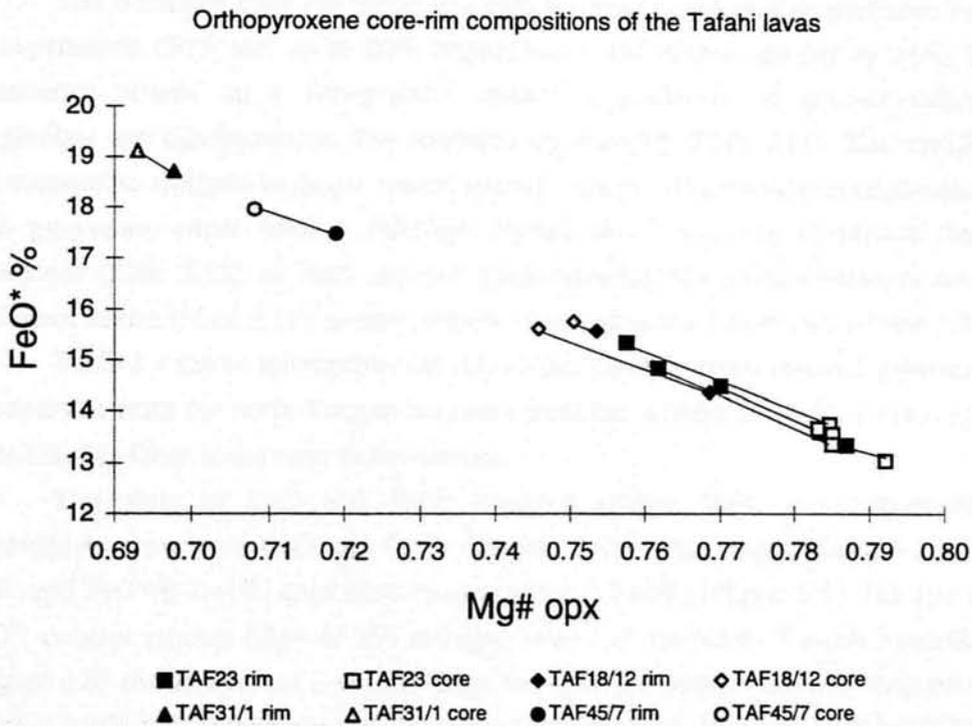
Figure 3.4: Plot of the FeO* content (total Fe as Fe^{II}) against the Mg# of the cores and rims of orthopyroxene phenocrysts of the Tafahi lavas.

3.4 Niuatoputapu

Volcanic debris-flows, massive lava-flows and flow-banded lavas are exposed on the volcanic ridge of Niuatoputapu (Section 2.4). The massive lava flows are mostly aphyric, but may contain a few microphenocrysts of plagioclase and clinopyroxene. The basaltic groundmass has been partially altered to clay minerals. The petrography of the clasts in the volcanic debris-flows varies (Table 2.1) and has been briefly described in Section 2.4.1. The flow-banded lavas have banding on a

0.5cm to cm scale. They do not contain any phenocrysts but do contain a few lithic clasts (up to 1cm in diameter).

3.5 The western ophiolite section from the Kallisto 1982 cruise

3.5.1 The north Tongan boninites

The boninites from the western ophiolite section contain clinopyroxene and orthopyroxene (10% and up to 20% respectively), and plagioclase (up to 15%) as phenocryst phases, in a fine-grained 'quench' groundmass of microcrystalline plagioclase and clinopyroxene. The boninites are vesicular (Plate 3.11). The vesicles are rounded to elongate in shape, where several adjacent vesicles have amalgamated. The pyroxenes either have a euhedral crystal-habit containing numerous fluid inclusions (Plate 3.12), or form rounded glomeroporphyritic clusters between 1mm and 4mm in size (Plate 3.11), similar to those observed in the Tafahi lavas (Plate 3.8).

Table 3.4 shows microprobe data of olivine, clinopyroxene and orthopyroxene phenocrysts from the north Tongan boninites from the western ophiolite section and from site 26, 40km to the west of the section.

The plots of CaO and FeO* contents against Mg# of clinopyroxene phenocrysts show their CaO and FeO* contents do not vary much (CaO:19.3-20.6 wt%, and FeO*:6-7 wt%, apart from one sample at 4.2 wt%) (Figure 3.5). The plot of FeO* content against Mg# of the orthopyroxenes of the north Tongan boninites (Figure 3.6) shows that the boninites from the ophiolite section are less magnesian (Mg# = 0.805-0.845) than most of those from the west (site 26; Mg# = 0.879-0.899). The orthopyroxenes from site 26 that are less magnesian are likely to be late-stage phenocrysts which formed after the host magma had cooled from its initial temperature.

3.5.2 The 'high level' plutonic sequence

The samples dredged from the 'high level' plutonic sequence are gabbro norites, tonalites, trondhjemites and a plagiogranite. Plate 3.13 shows a tonalite from this sequence which contains 20% quartz, 5% alkali feldspar, 70% plagioclase, 4% epidote and 1% chlorite. In places, the alkali feldspar and quartz have intergrown to give a granophyric texture. The tonalite also contains minor epidote with chlorite, which are the products of hydrothermal alteration. The plagioclase has undergone sericitic alteration during this hydrothermal event.
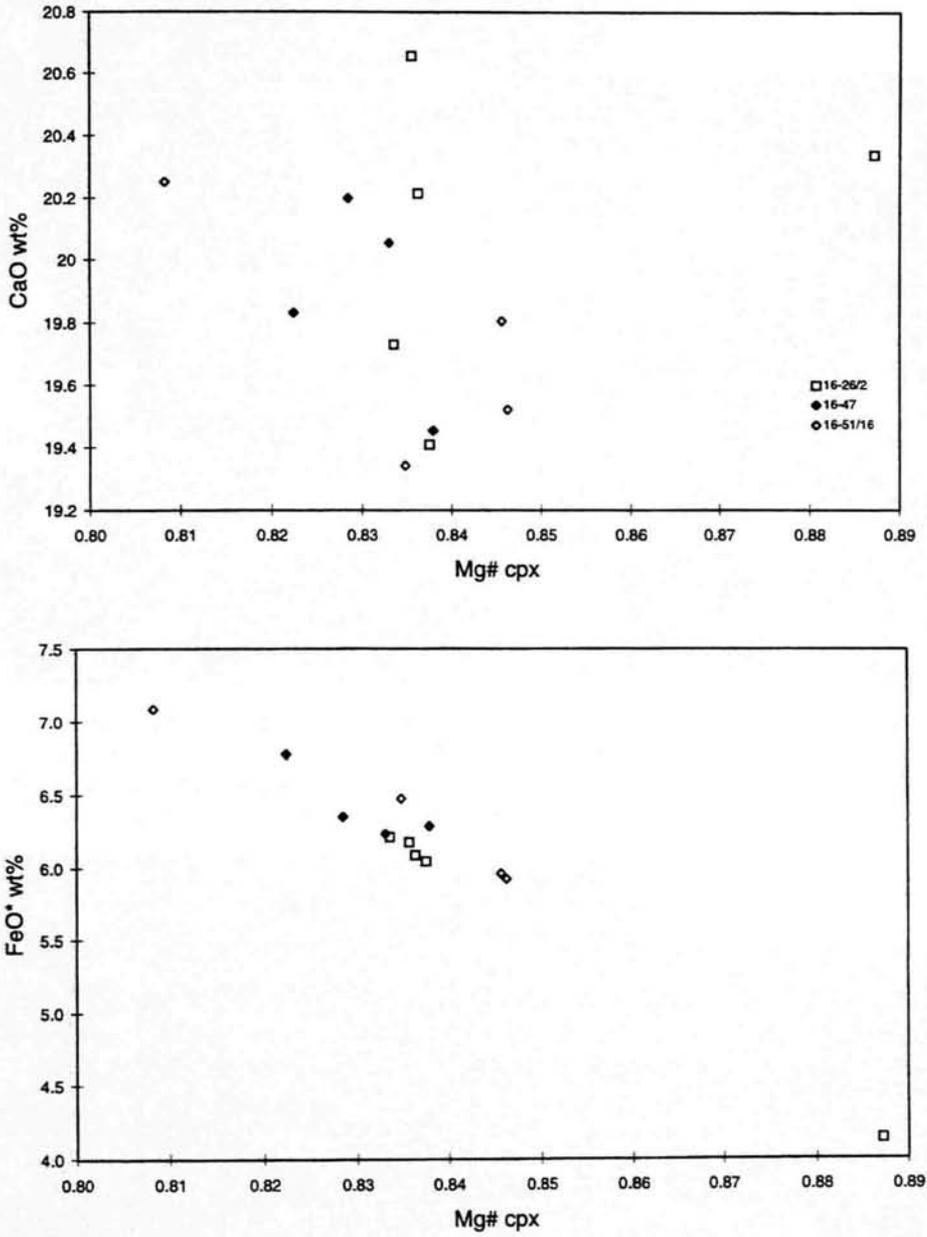
Figure 3.5 : *CaO and FeO* contents vs Mg# of the clinopyroxene phenocrysts of the north Tongan boninites. These diagrams show that the CaO and FeO* contents of the clinopyroxenes vary between 19.3-20.7wt% and 6-7wt%, respectively.*

sample	16-26/1	16-26/1	16-26/1	16-26/1	16-26/1	16-26/1	16-26/1	16-26/2	16-26/2	16-26/2	16-26/2	16-26/2
locality	core	core	rim	core	core	core	core	core	core	core	core	core
mineral	ol1	ol2	ol2	ol3	ol4	ol5	ol6	ol1	ol2	ol3	ol4	ol5
SiO_2	40.92	41.82	40.78	41.43	40.38	41.72	41.53	41.01	40.34	41.32	40.51	40.38
TiO_2	0.00	0.00	0.00	0.11	0.08	0.00	0.00	0.00	0.00	0.00	0.00	0.07
Cr_2O_3	0.13	0.00	0.00	0.10	0.00	0.00	0.00	0.00	0.05	0.00	0.12	0.08
Al_2O_3	0.00	0.00	0.00	0.25	0.00	0.00	0.00	0.25	0.07	0.21	0.24	0.00
FeO	8.53	9.10	10.63	9.25	8.48	8.92	8.53	9.41	9.63	12.31	9.85	10.02
MnO	0.00	0.00	0.00	0.00	0.00	0.15	0.13	0.20	0.17	0.17	0.06	0.22
MgO	48.92	50.01	48.54	49.45	48.89	50.52	50.02	49.68	47.51	46.20	47.64	48.16
CaO	0.17	0.21	0.21	0.10	0.11	0.18	0.14	0.09	0.15	0.28	0.17	0.14
Na_2O	0.41	0.34	0.32	0.33	0.32	0.42	0.34	0.14	0.19	0.31	0.20	0.70
K_2O	0.00	0.00	0.00	0.00	0.00	0.00	0.00	0.07	0.04	0.00	0.01	0.03
Total	99.08	101.47	100.48	101.00	98.26	101.91	100.70	101.14	98.46	101.13	99.13	100.01
Fo%	91.1	90.7	89.1	90.5	91.1	91.0	91.3	90.4	89.8	87.0	89.6	89.5

sample	16-26/2	16-26/2	16-47	16-47
locality	core	core	core	core
mineral	ol6	ol7	ol1	ol2
SiO_2	40.86	40.41	41.19	40.89
TiO_2	0.05	0.01	0.03	0.07
Cr_2O_3	0.00	0.00	0.04	0.10
Al_2O_3	0.13	0.46	0.20	0.28
FeO	9.04	10.28	9.19	9.64
MnO	0.26	0.29	0.04	0.08
MgO	48.18	46.44	49.73	49.69
CaO	0.20	0.35	0.00	0.06
Na_2O	0.71	0.45	0.54	0.00
K_2O	0.00	0.05	0.02	0.00
Total	99.42	98.93	101.28	100.90
Fo%	90.5	89.0	90.6	90.2

sample	16-47	16-47	16-47	16-47	16-51/16	16-51/16	16-51/16	16-51/16	16-51/16	16-51/16	16-51/16	16-51/16
locality	core	core	core	core	core	rim	core	core	rim	core	core	core
mineral	opx1	opx2	opx3	opx4	opx1	opx1	opx2	opx3	opx3	opx4	opx5	opx7
SiO_2	55.83	56.51	56.18	55.61	56.20	56.66	56.57	56.30	56.29	55.60	56.45	56.32
TiO_2	0.13	0.00	0.07	0.03	0.00	0.00	0.13	0.00	0.00	0.00	0.00	0.08
Cr_2O_3	0.25	0.17	0.28	0.18	0.50	0.28	0.21	0.50	0.35	0.41	0.32	0.32
Al_2O_3	1.29	1.06	1.55	1.42	1.14	0.75	0.87	1.26	0.87	1.22	0.62	0.70
FeO	12.01	11.32	10.64	12.23	10.25	10.10	10.23	10.29	10.28	10.30	9.77	10.37
MnO	0.23	0.31	0.13	0.22	0.20	0.30	0.30	0.18	0.26	0.31	0.21	0.31
MgO	28.55	29.73	30.28	28.38	30.60	30.67	30.63	30.30	30.14	30.29	30.64	30.53
CaO	2.32	2.14	1.64	2.14	2.26	2.14	2.18	2.15	2.29	2.24	2.27	2.25
Na_2O	0.00	0.11	0.17	0.00	0.34	0.19	0.28	0.29	0.13	0.19	0.26	0.40
K_2O	0.00	0.02	0.00	0.06	0.00	0.00	0.00	0.00	0.00	0.00	0.00	0.00
Total	100.77	101.44	100.95	100.29	101.47	101.08	101.39	101.27	100.61	100.57	100.53	101.28

sample	16-47	16-47	16-47	16-51/16	16-51/16	16-51/16	16-51/16
locality	core	core	core	core	core	core	core
mineral	cpx1	cpx2	cpx3	cpx1	cpx2	cpx3	cpx4
SiO_2	53.34	54.05	53.19	53.14	52.36	53.49	53.20
TiO_2	0.06	0.11	0.16	0.00	0.00	0.10	0.09
Cr_2O_3	0.34	0.08	0.30	0.83	0.50	0.67	0.62
Al_2O_3	1.91	1.87	2.51	2.50	3.07	1.69	1.49
FeO	6.77	6.23	6.35	6.47	7.08	5.96	5.92
MnO	0.34	0.23	0.21	0.15	0.18	0.11	0.18
MgO	17.61	17.47	17.21	18.37	16.76	18.31	18.28
CaO	19.83	20.05	20.20	19.34	20.25	19.80	19.52
Na_2O	0.10	0.22	0.11	0.23	0.42	0.34	0.27
K_2O	0.06	0.05	0.08	0.00	0.00	0.00	0.00
Total	100.35	100.36	100.43	101.03	100.63	100.48	99.57

Table 3.4 : *Microprobe analyses of olivines and pyroxenes from the north Tongan boninites.*

55

sample locality mineral	16-26/1 need opx1	16-26/1 core opx2	16-26/2 core opx1	16-26/2 core opx2	16-26/2 core opx3	16-26/2 core opx4	16-26/2 core cpx1	16-26/2 core cpx2	16-26/2 core cpx3	16-26/2 core cpx4	16-26/2 core cpx5
SiO_2	56.84	57.13	55.70	54.52	55.92	55.25	53.41	52.85	52.61	52.10	53.18
TiO_2	0.00	0.08	0.05	0.09	0.15	0.09	0.00	0.01	0.15	0.09	0.00
Cr_2O_3	0.56	0.37	0.30	0.43	0.34	0.21	0.55	0.61	0.54	0.66	0.78
Al_2O_3	0.58	0.95	1.80	1.50	1.68	1.29	2.28	2.53	2.33	1.95	1.37
FeO	7.47	7.88	10.89	10.12	10.22	10.99	6.18	6.21	6.09	6.04	4.13
MnO	0.00	0.00	0.29	0.43	0.36	0.27	0.22	0.06	0.00	0.24	0.06
MgO	32.73	32.36	29.36	29.30	29.69	29.03	17.65	17.47	17.47	17.49	18.25
CaO	1.60	1.65	2.25	2.17	2.32	2.10	20.66	19.73	20.22	19.41	20.34
Na_2O	0.25	0.38	0.09	0.22	0.34	0.05	0.17	0.14	0.24	0.23	0.31
K_2O	0.00	0.00	0.00	0.00	0.00	0.02	0.00	0.05	0.00	0.00	0.00
total	100.04	100.81	100.84	98.79	101.02	99.60	101.11	99.77	99.84	98.25	98.49

Table 3.4 cont.: Microprobe analyses of clinopyroxene and orthopyroxene phenocrysts from the north Tongan boninites.
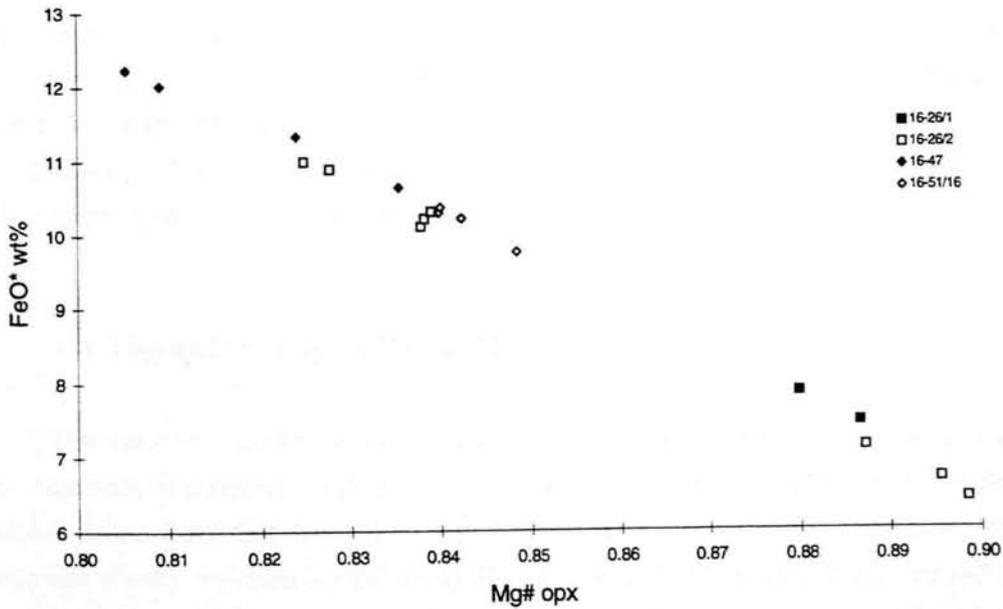
Figure 3.6: Plot of Mg# against FeO content where FeO*= total iron as Fe[II] of the orthopyroxene phenocrysts of the north Tongan boninites.*

The plagiogranite is composed of microcrystalline quartz (30%), alkali feldspar (20%), plagioclase feldspar (45%) and 5% calcite and hematite (Plate 3.14).

3.5.3 The cumulate sequence

The cumulate sequence lies stratigraphically below the plutonic sequence and contains cumulate ultramafics such as pyroxenites, and gabbros (Plate 3.15(a)). The gabbros have classic cumulate textures in which the olivine (<5%), clinopyroxene (up to 40%) and plagioclase (up to 60%) are closely intergrown (Plate 3.15). Plate 3.15(b) shows the same section as Plate 3.15(a) in plane polarised light, highlighting the high-relief olivine crystals, which are altered to iron-titanium oxides along cracks, and the slightly pleochroic hornblende phenocrysts which have strong cleavage planes at 60°.

3.5.4 The tectonised harzburgites

The tectonised harzburgites contain olivine and orthopyroxene which have been almost completely replaced by serpentine. Plate 3.16 shows olivine phenocrysts that have been 80% replaced by serpentine, but orthopyroxene, which is more resistant to serpentinisation, and is better preserved. The harzburgites contain up to 70% olivine and 30% orthopyroxene, but very little clinopyroxene (<5%). The original fabric of the harzburgite has been destroyed by the serpentinisation and by shearing, and only relic phenocrysts of orthopyroxene and olivine remain from the original rock.

3.6 The eastern ophiolite section

The eastern ophiolite section contains similar rocks to the western one. These are cumulate ultramafics and gabbros, tonalites from the plutonic sequence and diabase dykes, but it contains tholeiitic lavas rather than boninitic lavas. The tholeiitic lavas are wholly replaced by clay minerals and iron-titanium oxides, but some relict quench textures have been retained after alteration (Plate 3.17). Originally, these are likely to have been pyroxene phenocrysts. Similar textures have been observed in pyroxenes from Zone 2 and Zone 3 basalts form the margins of pillow lavas from Leg 83 of DSDP site 504B, from close to the Costa Rica Rift (*Kempton, 1985*).

The cumulate ultramafics and gabbros have cumulate textures. The gabbros contain up to 15% olivine, 35% clinopyroxene and 50% plagioclase. They contain

very little secondary amphibole, unlike the cumulate gabbros from the western section. The tonalites contain up to 70% plagioclase, 20% quartz, 5% alkali feldspar, 3% Fe-Ti oxides and 2% chlorite. The alkali feldspars have been partially replaced by clay minerals.

3.7 Site 26 from the Kallisto 1982 cruise

Boninites were dredged from site 26 of the 'Kallisto' 1982 cruise, which is located 40km west of the western ophiolite section (Figure 2.1(b)). This site had a similar location to Station 21 and 22 of the 'Natsushima' 1984 cruise (Section 2.5). These boninites are very phenocryst-rich compared with those from the western ophiolite section (Plate 3.18), containing up to 15% more olivine and 6% orthopyroxene and 1-5% clinopyroxene, but very little plagioclase. The olivine phenocrysts are up to 2mm in length and are in disequilibrium with their surrounding host liquid as they have complex resorbed boundaries (Plate 3.18). These phenocrysts are very magnesian, with forsterite contents between Fo_{88} and Fo_{91}. The groundmass is glassy to microcrystalline, suggesting that the rock quenched quickly.

Table 3.4 presents microprobe data of olivine, clinopyroxene and orthopyroxene phenocrysts of these boninites. These boninites are more magnesian than those from the western ophiolite section, which is reflected in the higher Mg#'s and lower FeO* contents of their orthopyroxene phenocrysts (Figure 3.6).

3.8 The Northern Lau Spreading Centre

The lavas from the Northern Lau Spreading Centre are vesicular, and contain olivine (<5%), plagioclase (12-15%) and clinopyroxene (<10%) phenocrysts. The plagioclases (0.25mm in length) form stellate clusters, and small (0.1mm in size) clinopyroxene phenocrysts are attached to these clusters (Plate 3.19). The phenocrysts are euhedral, showing no signs of any resorption, suggesting that they are in equilibrium with their host liquid. The compositions of the plagioclases vary between An_{59} and An_{80} *(Falloon et al., 1992)*. The Mg#'s of the clinopyroxenes vary between 0.70 and 0.90 and those of the olivines between 0.63 and 0.88. The groundmass of these lavas is glassy, and contains a high proportion of opaque minerals. A more detailed description of the lavas is given in *Falloon et al. (1992)*.

3.9 Two pyroxene geothermometry

Numerous workers have tried to extract thermometric information from coexisting pyroxenes (*Boyd, 1973; Wood & Banno, 1973; Saxena & Nehru, 1975; Saxena, 1976; Wells, 1977; Kretz, 1982; Mercier, 1976; Ishii, 1975*). The methods applied were for pyroxene pairs that plot onto the diopside-enstatite-hedenbergite-ferrosilite quadrilateral, that is wollastonite(Wo)-enstatite(En)-ferrosilite(Fs), which total 90% or more of the pyroxene composition. The methods involve plotting the pyroxene compositions onto the quadrilateral and then using them to calculate the temperature. *Ishii (1975)* used a three-pyroxene thermometer with augite + pigeonite + orthopyroxene. *Lindsley & Anderson (1983)* showed that only the two-pyroxene thermometers of *Ross & Huebner (1975)* and *Kretz (1982)* gave good results over a wide range of temperatures and compositions. The most common thermometers project the quadrilateral compositions onto a diopside-enstatite join and then use a phase diagram or solution to obtain the temperatures (*Lindsley, 1983*). The most successful thermometer is in *Lindsley & Anderson (1983)*, which uses the activities of Wo-En-Fs, and thus enables projection onto the pyroxene quadrilateral and the use of quadrilateral phase relations for thermometry.

Microprobe data of clinopyroxenes and orthopyroxenes from Tafahi lavas were used to calculate the Wo-En-Fs parameters according to the projection scheme suggested by *Lindsley & Anderson, (1983)*. Calculations were carried out on an IBM-PC computer using the PX program developed by *Gómez (1990)*. Figure 3.7 shows data plotted on the Di-En-Hd-Fs quadrilateral of *Lindsley (1983)* which is calibrated for 1 atmosphere and contoured at 100°C intervals using these Wo-En-Fs parameters (*Lindsey & Anderson, 1983*). At low pressures (≤5kbar) there was not much variation in the isotherms, so a pressure of 1 atmosphere was chosen for the thermometry. In fact, low-pressure diagrams would only be applicable if the host-magmas resided and fractionated in shallow-level chambers. The primary magmas for high-Ca boninites and high Mg-lavas, such as those of Tafahi, are produced at pressures less than 10kbar (*Duncan & Green, 1987; Van der Laan et al., 1989*), but are likely to segregate at shallow depths (<5kbar). Therefore, the 1 atmosphere thermometry is a good approximation.

Lindsley & Anderson (1983) estimated the errors in the calculation and placement of the isotherms to be ±20-30°C. The total error in the thermometry of pyroxenes containing very little non-quadrilateral components is about ±50°C (*Lindsley & Andersen, 1983*), taking into account the errors in the analyses of the pyroxenes. Pyroxenes containing 'other' components do not give accurate temperatures by the above method (i.e. Wo-En-Fs is less than 90% of the pyroxene
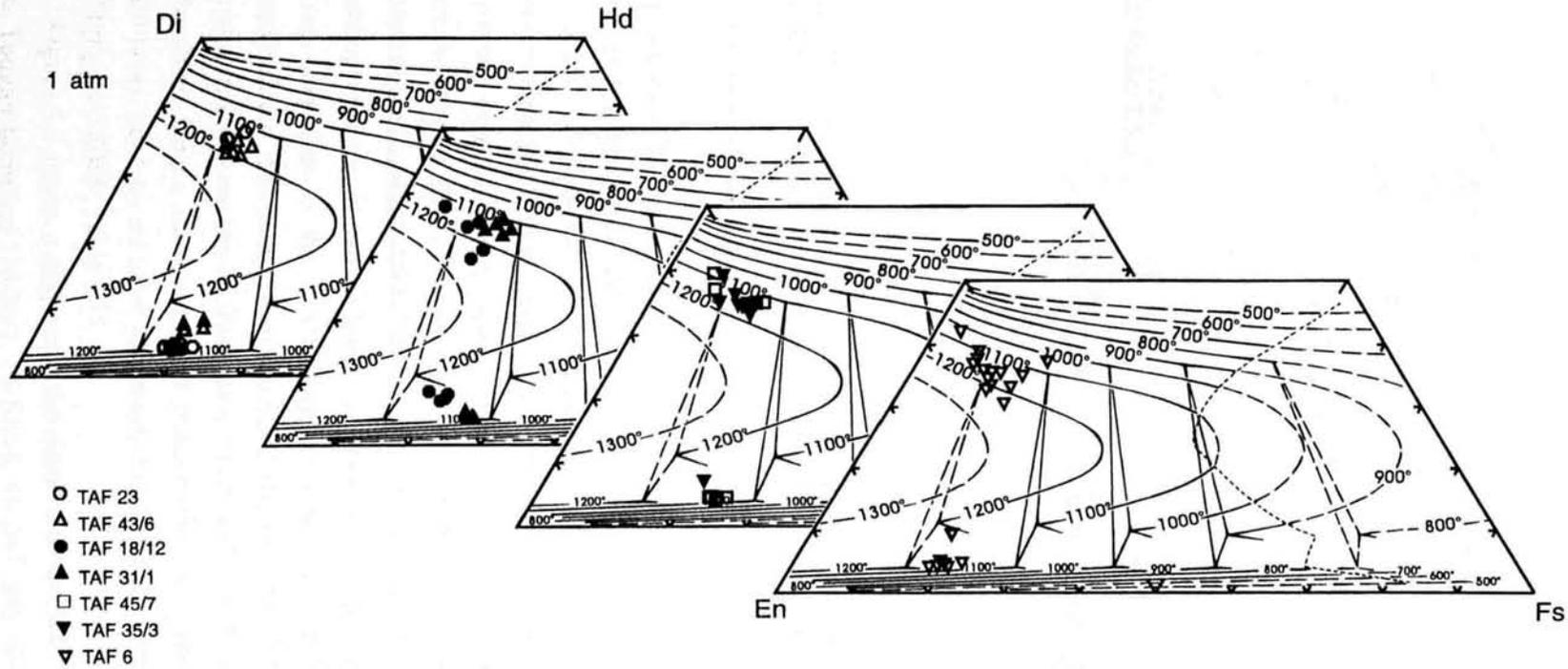
Figure 3.4(a): *Liquidus temperatures of pyroxenes from the lavas of Tafahi, on a Di-En-Hd-Fs quadrilateral of Lindsley (1983) which is calibrated to 1 atmosphere and contoured at 100°C intervals.*
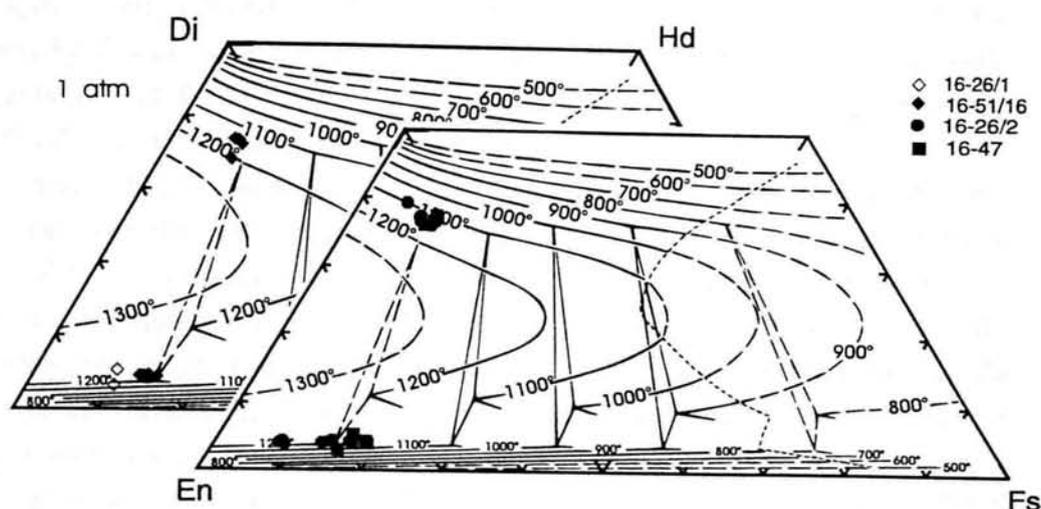
Figure 3.7b: Liquidus temperatures of pyroxenes of the north Tongan boninites on a Di-En-Hd-Fs quadrilateral of Lindsley (1983) which is calibrated to 1 atmosphere and contoured at 100°C intervals.

compositions). The uncertainty may increase by 5°C for each percentage point by which the non-quadrilateral components exceeds 2 mol%.

Figure 3.7 shows the two-pyroxene thermometry diagrams for both clinopyroxenes and orthopyroxenes from the lavas of Tafahi and two boninites from the western ophiolite section and two from site 26, and Table 3.5 shows the results. Figure 3.7 shows that clinopyroxene and orthopyroxene phenocrysts have similar temperatures of crystallisation. However, it is easier to determine the temperatures for the clinopyroxenes, due to the isotherms being further apart at the Ca-rich end of the diagram and due to the larger range of their Ca contents than those of the orthopyroxenes. The temperature ranges given in Table 3.5 are likely to be good estimates of the pyroxene crystallisation temperatures in the lavas. The pyroxenes in the boninites have a similar range of temperatures of crystallisation as those in the Tafahi lavas, but they are more magnesian-rich (Average whole rock $Mg\#_{bon}$= 0.9218 c.f. $Mg\#_{Taf}$ = 0.8064; Table 3.5).

Figure 3.8 shows a diagram of the range of temperature of crystallisation of the north Tongan boninites (16-26/1, 16-51/16, 16-26/2 and 16-47) and the lavas from Tafahi (TAF 23, 43/6, 18/12, 31/1, 35/3, 45/7 and 6), versus the magnesian number of

the host orthopyroxene. A best-fit straight line has been drawn through the data, and it can be extrapolated to higher Mg#'s to estimate the temperature of the primary magma of the boninites and the lavas from Tafahi. This is a similar method to that used by *Pearce et al. (1995a)* in their study of the volcanic rocks of the South Sandwich Islands. The primary magma is estimated to have a $Mg\#_{opx}$ of around 0.855-0.900. This assumes that the most primitive boninite (16-26/1) has the most magnesian $Mg\#_{opx}$, which is representative of the $Mg\#_{opx}$ of a boninite primary magma. Therefore, the orthopyroxene in this primary magma has a temperature of crystallisation of about 1150-1200°C which is approximately similar to, or just below, its initial temperature of formation. This assumes that orthopyroxene has reached the solidus at the time of magma generation, or just after, when the magma has cooled slightly. This also assumes that crystallisation begins soon after magma generation. The estimated temperature of the primary-magma of the lavas from north Tonga is similar to those of MORB generation (c.1280°C; e.g. *McKenzie & Bickle, 1988*).
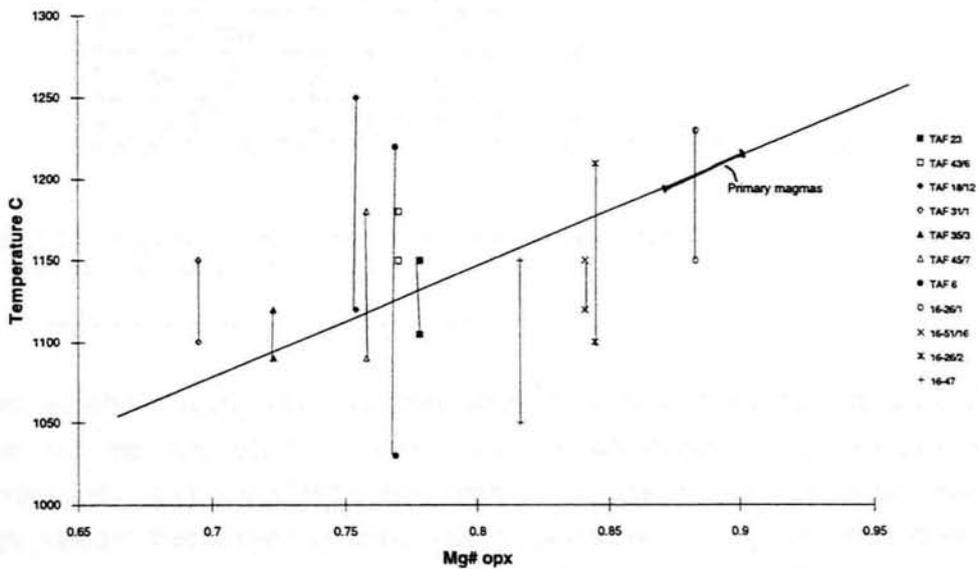
Figure 3.8: The range of the temperature of crystallisation from Table 3.4 versus magnesian number of host orthopyroxenes for the north Tongan boninites and lavas from Tafahi where Mg# = Mg/(Mg+Fe) and Fe is total Fe as Fe".

Sobolev & Danyushevsky (1994) estimate a range of temperatures of crystallisation of 1390-1150°C, for a pressure range 1.7 to 0.15 kbar, for pyroxenes

Sample	Rock type	MgO wt %	Range of temperatures of crystallisation (±50°C)
TAF43/6	Basaltic andesite	6.95	1150-1200°C
TAF23	Basaltic andesite	6.37	1105-1160°C
TAF18/12	Basaltic andesite	6.14	1130-1230°C
TAF31/1	Basaltic andesite	5.32	1100-1150°C
TAF35/3	Basaltic andesite	5.38	1090-1180°C
TAF45/7	Basaltic andesite	4.50	1090-1120°C
TAF6	Basaltic andesite	6.14	1100-1220°C
16-26/1	Boninite	14.10	1150-1230°C
16-51/16	Boninite	13.36	1150-1220°C
16-26/2	Boninite	28.35	1100-1215°C
16-47	Boninite	8.97	1100-1140°C

Table 3.5: Two pyroxene thermometer results of the samples from Tafahi and four north Tongan boninites from the Kallisto 1982 cruise.

---

from the same boninite samples as those used in this study, using fluid inclusion data from olivines and orthopyroxenes. However, according to the two-pyroxene thermometry of *Lindsley (1983)* this range of temperatures can only be obtained if high-pressure thermometry is used. This is clearly not the case as these magmas segregated at low pressures (<5kbar). *Sobolev & Danyushevsky (1994)* also estimate the primary magma temperature from these samples, to be around 1450-1550°C, which is considerably higher than the temperatures obtained from the two-pyroxene thermometry in this study (1090-1230°C).

The lavas from Tafahi have a similar range of temperatures of crystallisation, but lower Mg# of orthopyroxene, as they are more fractionated lavas than the north Tongan boninites. They lie approximately on the same line of descent as the north Tongan boninites (Figure 3.8) and their primary-magma compositions are estimated to be of approximately similar composition to those of the north Tongan boninites.

3.9.1 Evidence for the origin of the source to the north Tongan boninites and lavas from Tafahi

It is useful to estimate the temperatures of the primary magmas because it is one way to determine the nature and origin of the source of lavas that have erupted at the surface. *Sobolev & Danyushevsky (1994)* use their estimated high temperature of the primary magmas as evidence that their sources were residual plume mantle, as the temperatures they obtained are similar to those under a plume. They suggest that this residual mantle had influxed into the northern Lau Basin through the rip in the Pacific plate along the northern termination of the Tonga trench into the source region of the north Tongan boninites. They propose that the high temperatures of this mantle induced fluids to be released from the downgoing slab, which then led to melting and the production of boninitic primary melts, at pressures of 20-25 kbar. However, the temperatures obtained from this study, which are closer to those for MORB-generation, suggest that the boninite source was at a lower temperature than the Samoan plume, but of a similar temperature to that of the MORB-type mantle at the spreading centres of the northern Lau Basin.

In summary, the lower temperatures of the boninite primary magmas obtained in this study do not preclude the involvement of the Samoan plume in their petrogenesis. In fact, the trace element and isotope geochemistry show that the sources of the north Tongan boninites, the lavas from Tafahi (and Niuatoputapu) are residual plume mantle, which has originated from Samoa (Chapters 4, 5 and 6). This residual plume mantle influxed into their source regions from the northeast, through the rip in the Pacific plate (Figure 5.4). However, the temperatures of crystallisation for these lavas, obtained from two-pyroxene thermometry, imply that this plume mantle has cooled considerably to a temperature similar to that at which MORB is generated.

3.10 Chapter 3 Summary

The petrography of two ophiolite sections, from the inner wall of the northern Tonga trench, and lavas from Tafahi, Niuatoputapu and the Northern Lau Spreading Centre are described in this chapter. Two-pyroxene thermometry is applied, using microprobe data of pyroxene phenocrysts from the north Tongan boninites and the lavas from Tafahi, in order to estimate their temperatures of crystallisation and primary magmas. These temperatures are then used as evidence for the nature of their mantle sources.

• The lavas from Tafahi and the north Tongan boninites have both *intratelluric* and *quench* stage phenocrysts, whereas the lavas from Niuatoputapu and the Northern Lau Spreading Centre only have *quench* stage phenocrysts.

• The lavas from Tafahi have either porphyritic or glomeroporphyritic textures, with large phenocrysts of plagioclase, clinopyroxene and orthopyroxene, in a fine- to moderately coarse-grained 'quench' groundmass. The plagioclase phenocrysts have a modal abundance of between 15% and 30%, and a composition of An_{84} to An_{92} which is similar to the compositions of the groundmass plagioclases. Most of the plagioclase phenocrysts have more sodic rims than their corresponding cores, suggesting that some zoning has occurred. Olivine occurs as a minor intratelluric phase in some of the lavas, having a composition of Fo_{76} to Fo_{85}, which is less magnesian than the olivines in the north Tongan boninites (Fo_{78} to Fo_{91}).

The lavas contain up to 10% of clinopyroxene and 10% of orthopyroxene. The clinopyroxene rims have higher FeO* contents and lower Mg# than the cores, but the CaO contents of the rims are more variable compared to those of the cores. The variation in composition between the cores and rims of the clinopyroxenes suggests that some zoning has taken place and that the phenocrysts were not in equilibrium with their host magma as they grew. Most of the cores of the orthopyroxene phenocrysts have lower Mg#'s and higher FeO* contents than their corresponding rims, indicating that they are also zoned and were not in equilibrium with the host magma as they grew. Clinopyroxenes either have a tabular crystal-habit, or are resorbed, or form glomerocrysts, up to 3mm in diameter with orthopyroxene and plagioclase. Orthopyroxene also occurs either as singular subhedral phenocrysts, or in stellate clusters.

• The lava flows of Niuatoputapu are mostly aphyric, but may contain microphenocrysts of plagioclase and clinopyroxene.

• *The western ophiolite section of the 'Kallisto' 1982 cruise*

The north Tongan boninites from the western ophiolite section contain clinopyroxene (10%), orthopyroxene (up to 20%) and plagioclase (up to 15%) as phenocryst phases and have a quench groundmass of clinopyroxene and plagioclase. The pyroxenes have a euhedral crystal-habit, often forming glomerocrysts, similar to those observed in the Tafahi lavas. The CaO and FeO* contents of the clinopyroxenes in the boninites from the western ophiolite section, and from site 26, do not vary very much. However, the orthopyroxenes in boninites from the dredge section are less magnesian than those from Site 26 to the west.

Gabbro norites, tonalites, trondhjemites and a plagiogranite from the plutonic sequence were dredged. The tonalites contain up to 20% quartz, 5% alkali feldspar, 70% plagioclase, 4% epidote and 1% chlorite.

Cumulate ultramafics, such as pyroxenites and gabbros were dredged from the cumulate sequence. The gabbros have cumulate textures with intergrown olivine (<5%), clinopyroxene (up to 40%), plagioclase (up to 60%) and minor hornblende (<5%).

Tectonised harzburgites were also dredged on this section, which contain up to 70% olivine, 30% orthopyroxene, but very little clinopyroxene (<5%). The original fabric and minerals in the harzburgites have been almost completely destroyed by serpentinisation.

• *The eastern ophiolite section*

This section contains similar rocks to the western section: cumulate ultramafics and gabbros and tonalites, but has tholeiitic lavas rather than boninitic ones. Most of the original textures of the tholeiitic lavas have been replaced by clay minerals, but some relic quench textures remain.

The cumulate gabbros contain up to 15% olivine, 35% clinopyroxene and 50% plagioclase, but contain very little secondary amphibole, unlike the gabbros from the western section.

• *Site 26 of the 'Kallisto' 1982 cruise*

Boninites were dredged from site 26, which is located 40km west of the western ophiolite section. These boninites are very phenocryst-rich, containing up to 15% olivine, very little plagioclase (<3%), 6% orthopyroxene and 1-5% clinopyroxene. The olivines have compositions between Fo_{88} and Fo_{91}, and are in disequilibrium with their host magma, as is shown by their complex resorbed rims.

• Two-pyroxene thermometry at 1 atmosphere pressure has been used to estimate the temperatures of crystallisation of the north Tongan boninites and the lavas from Tafahi to within ± 50°C. The north Tongan boninites have a similar temperature range of crystallisation (1100-1230°C) to the Tafahi lavas (1090-1230°C), but they are more magnesian (Average whole rock $Mg\#_{bon}$ = 0.9128 c.f. $Mg\#_{Taf}$ = 0.8064). The temperature of crystallisation of orthopyroxenes in the boninite primary magmas is estimated to be 1150-1200°C, assuming that the Mg#'s of the primary magma orthopyroxenes are similar to those in the most primitive boninite. This temperature range is approximately similar to, or just below, the initial temperature of formation of the primary magma and is within the range for MORB generation.

However, *Sobolev & Danyushevsky (1994)* estimated a range of temperatures of crystallisation of 1390-1150°C for a pressure range 1.7 to 0.15 kbar for pyroxenes from the same boninites as in this study, using fluid inclusion data from olivines and orthopyroxenes. They estimate the initial primary-magma temperature to be around 1450-1550°C. These temperatures are similar to those under a mantle plume and led *Sobolev & Danyushevsky (1994)* to propose that the source to the north Tongan boninites was residual mantle from the Samoan plume. This plume mantle influxed into the source region through the rip in the Pacific plate at the northern termination of the Tonga trench.

The lower estimated temperature range of the boninite primary magmas obtained in this study suggests that either the boninites have plume mantle sources, which had cooled to a MORB-like geotherm before their magma genesis, or that the boninite source was residual mantle after production of basalts at a spreading centre. The trace elements and isotopes, however, indicate that the sources of the boninites, and the lavas from Tafahi (and Niuatoputapu) are residual plume mantle, which has influxed into the source region (Chapters 4, 5 and 6).

CHAPTER 4

Major and trace element geochemistry

4.1 Introduction

In this chapter, the major element geochemistry of the north Tongan boninites, and the lavas from Tafahi, Niuatoputapu and the Northern Lau Spreading Centre is described. This is then used to classify the lavas, and to determine their fractionation histories. The trace element characteristics of the lavas are identified, which are compared to those of the central Tofua arc. The major and trace elements are used to investigate whether the sources of the lavas from north Tonga were: (i) derived from either MORB-, or plume-like, mantle, or a mixture; (ii) enriched as a result of the addition of a component and/or the type of mantle in the region; and (iii) depleted due to a mantle process, such as previous partial melting episodes. The nature of any enrichments by a subduction component are identified, and whether this component is hydrous fluids derived from the subducting slab and sediments, or is generated by slab fusion, is elucidated. The % contributions to the elemental budgets of the lavas from the subduction component are estimated using the trace elements.

4.2 Major element characteristics

4.2.1 Classification of the lavas

Boninites are commonly divided into two main classes: high- and low-Ca boninites. The lavas from the western ophiolite section can be classified as boninitic on the basis of their high SiO_2 content (>53% SiO_2) and high MgO content (Mg# >0.6), where Mg# = Mg/(Mg+Fe), with Fe calculated from total Fe as Fe^{II} (*Crawford et al., 1989*). High-Ca boninites, such as the Upper Pillow Lavas of the Troodos Ophiolite (*Cameron, 1985; Rogers et al., 1989*), have SiO_2<56% and CaO/Al_2O_3>0.75, whereas low-Ca boninites such as the boninites from Cape Vogel, Papua New Guinea, have higher SiO_2 contents (>58%) and lower CaO/Al_2O_3 ratios (<0.75).

To classify the north Tongan boninites, plots of their SiO_2 contents and CaO/Al_2O_3 ratios versus their MgO contents (Figure 4.1) have been constructed. The compositions of boninites from some 'type' localities have also been plotted for comparison: high-Ca boninites from the Upper Pillow Lavas of the Troodos Massif Cyprus (*Cameron, 1985; Rogers et al., 1989*); low-Ca boninites from Cape Vogel, Papua New Guinea (Jenner, 1981); and intermediate- low Ca boninites from drill sites in the Izu-Bonin forearc from ODP Leg 125 (*Pearce et al., 1992*). It is apparent from Figure 4.1 that the north Tongan boninites have similar CaO/Al_2O_3 ratios (0.65-0.9) and MgO contents (9-15 wt%) to the high-Ca boninites from the Troodos Massif, Cyprus, but have slightly higher SiO_2 contents (50-54 wt% cf. 47-52 wt%) and a more variable MgO content. They have higher CaO/Al_2O_3 ratios than the low-Ca boninites from Cape Vogel and the Izu-Bonin forearc boninites. They thus fulfil the criteria of *Crawford et al.* (*1989*) for high-Ca boninites ($CaO/Al_2O_3 > 0.75$, $SiO_2 < 56\%$).

The boninites from the western ophiolite section and from site 26, 40km to the west of this section, also have similar major element geochemistry to those from Station 21 of the 'Natsushima' 1984 cruise. In particular, all three groups have similar SiO_2 contents and CaO/Al_2O_3 ratios. However, the three groups of boninites from north Tonga can be distinguished on the basis of their trace element geochemistry (Figures 4.5(a) to (d)).

Figure 4.2 is a diagram of total alkali (Na_2O+K_2O) versus SiO_2 contents for the north Tongan boninites, lavas from Tafahi and Niuatoputapu and tholeiites from Ata, Fonualei and Late, from part of the central Tofua arc. The Tafahi lavas have compositions almost entirely within the basaltic-andesite field, with SiO_2 contents between 52 and 57 wt %, but with lower total alkalis (1.0-1.5 wt%) than the basaltic andesitic lavas from Late (2.0-2.2 wt%) and Ata (2.5-3.0 wt%).

The lavas from Niuatoputapu have higher SiO_2 contents (58-61 wt%) than the Tafahi lavas, and are therefore classified as andesitic in composition, but they also have a lower total alkali content (2.0-2.5 wt%) than the andesitic lavas from Late (2.8-3.1 wt%) and Fonualei (3.5-3.7 wt%).

4.2.3 Comparison of major element geochemistry

Figure 4.3 shows the major element variations of the north Tongan boninites, and lavas from Tafahi and Niuatoputapu, compared with lavas from the central Tofua arc and the Northern Lau Spreading Centre. Several features are apparent:
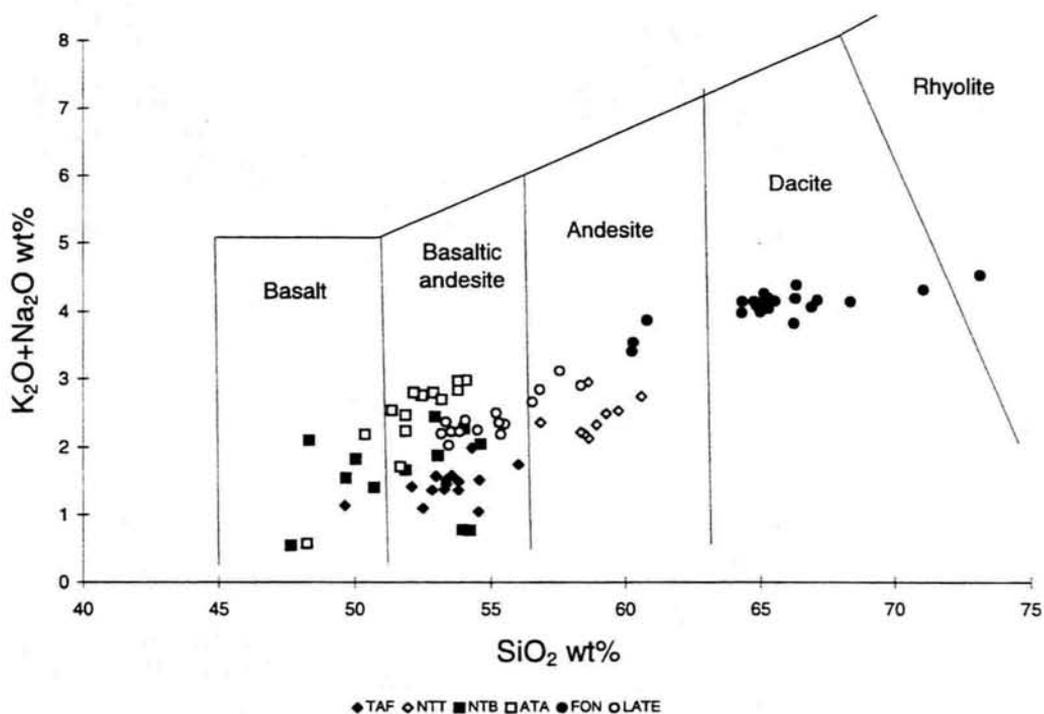
Figure 4.2: A plot of total alkalis (K_2O+Na_2O) versus SiO_2 content for the north Tongan islands of Tafahi (TAF) and Niuatoputapu (NTT), the north Tongan boninites (NTB) and the central Tofua arc islands of Ata (ATA), Fonualei (FON) and Late (LATE) in order to classify them. Suite boundaries and nomenclature from Le Maitre et al. (1989).

1. The north Tongan boninites have higher SiO_2 contents for a given MgO content (Figure 4.3(a)). As noted earlier, most satisfy the criteria for high-Ca boninites of high SiO_2 content (>53% SiO_2) at high MgO content (Mg#>0.6) proposed by *Crawford et al. (1989)*. Those that do not, have evolved from a boninite parent by either olivine accumulation (the relatively low SiO_2 contents) or fractional crystallisation (the relatively low MgO contents). The Tafahi lavas are intermediate between boninites and island arc tholeiites on this projection. However, Niuatoputapu lavas plot on the main arc trend.

2. On the Na_2O-MgO and K_2O-MgO plots, the compositions of lavas from Niuatoputapu and Tafahi are displaced to low K_2O and Na_2O contents relative to those of the lavas of the Tofua arc.

3. On the CaO-MgO plot (Figure 4.3(d)), the compositions of Tafahi and Niuatoputapu lavas plot within the Tofua arc array, consistent with the evidence from their phenocryst phase assemblage that they have a broadly similar fractional
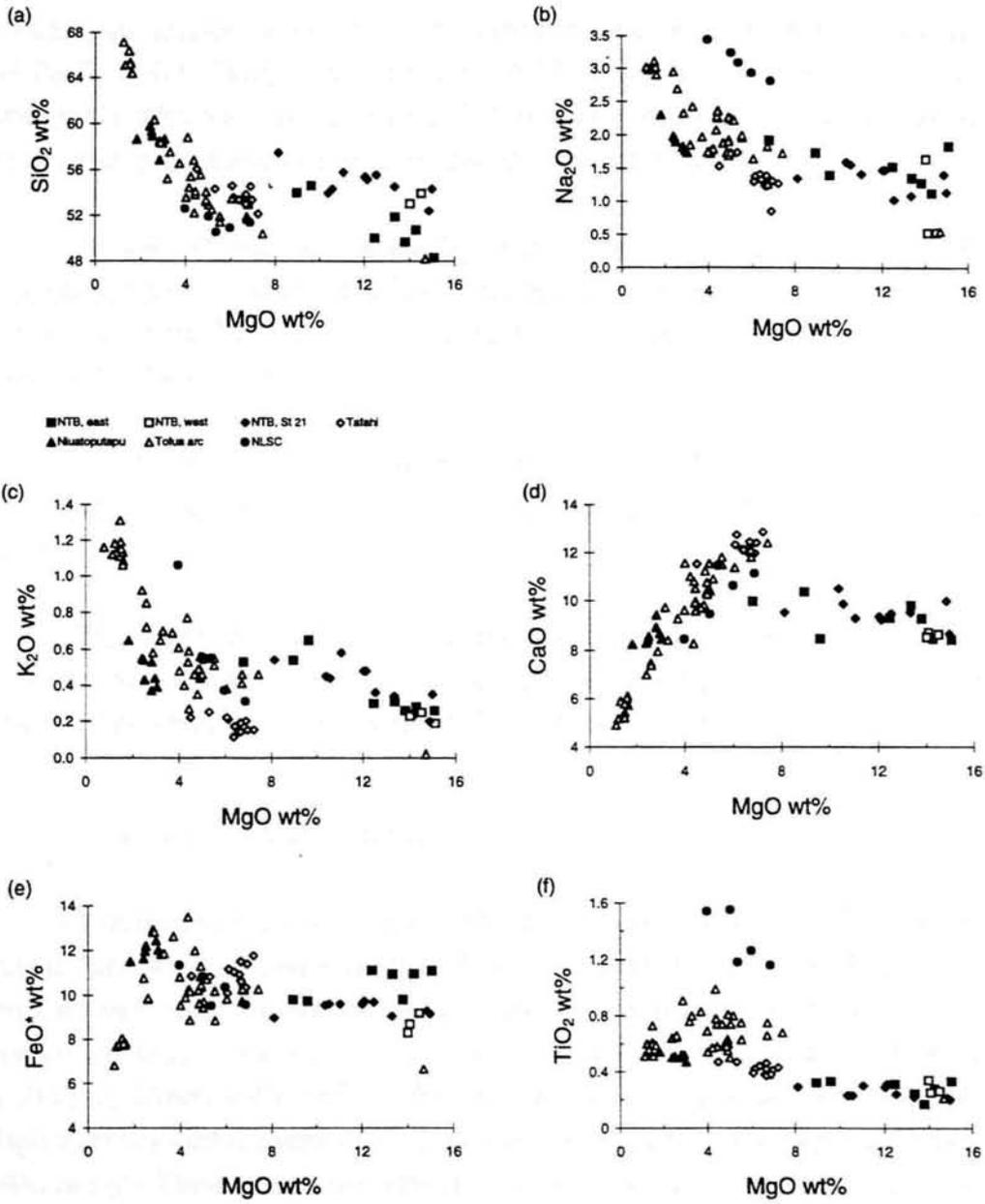
Figure 4.3 : Major element variation of the north Tongan boninites from the western ophiolite section dredged on the 'Kallisto' 1982 cruise (NTB, east), from site 26 (NTB, west) and from Station 21 of the 'Natsushima' 1984 cruise (NTB, St 21), and lavas from Tafahi, Niuatoputapu, the central Tofua arc and the Northern Lau Spreading Centre (NLSC).

crystallisation history, involving olivine, clinopyroxene, orthopyroxene, plagioclase and Fe-Ti oxides (*Ewart & Hawkesworth, 1987*). The boninites form a distinctive trend on this plot with CaO increasing slightly with decreasing MgO, which can be explained by plagioclase not having reached the liquidus (Figure 4.4).

4. On the TiO_2-MgO plot, the TiO_2 content for a given MgO content increases from the boninites, through Tafahi and Niuatoputapu, through the Tofua arc to the Northern Lau Spreading Centre. This variation relates to the Ti content of the mantle source and is discussed in Section 4.5.

5. On the plot of total Fe content (as FeO) against MgO content, Tafahi and Niuatoputapu appear to follow a trend of slightly greater Fe-enrichment than the main Tofua arc.

6. The Niuatoputapu lavas have low MgO content (3-4 wt%) and lie towards the more evolved end of the Tofua arc lavas (Figure 4.2), with high SiO_2 contents (58-60 wt%) and FeO contents (8.5-9.5 wt%) but low CaO contents (8.0-9.5 wt%).

4.2.4 Fractionation history

The fractionation history of the north Tongan boninites, Tafahi, Niuatoputapu and the Tofua arc can be observed from the major element geochemistry (Figure 4.4). The CaO and Al_2O_3 contents of the boninites and Tafahi are plotted against MgO contents on Figure 4.4(a) and (c), using the whole rock data. These data are included as fields on Figure 4.4(b) and (d). The olivine, clinopyroxene, orthopyroxene and plagioclase phenocryst compositions from microprobe data are also plotted on Figure 4.4(b) and (d). These microprobe data are useful for estimating the compositions of fractionation end-members. These diagrams are used to show fractionation trends (cf. *Pearce et al., 1986*).

The north Tongan boninite data form a trend towards olivine on the Al_2O_3-MgO plot and one sample (16-26/2) has a composition very close to that of olivine, suggesting that these boninites have experienced olivine accumulation. This evidence is supported by the CaO-MgO plot (Figure 4.4(a) and (b)), on which the boninites show a trend towards the olivine-clinopyroxene tieline. The trend intersects the line at 80% olivine, 20% clinopyroxene suggesting that these phases are fractionating from the boninite parent-magma in these proportions. Plagioclase does not reach the liquidus during the fractionation of the boninite parent-magma. The major element
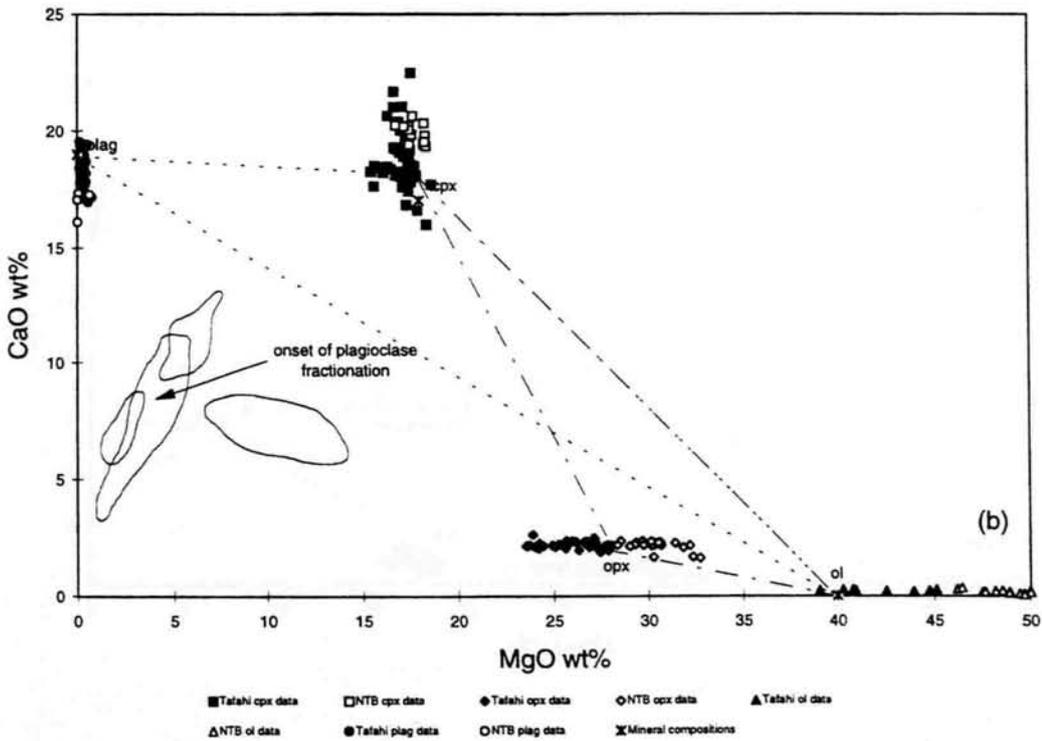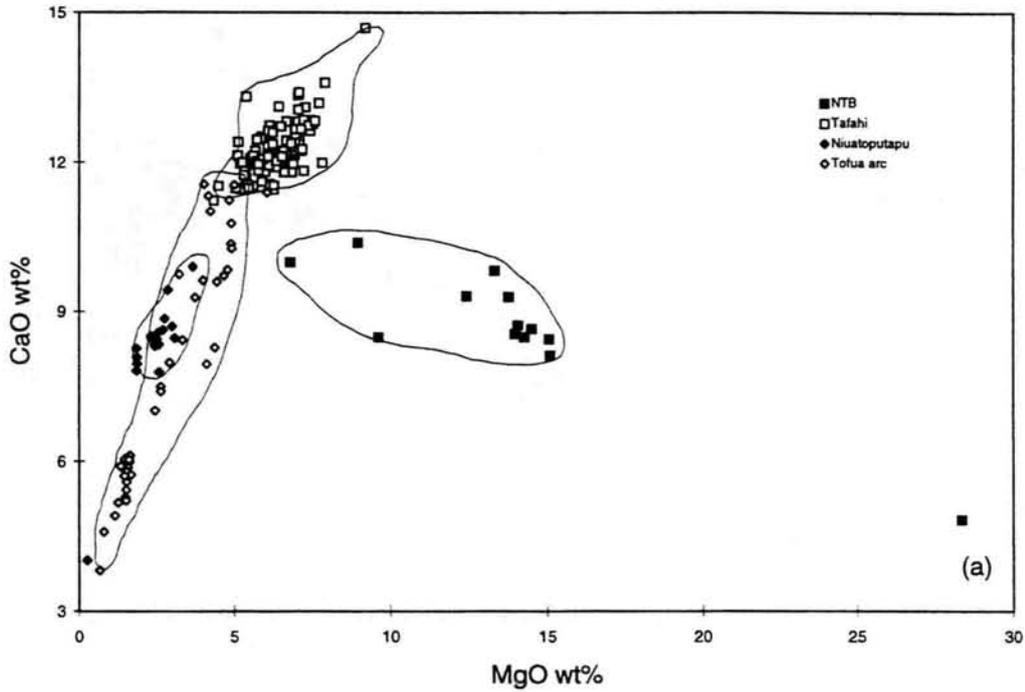
Figure 4.4 : These diagrams use the major element variation of the north Tongan boninites (NTB), lavas from Tafahi Niuatoputapu and the Tofua arc to highlight their fractionation histories. The upper diagrams (a) and (c) are more detailed plots of the variation of the compositions of the lavas, whereas the lower diagrams (b) and (d) show these data as fields and also microprobe data for olivine, clinopyroxene, orthopyroxene and plagioclase phenocrysts from from Tafahi lavas and the north Tongan boninites (Chapter 3). These microprobe data are representative of possible compositions of fractionation end-members. The dashed triangles are possible three-component fractionation assemblages.

77

(c)

(d)
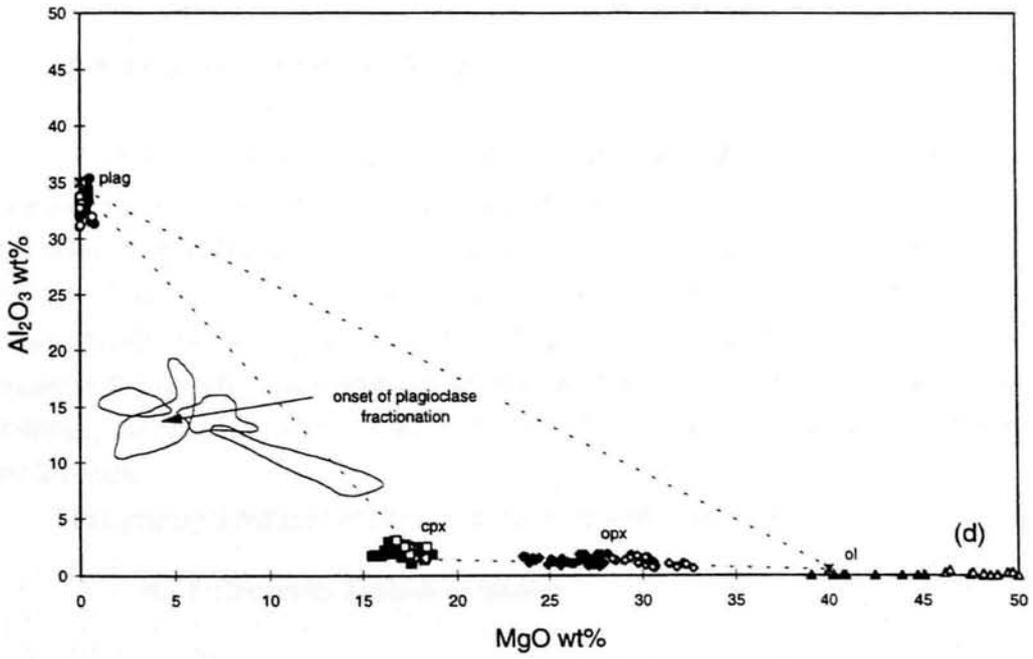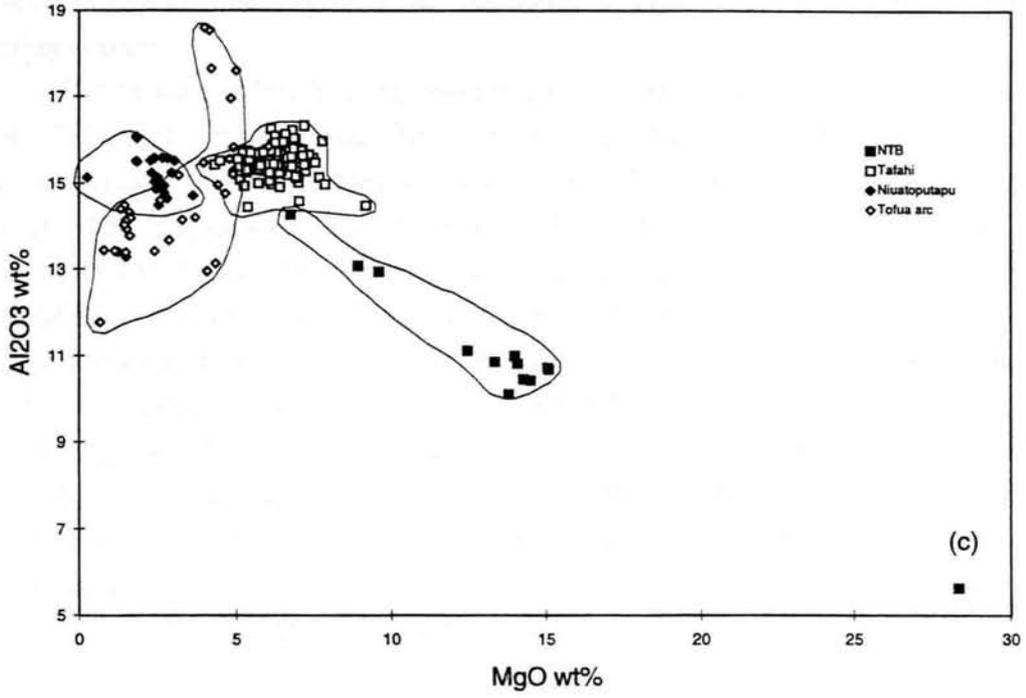
geochemistry can be explained by fractionation of olivine, clinopyroxene and orthopyroxene.

Plagioclase is a fractionating phase in the lavas from Tafahi, Niuatoputapu and the Tofua arc. Most of the lavas from Tafahi have undergone plagioclase accumulation as their compositions lie at CaO-MgO contents above the inflection point where plagioclase starts crystallising. The trend formed by the Tafahi data intersects the plagioclase-clinopyroxene tieline at 65% clinopyroxene and 35% plagioclase showing that these phases are fractionating in these proportions. Niuatoputapu plots are lower CaO and MgO contents than Tafahi suggesting that the former has undergone more fractionation. The trend shown by the Niuatoputapu data is steeper than that shown by the Tafahi data and intersects the plagioclase-clinopyroxene tieline at 60% plagioclase and 40% clinopyroxene, suggesting that plagioclase and clinopyroxene have fractionated in these proportions. Some of the lavas from the Tofua arc (Fonualei) have undergone more plagioclase fractionation than those from Niuatoputapu as they have lower CaO contents at a given MgO content.

4.3 Trace element variations

Figures 4.5(a)-(j) show the N-MORB-normalised trace element and chondrite-normalised rare-earth element (REE) patterns for the north Tongan boninites, from the western ophiolite section of the 'Kallisto' 1982 cruise, and those from Station 21 of the 'Natsushima' 1984 cruise, and a selection of the lavas from Tafahi, Niuatoputapu and the Northern Lau Spreading Centre. On the trace element variation patterns, the elements have been arranged in the order of compatibility during mantle melting, with the least compatible on the left of the diagram to the most compatible on the right.

The principal features of the lava groups are now described in turn:

4.3.1 The north Tongan boninites

The main features of the trace element and REE patterns (Figures 4.5(a) and (b)) are:

(i) a depletion in the middle-rare-earth-elements (MREE) and heavy rare earth elements (HREE) relative to N-MORB,

(ii) an enrichment in light-rare-earth-elements (LREE) relative to MREE,

North Tongan boninites (0.58-3.09Ma)
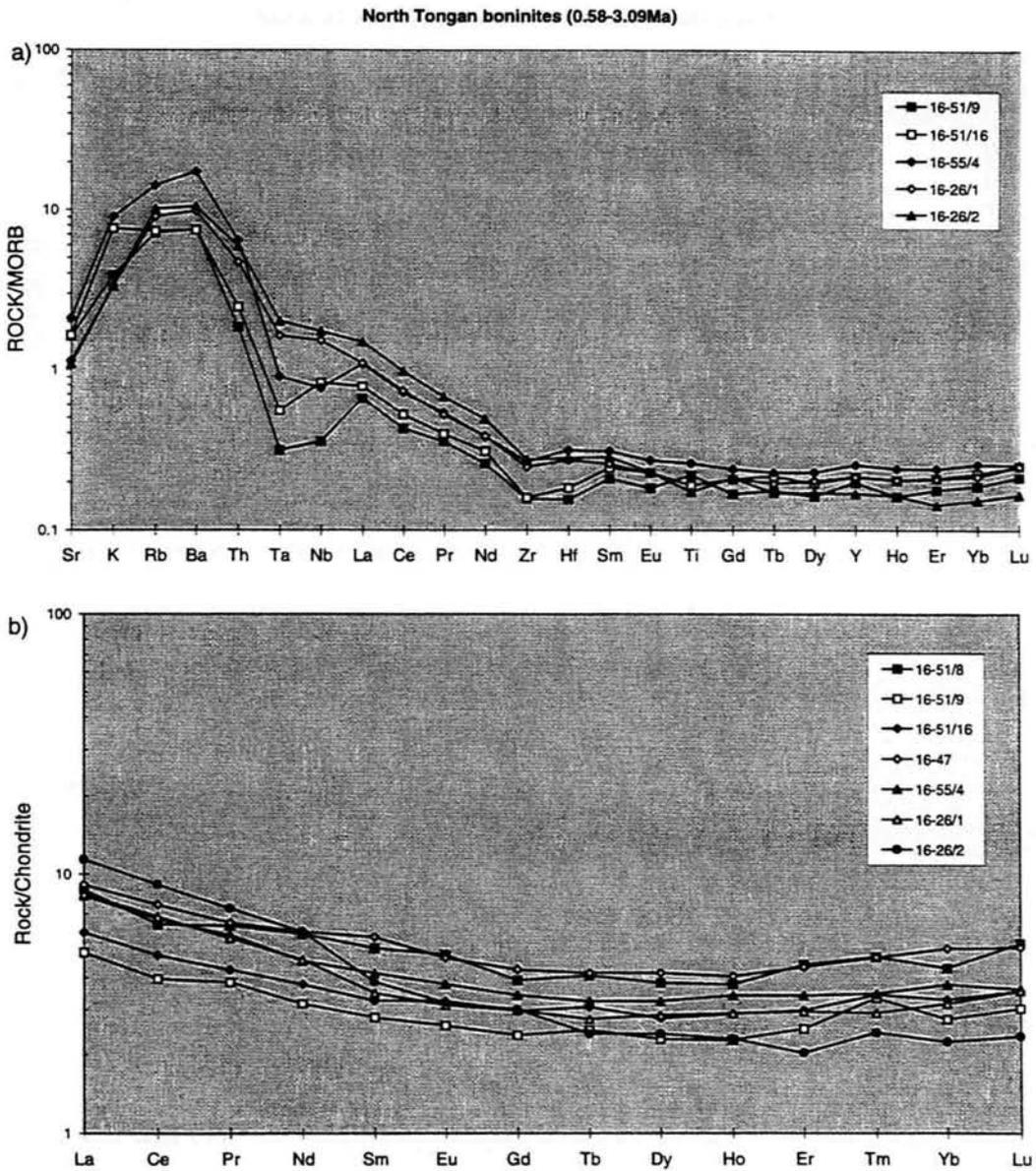
Figures 4.5(a)-(j): N-MORB-normalised trace element variation and chondrite-normalised REE patterns for: (a) and (b) the north Tongan boninites from the western ophiolite section and from the west (site 26), (c) and (d) the north Tongan boninites from Station 21 of the 'Natsushima' 1984 cruise, (e) and (f) the lavas from Tafahi, (g) and (h) the lavas from Niuatoputapu, (i) and (j) the lavas from the Northern Lau Spreading Centre. N-MORB- and chondrite-normalising values are taken from Sun & McDonough (1989) and Boynton (1984) respectively.

Station 21, north Tongan boninites (Falloon & Crawford, 1991)
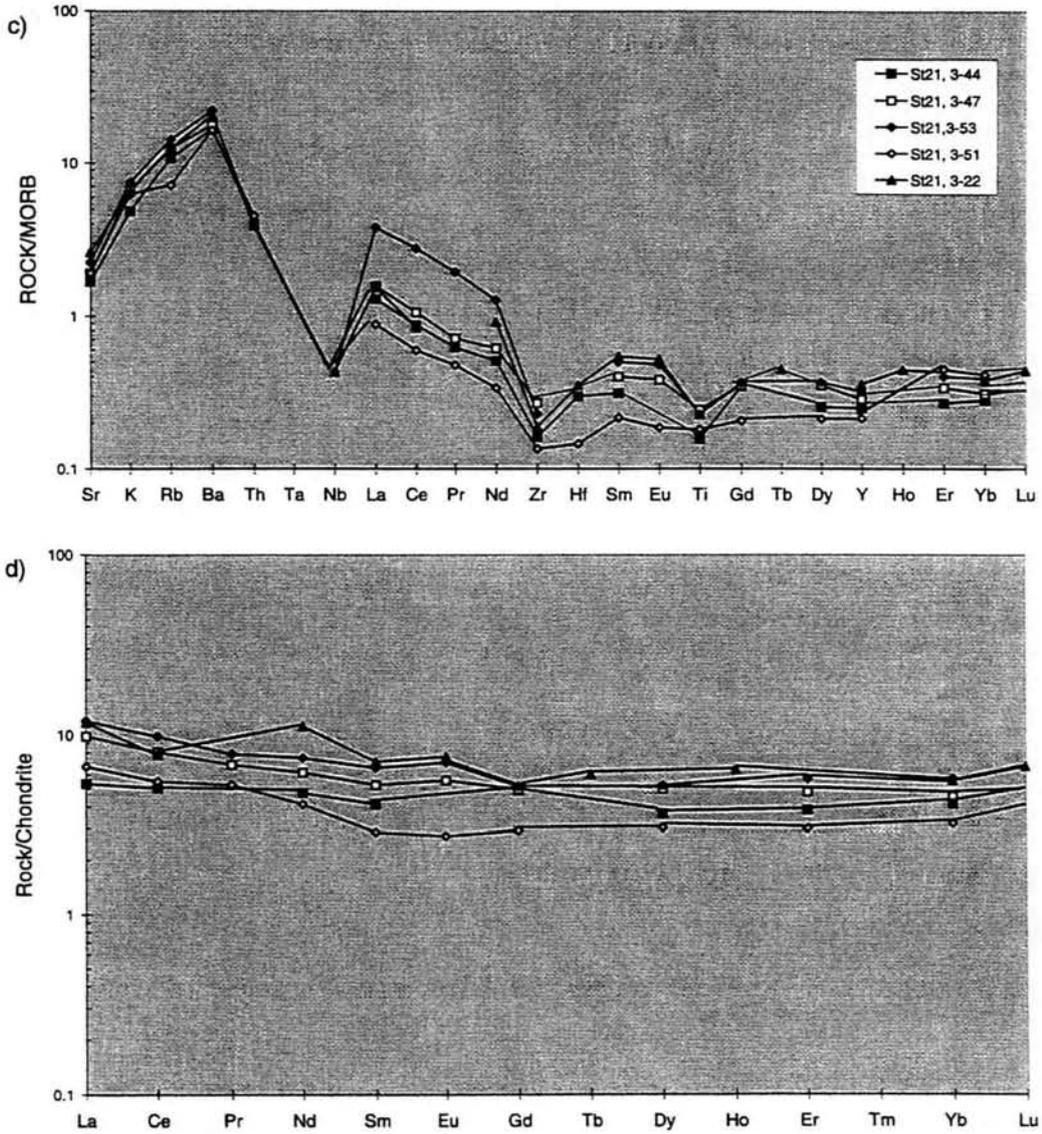
Figure 4.5 cont.

Tafahi (<7 Ma)

Figure 4.5 cont.

82
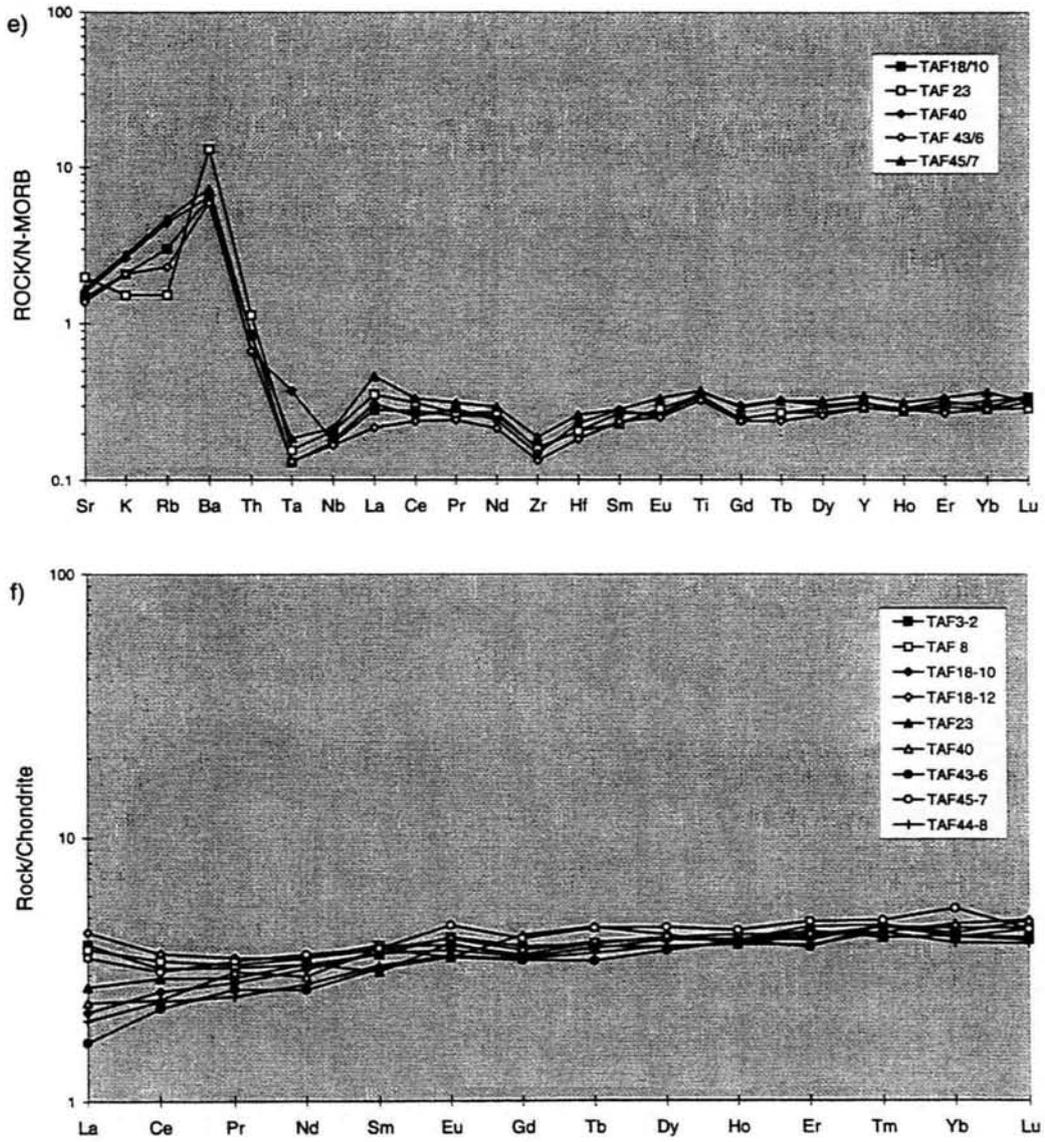
Niuatoputapu (1.5-3.0 Ma)

Figure 4.5 cont.

Northern Lau Spreading Centre (0-1.5Ma)
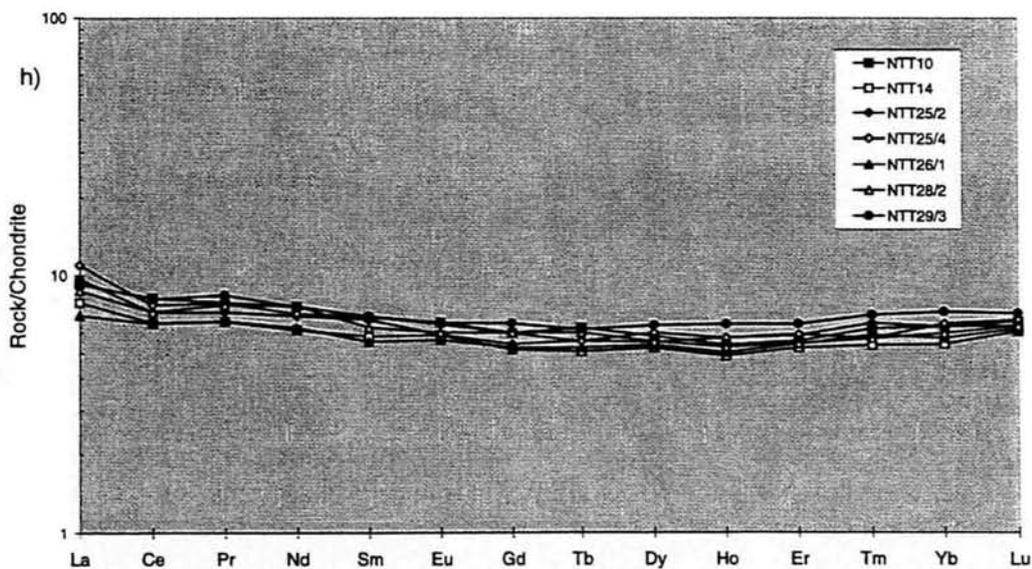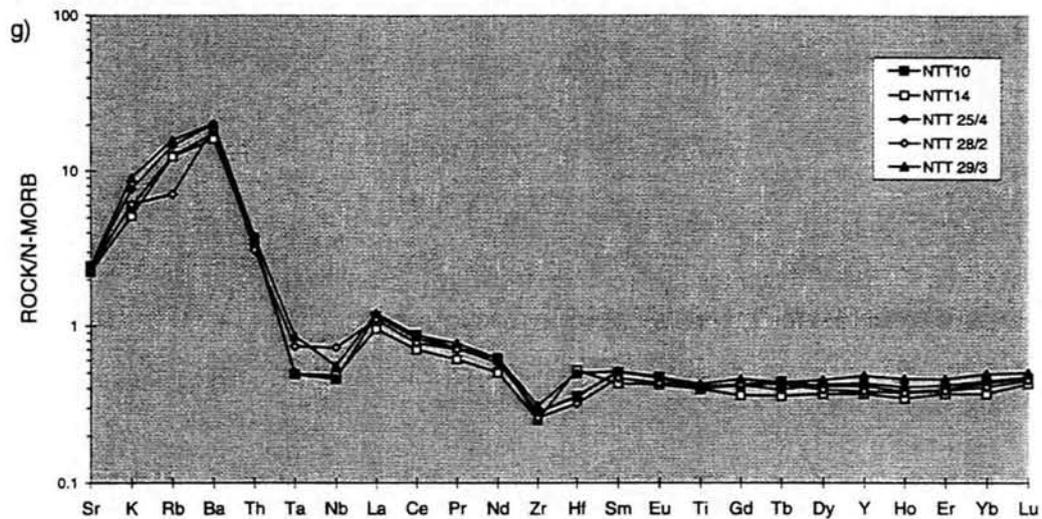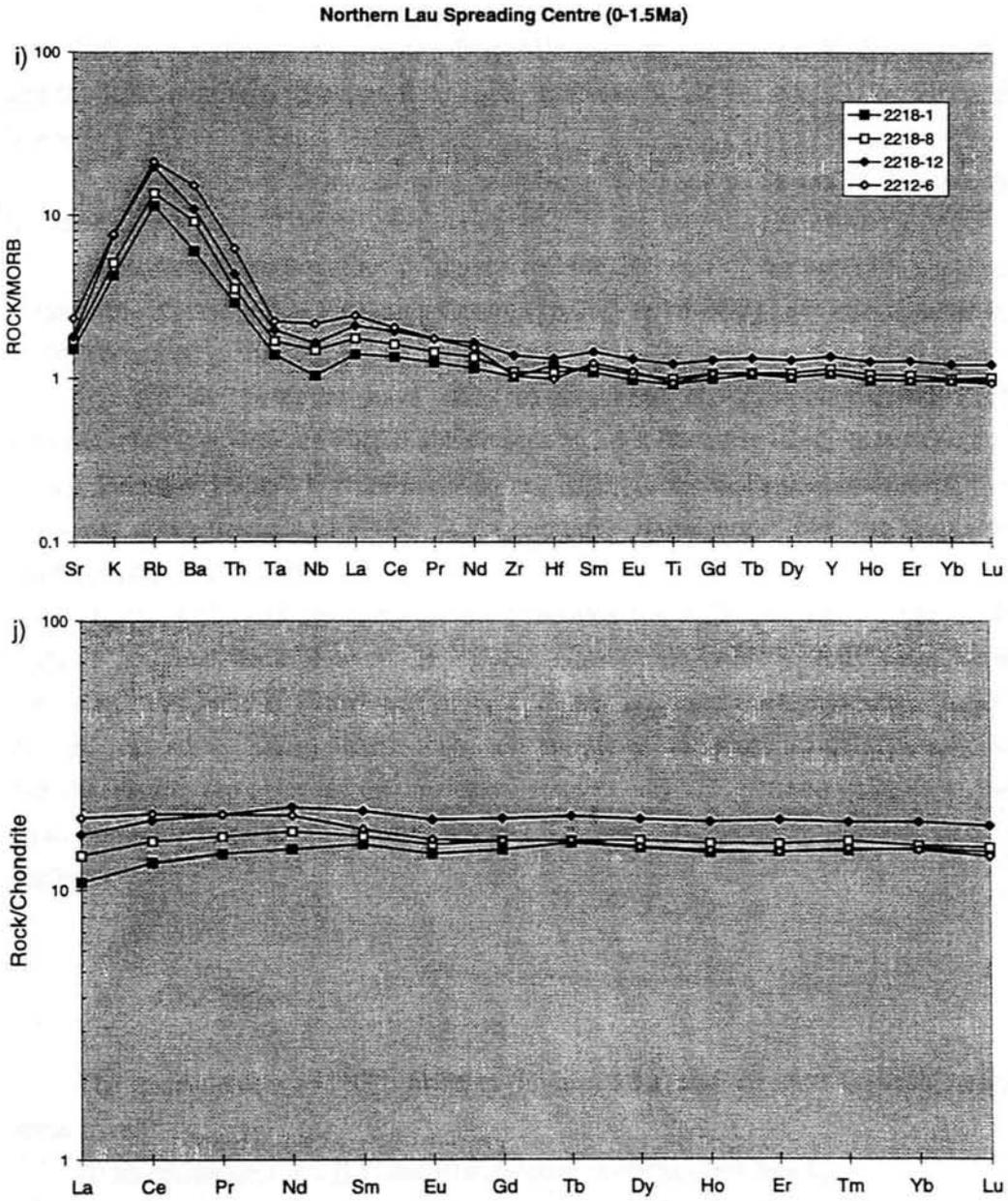
Figure 4.5 cont.

(iii) an enrichment in large-ion-lithophile-elements (LILE: Sr, K, Rb, Ba, Th) and the REE relative to the high-field-strength-elements (HFSE: Nb, Ta, Zr, Hf) and hence;

(iv) a depletion in Zr and Hf relative to Sm and Nd and in Ta and Nb relative to La and Th.

(v) However, the boninites dredged from site 26, west of the ophiolite section, close to the Northern Lau Spreading Centre (16-26/1 & 16-26/2) have *enrichments* in HFSE compared to the LREE.

(vi) All the boninites have dish- to U-shaped chondrite-normalised REE patterns, with low absolute HREE abundances at 2-5 x chondrite abundances (Figure 4.5(b)). Boninite 16-26/2 is more enriched in LREE (12 x chondrite abundances), but has lower concentrations of HREE (2.5 x chondrite abundances), than the boninites from the ophiolite section.

Figures 4.5(c) and (d) show the trace element and REE patterns for the north Tongan boninites from Station 21 of the 'Natsushima' 1984 cruise, using data presented in *Falloon & Crawford (1991)*. Data are lacking certain elements (Th, Ta, Nb, Hf and some REEs) where their concentrations are close to detection limit. Similar features are observed on these trace element and REE patterns to those of the other boninites from north Tonga, such as LILE- and LREE-enrichment and HFSE-depletion.

4.3.2 Tafahi

The trace element and REE patterns (Figures 4.5(e) and (f)) show that the Tafahi lavas have:

(i) an enrichment in LILE and REE relative to HFSE, and hence,

(ii) a depletion in Zr and Hf relative to Sm and Nd and in Ta and Nb relative to La and Th;

(iii) a flat M-HREE pattern at 0.2 x N-MORB abundances;

(iv) M-HREE abundances of 4 x chondrite;

(v) the lavas from two distinct groups, one having LREE-enrichment (up to 4.5 x chondrite abundances), the other LREE-depletion (1.7-2.2 x chondrite abundances). Sample TAF23 is transitional between the LREE-enriched and depleted groups.

4.3.3 Niuatoputapu

The trace element and REE patterns for Niuatoputapu (Figures 4.5(g) and (h)) show that the lavas have:

(i) an enrichment in LILE and LREE relative to the HFSE and M-HREE;

(ii) a flat M-HREE pattern at 0.45 x N-MORB abundances;

(iii) a pronounced depletion in Ta and Nb relative to Th and La, and Zr and sometimes Hf relative to Nd and Sm;

(iv) M-HREE abundances of 8 x chondrite and a slight LREE enrichment (up to 11 x chondrite abundances).

4.3.4 The Northern Lau Spreading Centre

The trace element and REE patterns for the Northern Lau Spreading Centre (Figures 4.5(i) and (j)) show that the lavas have:

(i) a LILE and a slight LREE enrichment relative to Ta and Nb and the M-HREE;

(ii) a flat REE pattern at abundances similar to N-MORB;

(iii) a slight depletion in Ta and Nb relative to Th and La;

(iv) M-HREE abundances of about 18 x chondrite on average. Three of the lavas (2218-1, 2218-8 and 2218-12) have a slight LREE depletion (down to 11-17 x chondrite abundances), whereas 2212-6 has a LREE enrichment (up to 19 x chondrite abundance).

4.4 Comparison with the central Tofua arc

Figures 4.5(n) and (o) show the N-MORB-normalised trace element and chondrite-normalised REE patterns for the typical samples from the north Tongan boninites, one sample from the boninitic ophiolite section (NTB, east) and one sample from Site 26, west of this section (NTB, west), and from Tafahi and Niuatoputapu, which are compared to patterns from the central Tofua arc volcano of Late. The following features are observed:

(i) the samples have flat M-HREE patterns on the MORB-normalised plot with the degree of depletion of these elements relative to N-MORB increasing from the Tofua arc, through to Niuatoputapu, Tafahi, through to the north Tongan boninite (west) to the north Tongan boninite (east);

(ii) all the samples have an enrichment in LILE relative to HFSE and REE;

Comparison of the trace element geochemistry of the north Tongan boninites, Tafahi and Niuatoputapu with that of the central Tofua arc.
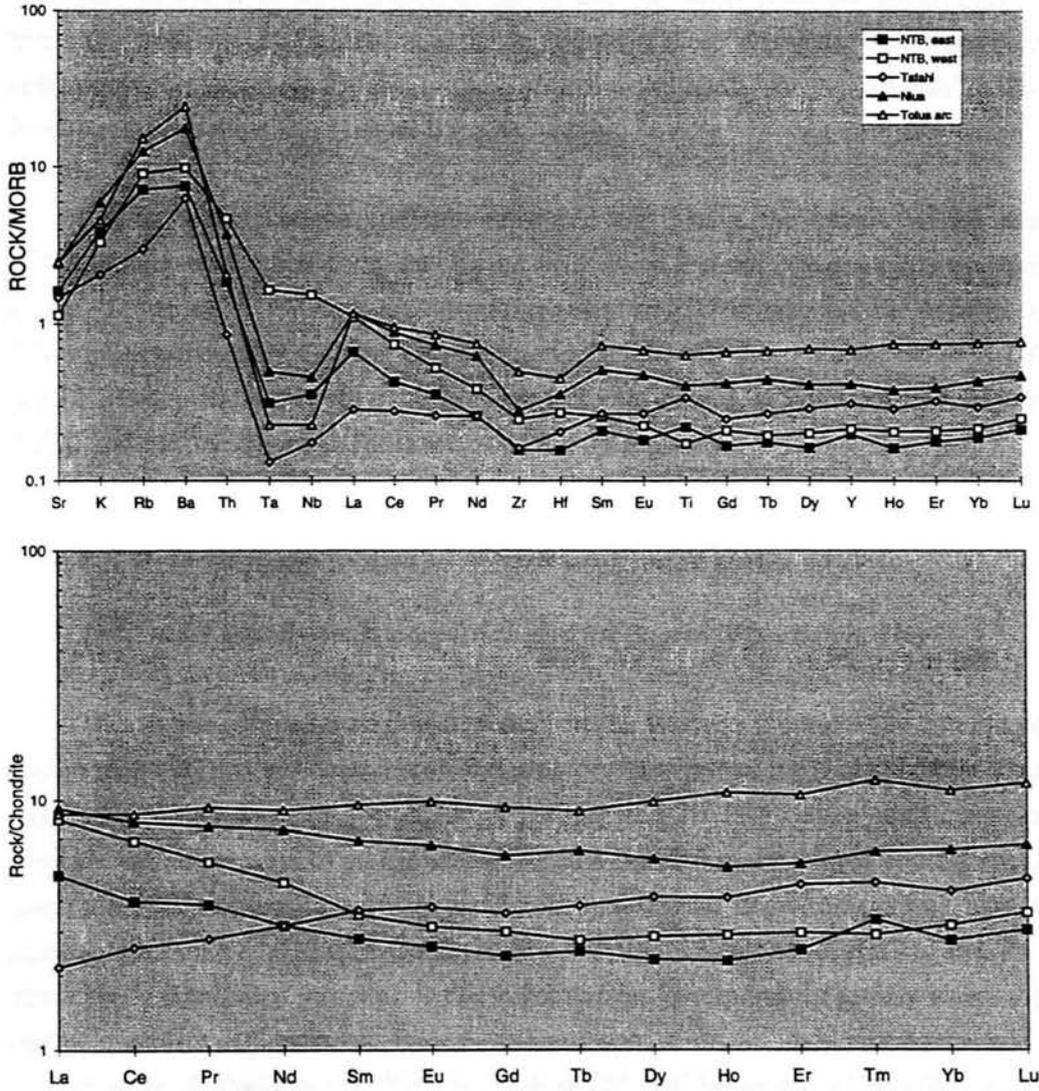
Figure 4.5(k) and (l) : N-MORB-normalised trace element variations and chondrite-normalised REE patterns of representative samples of the north Tongan boninites (NTB, east and west), Tafahi, Niuatoputapu and the Tofua arc to compare their trace element geochemistry.

87

(iii) all the lavas have depletions in Ta and Nb, apart from the north Tongan boninites from site 26, which have no depletion in these elements. The degree of depletion decreases from Tafahi, to the Tofua arc, the north Tongan boninite (east), Niuatoputapu to the north Tongan boninite (west).

(iv) the north Tongan boninites (east and west) have the lowest MREE and HREE abundances when compared to the lavas from Tafahi, Niuatoputapu and the central Tofua arc. They have a strong enrichment in LREE, whereas the lava from Niuatoputapu has only a slight LREE-enrichment; the one from Tafahi (TAF18/10) has LREE-depletion (but other samples from Tafahi have LREE-enrichment; Figure 4.5(f)) and the one from the Tofua arc has a flat REE pattern.

4.5 Petrogenesis from the major and trace element data

4.5.1 Mantle-source depletion and the degree of partial melting

The degree of mantle-source depletion can be taken to represent the amount of partial melt (%) that has been removed during previous partial melting episodes. This value is also dependent on the degree of melting and the distribution coefficients (a measure of the partition of an element between a mineral in the source and the melt) used: a similar composition can be produced by a smaller degree of melting from a less depleted source, as that from a more depleted source at higher degrees of melting. However, a significant variation in these parameters is required to greatly affect the degree of source depletion.

Pearce & Parkinson (1993) have modelled the behaviour of a selection of incompatible and compatible elements during melting for which there is no detectable slab contribution to the sources of arc volcanics. Details of the melting model applied are given in their paper. Table 4.1 and 4.2 present the partition and bulk distribution coefficients used in the modelling. Figure 4.6, which is taken from this paper, shows fertile MORB mantle- (FMM) normalised diagrams for these elements, of the melts produced from variably depleted mantle sources at different degrees of melting. As incompatible elements are preferentially taken up in the melts, the residual mantle becomes 'depleted' in them. Remelting of this 'depleted' mantle will therefore produce melts that are more highly depleted in incompatible elements (Figures 4.6(b)-(e)). Increasing the degree of melting will also decrease the incompatible element of the melt due to progressive dilution. Therefore, the incompatible element content of the melts is reduced by increasing the degree of melting and/or source depletion.

However, Figure 4.6(f) shows the variations in melt compositions for a constant degree of melting (10%) of variably-depleted mantle source. Figures 4.6(a) and (f) compare the relative effectiveness of source depletion and degree of melting in reducing the incompatible element content of the melts. They show that source depletion is a more effective method of doing this.
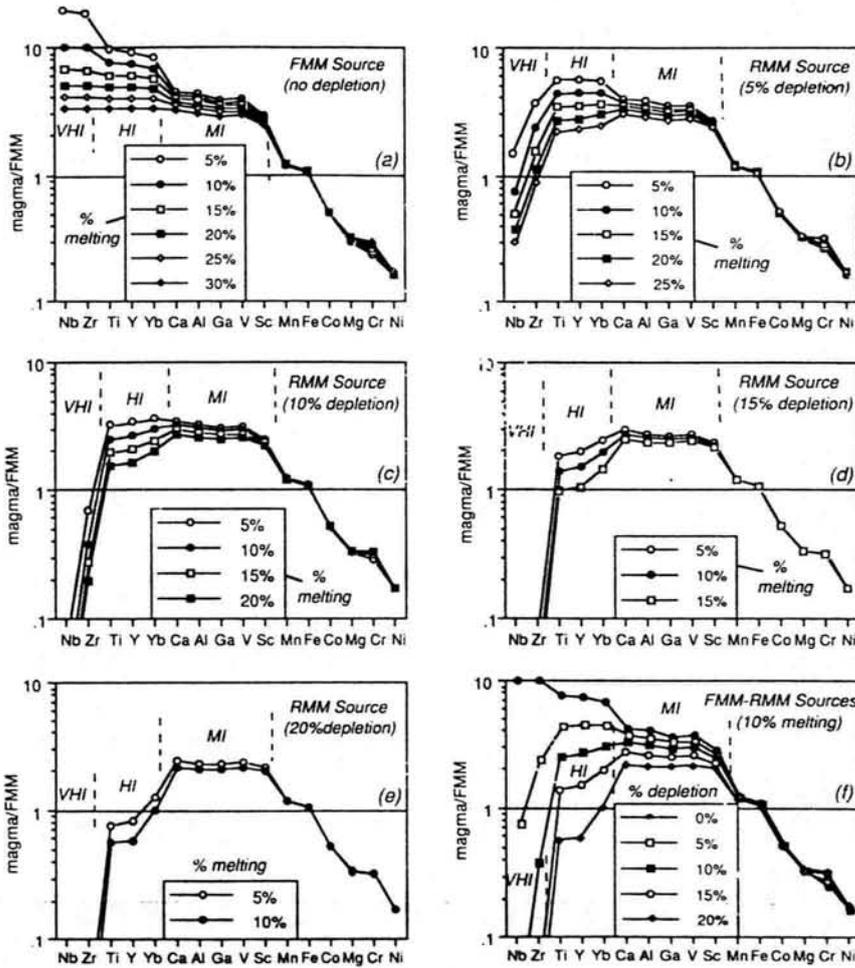
Figure 4.6: *Theoretical FMM-normalised patterns for sources of variable depletion or melt loss. Each diagram has been modelled for up to 30% melting (=sum of source depletion and % melting i.e. total melting). (f) modelling has used a constant degree of melting (10%) for a variably-depleted mantle. These diagrams show that increasing the degree of source depletion is a more effective method of depleting the incompatible element content of the melt than increasing the degree of partial melting.*

The observations made from this diagram are supported by the experimental studies of *Jaques & Green (1980)*, who produced magmas by anhydrous melting of pyrolite and depleted lherzolite. Melts produced from depleted lherzolite are strongly TiO$_2$ and alkali depleted, SiO$_2$-rich and strongly magnesian.

	ol/l		opx/l		cpx/l		gt/l		hbl/l		Al-sp/l		Data sources
	1300°C	1200°C	1300°C	1200°C	1300°C	1200°C	1300°C	1200°C	1300°C	1200°C	1300°C	1200°C	
Ni	9.0	15	2.5	4.5	1.5	2.5	1.3	2.5	1.5	2.0	7.5	12.0	3, 4, 10, 14, 15, 19, 31, 32
Cr	1.0	1.5	3.0	7.0	5.0	10	5.0	10	4.0	8.0	100	200	7, 10, 13, 14, 19, 31
Mg	3.9	4.2	2.8	3.2	1.9	2.1	2.2	2.4	1.5	1.6	3.0	3.5	8, 10, 18, 19, 21, 24, 34
Co	2.5	4.0	1.4	2.0	0.65	1.0	0.6	1.0	*1.0*	*1.4*	3.0	4.5	4, 7, 10, 15, 20, 27, 31
Fe	0.95	1.2	0.9	1.1	0.65	0.8	1.4	1.6	1.6	1.8	1.5	1.7	3, 5, 10, 18, 21, 29, 34
Mn	0.8	1.1	0.8	1.2	0.9	1.2	2.0	3.0	0.8	1.0	0.8	1.0	3, 4, 8, 10, 14, 18, 20, 21, 34
Sc	0.16	0.25	0.5	1.0	0.85	2.0	6.0	15.0	*1.0*	*2.0*	0.1	0.3	3, 4, 5, 13, 14, 15, 19, 25, 28, 31, 32
V	0.03	0.03	0.2	0.4	0.4	0.8	*0.8*	*1.3*	1.0	2.0	5.0	12.0	7, 10, 13, 14, 20, 30
Ga	*0.04*	*0.1*	*0.3*	*0.4*	*0.35*	*0.6*	*0.6*	*1.2*	*1.0*	*1.2*	*4.0*	*4.0*	22
Al	0.03	0.004	0.03	0.5	0.3	0.5	*1.5*	*1.5*	*1.0*	1.0	4.0	4.0	3, 4, 5, 10, 18, 21, 34
Ca	0.025	0.03	0.18	0.2	1.2	1.3	0.45	0.6	*1.0*	1.0	0.02	0.03	3, 4, 5, 8, 10, 19, 21
Yb	0.015	0.025	0.11	0.2	0.5	0.75	4.0	7.0	0.6	1.0	0.001	0.01	3, 4, 5, 8, 11, 15, 16, 21, 24, 25, 35
Y	0.005	0.015	0.08	0.15	0.5	0.7	1.0	2.0	0.6	1.0	0.001	0.01	3, 4, 5, 8, 11, 12, 15, 16, 21, 24, 25
Ti	0.01	0.04	0.11	0.25	0.35	0.4	0.3	0.4	1.2	2.0	0.1	0.15	1, 2, 7, 10, 12, 15, 16, 17, 18, 21, 28, 34
Zr	0.005	0.008	0.08	0.06	0.15	0.18	0.2	0.3	0.25	0.4	*0.01*	*0.02*	8, 11, 12, 15, 17, 22, 26, 35
Nb	0.001	0.001	0.01	0.01	0.06	0.08	0.1	0.01	0.3	0.6	*0.01*	*0.02*	8, 12, 14, 15, 16, 22
Al (15kb)			0.4	0.6	0.8	1.6					Cr-sp/l		
Al (1atm)			0.08	0.1	0.2	0.4					Cr 300	600	
											Al,Ga 1	1	

Table 4.1: The set of partition coefficients used in Pearce & Parkinson (1993) and to calculate the FMM-normalised patterns in Figure 4.6. Major element coefficients are for wt% oxides. Data sources used are 1: Bartels et al. (1991); 2: Beattie (1993); 3: Beattie et al. (1991); 4: Colson et al. (1988); 5: Colson & Gust (1989); 6: Dostsl et al. (1983); 7: Duke (1976); 8: Dunn (1987); 9: Dunn & McCallum (1982); 10: Dupuy et al. (1980); 11: Fujimaki et al. (1984); 12: Green et al. (1989); 13: Hervig et al. (1986); 14: Irving (1978); 15: Irving & Frey (1984); 16: Johnson & Kinzler (1989); 17: Kato et al. (1987); 18: Kinzler & Grove (1992); 19: Leeman & Scheidegger (1977); 20: Lindstrom & Weill (1978); 21: Liu et al. (1992); 22: McCallum & Charette (1987); 23: McKay & Mitchell (1988); 24: Mckay (1986); 25: Neilsen et al. (1992); 26: Ohtani et al. (1989); 27: Onuma et al. (1968); 28: Ray et al. (1983); 29: Roeder & Emslie (1970); 30: Shervais (1982); 31: Stosch (1981); Stosch & Seck (1980); 33: Takahashi (1978); 34: Tormey et al. (1987); 35: Watson et al. (1987). Coefficients based on a single value, or a series of inconsistent values, are given in italics. Data sources cited in Pearce & Parkinson (1993).

To illustrate the effect of mantle source characteristics on the major element composition of the lavas from north Tonga, their CaO/TiO_2 ratios have been plotted against their Al_2O_3/TiO_2 ratios (Figure 4.7). The idea of this plot is that the degree of mantle source depletion is reflected in the CaO/TiO_2 and Al_2O_3/TiO_2 ratios of the derived melts (*Sun & Nesbitt, 1978*). For comparison, data from the north Tongan

	sp. lhz.		gt. lhz.		hbl. lhz.		hz.	
	1300°C	1200°C	1300°C	1200°C	1300°C	1200°C	1300°C	1200°C
Ni	6.19	10.39	6.19	10.42	6.25	10.45	7.95	13.29
Cr	4.01	8.00	2.18	4.27	1.99	3.93	4.31	8.37
Mg	3.30	3.61	3.32	3.63	3.28	3.58	3.72	4.03
Co	1.96	3.06	1.91	3.01	1.99	3.09	2.33	3.69
Fe	0.90	1.12	0.97	1.20	1.00	1.23	0.95	1.19
Mn	0.80	1.13	0.95	1.35	0.80	1.12	0.80	1.12
Sc	0.34	0.67	0.95	2.24	0.37	0.70	0.21	0.37
V	0.22	0.47	0.18	0.31	0.19	0.37	0.11	0.21
Ga	0.23	0.32	0.18	0.33	0.22	0.32	0.09	0.16
Al	0.20	0.28	0.26	0.32	0.20	0.26	0.06	0.09
Ca	0.21	0.23	0.19	0.23	0.22	0.23	0.05	0.06
Yb	0.10	0.16	0.53	0.92	0.12	0.21	0.03	0.05
Y	0.09	0.14	0.17	0.32	0.11	0.18	0.02	0.04
Ti	0.08	0.14	0.09	0.15	0.18	0.32	0.03	0.07
Zr	0.03	0.04	0.05	0.07	0.05	0.07	0.01	0.02
Nb	0.01	0.01	0.02	0.01	0.04	0.07	0.003	0.003

Table 4.2: Table of bulk distribution coefficients of spinel, garnet and hornblende lherzolite and harzburgite at 1300°C and 1200°C for the elements used in the FMM-normalised pattern (Figure 4.6) and used in the modelling of Pearce & Parkinson (1993). Compatible elements are towards the top of the table, whereas highly incompatible elements are towards the bottom. The mantle compositions are taken to be : Spinel lherzolite, 0.575 ol+0.27 opx + 0.125 cpx + 0.02 Al-sp; Garnet lherzolite, 0.6 ol + 0.21 opx + 0.075 cpx + 0.115 gt; Hornblende lherzolite, 0.6 ol + 0.25 opx + 0.04 cpx + 0.11 hbl; Harzburgite, 0.83 ol + 0.16 opx + 0.01 Cr-sp. A table of the partition coefficients and the data sources are given in Pearce & Parkinson (1993).

boninites, Tafahi, Niuatoputapu, the central Tofua arc islands of Ata, Fonualei and Late, the Northern Lau Spreading Centre and the Central and Eastern Lau Spreading Centres have been plotted on the CaO/TiO_2-Al_2O_3/TiO_2 diagram (Figure 4.7). The north Tongan boninites and Tafahi lavas have higher CaO/TiO_2 and Al_2O_3/TiO_2 ratios (i.e. more 'depleted') than the Tofua arc, the Northern and Central Lau Spreading Centres and the Lau Basin lavas. Before Figure 4.7 can be interpreted entirely in terms of mantle source characteristics, the effects of fractional crystallisation and phenocryst accumulation have to be considered, as these processes have a marked

effect on the major element composition of the lavas. Plagioclase accumulation or fractionation will particularly affect the CaO/TiO_2 and Al_2O_3/TiO_2 ratios, increasing and decreasing them respectively.

An arrow has been drawn from a specific sample from Tafahi (TAF8) to represent the compositional vector for 20% plagioclase subtraction (for plagioclase composition An_{70}). Clearly, plagioclase accumulation can considerably increase the Al_2O_3/TiO_2 and CaO/TiO_2 ratios. To test the effects of plagioclase fractionation and
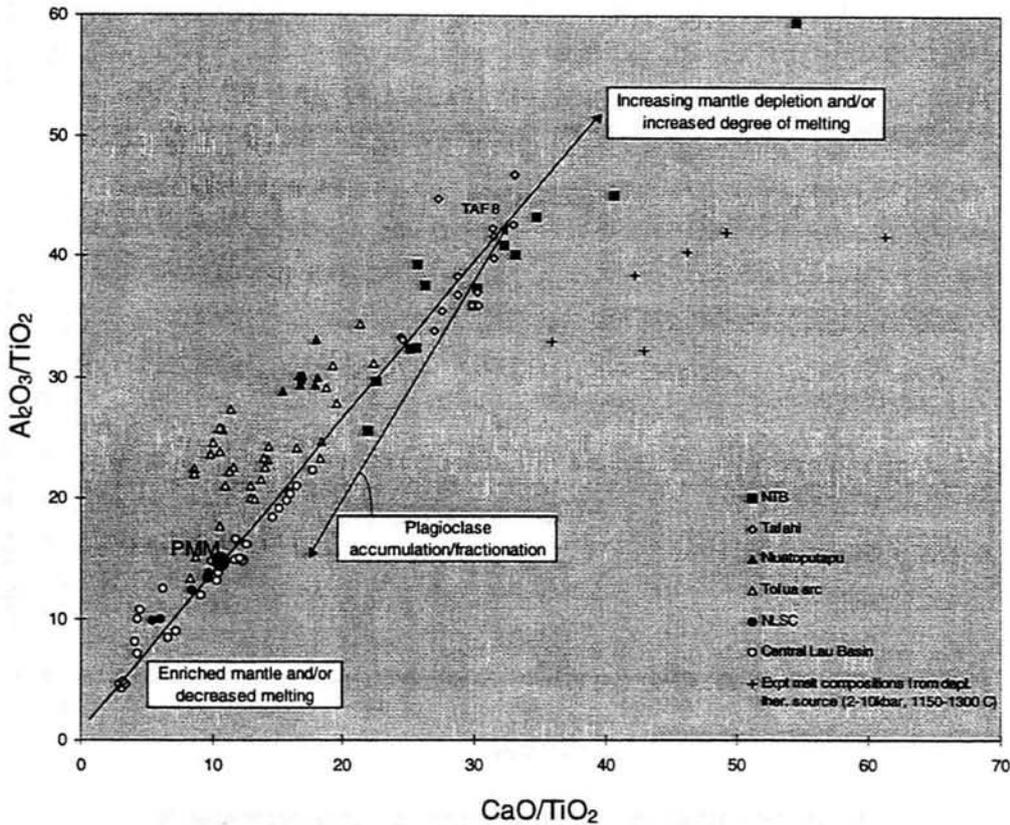
Figure 4.7: A plot of the CaO/TiO_2 ratios versus the Al_2O_3/TiO_2 ratios for the north Tongan boninites (NTB), the lavas from Tafahi, Niuatoputapu, the central Tofua arc, the Northern Lau Spreading Centre (NLSC) and the Central Lau Basin. The composition of Primitive MORB mantle (PMM) and melts produced from depleted lherzolite at 2-10kbar and 1150-1300°C in experiments (Jaques & Green, 1980) are also plotted. An increase in source depletion and/or the degree of melting causes an increase in the CaO/TiO_2 and Al_2O_3/TiO_2 ratios of the melts produced from that source (Sun & Nesbitt, 1978). Therefore, the trend for increasing mantle depletion and/or degree of melting is as shown. The vector for 20% plagioclase subtraction from a Tafahi sample (TAF8) is plotted to show that plagioclase accumulation can considerably increase the CaO/TiO_2 and Al_2O_3/TiO_2 ratios and therefore needs to be considered.

accumulation on the CaO/TiO_2 and Al_2O_3/TiO_2 ratios of the lavas, plots of their plagioclase phenocryst content versus CaO/TiO_2 and Al_2O_3/TiO_2 ratios have been made (Figure 4.8). Lines drawn through the data and extrapolated to zero phenocryst
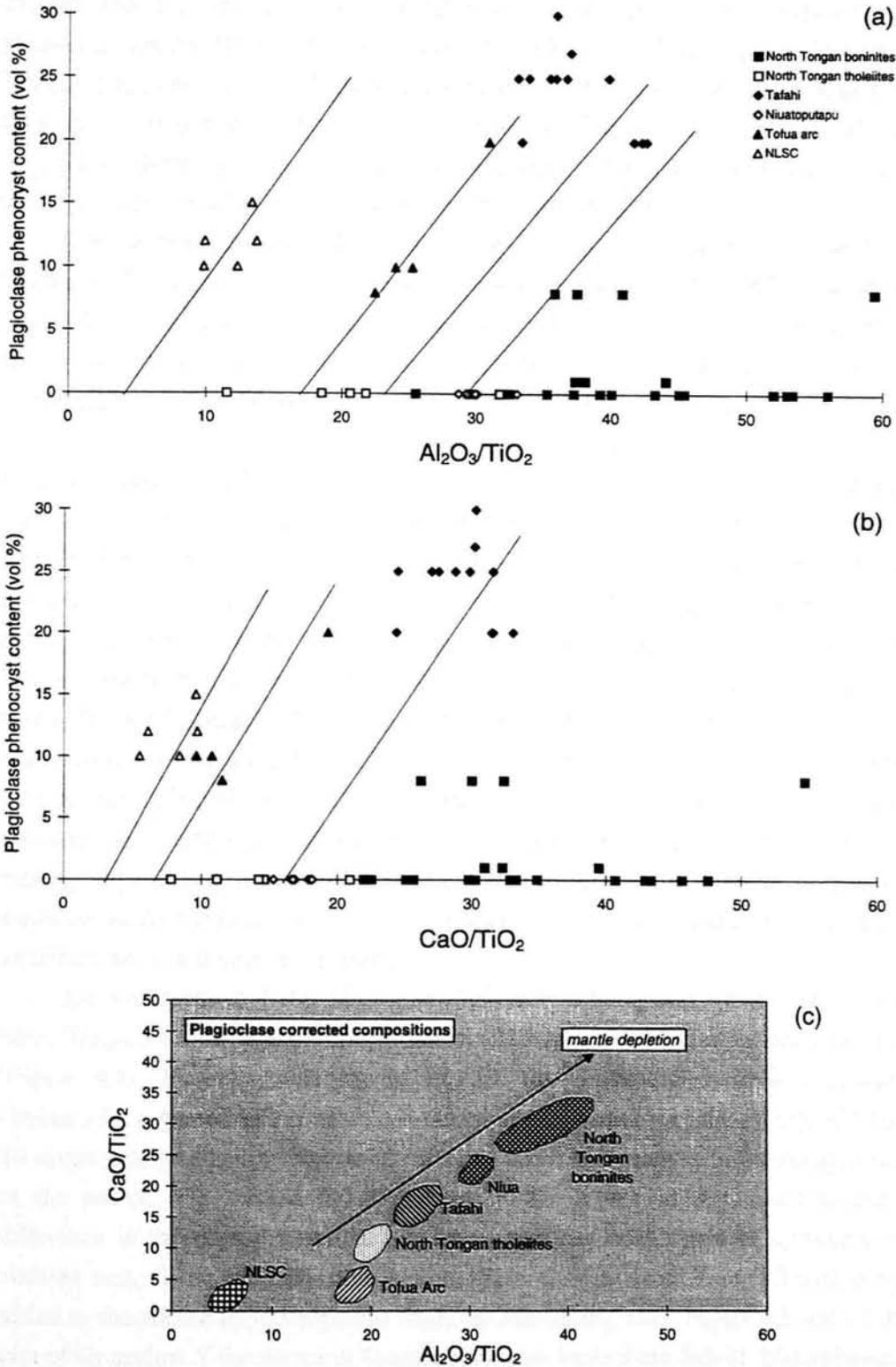
Figures 4.8(a)-(c): *(a) and (b) are plots of the plagioclase phenocryst content (volume %) of the lavas versus the Al_2O_3/TiO_2 and CaO/TiO_2 ratios respectively. Lines are drawn through the data to zero phenocryst content which gives the values of the Al_2O_3/TiO_2 and CaO/TiO_2 ratios corrected for plagioclase accumulation. This method assumes that all the plagioclase phenocrysts are accumulated, and therefore it is likely to overcorrect. (c) A plot of the CaO/TiO_2 vs Al_2O_3/TiO_2 ratios for the plagioclase corrected compositions. The north Tongan boninites have the most depleted source, then Tafahi, Niuatoputapu, the north Tongan tholeiites, the Tofua arc and finally the Northern Lau Spreading Centre, in the order of decreasing source depletion.*

93

content give the values of the CaO/TiO$_2$ and Al$_2$O$_3$/TiO$_2$ ratios, corrected for plagioclase accumulation. These values are then plotted on Figure 4.8(c). The north Tongan boninites have the highest CaO/TiO$_2$ and Al$_2$O$_3$/TiO$_2$ ratios and therefore have the most depleted sources. This method of correction assumes that all the plagioclase phenocrysts in the lavas are accumulated, rather than crystallising in situ in the lava, and therefore, it is likely that this method overcorrects.

The compositions of melts produced in melting experiments on a depleted lherzolite (Tinaquillo) in the pressure range 2-10kbar, and 1150°C-1300°C (*Jaques & Green, 1980*), are also plotted on Figure 4.7, for comparison with the compositions of the lavas. These ranges are chosen to be consistent with the upper range of temperatures of crystallisation obtained from two pyroxene geothermometry (Section 3.9) for the north Tongan boninites and Tafahi lavas, which is likely to be similar to melting temperatures. The lower temperature range is not used as it is likely not to correspond to melting temperatures because the magma temperature decreases with crystallisation. The experimental melts have high CaO/TiO$_2$ and Al$_2$O$_3$/TiO$_2$ ratios and their CaO/TiO$_2$ ratios are higher for a given Al$_2$O$_3$/TiO$_2$ ratio compared to the other lavas. All the lavas (corrected for fractionation), except some of the north Tongan boninites, have lower CaO/TiO$_2$ and Al$_2$O$_3$/TiO$_2$ ratios than those of the melts. The north Tongan boninites have the most similar CaO/TiO$_2$ and Al$_2$O$_3$/TiO$_2$ ratios to those of the melts from the depleted lherzolites, but the melts from the latter have higher CaO/TiO$_2$ ratios. This suggests that either the depleted lherzolites have different compositions to the sources of all the lavas from north Tonga, or that the melting experiments could not reproduce the conditions of melting at subduction zones due to the complexities of hydrous melting (see Figure 1.2), and therefore melts generated are of a different composition.

The variations in CaO, Al$_2$O$_3$ and MgO within the groups of the lavas from north Tonga have been explained in terms of crystal fractionation or accumulation (Figure 4.4). However, this cannot explain the concentration of incompatible elements for a given MgO content, and the Ni and Cr contents of the groups of lavas. To investigate whether this can be explained in terms of variations in the composition of the source (e.g. caused by differences in the degree of depletion) and/or a difference in the degree of partial melting, a plot has been made of a compatible element (e.g. Cr or Ni) against an incompatible element (e.g. Y or Ti) that is not added to the source by a component from the subducting slab. Figure 4.9 shows the plot of Cr against Y for the north Tongan boninites, lavas from Tafahi, Niuatoputapu, the Tofua arc and the Northern Lau Spreading Centre. Vectors for the effects of 20% fractional crystallisation of olivine, clinopyroxene, orthopyroxene, and plagioclase and 0.1% fractional crystallisation of Cr-spinel are also shown. In the description of

this plot it has been assumed that there was a constant degree of melting. Melting trends are superimposed on this plot using equations, distribution coefficients and parameters from *Murton et al. (1992)* and *Parkinson et al. (1992). Parkinson et al. (1992)* show, using peridotite data from the Izu-Bonin forearc, that pooled fractional melting (or incremental melting with very small increments) best approximates the melting process. Therefore, the composition of pooled melts from 10% fractional melting, at varying degrees of depletion (0-30%), for a MORB-mantle source (Cr = 2600 ppm, Y = 4 ppm) has been superimposed on Figure 4.9. The composition of melts from equilibrium (batch) melting, at varying degrees of depletion, has also been superimposed on the diagram. These compositions show that equilibrium melting cannot explain the low concentrations of Y in the most depleted lavas.

The north Tongan boninites have low Y contents (4-9 ppm) relative to the lavas from Tofua arc (10-22 ppm), the Northern Lau Spreading Centre (20-40 ppm) and the Central Lau Spreading Centre (17-170 ppm). They have a high Cr content (400-1250 ppm), whereas the lavas from Tafahi, Niuatoputapu, the Northern and Central Lau Spreading Centres have lower Cr contents.

The north Tongan boninites exhibit a variation in Cr and Y contents that can be explained by a small amount of olivine, clinopyroxene and orthopyroxene fractionation. The lavas from Tafahi and Niuatoputapu require higher degrees of fractionation of an assemblage that includes plagioclase, which decreases the Cr and increases the Y contents. The low Y content of the boninites is a result of their highly depleted source (15-20%), assuming 10% fractional melting. This is consistent with the predictions for boninitic magmas made by *Pearce & Parkinson (1993)*. The lower Y contents of the boninites compared to those of the lavas from the Tofua arc shows that their source is more depleted than that of the Tofua arc lavas. The lavas from Tafahi have undergone a greater fractionation of olivine, spinel and two pyroxenes than the north Tongan boninites, as shown by their lower Cr contents. However, the lavas from Tafahi, Niuatoputapu and the north Tongan boninites have similar Y contents, suggesting that their sources are likely to have undergone similar degrees of depletion. The lavas from Niuatoputapu have similar Cr contents to the more fractionated lavas from the Tofua arc, but have lower Y contents suggesting that their source was more depleted than that of the Tofua arc.

Figure 4.9 also shows that the lavas from Niuatoputapu can be formed by fractionation of clinopyroxene and orthopyroxene, and plagioclase from magmas with Cr-Y contents similar to the lavas of Tafahi. This is evidence that the lavas from Tafahi and Niuatoputapu may have a similar source and could be related by simple fractionation.

The lavas from the Northern Lau Spreading Centre and the Central Lau Spreading Centre lie in the MORB compositional field, suggesting that their source is more fertile.
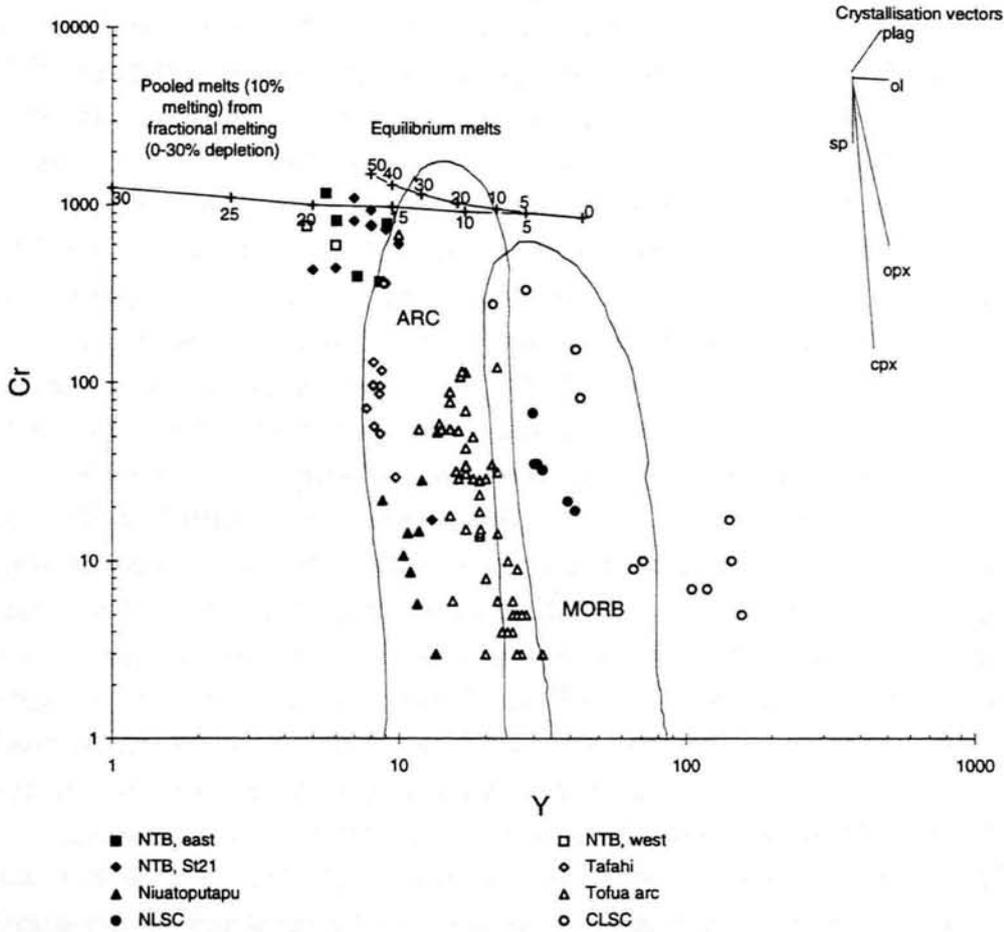
Figure 4.9: *A Cr-Y plot for the north Tongan boninites, Tafahi, Niuatoputapu, the Tofua arc and the Northern Lau Spreading Centre. Fields for arc volcanics and MORB (Pearce, 1975, 1982) are shown. The composition of pooled melts from 10% melting by fractional melting and equilibrium melts of a source that has been variably depleted (0-30%) are shown (Murton et al., 1992). Vectors for 20% fractional crystallisation of olivine, clinopyroxene, orthopyroxene and plagioclase and 0.1% fractional crystallisation of Cr-spinel.*

4.5.2 Possible explanations of the HFSE depletions in the subduction-related lavas?

The depletions in HFSE (Nb, Ta, Zr and Hf) relative to the REE and LILE observed on MORB-normalised trace element patterns is recognised as a geochemical characteristic of subduction-related lavas (*Pearce & Norry, 1979; Arculus & Powell,*

1986; Wilson, 1989; McCulloch & Gamble, 1991; Woodhead et al., 1993; Kelemen et al., 1990, 1993; Thirlwall et al., 1994). However, the explanation for this depletion is a controversial subject.

Briqueu et al. (1984) proposed that it is possible to produce the HFSE depletions observed in subduction-related magmas if titano-magnetite phases, such as titanite or rutile, were residual in their source. These minerals preferentially retain HFSE, particularly Nb, during partial melting due to their high mineral/melt partition coefficients (Average $K_dNb=26.5$, $K_dTa=44.0$ for rutile/andesitic melt; *Green & Pearson, 1987*). However, later work by *Ryerson & Watson (1987)* shows experimentally that basaltic and andesitic liquids need between 7 and 9 wt%, and 5 and 7 wt%, respectively, of TiO_2 in the liquid for rutile saturation at 8-30kbar. This pressure range is within that of magma generation at subduction zones. These TiO_2 concentrations are in excess of the concentrations found in subduction-related magmas, which contain less than 3 wt% TiO_2. Therefore, rutile could not be a residual phase at the conditions of magma genesis in subduction zones.

The presence of amphibole in the source is another mechanism for explaining the HFSE depletions in these magmas (*Woodhead et al., 1993; Wharton unpubl., 1993*). However, *Green (1973)* shows experimentally that amphibole should not be retained in the mantle at temperatures above 1200°C and conditions of water content of about 0.2%, which are similar to the conditions of magma genesis of the north Tongan boninites and the lavas from Tafahi ($T_{prim.mag.}$~1090-1230°C; Section 3.9). Therefore, residual amphibole is also not a viable option for explaining the HFSE depletions of the subduction-related volcanics of Tonga.

Other options use chromatographic processes to fractionate HFSE from REE (*Navon & Stolper, 1987; Kelemen et al., 1990, 1993*). *Navon & Stolper (1987)* propose that the mantle can behave like a chromatographic column, and therefore, as melt percolates through it, a mantle/melt interaction occurs due to their chemical disequilibrium. This interaction involves ion-exchange between the melt and the mantle, which will depend on the concentration and transport velocities of the ions in the melt, the partition coefficients of the elements and the diffusion rates. This leads to the fractionation of elements depending on their compatibility and transport velocities through the mantle. In order to generate the depletions in HFSE observed in subduction-related volcanics, the percolating melt in a Navon & Stolper-type chromatographic column has to pass through mantle that contains minerals which will retain HFSE after interaction. Amphibole is a possible retaining mineral, but as shown by *Green (1973)*, it is not stable in the mantle at the temperatures of boninite and Tafahi lava magma genesis.

Kelemen et al. (1990, 1993) have developed a different mantle/melt interaction model to explain the HFSE depletion in subduction-related magmas. They propose that as melt migrates up through the mantle wedge, it simultaneously dissolves out phases that have relatively low abundances of HFSE from the mantle, such as pyroxenes, and precipitates out phases with high HFSE abundances, and therefore develops a HFSE depletion.

Both of these models are elegant ways of explaining the depletions in HFSE and M-HREE observed in subduction-related volcanics, but they are dependent on many factors, particularly the accuracy and consistency of the partition coefficients used. *Kelemen et al. (1990)* note that not all the partition coefficients for the REEs, Ti and Zr which they used in their modelling were measured in the same experiment, which suggests that there could be errors in the modelling. Another problem with these models is the lack of knowledge of intracrystalline diffusion rates for trace elements in the phases present in the mantle wedge, which control the ion-transfer processes. If these rates are very much less than the transport velocities of the migrating melt then there is not enough time for a mineral/melt interaction to occur. The way the melt migrates, whether it migrates along porous or channel flows *(Iwamori, 1992, 1993)* will also determine if the melt remains chemically isolated from the surrounding mantle.

I prefer to explain the HFSE depletions in terms of differences in the depletion of the sources. Evidence that first linked the HFSE depletions in arc volcanics to mantle source depletion were the petrological observations that subduction zone peridotites are more depleted (i.e. they have had a higher amount of partial melt extracted) than the most refractory oceanic peridotites *(Bonatti & Michael, 1989; Dick & Fisher, 1984)*. Also, primitive arc-basalts crystallise extremely magnesian olivines (>Fo_{92}), which are slightly more magnesian than those from the north Tongan boninites (Fo_{88} to Fo_{91} Section 3.7), and Cr-rich spinels (100X$Cr/(Cr+Al)$) of 60-90). These occurrences can be associated with magma compositions derived from refractory peridotites.

Pearce & Parkinson (1993) demonstrated that the HFSE depletions of arc volcanics can be produced by the removal of a small (up to 5%) melt fraction from a source similar in composition to MORB-mantle, in spinel facies, prior to their production. They modelled the behaviour of a selection of HFSE and compatible elements for which the mantle contribution greatly exceeds any subduction contribution, during partial melting. Their models predict that the more extreme depletions in HFSE of boninites can be explained by extraction of 15% of melt from their sources prior to magma genesis. *Woodhead et al. (1993)* arrive at similar conclusions to explain the lower average abundances of incompatible HFSE and Y,

and the higher Ti/Zr, V/Ti and Sc/Y ratios of arc-volcanics compared with basalts from their adjacent back-arc basins. *Ewart & Hawkesworth (1987)* explain the increase in depletion in HFSE and H-MREE of the volcanics from south to north along Tofua arc by an increase in their source depletion. They suggest that the greater depletions of the sources of the volcanics from the northern islands can be explained if the greatest loss of melt has occurred from the back-arc basin mantle sources in the northern Lau Basin than in the southern Lau Basin.

Figure 4.10 is a FMM- (fertile MORB mantle or N-MORB) normalised diagram for the same selection of elements as those that *Pearce & Parkinson (1993)* modelled, for the north Tongan boninites (east and west), a lava from Tafahi, Niuatoputapu and the Tofua arc (Late). Normalising values are taken from *Pearce & Parkinson (1993)* and are also shown in Appendix 4. Table 4.2 shows bulk distribution coefficients for these elements for spinel, garnet and hornblende lherzolite and harzburgite, used in the modelling and shows the differences between the values for compatible elements ($D_{sp.lhz}.Cr=8.00$ at 1200°C) compared to those of incompatible elements ($D_{sp.lhz}.Nb=0.01$ at 1200°C). Either primitive compositions or compositions extrapolated to MgO=9 wt% are used for this plot.

Figure 4.10 shows that:

(a) the north Tongan boninites have FMM-normalised abundances in the order of VHI>HI<MI, where VHI are very highly incompatible elements, HI are highly incompatible elements and MI are moderately incompatible elements;

(b) the lavas from Tafahi have FMM-normalised abundances in the order of VHI≤HI<MI;

(c) the lavas from Niuatoputapu have a similar pattern to Tafahi, but are less enriched in Nb and some of the HI elements;

(d) the Tofua arc have FMM-normalised abundances in the order of VHI<HI≥MI;

(e) the lavas from the Northern Lau Spreading Centre have a pattern in the order of VHI=HI=MI, whereas the Samoa shield volcanics have one with VHI>>HI>MI.

The shapes of the patterns are dependent on the melting and depletion/enrichment events in the mantle. The patterns for the north Tongan boninites, Tafahi and Niuatoputapu are similar to theoretical patterns for melts produced from high degrees of melting of a depleted source (Figure 9(c)-(e) and Type 7 of Figure 11(g) of *Pearce & Parkinson, 1993*). However, all these patterns have higher concentrations of VHI elements than the theoretical modelling (Figure 9 of *Pearce & Parkinson, 1993*) which predicts that these elements are highly depleted in

melts from depleted sources. This is because VHI elements are preferentially taken up in melts produced from prior melting events due to their incompatibility ($D_{Nbsp. lhz.}$=0.01, $D_{Zrsp. lhz.}$= 0.04 at 1200°C; Table 4.1), leaving the residual mantle depleted. When this residual mantle is remelted the subsequent melts are also depleted in VHI elements. However, the north Tongan boninites and the lavas from Tafahi and Niuatoputapu do not have
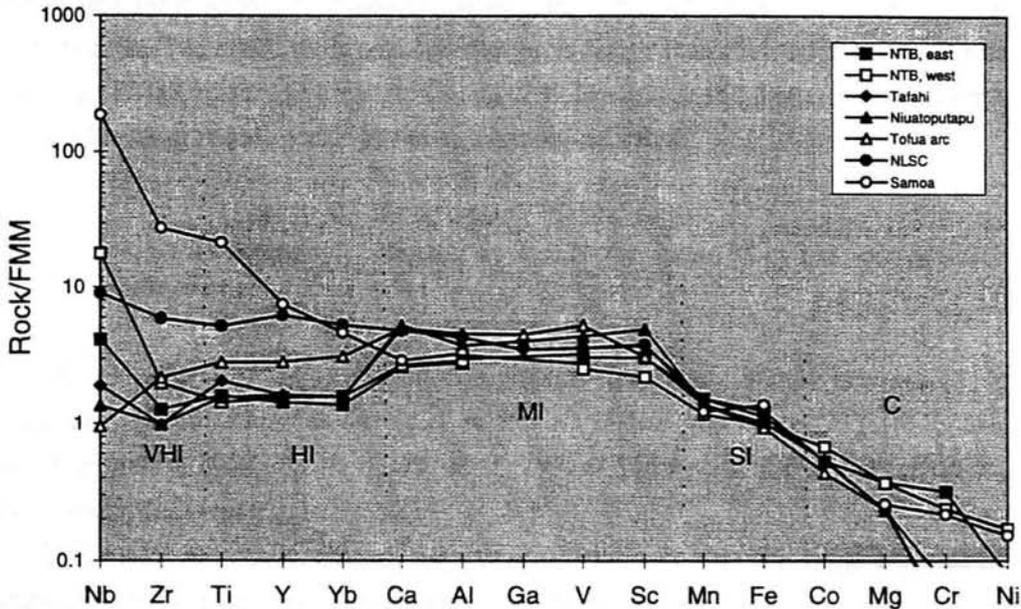
Figure 4.10: A fertile MORB mantle-(FMM) normalised pattern for a selection of HFSE and compatible elements for representative samples of the north Tongan boninites, Tafahi, Niuatoputapu, Tofua arc and the Samoan shield volcanics. Normalising values are taken from Pearce & Parkinson (1993). The data has been adjusted to MgO=9 wt%. VHI, very highly incompatible; HI, highly incompatible; MI, moderately incompatible; SI, slightly incompatible; C, compatible.

extremely low FMM-normalised abundances of VHI elements suggesting that either there has been some addition of these elements to their sources, or that their sources were 'enriched' relative to FMM.

The pattern for the Tofua arc is similar to the theoretical one for melts produced from high degrees of melting of a slightly depleted source (Type 5, Figure 11(e) of *Pearce & Parkinson, 1993*).

It is not particularly useful to compare the degrees of depletion of the lavas on Figure 4.10 as this assumes that they all have a FMM source. However, their sources may be more enriched, (or more depleted), than FMM and therefore, their actual depletion may be greater, (or less), than their apparent depletion relative to FMM, observed on Figure 4.10. For instance, the north Tongan boninites, and the lavas from Tafahi and Niuatoputapu have plume mantle rather than FMM sources, which are

more enriched, indicated by their high FMM-normalised Nb abundances compared with their HI element abundances (see also Figure 4.12). Undepleted plume mantle produces melts with a FMM-normalised pattern similar to Samoa, characterised by high abundances of all incompatible elements (Figure 4.10). Therefore, to explain the FMM-normalised patterns of the north Tongan boninites, the lavas from Tafahi and Niuatoputapu, their sources have to be residual plume-mantle in order to produce their considerable depletion compared with the pattern of a melt from non-residual plume-mantle. Therefore, their actual depletion is larger than their apparent depletion relative to FMM, observed on Figure 4.10. It is likely that the Tofua arc lavas have sources similar to FMM, which has been variably-depleted.

4.5.3 Incompatible element evidence for identifying the end-member components

The presence of end-member components has been widely recognised in subduction related volcanics (*Arculus & Powell, 1986; Wheller et al., 1987; Lin, Stern & Bloomer, 1989; Hawkesworth et al., 1991a; Stern et al., 1991; Tatsumi et al., 1991, 1992; McDermott et al., 1993*).

The major and trace element data provide evidence that the lavas from north Tonga are derived from a combination of (1) a variably-depleted source, (2) a component enriched in LILE ± LREE, and in the case of the North Tongan boninites, Tafahi and Niuatoputapu and the Northern Lau Spreading Centre lavas, (3) a contribution from a component enriched in LREE and HFSE.

Tatsumi, (1989) proposed that fluids are initially released from the slab by dehydration, at a depth of around 90km, due to the increasing pressure and temperature to which the downgoing slab is subjected. This fluid reacts with anhydrous mantle wedge above the slab to produce hydrous minerals (serpentine, talc, amphibole, chlorite and phlogopite). This hydrated peridotite is dragged down with the slab until it reaches depths of around 100km (depth of amphibole stability), when the hydrous minerals begin to dehydrate and release water. This hydrous component migrates laterally to the base of the melting column as shown in Figure 4.11 and Figure 2.1. This process has been theoretically modelled by *Tatsumi et al. (1993), Davies & Bickle (1991)* and *Davies & Stevenson (1992)*. Melting is initiated at the base of the melting column due to the depression of the mantle solidus by the presence of the fluid. The degree of melting that occurs will be dependent on the amount of this depression, the extent of adiabatic upwelling above the solidus and the composition of the mantle prior to melting.

Dehyration experiments on synthetic serpentine spiked with trace elements (Cs, Rb, K, Ba, Sr, La, Sm, Tb, Y, Yb and Nb) carried out by *Tatsumi et al. (1986)*, to represent the dehydrating process in the subducting slab, show that elements with a larger ionic-radius are more readily transported by an aqueous fluid phase during this process. This suggests that these elements are more likely to be carried in fluids from the dehydrating slab to the base of the melting column of the arc-volcanics. These fluids enrich the mantle in these elements, and due to their incompatibility during partial melting, the magmas produced during melting are also enriched. Therefore, it seems likely that the LILE (K, Ba, Sr and Th) enrichment observed in the lavas from north Tonga originates from a slab-derived fluid. Some of the LREE may also be carried by this fluid as well, as these elements have a moderate to high ionic-radius and are therefore incompatible.
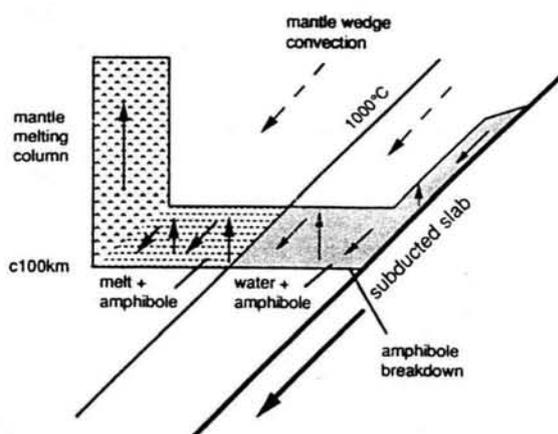
Figure 4.11: *Diagram illustrating the mechanism for melting above subduction zones, as proposed by Tatsumi et al. (1983), Davies & Bickle (1991) and Davies & Stevenson (1992), taken from Pearce & Parkinson (1993). The arrows indicate transport of mantle (dashed line), aqueous fluid (thin line), melt (intermediate line) and subducted slab (thick line).*

A second 'enriched' component has been recognised in other boninites and lavas from north Tonga (*Falloon & Crawford, 1991; Volpe et al., 1988; Sunkel, 1991*). This component is characterised by a LREE-enriched signature and high concentrations of HFSE. The U-shaped chondrite-normalised REE plot, which is a common feature of boninites (*Hickey & Frey, 1982*; Figure 4.5(b)), and enrichments in VHI elements compared with HI ones (Figures 4.10 and 4.5(a)) are usually attributed to this component. This component is likely to originate from the Samoan plume, but further evidence from other trace element plots (Figure 4.12) and the isotopes (Figures 5.6, 6.3, 6.4 and 6.5) are required to confirm its presence.
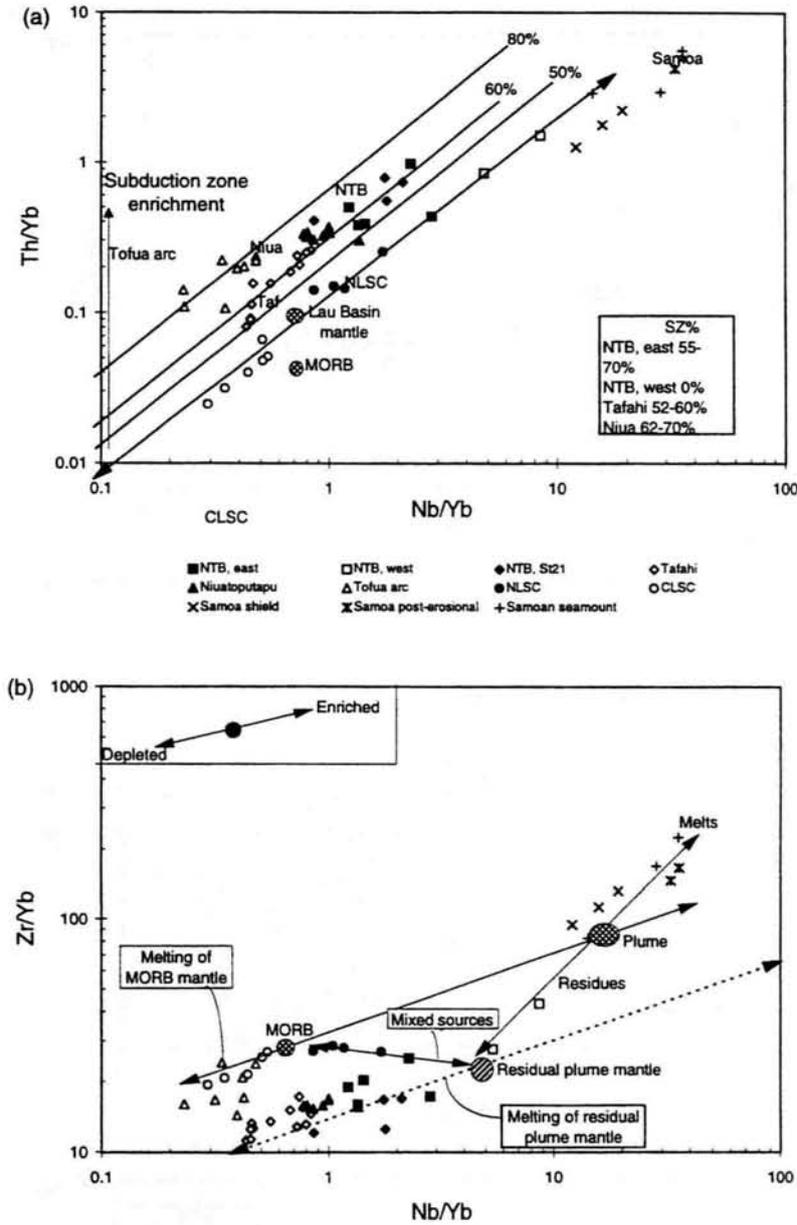
Figures 4.12 (a)-(h) : Plots of M/Yb vs Nb/Yb for the north Tongan boninites (NTB), from the east ('Kallisto' ophiolite section), site 26 from the west, and from Station 21 of the 'Natsushima' 1984 cruise, Tafahi, Niuatoputapu, the Samoan shield (SSh) and post-erosional volcanics (SPE) and seamount (SS), the Northern and Central Lau Spreading Centres (NLSC and CLSC) and the Tofua arc (Pearce et al., 1995). The double-headed arrow (solid) represents the MORB- plume array, which is the variation in the compositions of average N-MORB and arc volcanics (from Pearce, 1982; Pearce & Peate, 1995; Sun & McDonough, 1989). This array is produced by melting of variably-depleted MORB mantle in spinel facies. The dashed double-headed arrows represent the array of compositions produced by melting of variably-depleted residual plume mantle in spinel facies. The lavas from the NLSC are not significantly influenced by a subduction component. Their sources are mixtures of MORB-like and residual plume mantle, which is illustrated by the double arrow-head on (b). Another double-headed arrow, which has a steep positive slope through the composition of plume mantle represents the compositions of melts (increasing M/Yb and Nb/Yb) and those of the residues (decreasing M/Yb and Nb/Yb ratios) with increasing partial melting of plume mantle in garnet facies. The lines above, and parallel to, the MORB-plume array are the subduction zone contribution (%sz), calculated as the percentage subduction contribution for the element in question.

103

(c)

(d)

SZ%
NTB,east 93-97%
NTB, west 92-98%
Tafahi 88-95.8%
Niua 87-96.5%
Tofua arc 90-98%

(e)

SZ%
NTB,east 0-40%
NTB, west 0-30%
Tafahi 0-255
Niua 21-30%

(f)

(g)

(h)

105
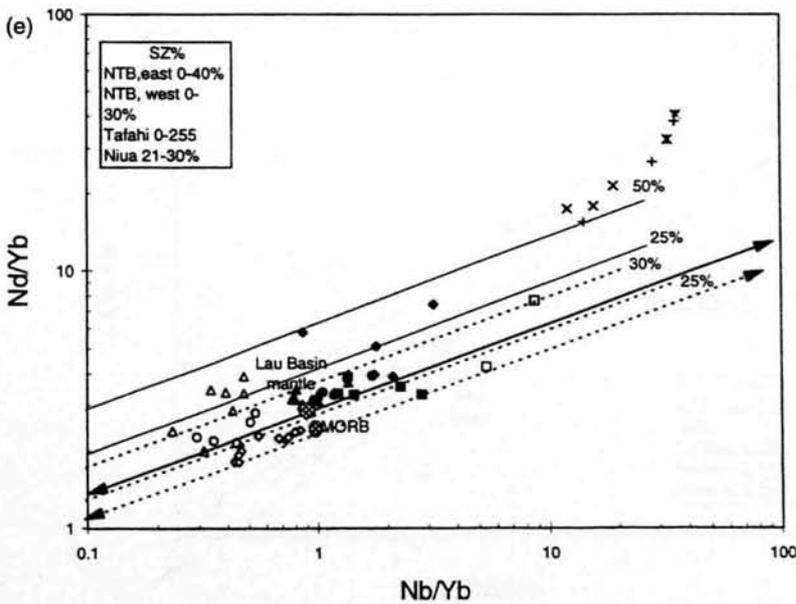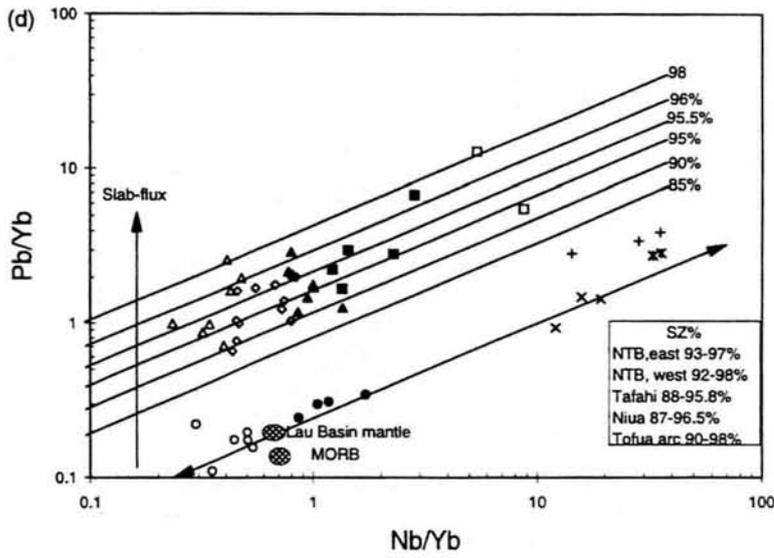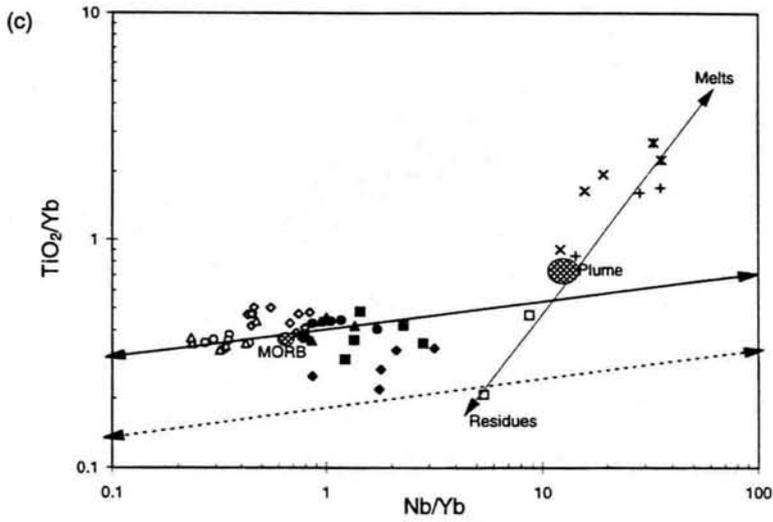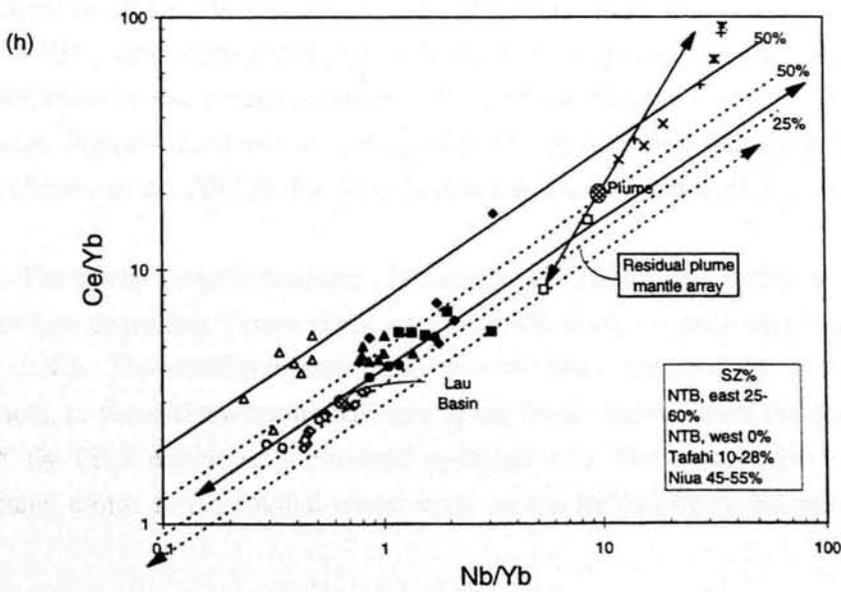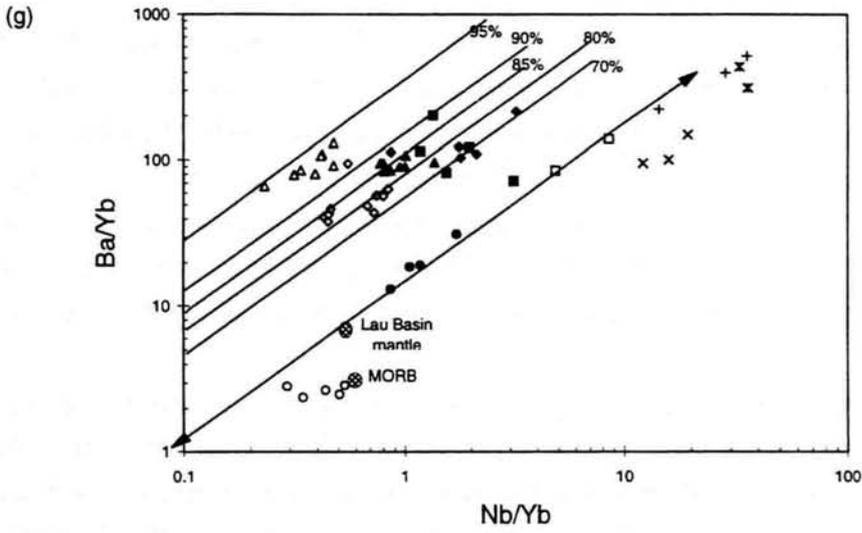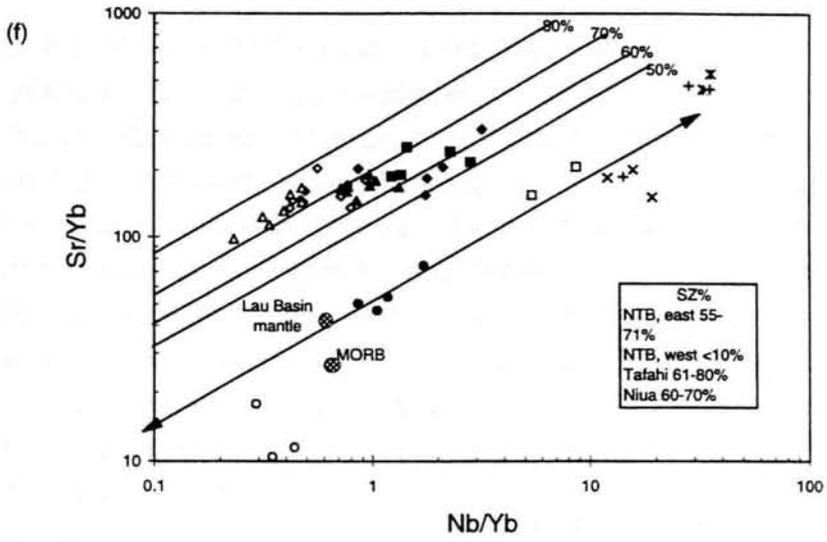
One way of assessing the relative contribution of these components to the magma genesis of the north Tongan boninites, the lavas from Tafahi, Niuatoputapu and the Northern Lau Spreading Centre, is to follow the approach of *Pearce (1982, 1983)* in plotting diagrams of the form M/Yb against Nb/Yb or Ta/Nb where M is the incompatible element of interest. These diagrams highlight differences in enrichments or depletions depending on whether M is an element for which there is, or is not, a detectable slab contribution to the source. Th, Pb, Sr, Ba, La and Ce are elements for which there *is* a detectable slab contribution. However, Zr, Ti and Nb are elements for which there is no detectable slab contribution. Therefore, the latter elements are useful in tracing the nature of the mantle source (see also Figures 4.6 and 4.10; *Pearce & Parkinson, 1993; Pearce & Peate, 1995*).

Figure 4.12(a)-(h) are plots for M = Th, Zr, TiO$_2$, Pb, Nd, Sr, Ba and Ce. Figure 4.12(a) is a plot of Th/Yb versus Nb/Yb (c.f. *Pearce & Peate, 1995*), based on the Th/Yb-Ta/Yb plot of *Pearce (1982)*. The normalising factor (Yb) is largely effective in eliminating variations due to partial melting and fractional crystallisation. The vector for enrichment due to a subduction component is marked on the diagram. The subduction component causes enrichments in Th (and Pb, Sr, Ba, La and Ce), but not Nb (or Yb), due to the relatively high compatibility of Th in fluids, and therefore this vector is sub-vertical. Enrichments due to a plume component affect Th and Nb equally and therefore this vector has a slope of unity (see Figures 4 and 5 of *Pearce, 1983*).

Variable depletion of the source will also take the composition parallel to the MORB-plume array, as removal of a melt removes Nb due to its incompatibility in melting. For example, depletion of a source and then enrichment by a subduction component of constant composition takes the composition above the MORB-plume array. Dynamic melting of this source leads to a distribution of data in a line parallel to the MORB-plume array, but displaced above it by an amount corresponding to the % contribution to the elemental budget of M in the sample from the subduction component. Figure 4.13 shows modelling of this using data from the South Sandwich Islands (*Pearce et al., 1995a*). The following features are observed in Figure 4.12:

1. The north Tongan boninites, Niuatoputapu, Tafahi, the Tofua arc and the Northern Lau Spreading Centre plot above the MORB-plume array when M=Th, Pb, Sr, Ba ± Ce. This confirms that they have all been enriched by a subduction component, as these elements are enriched in the fluids derived from the dehydrating slab (cf. the LILE enrichments observed in Figure 4.5). These data form a series of sub-parallel trends to the MORB-plume array on the M/Yb-Nb/Yb diagrams, where

M=Th, Pb, Sr, Ba and Ce. This suggests that the data distribution cannot simply be explained by enrichment of a single source by a subduction component which then undergoes dynamic melting (cf. the South Sandwich Islands data; *Pearce et al., 1995a*). The sub-parallel data trends of the lavas from north Tonga suggest that the degree of enrichment by the subduction component and/or its composition are variable. The data of the north Tofua arc islands of Tafahi and Niuatoputapu have higher Nb/Yb ratios than those of the central Tofua arc, which suggests that they have a distinct source (see discussion below).
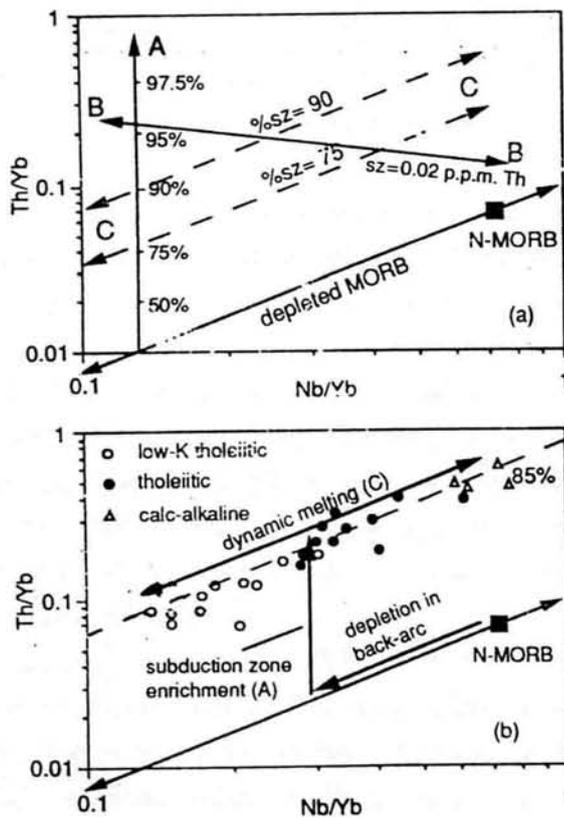
Figure 4.13: *Modelling of M/Yb vs Nb/Yb for the South Sandwich Islands, (Figure 10 from Pearce et al., 1995a) contrasts (A) variable addition of a subduction component to a constant mantle composition, (B) addition of a constant subduction component to a variable mantle composition, and (C) addition of a constant subduction component to a constant mantle composition followed by dynamic melting. (b) Explanation of the variation in the South Sandwich Islands by back-arc depletion, followed by subduction zone addition of Th, then dynamic melting.*

4. The Tafahi data form two distinct groups: Group 1 lavas with Nb/Yb ratios between 0.65 and 0.95, and Group 2 lavas with Nb/Yb ratios between 0.40 and 0.55. When M= Th, Ba, Sr, Pb on Figure 4.12, the Tafahi lava data are either very variable (e.g. for Pb), or form a series of trends, parallel to the MORB-plume array (for Th, Ba and Sr). However, when M=Ce and Nd these data form a single trend sub-parallel to the MORB-plume array. Therefore, the geochemical differences between the two groups are not likely to be the result of dynamic melting of a single source, which has been enriched by a constant subduction component (c.f. South Sandwich Islands; *Pearce et al., 1995a*). A more likely explanation is that there are two distinct sources of the Tafahi lavas, which have either (i) been variably enriched by a slab-flux with a constant composition, or (ii) had a constant enrichment by a slab-flux with a varying composition.

It is difficult to distinguish between (i) and (ii) as the processes of generation, transport of the slab-derived fluids to the base of the melting column and their interaction with the mantle (e.g. chromatographic processes) are not well understood (Figure 1.2; *Pearce & Peate, 1995*). Also, localised variations in compositions of slab and subducted material may affect the composition of the slab-flux, but are hard to trace unless the isotopes are invoked (see Sections 5.4 and 5.5; Figures 5.6 and 5.8).

5. The Northern Lau Spreading Centre (NLSC) lavas form a trend parallel to MORB-plume array, with higher Nb/Yb ratios than those of MORB. This suggests that mixing has occurred between MORB- and plume-mantle in their source region, which gives them high Nb/Yb ratios compared to those of MORB. A subduction component has not significantly enriched their sources as their Th/Yb, Ba/Yb and Ce/Yb ratios are similar to those of the MORB-plume array. The Pb isotopic compositions of the NLSC lavas support the trace element evidence for the involvement of a plume end-member in their magma genesis (Figure 5.6(b) and (c); Section 5.2). This can be contrasted with the compositions of the Central Lau Spreading Centre lavas, which are similar to those of MORB, which therefore indicate the absence of a plume end-member in their magma genesis.

4.5.4 Contributions from enriching components: subduction vs plume

The trace elements show that the north Tongan boninites, the lavas from Tafahi and Niuatoputapu have enrichments in LILE (Figure 4.5), which can be attributed to a subduction component (Section 4.5.3). This component may comprise fluids driven off dehydrating subducted oceanic crust and/or sediments (*Woodhead, 1989*), or a

silicate melt of the slab itself (*Pearce et al., 1992; Taylor et al., 1994*). It is enriched in LILE and often in LREE due to the high compatibility of these elements in fluids or melts (Figure 4.5; *Tatsumi et al., 1986; Tatsumi, 1989; Davies & Bickle, 1991*). Major and trace elements are used in Figures 4.15 and 4.16 to further investigate the origin of the subduction component, particularly to determine if a slab melt is present.
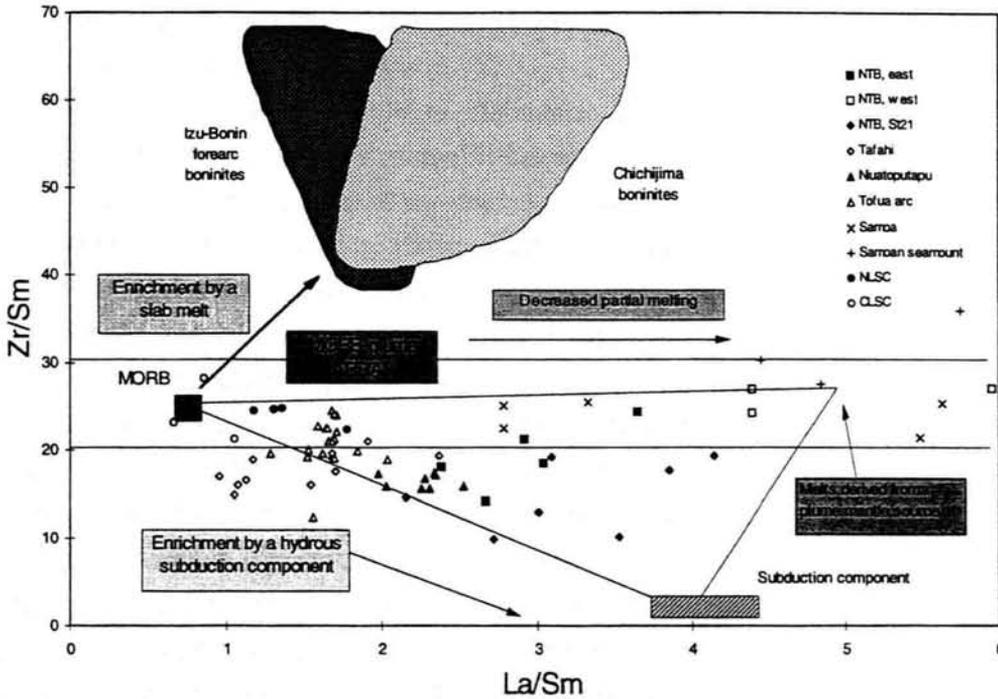
Figure 4.14: A plot of La/Sm vs Zr/Sm for the north Tongan boninites (NTB), Tafahi, Niuatoputapu, the Tofua arc, the Central and Northern Lau Spreading Centres (CLSC and NLSC), and the Samoan shield, post-erosional volcanics and seamount. Compositional fields for the boninites from the Izu-Bonin forearc and Chichijima (Pearce et al., 1992(a) and (b); Taylor et al., 1994) are shown. These boninites have higher Zr/Sm ratios than the MORB-plume array, which are a result of enrichment of their sources by a slab fusion component. The compositions of the lavas from north Tonga can be explained by the mixing between a subduction component and a plume end-member (see text for discussion).

Figure 4.14 is a plot of La/Sm against Zr/Sm ratios for the north Tongan boninites, Tafahi, Niuatoputapu, the Tofua arc, the Northern Lau Spreading Centre and boninites from Chichijima and the Izu-Bonin fore-arc (ODP Leg 125). It separates out enrichments by a subduction component due to either a slab melt or an hydrous fluid, from enrichment by a plume end-member, which are shown by the arrows and labels on this diagram. The trend for enrichment by a hydrous subduction component is towards lower Zr/Sm and higher La/Sm ratios than those of MORB, which is assuming that it does not contain any, or very little, Zr. This is probably a

fair assumption as HFSE, such as Zr, and HREE are not strongly partitioned into aqueous fluids (*Tatsumi, 1986; Tatsumi et al., 1989; Keppler, 1996*). However, *Pearce et al. (1992)* demonstrate that melting of the slab in amphibolite facies produces melts which are enriched in Zr and La relative to Sm. LILE, La, Ce, (± Pr and Nd) are favourably taken up by fluids *and* melts, due to their high mobility in both, relative to the MREE. Therefore enrichment trends for both types of subduction component are towards high La/Sm ratios, but only the one due to a slab melt is towards high Zr/Sm ratios.

Although this plot is able to distinguish between enrichments due to a subduction component and the plume, it cannot be used to determine whether the former one was derived from either altered oceanic crust or subducted sediments. This is because fluids derived from both altered oceanic crust and sediments are likely to have similar La/Sm and Zr/Sm ratios.

Enrichment due to a plume end-member forms a trend towards high La/Sm, parallel to the MORB-plume array, and also the partial melting trend, i.e. at a constant Zr/Sm ratio on Figure 4.14. This is due to the similar behaviour of Zr and Sm during partial melting i.e. they have similar bulk partition coefficients ($K_dZr=0.1294$ and $K_dSm=0.2677$ for melting of peridotite in spinel lherzolite facies; *Kelemen et al., 1993*), and therefore leads to no significant fractionation between these two elements. (see partial melting trend marked on Figure 4.14). The compositions of lavas from a Samoan seamount have also been plotted on Figure 4.14. Its La/Sm and Zr/Sm ratios lie within, or just above, the MORB-plume array, and are similar to those of the Samoan post-erosional volcanics. The Samoan shield has lower La/Sm ratios, but similar Zr/Sm ratios to the other Samoan volcanics.

The most striking feature of Figure 4.14 is the very high Zr/Sm ratios (40-60) of the Chichijima and Izu-Bonin fore-arc boninites compared to those of the lavas from north Tonga (10-25) and the MORB-plume array (c. 22-32). The north Tongan boninites have lower Zr/Sm ratios (10-20) compared to the other boninites, but these are similar or slightly lower than the MORB-plume array. Their La/Sm ratios are higher than those of MORB. Their data form a sub-trend towards high Zr/Sm and La/Sm ratios. Boninites 16-26/1 and 16-26/2 from the west have La/Sm and Zr/Sm ratios similar to the Samoan plume and lie within the MORB-plume array.

The Central Lau Basin lavas have Zr/Sm and La/Sm ratios similar to MORB, whereas the Northern Lau Spreading Centre lavas have Zr/Sm ratios similar to MORB, but higher La/Sm ratios, being displaced along the MORB-plume array towards ratios similar to the Samoan plume.

The fields of Zr/Sm and La/Sm ratios of the lavas from the Tofua arc, Tafahi, Niuatoputapu and some of the north Tongan boninites from the 'Kallisto' ophiolite section and those dredged from Station 21 (Figure 2.1) lie on a negative trend. The boninites have the highest La/Sm ratios, then in the order of decreasing La/Sm ratios, Niuatoputapu through to the Tofua arc to Tafahi. The lavas from Tafahi form a sub-trend from La/Sm ratios very similar to MORB to higher La/Sm ratios, at lower Zr/Sm ratios than MORB, whereas the lavas from Niuatoputapu have higher La/Sm and lower Zr/Sm ratios than MORB.

The high Zr/Sm ratios of the boninites from Chichijima and the Izu-Bonin fore-arc can be explained if their sources were enriched by a component with a high Zr/Sm ratio. A plume end-member could not produce Zr/Sm ratios as high as those observed in these boninites, and therefore another component has been invoked by *Pearce et al. (1992)* and *Taylor et al. (1994)*. They use these high Zr/Sm ratios as evidence that the boninite source has been enriched by a slab melt. However, the lack of such high Zr/Sm ratios in the lavas from north Tonga precludes the involvement of such a slab melt in their petrogenesis. Figure 4.15 presents further evidence for this.

The north Tongan boninite data are displaced toward high La/Sm ratios from MORB and some of the data lies below the MORB-plume array. This can be attributed to the addition of a subduction component to the boninite source, which appears to be MORB-like according to this diagram. The data also form a trend to high La/Sm *and* Zr/Sm ratios, towards the compositions of the Samoan plume. This trend can be taken as evidence that a plume end-member has enriched their source. The two boninites from site 26 (16-26/1 and 16-26/2) have higher La/Sm and Zr/Sm ratios than those of the other north Tongan boninites and similar to those of the Samoan plume. Their compositions lie within the MORB-plume array. This indicates either that their source was Samoan plume mantle, and supports evidence from Figure 4.12 that a subduction component does not significantly influence their compositions. On this diagram, the boninite sources appear to be MORB-like, apart for those of the boninites from the west. However, other geochemical evidence indicates that their sources are more likely to be residual plume mantle (Figures 4.12, 4.13, 5.6, 6.3 and 6.4).

Niuatoputapu lavas have higher La/Sm ratios than lavas from the Tofua arc and Tafahi, suggesting a greater enrichment by the LREE-enriched subduction component, but the data also show a trend to higher Zr/Sm and La/Sm ratios, similar to that shown in the north Tongan boninites. This trend suggests that the plume has influenced the compositions of the Niuatoputapu lavas. However, the isotope data (Figure 5.6) do not obviously indicate the presence of this component in their source.

The Northern Lau Spreading Centre lavas have higher La/Sm ratios than, and similar Zr/Sm ratios to, those of MORB, having compositions which lie within the MORB-plume array. This suggests that the compositions are not influenced by a subduction component. Therefore, the displacement to higher La/Sm ratios than those of MORB, towards the Samoan plume (Figure 4.14) suggests that their source contains a plume end-member. This supports evidence from the isotopes (Figure 5.6).

The Tofua arc and Tafahi have higher La/Sm and lower Zr/Sm ratios than those of MORB. This is along the trend of enrichment due to a hydrous subduction component. However, some of the lavas from Tafahi have La/Sm ratios which are similar to those of MORB, suggesting that their source has not been enriched by a subduction component that has high concentrations of LREEs (see Section 6.2.3; Figures 4.5(f) and 4.16).

4.5.5 Further evidence for the nature of the subduction component

Figure 4.14 shows the Eocene boninites from the Izu-Bonin fore-arc and from Chichijima, Bonin Islands have high Zr/Sm ratios (40-60). *Pearce et al. (1992)* and *Taylor et al. (1994)* used this as evidence that a Zr-rich component was added to their source. The lack of Zr/Sm ratios greater than those of the MORB-plume array of the lavas from north Tonga suggests that no such component has enriched their sources. Further evidence for this observation is shown in Figure 4.15(a) and (b), diagrams of Na_2O and CaO/Al_2O_3 against TiO_2.

The north Tongan boninites have the lowest Na_2O and TiO_2 contents and the highest CaO/Al_2O_3 ratios. Three of the boninites from the west (16-26) have very low Na_2O contents (<0.5 wt %). The compositional fields of the lavas from the Central Lau Spreading Centre, the Tofua arc, Niuatoputapu and Tafahi lie on a trend of decreasing Na_2O and increasing CaO/Al_2O_3 ratio with decreasing TiO_2. The Tofua arc, the Northern Lau Spreading Centre and Niuatoputapu are displaced to lower CaO/Al_2O_3 ratios than this trend, which can be attributed to plagioclase fractionation. The Izu-Bonin fore-arc boninites are displaced from this trend, to higher Na_2O contents and lower CaO/Al_2O_3 ratios for their TiO_2 contents.

The trend in the data fields, marked as an arrow on Figure 4.15, is a trend of increasing mantle depletion because melts from depleted sources have lower Na_2O and TiO_2 contents, as Na and Ti are highly incompatible elements during partial melting (see Figure 9 of *Pearce & Parkinson, 1993*). Therefore, these oxides are removed during previous melting events leaving a source that is depleted in Na_2O and TiO_2. The low TiO_2 and Na_2O contents and high CaO/Al_2O_3 ratio of the north

■ NTB, east   □ NTB, west   ◆ NTB, St 21   ◇ Tafahi
▲ Niuatoputapu   △ Tofua arc   ○ NLSC   ● CLSC
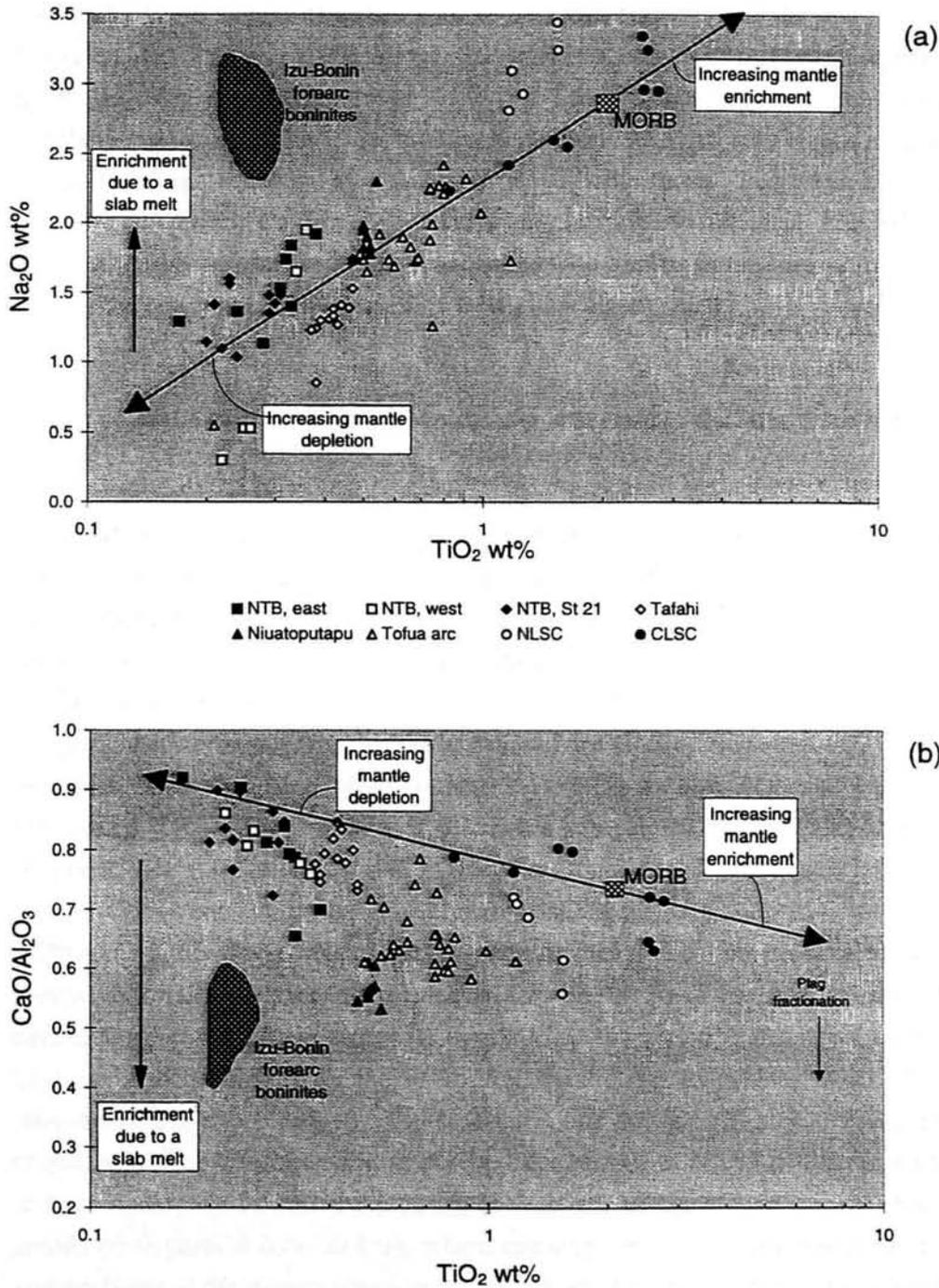
Figure 4.15 : Na₂O and CaO/Al₂O₃ vs TiO₂ for the north Tongan boninites, the lavas from Tafahi, Niuatoputapu, Tofua arc, the Northern and Central Lau Spreading Centres (NLSC and CLSC) and the Izu-Bonin forearc boninites (shown by the shaded field). The composition of average MORB is shown and the arrow indicates the trend for increased mantle enrichment or depletion towards decreasing and increasing TiO₂, respectively. The trend for plagioclase fractionation towards decreasing CaO/Al₂O₃ is shown by the pale arrow. The compositions of the Tongan lavas lie on the trend of mantle-depletion on (a) and on (b) the amount of their displacement from it is explained by plagioclase fractionation. The compositions of the Izu-Bonin forearc boninites are displaced to high Na₂O wt% and low CaO/Al₂O₃ ratios for a given TiO₂ which is explained by the enrichment of their sources by a slab fusion component.

Tongan boninites suggest that their sources are more depleted than the sources of the Tofua arc and Tafahi lavas. However, the boninites from the Izu-Bonin fore-arc lie above the mantle depletion trend. This has been explained in terms of source enrichment by a component with high concentrations of Al_2O_3 and Na_2O, such as a tonalitic melt produced by slab fusion in amphibolite facies (*Pearce et al., 1992; Taylor et al., 1994*). The low Zr/Sm ratios and the lack of enrichment in Al_2O_3 and Na_2O of the lavas from north Tonga compared with the Izu-Bonin fore-arc boninites, suggest they have not been enriched by a slab fusion component.

4.5.6 Comments about the melting processes of the lavas from north Tonga from their major element geochemistry

The melting process is likely to be one of the most important causes of element variation between the suites of lavas from north Tonga (Section 4.5.1; *Pearce et al., 1995a; Langmuir et al., 1993; Klein & Langmuir, 1987*). The approach taken to examine this, utilizes the methods of Langmuir and co-workers (e.g. *Langmuir et al., 1993*). Na and Fe, quoted for MgO=8.0wt% to correct for fractional crystallisation, are particularly effective. Figures 4.16(a) and (b) are plots of Na_2O and FeO* against MgO for lavas that have MgO contents >5wt% that allow Na8 and Fe8 to be determined. Liquid lines of descent (LLD) are sub-parallel on the Na_2O-MgO plot (Figure 1, *Klein & Langmuir, 1987*). Therefore, it can be inferred that differences in the Na_2O contents of lavas, at a chosen MgO content (e.g. 8wt%), are due to differences in the Na_2O content of their parental magmas. By projecting along a line parallel to the LLD, when MgO is less than 8.5wt%, the Na_2O content at an arbitrarily chosen MgO content can be inferred. 8 wt% MgO is selected as this reference point. This has also been done for the FeO*-MgO plot. Lines for which Na8=1.0-3.5 in intervals of 0.5, and Fe8=8-13, in internals of 1, are drawn on Figures 4.16(a) and (b) respectively. The lavas from Niuatoputapu have MgO<5wt% and are therefore likely to have undergone extensive fractionation. Vectors for plagioclase fractionation are shown on Figures 4.16(a) and (b), which can explain some of the variation in the compositions of the Niuatoputapu lavas. Therefore, the Na8 and Fe8 of Niuatoputapu has been calculated from the lavas with the highest MgO content.

Figure 4.16(c) is a plot of the Na8 versus Fe8 values for the north Tongan boninites (NTB, east and west), Tafahi (TAF) and Niuatoputapu (Niua) and the Tofua arc. Fields for Indian and Pacific MORB mantle and the Samoan plume have also been included on this diagram (from *Pearce et al., 1995a*). The MORB global trend is shown by the double-headed arrow with the negative trend, which is a result of differences in the compositions of MORB sources. The MORB local trend is also
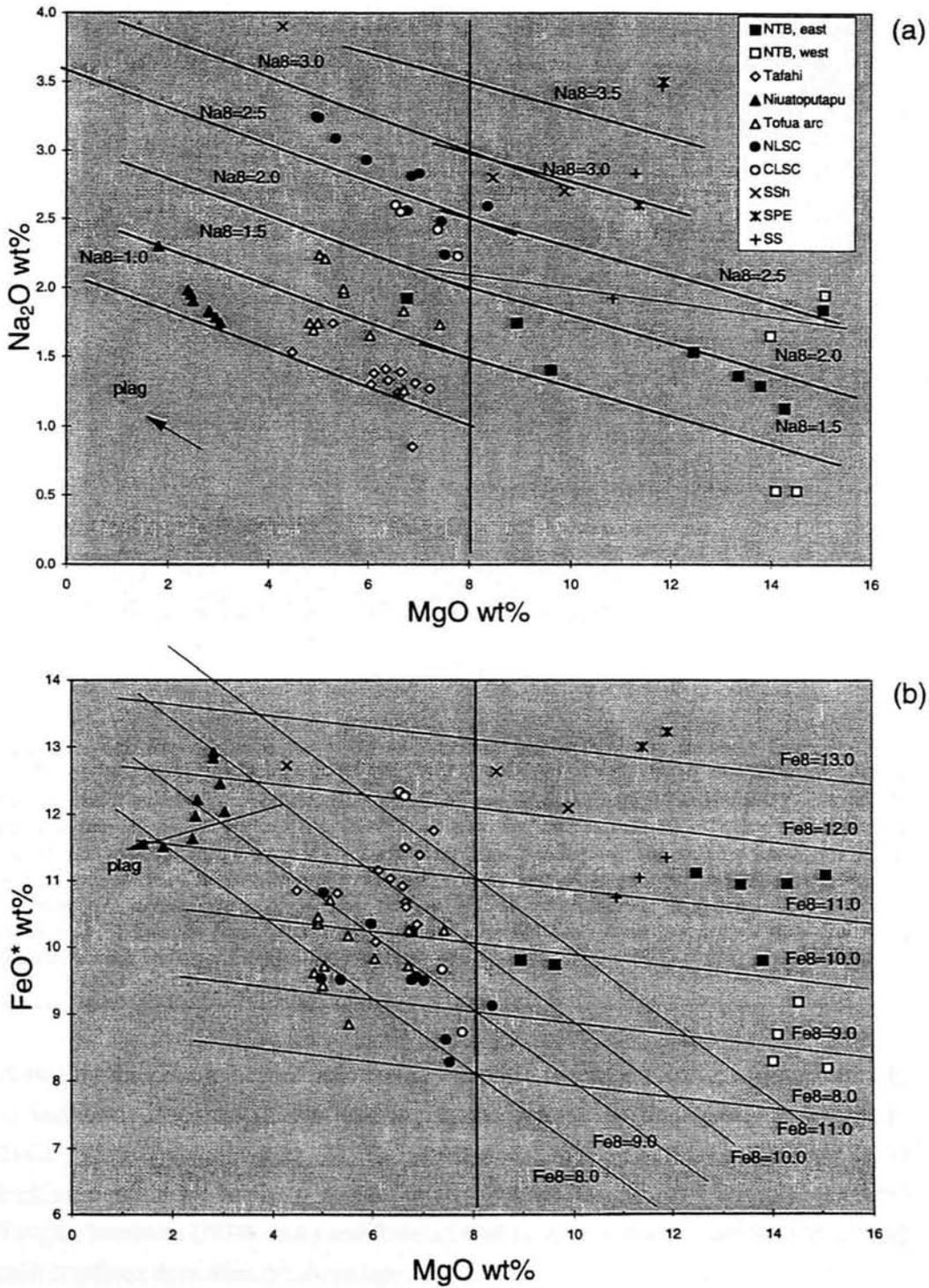
Figure 4.16 : Na$_2$O and FeO* wt% vs MgO wt% for the north Tongan boninites from the ophiolite section (east) and site 26 to the west, Tafahi, Niuatoputapu, the Tofua arc, the north Tongan tholeiites, 'Eua and the Northern and Central Lau Spreading Centres. FeO* is the total Fe as Fe^{2+}. Na8 and Fe8, the calculated Na$_2$O and FeO* contents at 8 wt% MgO, are derived from these plots, as described in the text.
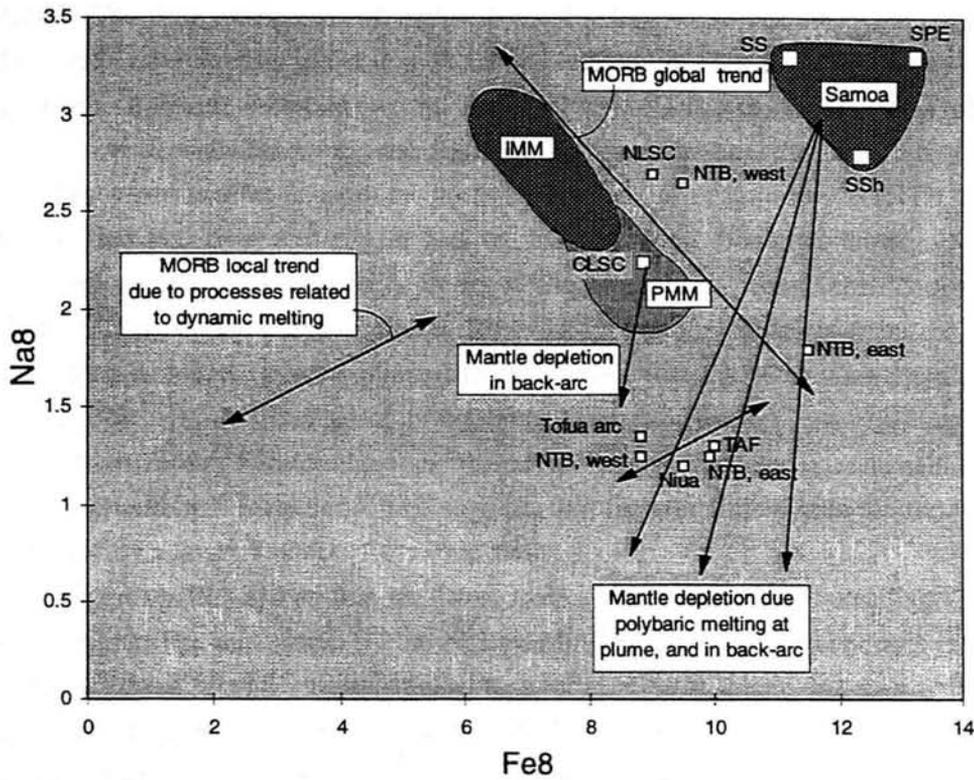
Figure 4.16(c): *Plot of Fe8 versus Na8 from Langmuir et al. (1993) for the north Tonga boninites (NTB, east and west), the lavas from Tafahi (TAF) and Niuatoputapu (Niua), the Tofua arc and the Central and Northern Lau Spreading Centres (CLSC and NLSC). Fields for Indian and Pacific MORB and the Samoan plume are superimposed. Double-headed arrows indicate MORB global and local trends (Langmuir et al., 1993). The variation in Na8 and Fe8 between the suites of lavas from Tonga may be explained by a MORB local trend, which is a result of dynamic melting. The north Tongan boninites are derived from mantle that has undergone an episode of depletion during polybaric melting at the Samoan plume and in the back-arc. The Tofua arc lavas are derived from Lau Basin mantle that has undergone depletion in the back-arc.*

shown by the double-headed arrow with the positive trend, which has been attributed to variations in compositions resulting from dynamic melting (*Klein & Langmuir, 1987, 1989; Langmuir et al., 1993*). Instantaneous melts generated at the base of the melting column are likely to contain relatively high Na and Fe. Therefore, the north Tongan boninites (NTB, east) and Tafahi lavas contain a greater contribution of deep melt fractions than does Niuatoputapu.

The trace element study in Figure 4.12 shows that there were at least two episodes of melting prior to that which generated the lavas from north Tonga: one prior to advection into the wedge (at the Samoan plume), which depleted the mantle in a small melt fraction, and one in the source regions of the different suites of lavas from north Tonga which generated these lavas by dynamic melting of the upwelling

117

mantle. The first episode, involving the loss of a small melt fraction would deplete the mantle more rapidly in Na than Fe, as Na is more incompatible. This could give the steep depletion vector shown on Figure 4.16(c). However, melting at a plume occurs over a wide range of pressures and therefore, the specific direction of this vector may be variable. Some of the north Tongan boninites from site 26 (NTB, west) have higher Fe8 than, and similar Na8 to, MORB. These boninites therefore, have 'enriched' sources compared with those of the other lavas from north Tonga and MORB. This supports evidence from Figure 4.12 that the boninites from the west have more enriched 'residual' plume mantle sources than the other lavas from north Tonga. However, the other group of boninites from the west has lower Na8 and Fe8 values than Tafahi, Niuatoputapu and the north Tongan boninites (east), but they lie on the same MORB local trend. This suggests that these boninites from the west were generated by a larger amount of dynamic melting.

Figure 4.16(c) shows that the lavas from the Northern Lau Spreading Centre have a higher Fe8 than, and a similar Na8 to, MORB. This is further evidence that the sources of these lavas are more enriched than those of MORB, and that they are likely to be, or partly be, plume mantle. Figure 4.12(b) suggests that this plume mantle is residual after melting at Samoa. Further evidence for the nature of the sources of the lavas from the Northern Lau Spreading Centre is discussed in Chapter 5.

4.6 Chapter 4 Summary

• Most of the north Tongan boninites are classified as high-Ca, in terms of their major element geochemistry ($CaO/Al_2O_3 > 0.75$; $SiO_2 > 53\%$; Mg# > 0.6). Those that are not have evolved from a boninitic parent by either olivine accumulation (low SiO_2 contents), or fractionation (low MgO contents). The major element variation in the boninites can be explained by fractionation of olivine, clino- and orthopyroxene. The boninites have a similar major element compositions to high-Ca boninites from the Upper Pillow Lavas of the Troodos Massif, Cyprus.

• The major element compositions of lavas from Tafahi and Niuatoputapu lie on the main Tofua arc trend on the CaO- and SiO_2-MgO plots. They have similar phenocryst assemblages to the Tofua arc, suggesting that they have undergone broadly the same fractionation history involving olivine, clinopyroxene, orthopyroxene, plagioclase and Fe-Ti oxides. Niuatoputapu lavas have lower CaO and MgO contents than the Tafahi lavas suggesting that they have undergone more fractionation.

• The north Tongan boninites have enrichments in LILE and REE relative to the HFSE, and in LREE relative to MREE. The boninites from the western ophiolite section have strong depletions in Zr and Hf relative to Sm and Nd and in Ta and Nb relative to La and Th, whereas the ones from west of the section do not have these depletions. The former boninites have similar trace element geochemistry to the boninites from Station 21 of the 'Natsushima' 1984 cruise.

The Tafahi lavas have enrichments in LILE and REE relative to HFSE, and hence have depletions in Zr and Hf relative to Sm and Nd, and Ta and Nb relative to La and Th. The lavas form two distinct groups, one having LREE enrichment and the other having LREE-depletion. One sample is transitional between the two groups.

The Niuatoputapu lavas have LILE- and a slight LREE-enrichment relative to the HFSE. They have a pronounced depletion in Ta and Nb relative to Th and La, and in Zr and Hf relative to Nd and Sm. The Hf depletion is not pronounced in all the Niuatoputapu lavas.

The lavas from the Northern Lau Spreading Centre also have LILE- and slight LREE-enrichments, but only have very slight depletions in the HFSE.

• Three end-member components have been identified in the Lavas from north Tonga from the trace element geochemistry:

1. *a subduction component* derived from the subducting slab and carrying high concentrations of incompatible elements (LILE and LREE) has enriched the sources of the north Tongan boninites (east), and the lavas from Tafahi and Niuatoputapu in these elements. The low Zr/Sm ratios and lack of enrichment in Na_2O and Al_2O_3 compared with the boninites from the Izu-Basin fore-arc and Chichijima indicate that this component is hydrous fluids, rather than a slab melt. The high La/Yb, Ce/Yb, Sr/Yb and Ba/Yb ratios compared to the MORB-plume array of the north Tongan boninites (east), Tafahi, and Niuatoputapu may also be attributed to the enrichment of their sources by a subduction component.

The lavas from the Northern Lau Spreading Centre (NLSC) do not have a significant geochemical signature from the subduction component. Their weak LILE and LREE enrichment relative to MORB is likely to be due to the influence of the Samoan plume. The compositions of boninites from site 26, from the west, lie within the MORB-plume array (apart from high Pb/Yb ratios which may be due to contamination), suggesting that they have an insignificant contribution from a subduction component.

2. *a residual plume mantle end-member:* The low concentrations of HFSE and the high Al_2O_3/TiO_2 and CaO/TiO_2 ratios relative to primitive MORB of the north Tongan boninites (east), Tafahi, Niuatoputapu are evidence that their mantle sources have been depleted by the removal of melt(s) at previous partial melting events. The depletion of the sources decreases from the north Tongan boninites through Tafahi and Niuatoputapu to the Tofua arc. The boninites, Tafahi and Niuatoputapu have a source depleted by removal of between 15 and 20% of melt from their source prior to their magma genesis, whereas the Tofua arc has had between 10 and 15% removed.

The low Zr/Yb and Nb/Yb ratios of north Tongan boninites, the lavas from Tafahi and Niuatoputapu compared with the MORB-plume array suggest that they have sources derived from partial melting of residual plume mantle.

3. *a depleted MORB mantle end-member:* The Tofua-arc lavas are depleted in incompatible mantle-derived elements relative to fertile MORB mantle and they have Zr/Yb and Nb/Yb ratios which lie on the MORB-plume array but are lower than those of MORB. This evidence suggests that their sources are depleted MORB mantle.

The lavas from the Northern Lau Spreading Centre are derived from a source with 'mixed' geochemical characteristics between those of MORB and residual plume-mantle.

CHAPTER 5

Isotope systematics

5.1 Introduction

In this chapter, the effects of post-eruption alteration on the lavas from north Tonga are assessed by comparing the isotopic composition of their leachates and residues after leaching with 6M HCl. Once the 'primary' isotopic compositions of the lavas are constrained, possible isotopic end-members, which originate from the subduction component and the mantle wedge, are identified. The Sr, Nd and Pb isotopic characteristics of these lavas are then described and used to propose initial models for their magma genesis in terms of mixing of isotopic end-members.

5.2 Assessing the effects of seawater alteration

The north Tongan boninites and tholeiites, and the lavas from Tafahi, Niuatoputapu and the Northern Lau Spreading Centre have all undergone some form of post-eruption alteration. This alteration took place at low temperatures, as none of the lavas have high temperature mineral assemblages or have intense alteration, and is characterised by clay and/or serpentine minerals (Chapter 3). The lavas from Tafahi and Niuatoputapu contain lower proportions of clay minerals than the north Tongan boninites and tholeiites and the lavas from the Northern Lau Spreading Centre, which suggests that they have not experienced as much alteration.

Previous studies by *McDonough & Chauvel (1991)* on the contamination of ocean island basalts from the Rurutu and Sasha seamounts showed that their Pb isotopic compositions were considerably affected by a contaminant with a different isotopic composition. They showed that leaching of the samples was an effective way of isolating the contaminant and thus enabled the true pre-alteration Pb isotopic composition of the samples to be determined. In order to assess the effects of low-temperature alteration on the isotope systematics of the lavas from north Tonga, the samples were similarly leached for 30 minutes on a hotplate using 6M HCl before

being run through the isotope separation columns. The experimental details of this process are in Appendix 1.

The leaching extracts into solution any elements loosely-held on alteration phases, and leaves a residue. In the following sections it is assumed that the isotopic composition of the residues is the same as that of the samples prior to alteration. This is a reasonable assumption because, when a few of the samples were leached a second time and re-analysed, the isotopic composition of the residues duplicated the composition of those from the first analysis. The leachates were also analysed for their Pb, Nd and Sr isotopic compositions as these should have the isotopic signature of the alteration component (Appendix 2). The leachate analysis can be used to assess the degree and nature of alteration in the samples because, if they have undergone alteration by a component, there will be a difference between the isotopic composition of the residue and the leachate.

If the samples are fresh and geologically young then the leachate will have the same, or similar, composition as the sample itself. If the samples are old then there is a possibility that their isotopic compositions have changed due to radiogenic growth of a daughter isotope by the decay of its parent isotope. This occurs if the age of the samples is significantly greater than the half-life of the parent isotope. For instance, for samples older than about 1 Ma, the ^{87}Rb within them will decay radiogenically to ^{87}Sr, which will progressively increase their ^{87}Sr/^{86}Sr ratios with time. This scenario could also occur if Rb was added during alteration. However in the latter case, as leaching removes the alteration minerals and hence, with them, all the Sr produced by radiogenic decay, the leachate will have the Sr isotopic composition of the alteration component, whereas the residue will have the original composition of the sample prior to alteration. The samples from Tafahi (c.10-20ka, *S. Turner pers. comm.*), Niuatoputapu (<2.8 Ma but >c. 350ka, *J. Mitchell* and *S. Turner pers. comm.*) and the north Tongan boninites (<3.1 Ma) are all young and therefore it is assumed that there has been no radiogenic growth of ^{87}Sr due to Rb added by alteration. However, the north Tongan tholeiites from the eastern ophiolite section, from the inner wall of the Tonga trench, have a K-Ar age of around 50 Ma and therefore, there is a possibility of addition of ^{87}Sr by radiogenic decay of Rb added by alteration.

It has been recognised that the upper crust is a sink for the alkali metals Li, K, Rb and Cs, and other elements such as U, during weathering and low-temperature (<100°C) alteration by the hydrothermal circulation of seawater. *Hart & Staudigel (1982)* evaluated mobile element fluxes by comparing average compositions of altered crustal compositions from DSDP Sites 418A (550m deep), 417A and 417D in the western Atlantic with those of average MORB mantle. This study provided more quantitative information on these fluxes than previous ones (*Hart, 1969; Thompson,*

1973) and can be used in predicting the geochemical characteristics of seawater alteration.

	^{87}Rb/^{86}Sr	^{147}Sm/^{144}Nd	^{238}U/^{204}Pb	^{232}Th/^{204}Pb	^{232}Th/^{238}U
Average unaltered oceanic crust	0.0413	0.1968	7.75	30.8	3.98
Average altered oceanic crust	0.223	0.1995	30	6.96	0.232

Table 5.1: Table showing the ^{87}Rb/^{86}Sr, ^{147}Sm/^{144}Nd, ^{238}U/^{204}Pb, ^{232}Th/^{204}Pb, and ^{232}Th/^{238}U ratios of unaltered and altered oceanic crust (Cohen & O'Nions, 1982; Hart & Staudigel, 1989). The data for altered oceanic crust is obtained from the DSDP Site 418A. This data shows that the average ^{87}Rb/^{86}Sr and ^{238}U/^{204}Pb ratios of oceanic crust are greatly increased by hydrothermal alteration by seawater, whereas the average ^{232}Th/^{204}Pb and ^{232}Th/^{238}U ratios are decreased and the average^{147}Sm/^{144}Nd ratio is changed very little.

Table 5.1 shows a comparison of the ^{87}Rb/^{86}Sr, ^{147}Sm/^{144}Nd, ^{238}U/^{204}Pb, ^{232}Th/^{204}Pb, and ^{232}Th/^{238}U parent/daughter element ratios of unaltered and altered oceanic crust, taken from *Hart & Staudigel (1989)*. If the magnitude of the changes of these ratios in the samples, which is due to alteration, is large, then there is the potential also of further changing these ratios with time, owing to radioactive decay. Hence the ^{87}Rb/^{86}Sr, ^{143}Nd/^{144}Nd, ^{206}Pb/^{204}Pb, ^{207}Pb/^{204}Pb and ^{208}Pb/^{204}Pb daughter isotope ratios are also changed as a result of alteration. However, the concentration of the daughter element in the alteration component also has to be considered. In the case of seawater alteration of oceanic crust, the Sm/Nd ratio of oceanic crust is not greatly changed (Table 5.1), and seawater contains low concentrations of Nd ($2.58 \pm 0.23 \times 10^{-6}$ ppm in Pacific seawater: *Piepgras et al., 1979; Faure, 1986*), both of which lead to the ^{143}Nd/^{144}Nd ratios of oceanic crust being little changed from those of MORB by seawater alteration.

Similarly, the low concentrations of Pb in seawater (3×10^{-5} ppm; *Holland, 1978*) does not give oceanic crust a different Pb isotopic composition at the time of alteration, but the increased U/Pb ratio leads to a time-integrated increase in the ^{206}Pb/^{204}Pb ratio, and the decreased Th/U ratio, a time-integrated decrease in the ^{208}Pb/^{204}Pb ratio. This only occurs if the samples are old (i.e.>~50-100 Ma; *Hart & Staudigel, 1989*). Therefore, it is unlikely that the Pb isotopes of the lavas from north Tonga, apart from perhaps the north Tongan tholeiites (50Ma), have been significantly changed due to seawater alteration, as they are too young.

The Rb/Sr ratio of oceanic crust is increased by a factor of about 5 by seawater alteration (Table 5.1). This supports evidence from *Hart & Staudigel (1982)* that Rb is

preferentially added to oceanic crust, and so more ^{87}Rb is available for radiogenic decay to ^{87}Sr. This process also occurs in lavas erupted at the earth's surface that have undergone some seawater alteration if they are older than about 1 Ma. Seawater contains about 7.7 ppm Sr and has a high ^{87}Sr/^{86}Sr ratio. These factors lead to an apparent increase in the ^{87}Sr/^{86}Sr ratios of oceanic crust or any sample which has undergone seawater alteration, at the time of this event and subsequently.

In applying the work of *Hart & Staudigel (1982, 1989)*, which uses the compositions of oceanic crust from the western Atlantic, generated at the mid-Atlantic ridge, to the lavas from north Tonga, it has been assumed that alteration by hydrothermally circulated seawater produces similar geochemical characteristics to those of surficial seawater alteration during and/or post-eruption. It is a reasonable assumption as both produce similar geochemical characteristics, such as elevated ^{87}Sr/^{86}Sr ratios and enrichments in alkali metals and U, but the degree of alteration by the latter process may be less.

This is supported by the work of *Kimball & Gerlach (1986)*, who also recognised that differences in the Sr isotopic composition of ultramafic rocks from two oceanic fracture zones in the South Atlantic Ocean were due to the type of alteration they had undergone. They recognised a high-temperature reaction resulting from the hydration by fluids with a relatively *strong* basaltic signature, characterised by low ^{87}Sr/^{86}Sr ratios, and a low-temperature reaction resulting from the hydration by fluids with a *weak* basaltic signature and a strong seawater signature, characterised by high ^{87}Sr/^{86}Sr ratios.

Figure 5.1 shows ^{87}Sr/^{86}Sr-^{143}Nd/^{144}Nd, ^{208}Pb/^{204}Pb- and ^{207}Pb/^{204}Pb-^{206}Pb/^{204}Pb plots for the residues and leachates for the north Tongan boninites and tholeiites, and for lavas from Tafahi and Niuatoputapu. The ^{87}Sr/^{86}Sr and ^{143}Nd/^{144}Nd isotopic composition of Pacific seawater is taken from *Fauré (1986)*. It is assumed that Pacific seawater contains 7.7 ppm Sr and 2.58±0.23x10^{-6} ppm Nd (*Piepgras et al., 1979; Fauré, 1986*). Seawater has high ^{87}Sr/^{86}Sr and low ^{143}Nd/^{144}Nd ratios (0.708-0.709 and 0.5120-0.5130 respectively).

The alteration vectors drawn on Figure 5.1(a) are taken as simple mixing curves between seawater and other end-members, which have the isotopic compositions of fresh samples from (a) the north Tongan boninites, (b) north Tongan tholeiites, and (c) Niuatoputapu. These vectors are sub-horizontal because the Sr content of seawater is much higher than Nd, except for very high water/rock ratios. As the lavas from north Tonga have undergone low-temperature alteration, leaching experiments would test whether this alteration was due to seawater, or to another type of low-temperature alteration. The leachates of the north Tongan boninites and tholeiites show a
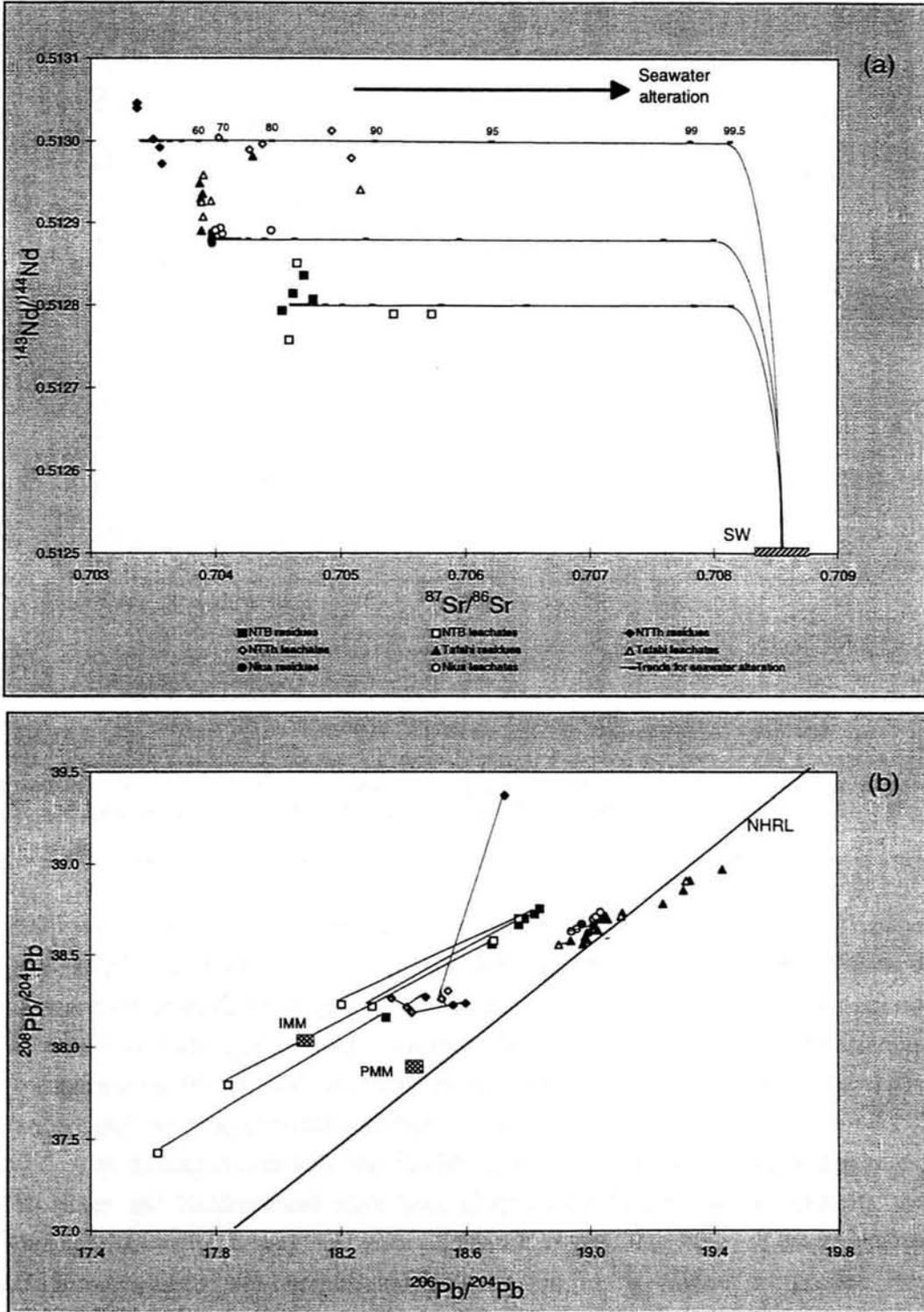
Figures 5.1(a) and (b): $^{143}Nd/^{144}Nd$-$^{87}Sr/^{86}Sr$ and $^{208}Pb/^{204}Pb$-$^{206}Pb/^{204}Pb$ plots for the leachates and residues of the north Tongan boninites (NTB) and tholeiites (NTTh), Tafahi and Niuatoputapu. Simple mixing curves for mixing between Pacific seawater and average end-members of the NTB, NTTh and Tafahi are superimposed on the Sr-Nd plot. The lines on the Pb isotope plots are between leachate-residue pairs. The leachates of the NTB have a lower $^{208}Pb/^{204}Pb$-$^{206}Pb/^{204}Pb$ composition than the corresponding residues. The leachates and residues of the lavas from Tafahi and Niuatoputapu have very similar compositions.

125
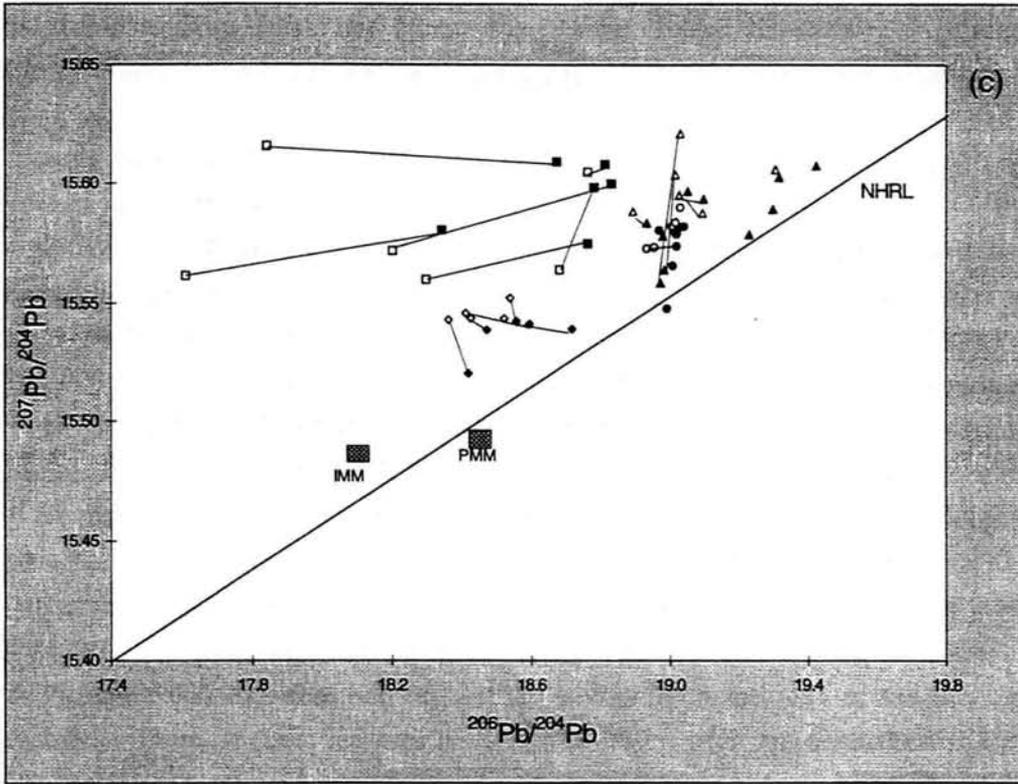
Figure 5.1(c): $^{207}Pb/^{204}Pb$ vs $^{206}Pb/^{204}Pb$ plot of the residues (closed symbols) and corresponding leachates (open symbols) of the north Tongan boninites, Tafahi, Niuatoputapu and north Tongan tholeiites. Data for residue-leachate pairs are joined by a line. The boninites contain an alteration component that has similar isotopic characteristics as Indian MORB mantle.

horizontal displacement from the residue trend to higher $^{87}Sr/^{86}Sr$ ratios which can be explained by seawater alteration. One sample from Tafahi and one from Niuatoputapu appear to be displaced to higher $^{87}Sr/^{86}Sr$ ratios and these are therefore also assumed to have also undergone seawater alteration. For the rest of the samples the isotopic composition of the leachates are very similar to the residues, suggesting that they have undergone very little seawater alteration.

The mixing curves between Pacific seawater and the north Tongan boninites, tholeiites and Niuatoputapu have been plotted onto Figure 5.1(a) to quantify the degree of alteration undergone by the samples. Between 80 and 90% of the Sr isotope composition of the two boninite samples is derived from a seawater component. This component contributes between 69 and 87% to that of the tholeiites and 61% to that of the Niuatoputapu sample. These estimates assume that there is no radioactive growth of Sr due to Rb added by alteration. The north Tongan boninites and tholeiites have undergone a greater amount of alteration due to their sub-aqueous eruption, and due to their greater opportunity to react with seawater since their eruption. It is likely

that the lavas from Tafahi and Niuatoputapu were erupted sub-aerially or uplifted soon after eruption and therefore had less opportunity to undergo seawater alteration.

On the $^{208}Pb/^{204}Pb$- and $^{207}Pb/^{204}Pb$-$^{206}Pb/^{204}Pb$ plots, tie-lines have been drawn between the isotopic compositions of the leachates and corresponding residues for the north Tongan boninites and tholeiites, Tafahi and Niuatoputapu. The residues and leachates of the samples from Tafahi and Niuatoputapu have similar compositions on the $^{208}Pb/^{204}Pb$-$^{206}Pb/^{204}Pb$ plot, but there is some scatter on the $^{207}Pb/^{204}Pb$-$^{206}Pb/^{204}Pb$ plot. The leachate data of the north Tongan boninites have lower $^{208}Pb/^{204}Pb$ and $^{206}Pb/^{204}Pb$ ratios than the corresponding residues, which lie within the field of Indian MORB mantle isotopic compositions. This may indicate alteration by a component with low $^{208}Pb/^{204}Pb$ and $^{206}Pb/^{204}Pb$ ratios, such as altered oceanic crust. This component could not be derived from ancient altered oceanic crust (>~0.1 b.y), as this is likely to have higher $^{206}Pb/^{204}Pb$ ratios with time compared with those of MORB, due to its high time-integrated U/Pb ratio (Table 5.1; *Hart & Staudigel, 1989*), and could therefore not explain the isotopic compositions of the boninite leachates. There is one leachate sample (16-26/2) with an anomalously high $^{207}Pb/^{204}Pb$ ratio which requires a complex alteration history to be invoked. The north Tongan tholeiite leachates have slightly lower $^{206}Pb/^{204}Pb$, similar or slightly higher $^{207}Pb/^{204}Pb$, and similar $^{208}Pb/^{204}Pb$ to their corresponding residues. One sample has an anomalously high $^{208}Pb/^{204}Pb$ which does not appear to be an analytical error, but could be indicative of a contaminant.

5.3 Isotope systematics

5.3.1 Introduction

Isotopes are useful to subduction zone geochemists as they are not affected by fractionation or partial melting processes, and are therefore indicative of the source compositions, or are good tracers of components which have been added to the source regions of arc-related volcanics. The possible source components of arc lavas are likely to have different time-integrated parent/daughter ratios and therefore, have different isotope ratios. Trends in isotopic data, such as those shown by arc lavas, may therefore be explained either in terms of mixing between the various end-member components, or are a result of time evolution. As the lavas from north Tonga (except for the north Tongan tholeiites; Chapter 7) are young (<3Ma), the latter explanation is invalid. The former explanation assumes that these end-members can be identified and that their isotopic or trace element compositions can be constrained. End-

members could be either derived from the subducting slab (altered oceanic crust), subducted pelagic or volcanogenic sediments, or from the mantle wedge which could have MORB- or plume-like isotopic characteristics, or a mixture of both (*Arculus & Powell, 1986; Lin et.al., 1989; Woodhead, 1989; Wharton, unpubl. 1993; Falloon & Crawford, 1991; Hawkesworth et al., 1991a, b; Hickey-Vargas, 1992; Morris et al., 1990; Ishikawa & Nakamura, 1994*).
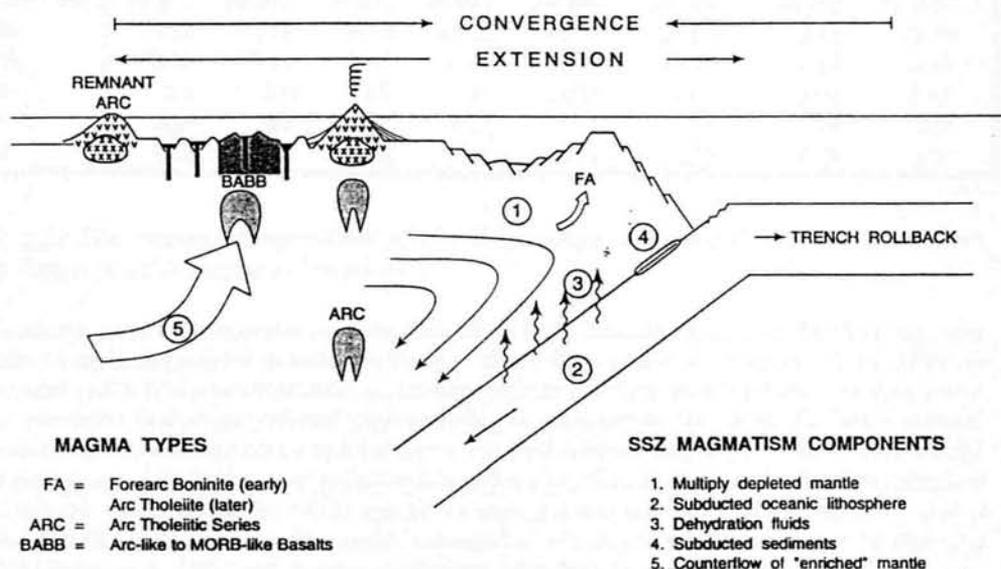
Figure 5.2: *A schematic diagram of a supra-subduction zone, from Hawkins (1995), illustrating the origins of possible end-members which may influence the compositions of lavas erupted at this setting. These end-members may be derived from: (1) a multi-depleted mantle; (2) subducted oceanic crust; (3) dehydration fluids; (4) subducted sediments, and; (5) a counterflow of 'enriched' mantle.*

Figure 5.2 is a schematic cross-section of an intra-oceanic convergent margin taken from *Hawkins (1995)*, (see also Figure 1.2 for a more detailed section), showing the origins of some of the possible end-members, which are numbered on this diagram. These are (1) a multiply-depleted mantle, (2) subducted oceanic crust, (3) dehydration fluids, (4) subducted sediments, and (5) counterflow of 'enriched' mantle.

The trace and major element compositions of the lavas from north Tonga indicate that their magma genesis can be explained in terms of: (a) a subduction component, and (b) a variably depleted mantle source with either MORB- or plume-like geochemical characteristics, or a mixture of both. Table 5.2 gives the average isotopic compositions of possible end-members contributing to these magma genesis. The following sections describe: (i) how the composition of the subduction component of the lavas from north Tonga may vary, (ii) the mantle dynamics that have influenced the composition of the mantle wedge in north Tonga, and (iii) the modelling of the interaction between end-members.

	SSh	SPE	SS	Residual Samoan mantle[1] (average)	Central Lau Basin mantle[2]	Average fluids from PPS (Sp)[3]	Average fluids from PVS (Sv)[3]	Fluids from altered oceanic crust (A)[3]
$^{87}Sr/^{86}Sr$	0.70520	0.70570	0.70518	0.70550	0.70323	0.70850	0.70700	0.70464[4]
$^{143}Nd/^{144}Nd$	0.51280	0.51270	0.51241	0.51276	0.51312	0.51245	0.51290	0.51316[5]
$^{206}Pb/^{204}Pb$	19.075	18.748	18.374	18.916	18.114	18.788	19.100	18.450[5]
$^{207}Pb/^{204}Pb$	15.597	15.614	15.612	15.606	15.472	15.630	15.555	15.494[5]
$^{208}Pb/^{204}Pb$	39.162	39.011	38.490	39.089	37.994	38.700	38.750	37.905[5]
Δ8/4	47.34	71.79	64.88	59.22	46.72	35.83	3.11	-2.79
Δ7/4	3.95	9.20	12.93	6.40	1.74	10.24	-0.64	0.30
Pb	2.8	5.0	8.8	0.53	0.025	1.65	1.65	1.65
Sr	829	508	851	82.5	16.4	124	124	124
Nd	14.4	68.0	63.4	9.6	0.79	0.29	0.29	0.29

Table 5.2: The isotopic compositions of possible isotopic end-members of the lavas from north Tonga (used in mixing calculations):

*(i) The **plume-mantle end-member** is residual mantle from the Samoan plume, and therefore may have a similar isotopic composition to either the Samoan shield (SSh), or the post-erosional lavas (SPE), or the seamount (SS), or a mixture of them. An average isotopic composition of the Samoa, excluding that of the seamount (=average residual plume-mantle) is included in the table. The trace element composition of this average plume end-member is not well constrained due to the lack of knowledge about the degree of its depletion or partial melting. However, this has been estimated, using standard batch melting equations (Shaw, 1970) and an average Samoan melt composition, assuming that it underwent 15% partial melting. The modal composition of Samoan mantle is taken to be that of a xenolith (Hauri et al., 1993) and partition coefficients taken from Parkinson (1993).*

*(ii) The **MORB-mantle end-member** has the average isotopic composition of the Indian MORB mantle erupted at the Central Lau Spreading Centre, but its trace element composition may vary between that of depleted- and fertile-MORB mantle, depending on the degree of partial melting it has undergone.*

*(iii) The **subduction component** has an isotopic composition of fluids derived from the subducting Pacific plate (altered oceanic crust [A], with an isotopic composition similar to that of PMM, except for an elevated $^{87}Sr/^{86}Sr$ ratio) and Pacific pelagic and/or volcanogenic sediments (PPS and PVS), (=average of combination of that of A, PPS and PVS). The trace element compositions of these fluids can be estimated from the trace element compositions of the lavas from north Tonga[3] (Figure 4.12).*

[1] Average isotope compositions of the Samoan plume volcanics from *Wright & White (1986/87)*.

[2] Average isotope compositions of CLSC lavas from *Pearce et al. (1995b)*, and Pb, Sr and Nd concentrations for ~MORB mantle from *Hilton et al. (1993)* and *Cohen & O'Nions (1982)*.

[3] Estimated Sr, Nd and Pb concentrations in fluids derived from PPS, PVS and altered oceanic crust estimated from Figure 4.12, using the method of *Pearce et al. (1995a)*. Isotopic compositions of PPS and PVS from *Pearce & Hergt (unpubl. data)*.

[4] Maximum value of the $^{87}Sr/^{86}Sr$ ratio for altered oceanic crust taken from *Hart & Staudigel (1989)*, assuming about 80% water/rock ratio (Figure 5.1(a)). The actual ratio may be between this value and that of PMM (unaltered; =0.70246) depending on the degree of interaction with seawater.

[5] Isotopic composition of average PMM which is assumed to be similar to the composition of the subducting slab (see text for discussion).
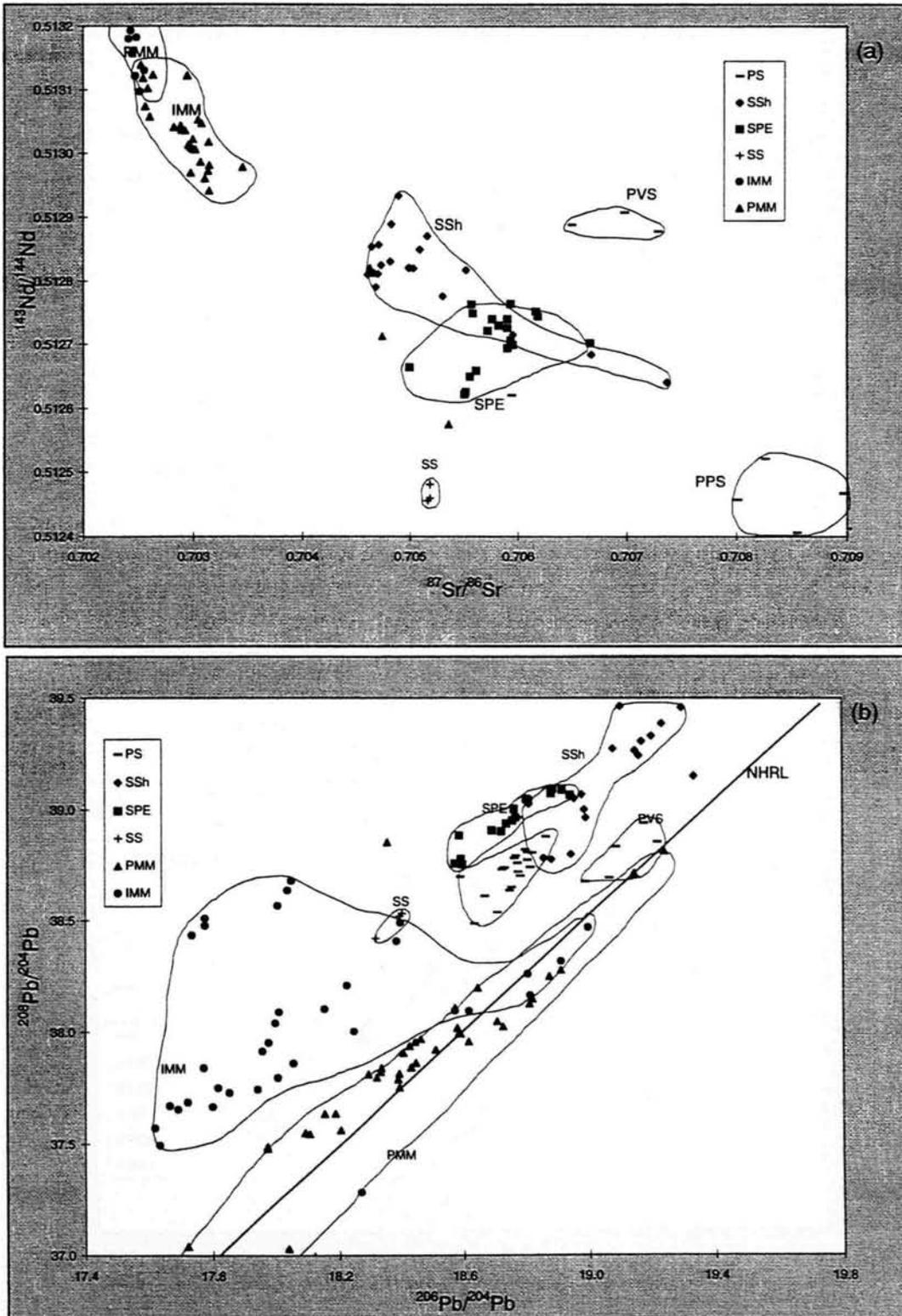
Figures 5.3(a)-(d): $^{143}Nd/^{144}Nd$-$^{87}Sr/^{86}Sr$ and $^{208}Pb/^{204}Pb$-, $^{207}Pb/^{204}Pb$- and $^{143}Nd/^{144}Nd$-$^{206}Pb/^{204}Pb$ showing fields outlining the isotopic data of the Samoan shield (SSh) and post-erosional volcanics (SPE), Pacific pelagic and volcanogenic sediments (PPS and PVS) and Indian and Pacific MORB mantle (IMM and PMM). Data sources are given in the text. These fields are used on the other isotopic plots (Figures 5.5, 5.6 and 5.8). It is not necessary for the precision of the placement of the field boundaries to be highly accurate (i.e statistically determined) in this study as they are meant to be illustrative of the possible isotopic compositions of end-members rather than for calculating precise ones.
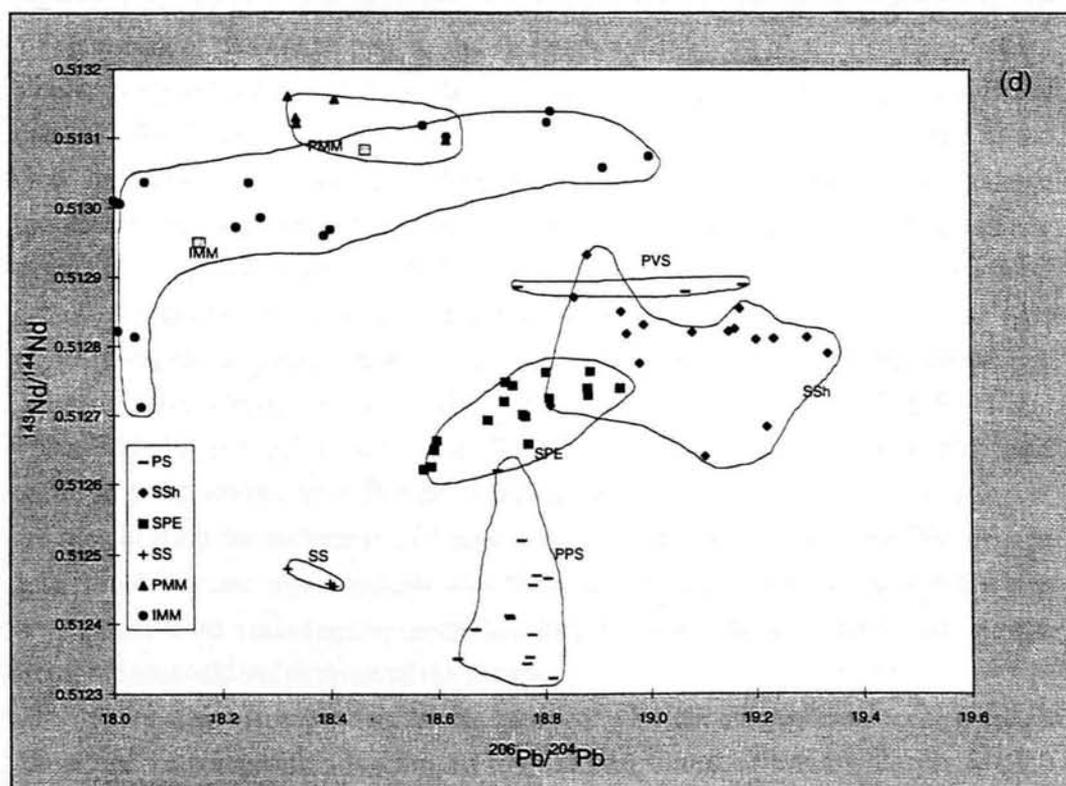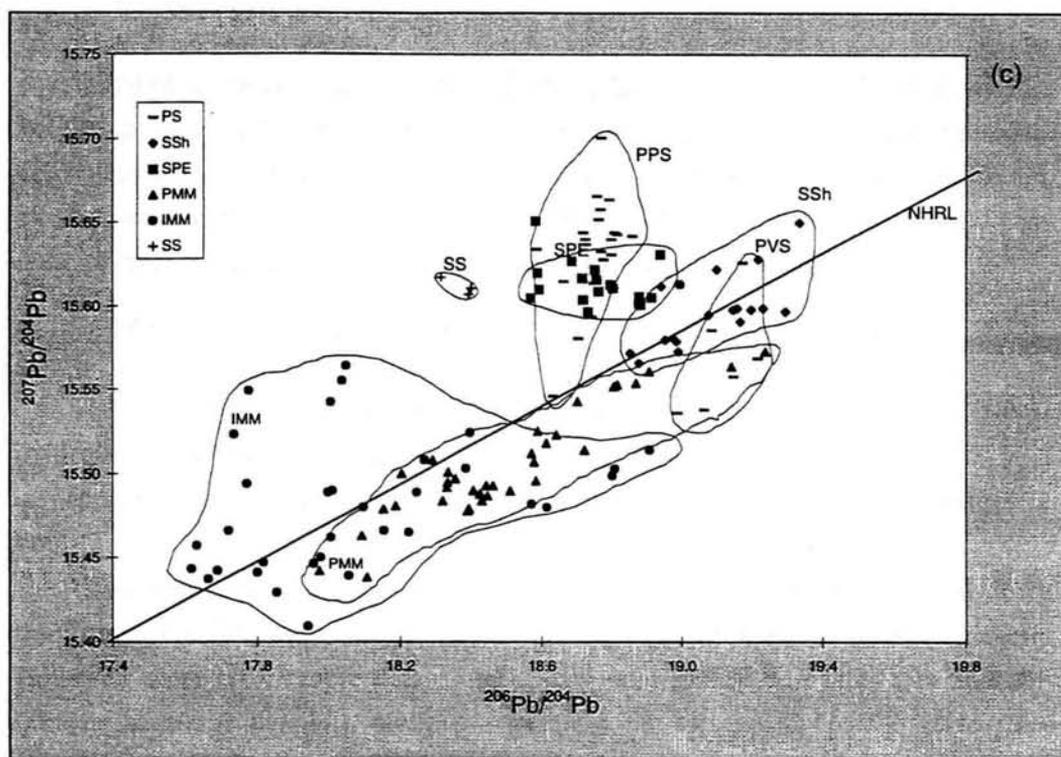
Figures 5.3(a)-(c) show fields defining data for the Pacific MORB mantle, Pacific pelagic and volcanogenic sediments, the Samoan shield, post-erosional volcanics, a seamount associated with the Samoan plume and Indian MORB mantle, all of which are possible end-member components of the lavas from north Tonga. The reasons for the choice of these as end-members are discussed below:

5.3.2 The subduction component

Isotopically, the subduction component may have the composition of fluids (hydrous or siliceous), or melts, derived from either the subducted slab, i.e. a signature of altered Pacific oceanic crust, or subducted sediments, or a mixture of both.

The actual composition of sediments and oceanic crust being subducted down the Tonga trench is not available due to the logistical problems of sampling them. However, there are isotopic data of sediments from DSDP drill sites 204 and 595 (*Pearce & Hergt unpubl.*), and from locations on the central Pacific plate (*Ben Othman et al., 1989*). These drill sites are respectively located approximately 100 and 1000km east of the Tonga trench, and therefore are likely to contain sediments with similar compositions to those which are being subducted. In north Tonga, it is likely that both Pacific pelagic *and* volcanogenic sediments are being subducted due to the close proximity of Samoa and Samoan seamounts to the trench. The relative proportions of each type of sediment being subducted are likely to vary along the trench and cannot be constrained. The isotopic compositions of sediments from these drill sites indicate that there are two distinct types of sediment (Figure 5.3). One type of sediment has a similar range of isotopic compositions to those of Pacific pelagic sediment (*Ben Othman et al., 1989*). The other type has higher $^{143}Nd/^{144}Nd$ and $^{206}Pb/^{204}Pb$, lower $^{87}Sr/^{86}Sr$ ratios than those of PPS. I have labelled the field defined by these compositions with Pacific volcanogenic sediments (PVS) as these samples are mostly from the sediments of Cretaceous or older age from drill site 204 (Figure 2.7), which contain large amounts of tuffaceous material. However, these sediments are distinct from volcanogenic sediments derived from Samoa, which have similar isotopic compositions to those of the plume.

There are no isotopic data for the subducting Pacific slab (altered oceanic crust). Therefore, its composition is assumed to be similar to that of average Pacific MORB mantle from the East Pacific Rise (*Hamelin et al., 1984; White et al., 1987; Ito et al., 1987*). This is a fair assumption if the slab is young, for its Nd and Pb isotopic composition, as interaction with seawater will cause very little change in these isotopes (Figure 5.1(a)). However, its 87/86 ratio of Sr is increased due to the high

Sr/Nd ratio of seawater. Also, if the subducting slab is old then its high U/Pb and low Th/U ratios will lead to increased $^{206}Pb/^{204}Pb$ and decreased $^{208}Pb/^{204}Pb$ ratios respectively, relative to unaltered Pacific crust (Table 5.1). The extent of this interaction is unlimited, but data from oceanic crust elsewhere suggest that an approximate increase of 30% of its Sr content occurs as a result of interaction with seawater (*Pearce et al., 1995a*). Therefore, these factors contribute to making the isotopic composition of the subduction component hard to constrain.

5.3.3 The isotopic composition of the mantle wedge

The Indian MORB mantle isotopic compositions of the Eocene lavas from 'Eua, the lavas from Central Lau Spreading Centre and the northern Lau basin and from the drill sites in the younger parts of the central Lau Basin (*Kempton & Tappin, 1994; Loock et al., 1990; Hergt & Hawkesworth, 1994; Pearce et al., 1995b*) suggest that a reservoir with this signature has been present under the Lau Basin since at least the Eocene. The south-east Indian Ridge (SEIR) is one of the spreading centres associated
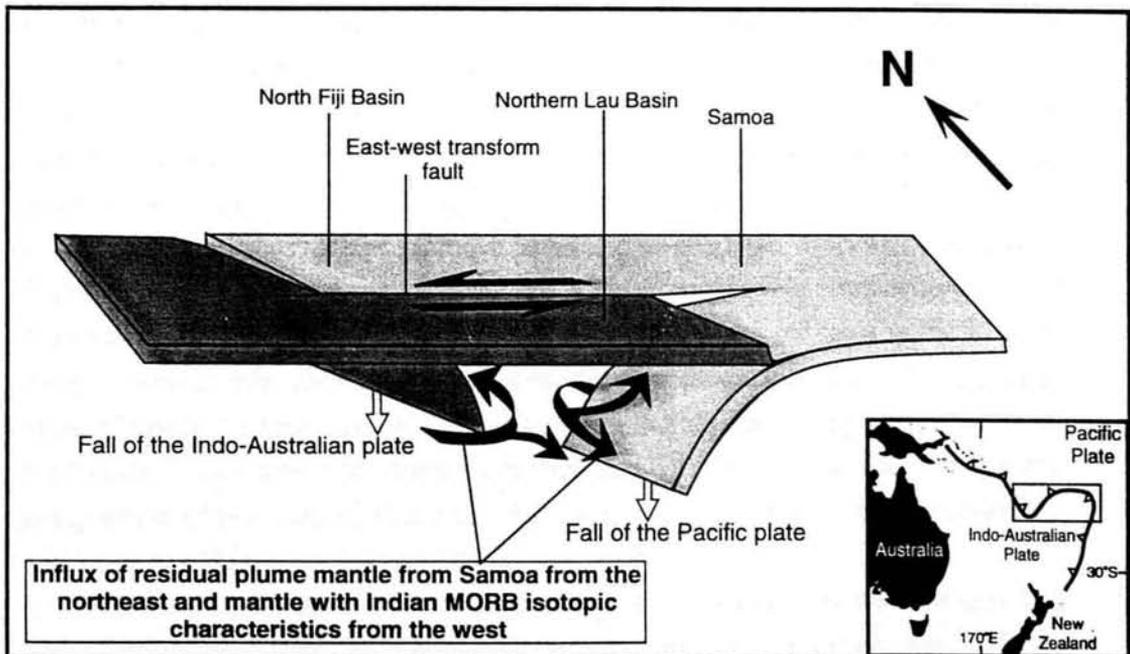
Figure 5.4: A three-dimensional diagram of the northern Lau Basin (area indicated by the box on inset geographical diagram of the southwest Pacific), adapted from Cann (1994), showing the structure of the Pacific plate at the northern termination of the Tonga trench. Vectors also indicate the gravitational forces on the Pacific and Indo-Australian plates, which result in slab roll-back at the trench. Vectors for the possible influxes of aesthenospheric mantle from the Samoan plume in the northeast, and MORB mantle from the west, which are a result of processes related to slab roll-back, are also shown.

with the Indian plate, for which there are isotopic data available. It is the closest one to the Lau Basin, and therefore, the compositions of lavas from it are assumed to be possibilities for those of the Indian MORB mantle that is present under the Lau Basin. *Klein et al. (1988)* found that basalts from the SEIR form two isotopically and geographically distinct groups, having affinities with either Indian Ocean or Pacific Ocean isotope compositions (Figures 5.3(b) and (c)). I have included all the SEIR data in one field which I have called Indian MORB mantle (IMM), despite its overlap with compositions similar to those of Pacific MORB mantle (*Hamelin et al., 1984; Michard et al., 1986; Klein et al., 1988*). This compositional field has been used on the isotope plots in this thesis, as it may contain some possible end-member compositions of the mantle wedge.

The mantle sources of the north Tongan boninites, and the lavas from Tafahi, Niuatoputapu and the Northern Lau Spreading Centre have plume-like geochemical characteristics (Figure 4.12), suggesting they are likely to be, or partly be, residual mantle from the Samoan plume. Influx of this mantle into their source regions is from the north-east through the rip in Pacific plate at the northern termination of the Tonga trench. Figure 5.4 is a diagram adapted from *Cann (1994)*, showing the possible vector of this influx, which is induced by the suction forces produced by subduction roll-back, as the Lau Basin opens. These source regions could therefore have a similar isotopic composition to that of residual plume mantle that may have produced the magmas associated with either the Samoan shield, or post-erosional volcanics, or lavas from a Samoan seamount. On the isotope plots in this thesis, fields for the isotopic compositions of the Samoan shield, post-erosional volcanics (*Wright & White, 1986/87*) and the Samoan seamount are used as possible compositions of the plume end-member (Figures 5.3(a)-(c)). These are likely to be the same as the isotopic compositions of their associated residual mantle sources, and hence may be similar to those of residual plume mantle that has influxed into the source regions of the lavas from north Tonga. Therefore, there are a large number of possibilities for the isotopic composition of this mantle. These are discussed when the isotopic data are described and interpreted (Sections 5.4 and 5.5).

To summarise, there exist two possible mantle domains in the northern Lau Basin, which may form the sources of the lavas from north Tonga, one with the isotopic characteristics of Indian MORB mantle, and the other with those of residual Samoan plume mantle. It is possible that mixing between these domains can occur in specific cases, and therefore produce a 'mixed' mantle source. I have therefore shaded the region between these end-members on the isotope plots in this chapter, calling it the *mantle array*. This shaded area represents the possible isotopic compositions of

the mantle wedge in the region of the partial melting that produced the primary magmas associated with the lavas from north Tonga.

5.3.4 Interaction between end-members

The interaction between two end-members of different isotopic compositions is assumed to take place by simple bulk-mixing. The locus of isotopic compositions produced by the mixing of two end-members will depend on the degree that each component contributes to the isotopic signature, and also on the concentration of the element in question in each component. The mixing equations are taken from *Fauré (1986)*. Simple bulk mixing is likely to be a good approximation of this process, but is too simplistic. The system may actually be more complex, containing more than two components and/or the resulting mixtures may be modified by further reactions or processes after mixing has taken place. Also, little is known about the way these components actually interact, such as whether it occurs during partial melting, or by a diffusive process, or by physical interaction between the two types of mantle in the solid state.

Figures 5.5(a)-(d) are isotope plots showing the possible compositions of magmas which are produced by the interactions between end-members from the mantle wedge and the subduction component. Figures 5.5(c) and (d) show the possible compositions of the subduction component of the lavas from north Tonga: there are three possible end-members from which this component could be derived, altered oceanic crust (A), Pacific pelagic and volcanogenic sediment (Sp and Sv). If the proportion of Sp:Sv being subducted is known (i.e. point S), then the composition of the subduction component is constrained to lie on an AS line. If the proportion of the crust:sediment contributions to the subduction component is known then its composition can be further constrained to a *point* on line AS. Figures 5.5(c) and (d) show that enrichment due to a subduction component leads to an increase in $^{87}Sr/^{86}Sr$, $^{206}Pb/^{204}Pb \pm ^{207}Pb/^{204}Pb$ and $^{208}Pb/^{204}Pb$ ratios, and a decrease in $^{143}Nd/^{144}Nd$ ratios (for high fluid/magma ratios) compared with those of MORB.

Figures 5.5(a) and (b) show a three-component model that may explain the possible magma compositions produced by the interaction between the chosen isotopic end-members. The position of W (the composition of the mantle wedge) may vary depending on the proportion of Indian MORB- to plume-mantle in the source of the particular lavas, as shown by the double-headed arrow. The isotopic composition of the subduction component may also vary, as shown in Figures 5.5(c) and (d), depending on the relative contributions of fluids derived from altered oceanic crust

135

(A) and subducted sediment (S). The composition of S depends on the relative contribution of Pacific pelagic and volcanogenic sediments to these fluids. A source containing a high proportion of plume-mantle leads to an increase in $^{206}Pb/^{204}Pb$, $^{207}Pb/^{204}Pb$ and $^{208}Pb/^{204}Pb$, and $^{87}Sr/^{86}Sr$ ratios and a decrease in $^{143}Nd/^{144}Nd$ ratios compared with those of MORB.

5.4 Isotopic characteristics of the lavas from north Tonga

In this section the isotopic characteristics of the lavas from north Tonga are described, and the end-member components in each location are identified. The extent to which a three-component ('W-A-S') model can be applied to these data is then investigated in Section 5.5.

Figure 5.6(a)-(d) are $^{87}Sr/^{86}Sr$-$^{143}Nd/^{144}Nd$, $^{208}Pb/^{204}Pb$-, $^{207}Pb/^{204}Pb$- and $^{143}Nd/^{144}Nd$-$^{206}Pb/^{204}Pb$ plots for the north Tongan boninites, the lavas from Tafahi, Niuatoputapu, the Tofua arc, the Northern and Central Lau Spreading Centres and Niua Fo'ou (This thesis; *Ewart & Hawkesworth, 1987; Volpe et al., 1988; Loock et al., 1990; Falloon & Crawford, 1991; Hergt & Hawkesworth, 1994; Pearce et al., 1995b*). Data from lavas of the northern Lau Basin and the Peggy Ridge are also included on the $^{87}Sr/^{86}Sr$-$^{143}Nd/^{144}Nd$ plot (*Loock et al., 1990; Volpe et al., 1988*). The Northern Hemisphere Reference Line of *Hart (1984)* is also shown on the Pb isotope plots (Figures 5.6(b) and (c)). Data fields for the Samoan shield, post-erosional volcanics and seamount, Pacific pelagic and volcanogenic sediments, and Indian and Pacific MORB mantle are also shown (from Figure 5.3). The Samoan seamount has anomalous Sr and Nd isotopic compositions compared with those of the other plume volcanics, which are also very different from those of all the lavas from north Tonga. This suggests that the seamount does not have an isotopic composition that is typical of the Samoan plume, and therefore, is probably not a suitable candidate for an isotopic end-member of these lavas.

5.4.1 The north Tongan boninites

The north Tongan boninites have low $^{143}Nd/^{144}Nd$ and high $^{87}Sr/^{86}Sr$ ratios that are very similar to those of the Samoan plume. They have Pb isotopic compositions that plot above the Northern Hemisphere Reference Line (NHRL) and overlap with those of Pacific pelagic sediments (PPS). The $^{207}Pb/^{204}Pb$-$^{206}Pb/^{204}Pb$ compositions of the boninites also overlap with those of the Samoan shield (SSh) field. Their

$^{208}Pb/^{204}Pb$–$^{206}Pb/^{204}Pb$ compositions form a trend which can be explained by mixing between a component with an isotopic signature similar to that of Indian MORB mantle (IMM) and one with higher $^{208}Pb/^{204}Pb$ and $^{206}Pb/^{204}Pb$ ratios. The origin of this radiogenic component is ambiguous, with a possibility of having a similar isotopic composition to either those of Pacific pelagic sediments or the Samoan shield. The evidence for the origin of this component is discussed in Section 5.5.

5.4.2 Tafahi

Two distinct groups in the Tafahi lavas have been recognised in the trace element geochemistry (Section 4.5.3). These groups are also represented in their Pb isotope compositions: Group I having $^{206}Pb/^{204}Pb$ ratios of 18.90-19.10 and Group II having ratios of 19.20-19.40. The $^{143}Nd/^{144}Nd$ and $^{87}Sr/^{86}Sr$ compositions of all the lavas are displaced to higher $^{87}Sr/^{86}Sr$ and lower $^{143}Nd/^{144}Nd$ ratios than IMM and PMM, and lie on the edge of the Tofua arc field. Their Pb isotopic compositions form a distinct trend, sub-parallel to that of the north Tongan boninites, but displaced to higher $^{206}Pb/^{204}Pb$ ratios (18.85-19.33) on the $^{208}Pb/^{204}Pb$- and $^{207}Pb/^{204}Pb$–$^{206}Pb/^{204}Pb$ diagrams (Figures 5.6(b) and (c)). Their compositions straddle the Northern Hemisphere Reference Line, and overlap the field for Pacific volcanogenic sediments (PVS).

The overlap of the trend in the Tafahi isotopic data with the field of the isotopic compositions of PVS, suggests that fluids derived from the latter are likely to be an end-member component of the Tafahi lavas. Another end-member may exist, which has higher $^{208}Pb/^{204}Pb$, $^{207}Pb/^{204}Pb$ and $^{206}Pb/^{204}Pb$ ratios than those of both average Pacific and Indian MORB mantle (PMM and IMM). On Figure 5.6, it appears that this end-member does actually lie close to, or within, the PMM and IMM fields, but this depends on where the boundary of these fields are drawn. Figure 5.6 shows that the majority of the PMM data lie at $^{208}Pb/^{204}Pb$ and $^{206}Pb/^{204}Pb$ compositions less than 38.4 and 19.0 respectively, and the IMM field is not well defined at that point. Two PMM data points have compositions similar to those of Tafahi, which may, or may not, be taken as atypical of PMM. When the origins of this end-member are discussed in Section 5.5.2, it is assumed that these data points are atypical, even though they are included in the PMM data field on Figures 5.6(b) and (c). It is also assumed that the $^{208}Pb/^{204}Pb$ ratio of this component are too high at its $^{206}Pb/^{204}Pb$ for it to be IMM. A third end-member with higher $^{206}Pb/^{204}Pb$ than PVS has to be invoked to explain the compositions of the Group 2 lavas ($^{206}Pb/^{204}Pb$ 19.2-19.4). Therefore, the magma genesis of the Tafahi lavas is complex, involving at least three components!

5.4.3 Niuatoputapu

The lavas from Niuatoputapu have lower $^{143}Nd/^{144}Nd$ and higher $^{87}Sr/^{86}Sr$ ratios than the Tofua arc and Tafahi. These ratios are similar to those of some of the northern Lau Basin lavas. There is also not much variation in these ratios between the Niuatoputapu lavas. The lower values of the $^{143}Nd/^{144}Nd$ ratios of the Niuatoputapu lavas compared with those of the Tofua arc and Tafahi lavas may suggest that their source contained a higher proportion of a component with a low $^{143}Nd/^{144}Nd$ ratio. The nature of this component is ambiguous, as with the north Tongan boninites.

The Niuatoputapu lavas have similar Pb isotopic compositions to those of the Tafahi lavas with lower $^{206}Pb/^{204}Pb$ ratios. This suggests that Niuatoputapu is likely to have similar end-member components to those of Tafahi, namely fluids derived from Pacific volcanogenic sediments and possibly two others, one with $^{208}Pb/^{204}Pb$, $^{207}Pb/^{204}Pb$ and $^{206}Pb/^{204}Pb$ ratios higher than IMM and PMM, and the other with $^{206}Pb/^{204}Pb$ ratios higher than PVS.

5.4.4 The Northern Lau Spreading Centre

The lavas of the Northern Lau Spreading Centre (NLSC) have lower $^{143}Nd/^{144}Nd$ and higher $^{87}Sr/^{86}Sr$ ratios than PMM and IMM, similar to those of the northern Lau Basin and of Niuatoputapu lavas. This is in contrast to those of the Central Lau Spreading Centre lavas, which have similar $^{143}Nd/^{144}Nd$ to, and higher $^{87}Sr/^{86}Sr$ ratios than, IMM.

The NLSC data form a trend close to that of the north Tongan boninites on the $^{208}Pb/^{204}Pb$-$^{206}Pb/^{204}Pb$ plot (Figure 5.6(b)), but have slightly lower $^{206}Pb/^{204}Pb$ ratios. They are displaced to higher $^{208}Pb/^{204}Pb$ and $^{206}Pb/^{204}Pb$ ratios from the compositions of the northern Lau Basin and Central Lau Spreading Centre lavas, which lie within the IMM field. Their $^{207}Pb/^{204}Pb$ and $^{206}Pb/^{204}Pb$ ratios are higher than those of IMM, but lower than those of the north Tongan boninites.

The low $^{143}Nd/^{144}Nd$ and high $^{87}Sr/^{86}Sr$, $^{208}Pb/^{204}Pb$ and $^{206}Pb/^{204}Pb$ ratios of the NLSC lavas compared with those of IMM, PMM and the CLSC, suggests that their sources contain an end-member with low $^{143}Nd/^{144}Nd$ and high $^{87}Sr/^{86}Sr$, $^{208}Pb/^{204}Pb$ and $^{206}Pb/^{204}Pb$ ratios. The two possibilities for this end-member are plume-mantle and a subduction component derived from predominantly Pacific pelagic sediments. The trace elements suggest that the sources to these lavas have had only a very minor influence from a subduction component (Figure 4.12). Therefore, the unidentified end-member is more likely to originate from the Samoan plume than from a

subduction component. The Pb isotopic compositions of these lavas are therefore indicative of mixing between Indian MORB- and plume-mantle in their source region.

5.4.5 The Central Lau Spreading Centre, central Tofua arc and the Peggy Ridge

The Central Lau Spreading Centre lavas have similar $^{143}Nd/^{144}Nd$ ratios (0.51308-0.51314) to, higher and $^{87}Sr/^{86}Sr$ ratios (0.7030-0.7033) than, those of IMM. The Pb isotopic compositions of these lavas lie within the IMM field on both Figures 5.6(b) and (c).

The Peggy Ridge lavas have a large range of $^{143}Nd/^{144}Nd$ ratios (0.51318-0.51288), but low $^{87}Sr/^{86}Sr$ ratios (0.7029-0.7038). They vary from compositions similar to those of the CLSC, to ones similar to those of the NLSC and Niuatoputapu. This suggests that their sources are isotopically heterogenous. Dredged rocks from the Peggy Ridge include rock-types similar to back-arc basin basalts (*Hawkins & Melchior, 1985*), MORB-like basalts and highly-depleted high-Ca boninites, which were derived from a highly-depleted source by high degrees of partial melting (up to 30%). *Hawkins (1995)* argues that these samples may represent some of the first magmas erupted as the Lau Basin began to open, as they have similar geochemistry to the early-formed melts in other supra-subduction zone settings. He suggests they are not likely to be derived from magma-leakage on the transform fault, as proposed previously by *Parson & Tiffin (1993)*, owing to the large amount of melting, and unfractionated compositions, that their chemistry implies. The Peggy Ridge may comprise old crustal blocks forced up by transpression on the northwest-trending transform fault, similar to those of the older parts of the central Lau Basin (Figure 2.1; *Hawkins, 1995*).

The Tofua arc lavas have higher $^{87}Sr/^{86}Sr$ than those of MORB, and $^{143}Nd/^{144}Nd$ mostly lower than those of MORB, and similar to those of Tafahi. They have $^{208}Pb/^{204}Pb$-$^{206}Pb/^{204}Pb$ compositions which lie on the edge of the PMM field, and their $^{207}Pb/^{204}Pb$-$^{206}Pb/^{204}Pb$ ratios extend from the PMM field to higher $^{207}Pb/^{204}Pb$. *Ewart & Hawkesworth (1987)* explain that this trend is a result of a subduction component, which was a mixture of a slab-derived component, with a Pb isotopic composition similar to PMM, and one derived from PPS. The compositions of the Tofua arc lavas indicate that their Pb isotopic signatures are dominated by that of the subduction component rather than that of the mantle wedge (Figure 5.6(b) inset).

5.5 Preliminary discussion on the magma genesis of the lavas from north Tonga from the isotopes

5.5.1 A three-component model for the magma genesis of the lavas from north Tonga?

A three-component ('W-A-S') model has been introduced to explain the isotopic compositions of the lavas from north Tonga. This involves an end-member derived from the mantle wedge (W), which has been shown to have a composition similar to Indian MORB- or plume-mantle, or one derived from mixtures of these end-members. The other two end-members contribute towards the subduction component: fluids derived from altered oceanic crust (A) and from sediments (S). If this model is applicable to the magma genesis of the lavas from north Tonga, then the variations in their isotopic compositions are explained by mixing between these end-members. Their compositions will also lie within the cross-hatched area on Figures 5.6(a)-(c), for a particular W and S.

Figure 5.7 summarises the trace element evidence for the existence of two distinct mantle domains, one with MORB-like and the other plume-like geochemical characteristics, and also the nature of the sources (or end-member W) of the lavas from north Tonga. Trend 1 shown on Figure 5.7 is the locus of the compositions of residual plume-mantle after melting in garnet facies. This trend is towards decreasing Zr/Yb and Nb/Yb ratios with increasing depletion assuming that Yb is retained in garnet in the residue during partial melting. Trend 2 is the locus of the compositions of plume residual mantle if it is then partially melted in spinel facies. Trend 3 is the locus of the composition of MORB-mantle residues (or MORB-plume mantle mixtures) after melting in spinel facies. Trend 4 is produced by mixing between MORB- and residual plume mantle.

The north Tongan boninites and the lavas from Tafahi and Niuatoputapu have a source in the wedge (or W) that is residual plume-mantle, as their compositions lie within the tramlines of melt compositions produced by melting of this type of mantle in spinel facies. However, the compositions of the lavas from the Central Lau Spreading Centre and the Tofua arc lie within the tramlines of those of melts produced by melting MORB-type mantle. The lavas from the Northern Lau Spreading Centre have higher Nb/Yb for their Zr/Yb ratios compared those of MORB melts. Their compositions form a trend that may be explained if their source is a mixture of residual MORB- and plume-mantle (Figure 5.7). This mixing may have occurred if plume-mantle was entrained during their magma genesis.

The $^{208}Pb/^{204}Pb$-$^{206}Pb/^{204}Pb$ compositions of the north Tongan boninites form a trend parallel to the mantle array, but displaced towards the line AS. The exact

position of AS cannot be constrained due to the lack of knowledge of the composition of sediments being subducted, but it is likely to be dominated by the composition of PVS, rather than PPS. This may suggest that boninite magma genesis involved a variable W (i.e. varying proportions of an Indian MORB mantle and plume end-members in the source region, but dominated by the latter) mixing with a subduction component. The composition of the plume end-member could lie anywhere within the fields for the Samoan shield and post-erosional volcanics. However, I have assumed its composition is similar to that of the average of Samoa. The subduction component may have a constant or variable composition to explain the linear trend in the boninite Pb isotopic data. The low $^{143}Nd/^{144}Nd$ ratios of the north Tongan boninites, which are within the mantle array, also imply that they have a plume-dominated W, and the shift to high $^{87}Sr/^{86}Sr$ ratios suggests that mixing may have occurred between this and a subduction component. However, these $^{87}Sr/^{86}Sr$ ratios also lie within the field of the isotopic compositions of the Samoan shield volcanics and therefore could be related to heterogeneities within the plume, rather than to the addition of a subduction component. The boninites from the west, from close to the Northern Lau Spreading Centre, lie within the mantle array on Figure 5.6(a). This may suggest that their
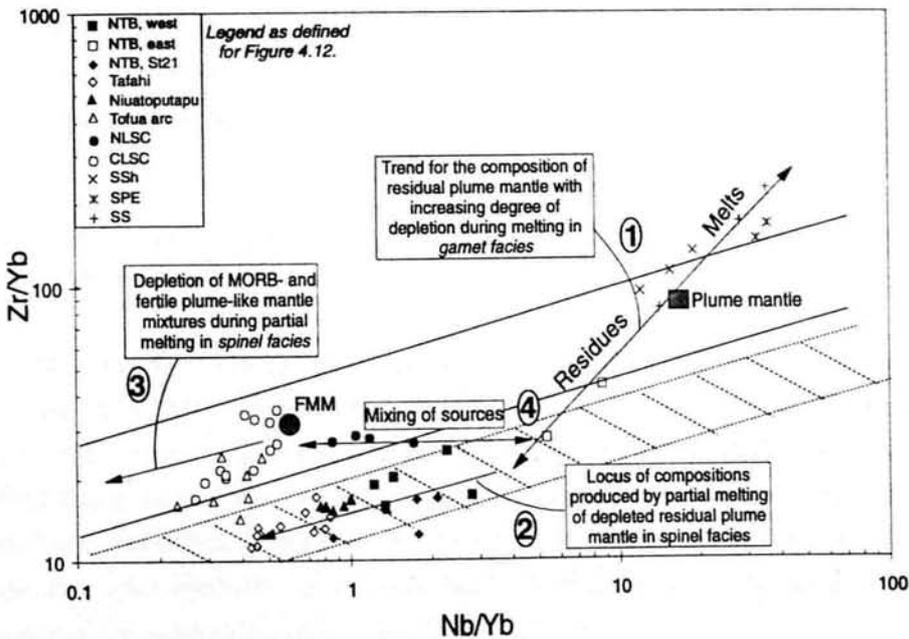
Figure 5.7: *Zr/Yb-Nb/Yb plot for the north Tongan boninites, the lavas from Tafahi, Niuatoputapu, the Tofua arc, and the Northern and Central Lau Spreading Centres. The solid tramlines indicate compositions of melts produced by partial melting of MORB mantle in spinel facies and the dashed ones those produced by melting of residual plume-mantle in spinel facies. The locus for the composition of residual plume-mantle after increasing degrees of partial melting in garnet facies is also shown.*

isotopic compositions have very little influence from the subduction component, if the shift to high $^{87}Sr/^{86}Sr$ ratios of the other boninites is related to this. The trace elements also support this (Figure 4.12).

The isotopic compositions of the lavas from the Northern Lau Spreading Centre lie within the mantle array on the Sr-Nd and Pb isotopic plots. This, therefore, suggests that the magma genesis of these lavas has had a negligible influence from a subduction component and that Indian MORB- and plume-mantle domains have mixed in their source region to explain their compositions.

The plume-mantle domain does not extend as far south as the central Tofua arc (Figure 5.6) and therefore a domain with isotopic characteristics similar to those of the CLSC or ELSC, i.e. Indian MORB mantle, is likely to underlie this region. The subduction component south of the northern Lau Basin is likely to contain very little PVS as there is no source for this sediment-type compared with in the north, where it is derived from Samoa and its associated seamounts, and from other volcanogenic sources (Figure 2.7). Hence, S lies in, or very close to, PPS. The inset to Figure 5.6(b) shows a possible three-component model for the lavas from the Tofua arc. However, the compositions of these lavas are dominated by that of the subduction component as they lie on the mixing line (AS) between fluids derived from altered oceanic crust (A) and from PPS (S). Another complication exists in the north, as it is possible that plume crust is subducted at the Tonga trench in this region. This would cause any slab-derived fluids to acquire the isotopic signature of the plume (Section 6.2.1).

5.5.2 The origin of the isotopic compositions of the Tafahi and Niuatoputapu lavas

The lavas from Tafahi and Niuatoputapu have low $^{143}Nd/^{144}Nd$ ratios compared with those of MORB. The lavas from Niuatoputapu have similar $^{143}Nd/^{144}Nd$ ratios to those from the northern Lau Basin and the Northern Lau Spreading Centre, but higher $^{87}Sr/^{86}Sr$ ratios, on the edge, or just above, the mantle array. Similarly, the lavas from Tafahi have higher $^{87}Sr/^{86}Sr$ ratios than those of the mantle array. As with the north Tongan boninites (Section 5.5.1), these high $^{87}Sr/^{86}Sr$ ratios can be attributed to the influence of the subduction component (Section 5.4.3).

The Pb isotope data of these lavas can be explained in several ways (Figure 5.8). Some of the Tafahi lavas have higher $^{206}Pb/^{204}Pb$ ratios than PVS, suggesting that a simple 'W-A-S' model cannot be applied to their magma genesis unless another unknown end-member (X) is invoked. This end-member has a composition lying outside the original triangle of possible end-members proposed in Figure 5.5. This

could be possible if the sediments analysed from DSDP sites 204 and 595 are not completely representative of those being subducted at the northern Tonga trench, which may actually include ones with more extreme isotopic compositions. If this is the case, then the Tafahi and Niuatoputapu Pb isotope data form a trend between this end-member (X) and one with lower $^{208}Pb/^{204}Pb$ and $^{206}Pb/^{204}Pb$ ratios (C). Two possible models for the magma genesis of these lavas have been proposed below:

Model 1: *Ewart et al. (1994)* and *Hergt & Hawkesworth (1994)* suggest that end-member C_1 has a similar composition to a slab-flux from the 'original' arc. The isotopic composition of C_1 lies on an AS line (within the 'WAS' model) which may be similar to that of the subduction component associated with early-arc magmatism (> 6Ma). This is because its composition overlaps with possible ones of slab-fluxes of lavas associated with the early-arc (see the trend of the isotopic data of the Eocene 'Eua lavas on Figure 5.8(a), which converges to the composition of C_1). The trend in the Pb isotopic data of the Tafahi lavas is therefore produced by mixing between this slab-flux and the unknown end-member (X).

Model 2: An alternative to this model also proposes that the Pb isotopic compositions of the Tafahi and Niuatoputapu lavas are part of a ('W-A-S') three-component model, but are dominated by that of a slab-flux (c.f. South Sandwich Island lavas; *Pearce et al., 1995a*). The composition of this slab-flux lies between that of fluids derived from the subducting slab (A) and subducted Pacific volcanogenic sediments (Sv). The Pb compositions of the Niuatoputapu and Group 2 Tafahi lavas lie on this A-Sv line, but the more extreme compositions of the Group 1 Tafahi lavas are explained if the unknown end-member (X) mixes with this slab-flux.

These models for the magma genesis of the Tafahi lavas are further developed in Section 6.2.3, using evidence from the variations in their trace element *and* isotopic compositions.

5.6 Chapter 5 Summary

• The effects of alteration of the lavas from north Tonga are studied by comparing the isotopic compositions of their leachates and residues. Alteration minerals are removed during leaching and therefore the leachates have the isotopic signature of this alteration component, whereas the residues have that of the sample prior to alteration. The leachates of the north Tongan boninites and tholeiites and a few of the lavas from Tafahi and Niuatoputapu have elevated $^{87}Sr/^{86}Sr$ compared with their residues, suggesting that seawater alteration of these samples has occurred. The

leachates of the north Tongan boninites have Pb isotopic compositions similar to those of Indian MORB mantle. This suggests that they have been altered by a mantle component with this isotopic composition, which may originate from altered oceanic crust. The leachates and corresponding residues of the north Tongan tholeiites and the lavas from Tafahi and Niuatoputapu have similar Pb isotopic compositions, suggesting that either these samples have not been affected by alteration, or that Pb was not mobile during it.

• The isotope systematics:

The isotopic signatures of the lavas from north Tonga originate from those of the subduction component and the mantle wedge. The compositions of the subduction component and the mantle wedge are derived from a combination of isotopic end-members. The subduction component is comprised of fluids, which may be derived from the subducting slab (altered oceanic crust), Pacific pelagic and/or volcanogenic sediments, or a mixture of these. Evidence from the trace elements (Figure 5.7) and isotopes, suggest that the composition of the mantle wedge may be derived from up to two isotopic end-members in north Tonga: Indian MORB- and/or Samoan plume-mantle. The IMM domain is likely to have similar compositions to those of the lavas from the Central Lau Spreading Centre, and the plume one probably has compositions similar to that of an average of the Samoan plume volcanics (=isotopic composition of average residual plume-mantle). The *mantle array* represents the range of compositions of the mantle wedge between these end-member compositions. I have assumed that the isotopic compositions of the lavas depend on the relative contribution of their isotopic end-members to their magma genesis.

• I have attempted to use *the isotopic characteristics* of the lavas from north Tonga to identify their isotopic end-members and hence, to propose models to explain their magma genesis in terms of mixing between them:

(a) The north Tongan boninites:

These have low $^{143}Nd/^{144}Nd$ and high $^{87}Sr/^{86}Sr$ ratios compared with those of MORB, but which are similar to those of the Samoan plume. These can be explained if their source was residual plume-mantle, but the variation in their $^{87}Sr/^{86}Sr$ ratios could be attributed either to heterogeneities within this mantle, or to the influence of a subduction component. Their Pb isotopic compositions overlap with those of the Samoan shield and form a trend on the $^{208}Pb/^{204}Pb$-$^{206}Pb/^{204}Pb$ plot that can be

explained by mixing between a component with a similar isotopic signature as Indian MORB mantle, and one with high $^{208}Pb/^{204}Pb$ and $^{206}Pb/^{204}Pb$ ratios. The latter could either be derived from a subduction component dominated by a contribution from Pacific pelagic sediments, or from the Samoan plume. The trace elements (Figure 5.7; Chapter 4) suggest that the Pb isotopic compositions of the north Tongan boninites are dominated by the signature of the plume rather than that of PPS. The isotopic compositions of the lavas from Tafahi and Niuatoputapu suggest that predominantly PVS are being subducted at the northern Tonga trench. The isotope compositions of the north Tongan boninites are dominated by the signature of an IMM-plume mixture of variable composition, but with a small influence of a subduction component (variable or constant composition?).

(b) the lavas of Tafahi:

These are characterised by a shift to lower $^{143}Nd/^{144}Nd$ and higher $^{87}Sr/^{86}Sr$ ratios from those of MORB. Their Pb isotopic compositions form two groups: Group 1 with $^{206}Pb/^{204}Pb$ of 18.90-19.20 and Group 2 with $^{206}Pb/^{204}Pb>19.20$, which lie on a trend straddling the Northern Hemisphere Reference Line, and overlapping with the compositions of Pacific volcanogenic sediments (PVS).

The low $^{143}Nd/^{144}Nd$ ratios can be explained if the sources were from within a plume-mantle domain. This is supported by evidence from the trace elements (Figure 5.7). The high $^{87}Sr/^{86}Sr$ ratios are a result of the influence of a subduction component. There are several possible ways of explaining the trend in the Pb data:

Model 1: the isotopic compositions of the lavas are a result of mixing between two unidentified end-members (X and C_1). X may represent a subduction component derived from subducted sediments that have more extreme isotopic compositions than those of PVS (from DSDP sites 204 and 595). The other has a similar isotopic composition as some of the Eocene volcanics of 'Eua and therefore it could represent a subduction component similar to the one associated with the early-arc (pre-Lau Basin).

Model 2: this is similar to Model 1, except that C_2 is a subduction component derived from altered oceanic crust and PVS, which is not necessarily similar to that of the 'original' arc. This, then, selectively mixes with X to explain the compositions of the Group 2 lavas ($^{206}Pb/^{204}Pb>19.2$). An end-member from the mantle array may also

149

be present (i.e. plume-mantle), but the isotopic compositions of the Tafahi lavas are dominated by the signature of the subduction component.

(c) the lavas from Niuatoputapu:

These have lower $^{143}Nd/^{144}Nd$ and higher $^{87}Sr/^{86}Sr$ ratios than those of MORB, the Tofua arc and Tafahi, but similar ones to the lavas from the northern Lau Basin and Niua Fo'ou. Their Pb isotopic compositions are similar to those of Group 1 Tafahi lavas ($^{206}Pb/^{204}Pb<19.2$).

The low $^{143}Nd/^{144}Nd$ and high $^{87}Sr/^{86}Sr$ ratios can be explained if the source region to these lavas was residual plume-mantle, but the high $^{87}Sr/^{86}Sr$ ratios (above the mantle array) are more likely to be due to the influence of a subduction component. The trace elements also support evidence for the plume-mantle source of these lavas (Figure 5.7). The similarity of the Pb isotopic compositions between the lavas from Niuatoputapu and those of Group 1 Tafahi lavas suggest that they may be explained by similar models.

(d) the lavas from the Northern Lau Spreading Centre:

These lavas have lower $^{143}Nd/^{144}Nd$ and higher $^{87}Sr/^{86}Sr$ than those of MORB. Their Sr and Nd isotopic compositions are similar to those of the northern Lau basin lavas and Niuatoputapu. Their Pb isotopic compositions form a trend close to that of the north Tongan boninites, but with lower $^{206}Pb/^{204}Pb$. Their compositions are displaced to higher $^{208}Pb/^{204}Pb$ and $^{206}Pb/^{204}Pb$ from those of field of IMM, and those of the Central Lau Spreading Centre lavas, towards the fields of the compositions of the Samoan shield and Pacific pelagic sediments. Both the Samoan shield and a component derived from Pacific pelagic sediments may be the $^{208}Pb/^{204}Pb$ and $^{206}Pb/^{204}Pb$ end-member. However, the trace elements suggest that the NLSC lavas contain a geochemical signature from the plume, but a very weak one from the subduction component (Figure 4.12). Therefore, the end-member with high $^{208}Pb/^{204}Pb$ and $^{206}Pb/^{204}Pb$ is more likely to originate from the plume rather than a subduction component dominated by the composition of PPS. The isotopic signatures of the Northern Lau Spreading Centre lavas are a result of mixing between Indian MORB- and plume-mantle in their source region.

CHAPTER 6

Magma genesis of the young lavas from north Tonga

6.1 Introduction

The three-component model, which was introduced in Chapter 5, for the magma genesis of the lavas from north Tonga, is developed in this chapter, using combinations of the available trace element and isotope data. Often the trace element data have proven more useful than the isotope data (Section 4.5.3 and following sections).

In this chapter, the following are further investigated:

(1) the nature of the subduction component, using the Pb isotopes and Ce/Pb ratios of the lavas from north Tonga;

(2) evidence for the plume mantle sources of some of the lavas;

(3) the possible origins of the geochemical signatures of the Tafahi lavas, i.e. whether they are a result of a variable source or subduction component, or both.

6.2 Isotope-trace element variation

It has already been shown from the isotopes and the trace elements that the lavas from north Tonga have variable mantle sources, which may have the isotopic characteristics of either Indian MORB mantle, or the Samoan plume, or a mixture of both. These sources may be enriched in LILE ± LREE by a subduction component (Figures 4.5, 4.12 and 4.13), which comprises hydrous fluids derived from subducted Pacific slab and sediments.

6.2.1 The origin of the subduction component?

Supra-subduction zone volcanics have low Ce/Pb ratios (c. 3) compared with those of oceanic basalts (c. 25) and Bulk Earth (c.10), (Figure 6.1(a); *Miller et al., 1994*). Pb and Ce have similar bulk solid/liquid partition coefficients ($K_d$clinopyroxene/liquid Pb=0.072, Ce=0.098; *Keppler, 1996*; *Parkinson, 1993*),

suggesting that they are not likely to be significantly fractionated during mantle melting processes *(Hoffman et al., 1986)*. Therefore, Ce/Pb ratios of a melt should approximately reflect that of its source *(Hofmann et al., 1986)*. *Miller et al. (1994)* showed that the Ce/Pb and $^{207}Pb/^{204}Pb$ ratios of lavas from two adjacent volcanoes on Umnak island, Aleutian Islands, Alaska, form a trend between a component with a low
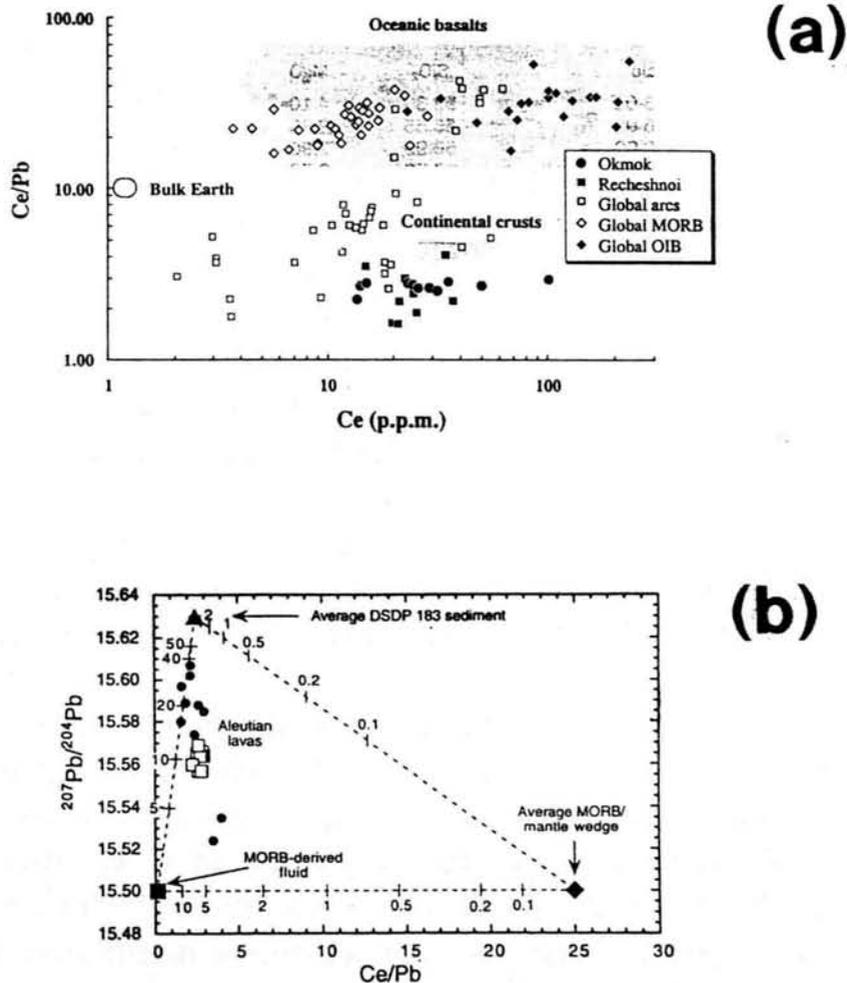
Figure 6.1: (a) *A global comparison of the Ce/Pb ratios of oceanic basalts, convergent margin lavas, the continental crust and bulk Earth (from Miller at al., 1994). Okmok and Recheshnoi are volcanoes from Umnak island, Aleutian Islands. This diagrams illustrates the low Ce/Pb ratios of arc-related volcanics compared with MORB and OIB; (b)* $^{207}Pb/^{204}Pb$ *vs Ce/Pb ratios for lavas from the Okmok (filled circles) and Recheshnoi (open squares) volcanoes (Miller et al., 1994; Brenan et al., 1995). The variations in the data are a result mixing between a component derived from average pelagic sediments (DSDP 183) and one with low Ce/Pb and* $^{207}Pb/^{204}Pb$ *ratios (MORB-derived fluid). Tick marks correspond to weight % of one end-member in each binary mixture.*

Ce/Pb ratio (c. 2.5) and high [207]Pb/[204]Pb ratio (15.63) and one with a low Ce/Pb ratio (<5) and [207]Pb/[204]Pb ratio (15.50), (Figure 6.1(b)). They showed that the latter component could not originate from the mantle wedge (Ce/Pb~25), but could be a MORB-derived fluid (Ce/Pb<5), due to the fact that its [207]Pb/[204]Pb ratio is similar to that of MORB and its Ce/Pb ratio is low.

Brenan et al. (1995) carried out experiments, at 2.0 GPa and 900°C, to estimate the Ce/Pb ratios of fluids coexisting with phases (clinopyroxene and garnet) that may be residual during the dehydration of basalt at high-pressure. They assumed that this process leaves a residue of garnet and clinopyroxene in a proportion 60:40 respectively, and used bulk rock/fluid partition coefficients, as calculated from average mineral/fluid values, of ~0.05 for Pb and ~11 for Ce. Their calculations show that, for average MORB, containing 7.5 ppm Ce and 0.3 ppm Pb *(Miller et al., 1994)*, the Ce/Pb ratio of fluid (2%) derived from it would be approximately 0.16. This demonstrates experimentally that the component with a low Ce/Pb ratio and [207]Pb/[204]Pb could be a MORB-derived fluid.

However, in 'real' systems, it is likely that the slab dehydrates over a large range of temperatures and pressures. As fluid/rock partition coefficients are temperature and pressure dependent, this results in difficulty in constraining their values. The composition of the slab during the dehydration process is also hard to constrain as it varies with temperature and pressure. Therefore, estimates of the composition of the slab-derived fluid, using partition coefficients are not likely to be representative of fluids generated in 'real' subduction zones *(Miller et al., 1994; Brenan et al., 1995; Keppler, 1996)*.

I have used the [207]Pb/[204]Pb-Ce/Pb plot from *Miller et al. (1994)* and *Brenan et al. (1995)*, and also a [208]Pb/[204]Pb-Ce/Pb plot to attempt to describe the magma genesis of the lavas from north Tonga in a similar way (Figures 6.2(a) and (b)). I have included an average composition of the Samoan plume (≈average plume mantle from Table 5.2), which has high [207]Pb/[204]Pb, [208]Pb/[204]Pb and a high Ce/Pb ratio (20), as the isotopes and trace elements suggest that this is the source of some of the lavas (Figures 5.6 and 5.7). The compositions of average MORB, average MORB-, and sediment-derived fluids are also plotted on this diagram *(Hamelin et al., 1984, 1986; Michard et al., 1986; Ito et al., 1987; White et al., 1987; Klein et al., 1988; Ben Othman et al., 1989; Hergt & Pearce, unpubl.; Brenan et al., 1995)*. However, the compositions of fluids derived from pelagic and volcanogenic sediments are not distinguishable on these diagrams.

The subduction-related lavas from north Tonga have low Ce/Pb ratios: 0.8-3.5 for the north Tongan boninites , 1.5-3.2 for Tafahi, and 2-4 for Niuatoputapu. The Tofua arc lavas also have low Ce/Pb ratios (0.7-4.0), but lower [207]Pb/[204]Pb and
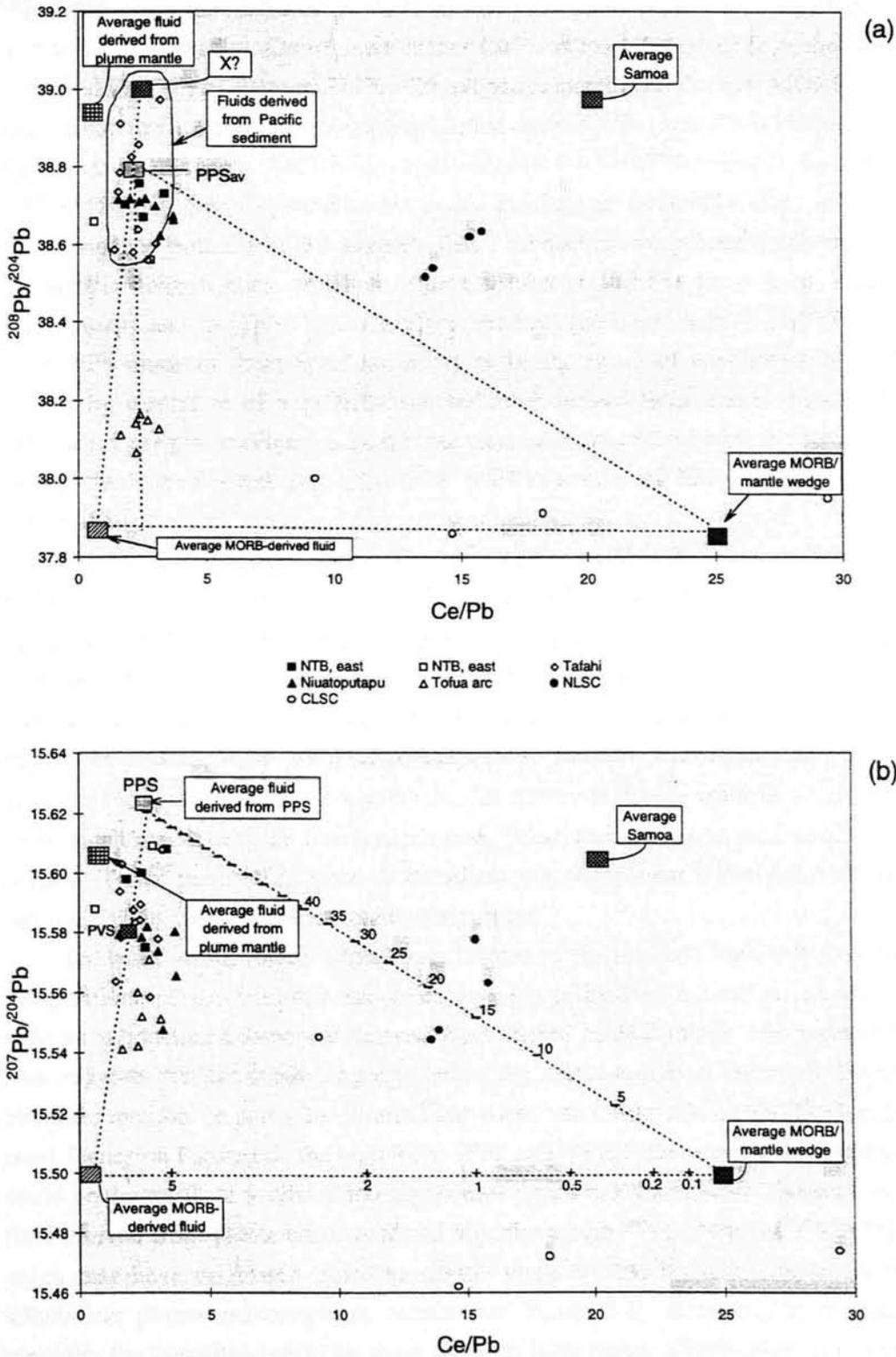
Figure 6.2 : $^{208}Pb/^{204}Pb$ and $^{207}Pb/^{204}Pb$ vs Ce/Pb plots for the north Tongan boninites, lavas from Tafahi, Niuatoputapu, the Tofua arc and the Northern and Central Lau Spreading Centres (c.f. Miller et al., 1994; Brenan et al., 1995). The compositions of average MORB, MORB-derived fluid, average Samoa, and those of fluids derived from average plume mantle and Pacific pelagic and volcanogenic sediments are plotted. Mixing lines between average MORB and MORB-derived fluid, and between MORB and average fluids derived from PPS are also shown.

154

$^{208}Pb/^{204}Pb$ ratios than those of the other subduction-related lavas. The lavas from the Northern Lau Spreading Centre have higher Ce/Pb ratios (13.5-16.0) than the other lavas, and high $^{207}Pb/^{204}Pb$ and $^{208}Pb/^{204}Pb$ ratios compared with those of MORB. The lavas from the Central Lau Spreading Centre have Ce/Pb and $^{208}Pb/^{204}Pb$ ratios between those of average MORB, or slightly higher, and MORB-derived fluids. Their $^{207}Pb/^{204}Pb$ ratios are more variable, but within the range of those of MORB.

Evidence from Figure 5.6 suggests that a subduction component dominates the Pb isotopic compositions, and hence the Ce/Pb ratios, of the lavas from Tafahi, Niuatoputapu and the Tofua arc. Therefore, the low Ce/Pb and high $^{207}Pb/^{204}Pb$ and $^{208}Pb/^{204}Pb$ ratios of these lavas are likely to be the result of enrichment of their sources by a mixture of a MORB- and sediment-derived fluid, rather than to the influence of the plume (Figure 6.2). It is not clear on Figure 6.2 whether the sediment-derived fluids are derived from either PPS or PVS, as both are likely to have similar compositions.

Figure 6.2 is not particularly effective in distinguishing between a subduction component with an isotopic signature of a mixture of MORB- and sediment-derived fluids and one that has an isotopic signature of the Samoan plume (either originating from the mantle wedge, or from subducted plume crust). The subduction component may acquire a plume isotopic signature if plume crust is subducted at the Tonga trench. At present, there are a large number of Samoan seamounts close to the northern Tonga trench and it is also likely that there was crustal material originating from the plume close to the trench in the past. This material may be subducted at the northern Tonga trench. Therefore, if the subduction component is derived from this material, it may acquire a plume isotopic signature.

Evidence from other plots (e.g. Figure 5.6) suggest that the isotopic compositions of the boninites are more strongly influenced by the plume than a hydrous subduction component derived from altered MORB-mantle and sediments. This suggests that the subducting slab below the source region of the north Tongan boninites may be, or partly be, plume lithosphere rather than altered Pacific oceanic crust. Hence on Figure 6.2, the high $^{207}Pb/^{204}Pb$ and $^{208}Pb/^{204}Pb$ ratios of the boninites could be the result of a subduction component which has the isotopic signature of a fluid derived from plume crust. Alternatively, these high $^{207}Pb/^{204}Pb$ and $^{208}Pb/^{204}Pb$ ratios may have originated from the mantle wedge in the boninite source region, which was plume asthenospheric mantle (see Figure 5.4). However, in the latter scenario, the boninites would be more likely to have higher Ce/Pb ratios (i.e. more like the Samoan plume rather than a fluid derived from subducted plume crust).

However, it is possible that the low Ce/Pb ratios of the boninites are a result of alteration, as Pb is a highly mobile element during alteration. Figure 4.12(d), a

diagram of Pb/Yb versus Nb/Yb, shows that Pb has not behaved in a similar way to other incompatible elements such as Th, Ba, Ce and Sr (Figure 4.12). The boninites from the west (16-26/1 and 16-26/2) have higher Pb/Yb ratios than the MORB-plume array, which either indicates a significant contribution of Pb to their sources by a subduction component, or they have undergone alteration. Other evidence suggests that these boninites do not have a significant influence from a subduction component (Figure 4.12). Therefore, the Pb trace element data are likely to be strongly affected by alteration. The isotopic data are of the residues of the samples, after leaching, and therefore any affects on these by alteration are likely to have been removed (Section 5.2). Therefore, the low Ce/Pb ratios and high $^{207}Pb/^{204}Pb$ and $^{208}Pb/^{204}Pb$ ratios of the north Tongan boninites are more likely to be a result of the influence of an hydrous subduction component derived from subducted plume crust.

Another possibility is that the fluids derived from the subducting slab and sediments acquire the isotopic signature of the plume as they percolate through the mantle wedge. *Hawkesworth et al. (1991b)* and *Stern et al. (1991)* point out that for the elements with isotope ratios, the apparent subduction zone input of dominantly slab-derived elements, as calculated from element abundances, is greater than estimates of the input based on the isotope ratios. They suggest that the selective enrichment of these elements is not solely due to the slab contribution, but also results from these elements being extracted from the mantle by aqueous, slab-derived fluids. However, *Pearce & Peate (1995)* also point out that: (1) these elements might actually be lost to, rather than extracted from, the mantle unless partition coefficients are in error, and (2) isotopes may exchange rather than extract elements from the mantle, in which case elements would be expected to give higher flux estimates than the isotopes. Hence, it is difficult to confirm from the compositions of the lavas from north Tonga whether their subduction components have acquired the isotopic signature of the plume from the mantle wedge.

The high Ce/Pb ratios of the Northern Lau Spreading Centre lavas compared with those of the other lavas from north Tonga and the Tofua arc suggest that it is not likely that their source contained a hydrous subduction component.

In summary, the low Ce/Pb, and high $^{207}Pb/^{204}Pb$ and $^{208}Pb/^{204}Pb$ ratios of the subduction-related lavas from north Tonga (north Tongan boninites, Tafahi, Niuatoputapu) are a result of enrichment of their sources by hydrous subduction components, which contain high concentrations of Pb relative to Ce. However, the low Ce/Pb, and high $^{207}Pb/^{204}Pb$ and $^{208}Pb/^{204}Pb$ ratios of the north Tongan boninites are more likely to originate from either a subduction component that was derived from subducted plume crust, or the mantle wedge, or an alteration effect.

6.2.2 Isotope-trace element variations: is a three-component model applicable?

Figure 6.3 is a plot of Zr/Sm against $^{143}Nd/^{144}Nd$ for the lavas from north Tonga, the Central Lau Spreading Centre and the Tofua arc. A field for possible compositions of the subduction component is shown (cross-hatched area). The isotopic compositions of mixtures of fluids derived from altered oceanic crust, sediments (PPS and PVS), and plume crust overlap, and therefore this field covers a large range of $^{143}Nd/^{144}Nd$ ratios, but is at low Zr/Sm ratios due to the immobility of Zr in fluids (Section 4.5.4). Therefore, trends in data towards low Zr/Sm ratios may be indicative of addition of a subduction component (unspecified) to a mantle source.

All of the north Tongan boninites have $^{143}Nd/^{144}Nd$ ratios similar to those of the Samoan plume, but some of them have lower Zr/Sm ratios. Both the Zr/Sm and $^{143}Nd/^{144}Nd$ ratios of the lavas from the Northern Lau Spreading Centre are similar to those of the plume. The lavas from the Central Lau Spreading Centre have $^{143}Nd/^{144}Nd$ ratios similar to those of MORB, but a range of Zr/Sm ratios which lie within the MORB-plume array, shown as a shaded area.

The following is one, but not necessarily the only, explanation of the data. The trends in the Tofua arc data can be explained by mixing between a depleted-MORB end-member and a subduction component. The trend in the Tafahi, Niuatoputapu and boninite data may be explained by mixing between a plume end-member and a subduction component. The compositions of the two boninites from site 26 (NTB, west) plot within the field of compositions of the Samoan plume. The other boninites also have $^{143}Nd/^{144}Nd$ ratio similar to those of the Samoan plume, but some have lower Zr/Sm ratios than those of average Samoa. The low Zr/Sm ratios of the boninites from the ophiolite section (NTB, east) are likely to be a result of enrichment of their sources by a subduction component. This supports other geochemical evidence (Figures 4.12, 5.6, 5.7) that the boninites have plume mantle-related sources, but that unlike the boninites from the section, the compositions of the boninites from the site 26 are not significantly influenced by a subduction component.

Figure 6.3 shows the anomalously low $^{143}Nd/^{144}Nd$ ratios of the Samoan seamount (SS) compared with those of the other Samoan volcanics. Its $^{143}Nd/^{144}Nd$, $^{207}Pb/^{204}Pb$ and $^{208}Pb/^{204}Pb$ ratios are similar to, and its $^{87}Sr/^{86}Sr$ ratios are lower than, those the Pacific pelagic sediments (see also Figures 5.3(a) and 5.6(a)). Therefore, it is possible that the Pb isotopic composition of the seamount could originate from a recycled sediment component, as this lies close to the locus of compositions of sediments subducted in the past (*Hart & Staudigel, 1989*). This locus is towards decreasing $^{206}Pb/^{204}Pb$, but increasing $^{208}Pb/^{204}Pb$ and $^{87}Sr/^{86}Sr$ ratios with time.
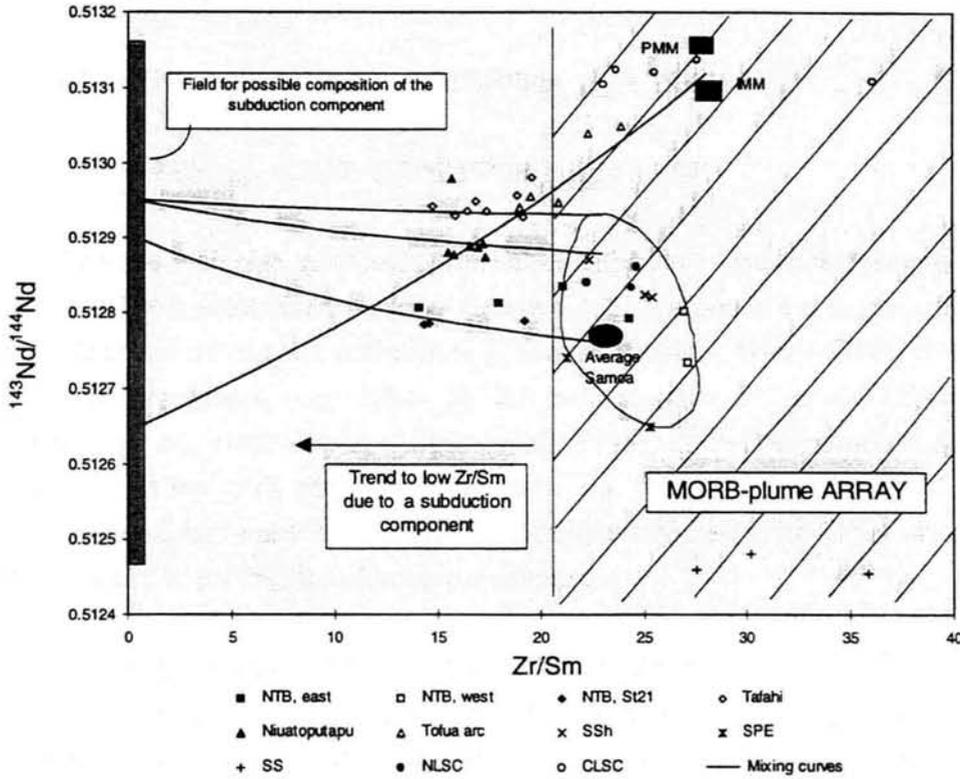
Figure 6.3: $^{143}Nd/^{144}Nd$ against Zr/Sm ratios of the north Tongan boninites (NTB, east and west), the lavas from Tafahi, Niuatoputapu, the Tofua arc, the Northern and Central Lau Spreading Centres (NLSC and CLSC) and the Samoan shield (SSh), post-erosional volcanics (SPE) and seamount (SS), average Samoa, Pacific and Indian MORB mantle (PMM and IMM) and the MORB-plume array. A field for possible compositions of the subduction component is shown at very low Zr/Sm ratios, but over a large range of $^{143}Nd/^{144}Nd$ ratios. The trend, which is a result of 'enrichment' by this component, is also shown. A point for the average composition of Samoa. Mixing curves have been superimposed on this diagram which illustrate one possible interpretation of the data (see text for description).

Therefore, the low $^{87}Sr/^{86}Sr$ ratios of the seamount compared with those of PPS (and any ancient subducted sediments) precludes the involvement of an ancient subducted sediment component. Hence, it is likely that there is another explanation for the anomalous isotopic composition of the Samoan seamount.

$\Delta7/4$ and $\Delta8/4$ are a measure of the displacement of the data from the Northern Hemisphere Reference Line (NHRL: *Hart, 1984*). Equations to calculate $\Delta7/4$ and $\Delta8/4$ are from *Hart (1984)*:

$$\Delta7/4 = [(^{207}Pb/^{204}Pb)_{sample} - (^{207}Pb/^{204}Pb)_{NHRL}] \times 100$$

$$\Delta 8/4 = [(^{208}Pb/^{204}Pb)_{sample} - (^{208}Pb/^{204}Pb)_{NHRL}] \times 100$$

$$(^{207}Pb/^{204}Pb)_{NHRL} = 0.1084 \times (^{206}Pb/^{204}Pb)_{sample} + 13.491$$

$$(^{208}Pb/^{204}Pb)_{NHRL} = 1.209 \times (^{206}Pb/^{204}Pb)_{sample} + 15.627$$

Samples with high $\Delta 8/4$ and $\Delta 7/4$ values either: (a) have high time-integrated Th/U and Th/Pb ratios respectively, or (b) are old, or (c) contain a component derived from either ancient recycled sediment (e.g. Samoa; *Wright & White, 1986*), or ancient subducted lithosphere, (e.g. Indian MORB mantle; *Mahoney et al., 1989, 1992; Staudigel et al., 1991; Hickey-Vargas et al., 1995*), or Pacific pelagic sediments. Samples with low $\Delta 8/4$ and $\Delta 7/4$ values have low time-integrated Th/U and Th/Pb ratios respectively, which may contain a component derived from either (a) altered oceanic crust, or (b) Pacific volcanogenic sediments.

Figures 6.4(a) and (b) are plots of the $\Delta 7/4$ and $\Delta 8/4$ values against Zr/Sm ratios of the lavas from north Tonga, the Tofua arc and the Central Lau Spreading Centre, and the Samoan plume volcanics. These attempt to explain the displacements of the compositions of these lavas from the NHRL in terms of mixing between end-member components. The average compositions of Indian and Pacific MORB-mantle (IMM and PMM), the Samoan plume and a field defining possible compositions of the subduction component ($\approx$fluids derived from altered Pacific oceanic crust, plume mantle and sediments) are shown on Figures 6.4(a) and (b). Average Samoa and IMM have similarly high $\Delta 8/4$ values (~55). The subduction component has a low Zr/Sm ratio (<2; Figure 4.13), but a large range of $\Delta 8/4$ and $\Delta 7/4$ values (50 to -50 and 11.7 to -3 respectively).

Fields for the compositions of boninites from Chichijima and the Izu-Bonin fore-arc are also shown *(Pearce et al., 1992a, b; Taylor et al., 1994)*, which further illustrate their anomalously high Zr/Sm ratios compared with those of the MORB-plume array and the lavas from north Tonga (Figure 4.13). These have already been shown to be a result of enrichment of their source by a slab-fusion component (Figures 4.14 and 4.15). An arrow on Figure 6.4(b) indicates the vector for the composition of altered oceanic crust with time. This vector is towards very low $\Delta 8/4$ values with time, because of its low time-integrated Th/U ratio. Therefore, a component derived from altered oceanic crust is a possible end-member component of lavas with very low $\Delta 8/4$ values.
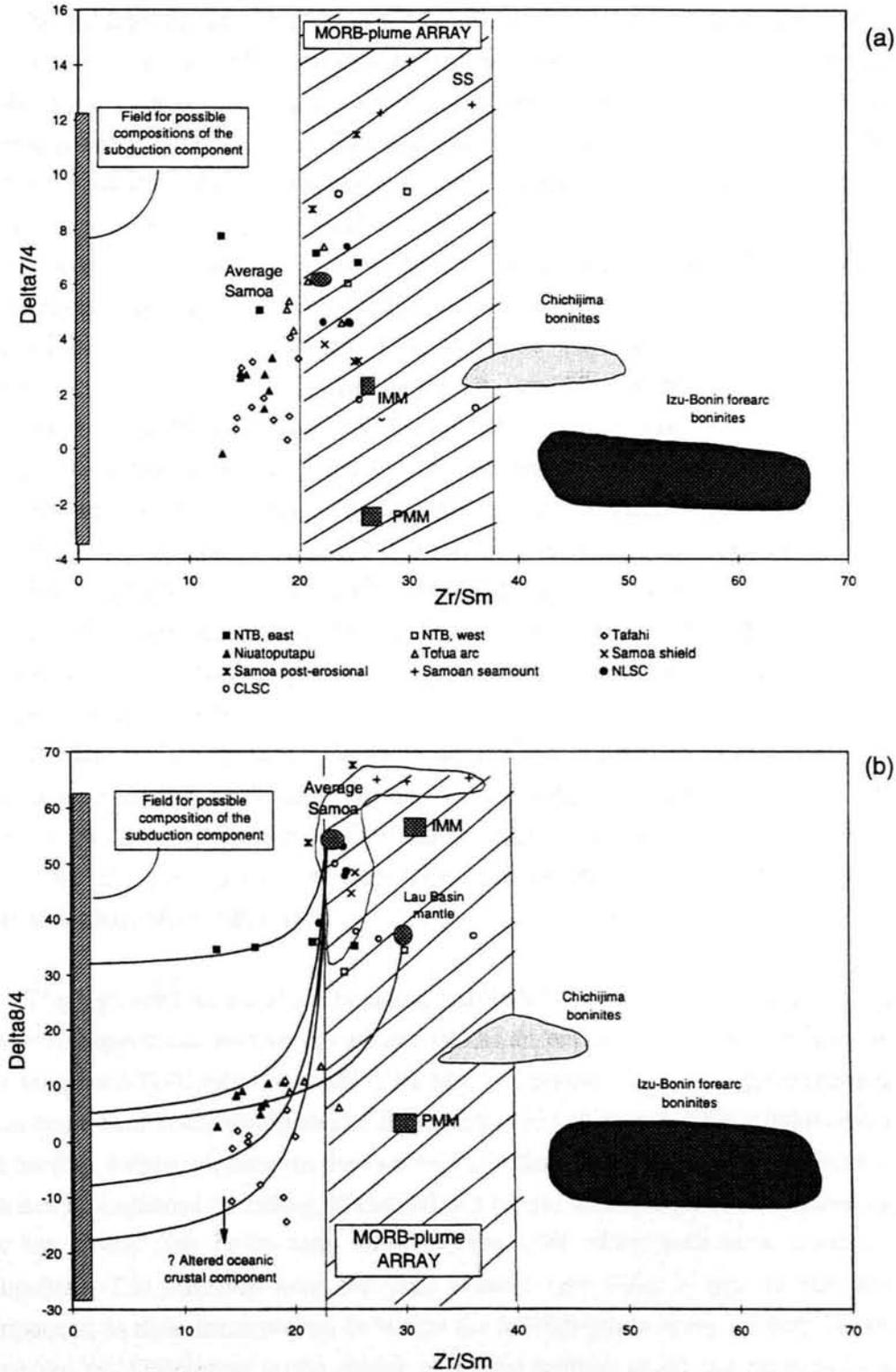
Figure 6.4 : *Delta8/4 and Delta7/4 against Zr/Sm ratios for the north Tongan boninites (NTB), the lavas from Tafahi, Niuatoputapu, and the Tofua arc, and the Samoan shield (SSh), post-erosional volcanics (SPE) and seamount (SS). A field for possible compositions of the subduction component is shown, which may be a mixture of fluids derived from the subducted slab (altered oceanic or plume crust) and Pacific sediments (PVS or PPS). Mixing curves between end-members have been superimposed on the diagrams. The positions of these are not well-constrained due to the difficulty in constraining the composition of the subduction component. These diagrams illustrate that the boninites from Chichijima and the Izu-Bonin fore-arc have higher Zr/Sm ratios than the MORB-plume array (also Figure 4.13). These ratios are a result of enrichment of their sources by a component derived from fusion of the slab (Pearce et al.,1992; Taylor et al.,1994).*

On the $\Delta 8/4$-Zr/Sm plot (Figure 6.4(b)), the north Tongan boninite data form a trend at constant $\Delta 8/4=35$, a value significantly higher than that of the NHRL ($\Delta 8/4=0$). This trend is from a point within the MORB-plume array towards the field defining possible compositions of the subduction component. On the $\Delta 7/4$-Zr/Sm plot (Figure 6.4(a)), these data form a group with $\Delta 7/4$ values similar to, and Zr/Sm ratios similar to, or lower than, those of average Samoa.

In both plots, the lavas from Tafahi and Niuatoputapu have $\Delta 8/4$ and $\Delta 7/4$ values close to, or just above, the NHRL (i.e. 0). However, on Figure 6.4(b), there is a group of four Tafahi lavas with $\Delta 8/4$ values of around -10, which are lower than those of the others (+0 to +5). This separate group of data is not evident on Figure 6.4(a). The two groups have been labelled on Figure 6.4(b): Group 1 has low $\Delta 8/4$, whereas Group 2 has higher $\Delta 8/4$. The possibilities for the origins of the different geochemical characteristics of the two groups are discussed in Section 6.2.3. The Zr/Sm ratios of the Tafahi and Niuatoputapu lavas (13-19) are lower than those of MORB (~25).

The Northern Lau Spreading Centre lavas have $\Delta 7/4$ values similar to, or just below, those of average Samoa. Their Zr/Sm ratios lie within the field defined by the compositions of the Samoan plume volcanics, but are transitional between those of average Samoa and IMM.

The Central Lau Spreading Centre lavas have higher $\Delta 7/4$ and lower $\Delta 8/4$ values than those of average IMM (point plotted), but are within the range of those of IMM ($\Delta 7/4=+1.2-+2$; $\Delta 8/4=+37-+50$). Their Zr/Sm ratios lie within the MORB-plume array. One data point has a very high $\Delta 7/4$ value (9.5), which is similar to that of average Samoa rather than IMM.

The high $\Delta 8/4$ values of the boninites ($\Delta 8/4=32$) compared to that of the NHRL ($\Delta 8/4=0$), suggest that their source either contains an 'enriched' component with a high time-integrated Th/U ratio, or is old (>200Ma??). Possible origins for this component are average Samoa ($\Delta 8/4=59$) and/or IMM ($\Delta 8/4=53$), (Figure 6.4(b)). Unfortunately it is hard to distinguish between the two on these diagrams. The trend in the boninite data can be explained by mixing of this 'MORB/plume' end-member with another one that has a very low Zr/Sm ratio and a similar $\Delta 8/4$ value, such as a subduction component. The boninites from the west contain very little, if any, of the latter component, as their compositions lie within the MORB-plume array on both Figures 6.4(a) and (b). Differences in the degree of partial melting could not be used as an explanation of this trend as the Zr/Sm ratio is not affected by this process (Section 4.5.4). $\Delta 7/4$ and $\Delta 8/4$ values are also unaffected by partial melting as isotopic compositions of melts reflect their source, unless there are heterogeneities within it.

On Figure 6.4(a), only two of the boninites have Zr/Sm ratios below the MORB-plume array. This suggests that only the compositions of these boninites have been significantly influenced by a subduction component and a plume. The compositions of the other boninites are dominated by that of the plume, with very little influence from a subduction component. A mixing curve are shown on Figure 6.4(b), between a plume end-member and a subduction component, which illustrates this.

The low Zr/Sm ratios of the Tofua arc, Tafahi and Niuatoputapu compared with those of MORB suggest that, as for the north Tongan boninites, their sources are likely to contain a component which has a very low Zr/Sm ratio i.e. a subduction component. The low $\Delta 8/4$ values for the Group 2 Tafahi lavas suggest that their source must contain a component with a low Th/U ratio, which is not present in the sources of the other lavas. It also appears that this component only affects the $^{208}Pb/^{204}Pb$ and possibly $^{206}Pb/^{204}Pb$ ratios, as these lavas do not form a separate group on Figure 6.4(a). Altered oceanic crust is a possibility for this component, as it has a low time-integrated Th/U ratio. The trend for addition of this component is shown on Figure 6.4(b), and the possibility of its presence is discussed in Section 6.2.3.

The Tofua arc lavas have similar $\Delta 7/4$ values and Zr/Sm ratios to the Samoan plume, but lower $\Delta 8/4$ values. Their trace element and isotope compositions do not indicate that they have been influenced by the plume (Figures 4.5, 4.12, 5.6 and 5.7). Therefore, the most likely explanation of the variations in the compositions of the Tofua arc lavas in Figure 6.4 is that they are a result of enrichment of an IMM source by a subduction component. Mixing curves between IMM and unspecified subduction components have been drawn on Figures 6.4(a) and (b) to illustrate these explanations.

These diagrams support the evidence from Figure 5.6 that the isotope compositions of the north Tongan boninites are similar to that of the Samoan plume, and may be influenced by a subduction component. However, the relative contributions of fluids derived from altered oceanic crust, plume crust, PVS and PPS to the subduction component is not known, and therefore its composition cannot be constrained.

The low Zr/Sm ratios, and $\Delta 7/4$ and $\Delta 8/4$ values of the lavas from Tafahi and Niuatoputapu supports other evidence from Figure 5.6, that their isotopic compositions are dominated by that of a subduction component. However, other plots are required (e.g. Figures 5.6 and 5.7) to distinguish between Indian MORB- and residual plume mantle end-members.
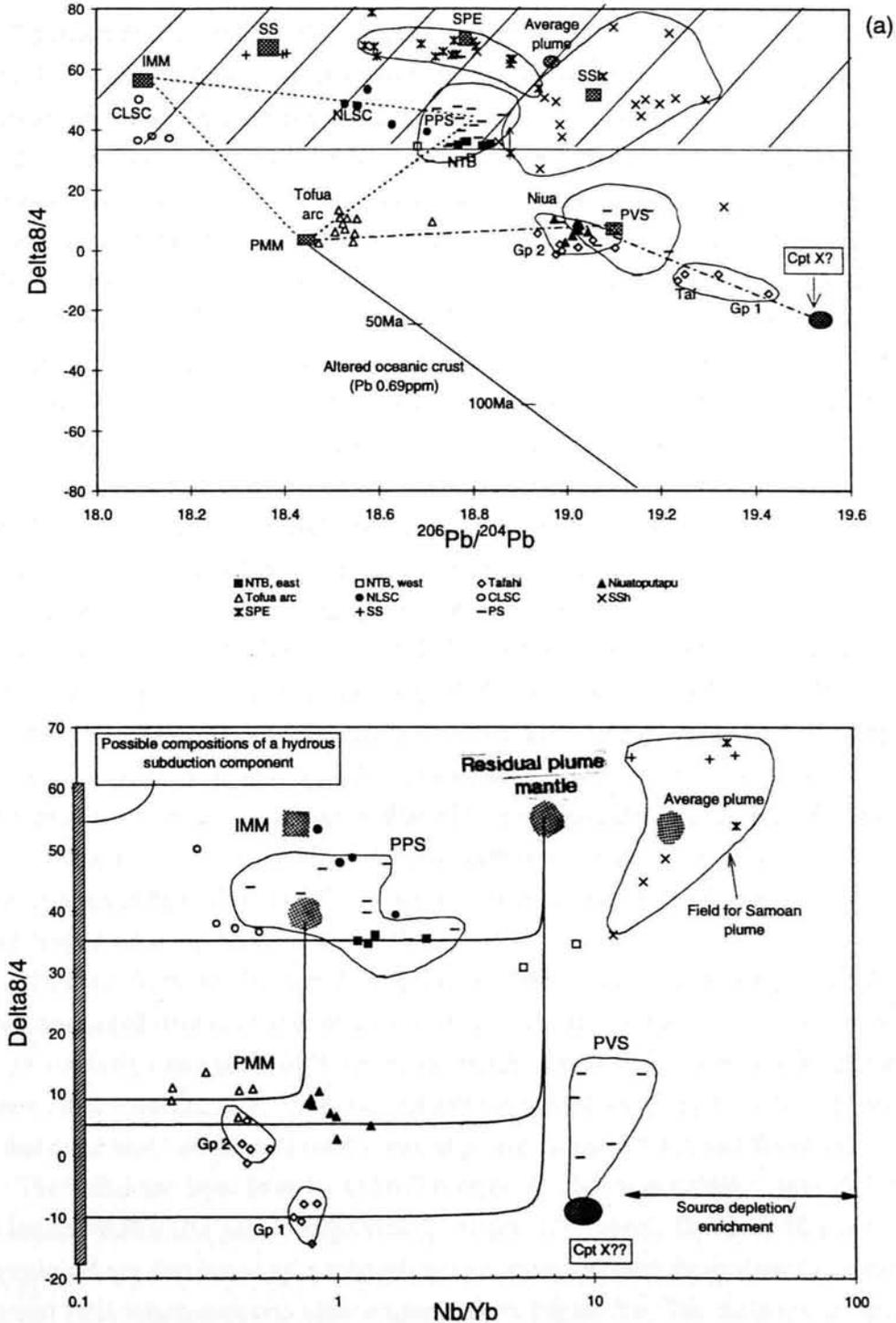
Figures 6.5(a) and (b) : Delta8/4 vs $^{206}Pb/^{204}Pb$ and Nb/Yb for the north Tonga boninites (NTB), the lavas from Tafahi, Niuatoputapu, the Tofua arc, and the Northern and Central Lau Spreading Centres. Fields for the Samoan plume, Pacific pelagic and volcanogenic sediments, and the compositions of fluids derived from these sediments and plume crust are shown. Average compositions of Indian and Pacific MORB and that of average Samoa are plotted. This diagram shows the compositional differences between the two groups of Tafahi lavas, which have been labelled Groups 1 and 2. It aims to show possible mixing models that may explain these differences. Mixing curves between end-member components have been superimposed on this diagram to do this. X is an hypothetical end-member component of the Tafahi lavas. The vector for the composition of altered Pacific oceanic crust with time, on (a), shows it cannot be a possibility for end-member X.

163

Figures 6.5(a) and (b) are plots of $\Delta 8/4$ versus $^{206}Pb/^{204}Pb$ and Nb/Yb ratios for the north Tongan boninites, the lavas from Tafahi and Niuatoputapu (Section 6.2.3), and those from the Northern and Central Lau Spreading Centres and the Tofua arc. Mixing curves have been superimposed on these plots between possible end-member components of the lavas: residual plume mantle, Indian MORB, and subduction components. The composition of the subduction component is hard to constrain for similar reasons as on Figures 6.3 and 6.4. It is assumed that the subduction component contains very little Nb due to the immobility of this element in aqueous fluids (*Tatsumi, 1989; Keppler, 1996*). Figures 4.12 and 5.7 show that the sources of the north Tongan boninites and the lavas from Tafahi and Niuatoputapu are residual plume mantle. However, the degree of depletion of this plume mantle, and hence its Nb/Yb ratio and Yb content, is hard to constrain. Therefore, the mixing curves on Figure 6.5(b) have been calculated using the composition of a possible 'extreme' end-member for this mantle, which assumes that the least 'depleted' residual plume mantle forms the sources of the north Tongan boninites from the west (see Figure 4.12).

The north Tongan boninites have high $\Delta 8/4$ values (30-35), which lie within the MORB-plume array, but at lower values than both average Indian MORB (55) and Samoan plume (55). The boninites from the west have Nb/Yb ratios (5-8) slightly lower than those of the plume (11-40), whereas those from the ophiolite section have significantly lower ratios (1-3). Their $^{206}Pb/^{204}Pb$ ratios overlap with those of PPS, but are most likely to be the result of mixing between a plume end-member and a subduction component (Figure 5.6). However, the boninites from the west contain a higher proportion of the former end-member.

The lavas from the Northern Lau Spreading Centre have Nb/Yb and $^{206}Pb/^{204}Pb$ ratios transitional between those of Indian MORB and the plume (0.7-1.5 and 18.5-18.7 respectively) and their $\Delta 8/4$ values lie within the MORB-plume array. These support other evidence from the trace elements and isotopes (Figures 4.12, 5.6 and 5.7) that these lavas are derived from a 'mixed' plume-Indian MORB mantle source.

The Tofua arc lavas have lower Nb/Yb ratios (0.25-0.5) and $\Delta 8/4$ values (5-12) than Indian MORB (0.7 and 55 respectively). Figure 6.5(a) shows that their Pb isotope compositions are dominated by a subduction component derived from altered oceanic crust and PPS, which supports other evidence from Figure 5.6. The variation in their compositions on Figure 6.5(b) can be explained by mixing between Indian MORB mantle and a subduction component.

These diagrams generally agree with the petrogenetic model introduced in Chapter 5, but are limited by the lack of constraint on the trace element and isotopic composition of the subduction component.

6.2.3 Tafahi: a variable source or subduction component?

The trace elements and Pb isotopes show that the Tafahi data form two distinct groups (Figures 4.5, 4.8, 5.6(b) and (c), 6.1 and 6.4(b)). The lavas in each of the groups are not all from any particular part of the island (Figure 2.3). However, most of those from Group 2 are from the southwestern gully sections, or from that region. Table 6.1 presents the different characteristics of the two groups. Group 1 and 2 lavas from Tafahi are labelled on Figures 6.5(a) and (b), which highlight some of the geochemical differences between them.

The Pb isotope data ($\Delta 8/4$ values and $^{206}Pb/^{204}Pb$ ratios) distinguish the two groups most effectively: Group 1 have $^{206}Pb/^{204}Pb > 19.2$ and $\Delta 8/4 < 0$, whereas Group 2 have $^{206}Pb/^{204}Pb < 19.2$ and $\Delta 8/4 > 0$ (Table 6.1 and Figure 6.5). However, Figure 6.5

	Characteristics	**Lavas**
Group 1	$\Delta 8/4 < 0$, Nb/Yb>0.70, $^{206}Pb/^{204}Pb > 19.2$, LREE enrichment generally	TAF3/2, TAF8, TAF18/12, TAF31/1, TAF54
Group 2	$\Delta 8/4 > 0$, Nb/Yb<0.70, $^{206}Pb/^{204}Pb < 19.2$, LREE depletion generally	TAF18/10, TAF23*, TAF40, TAF43/6, TAF44/8, TAF45/7*

Table 6.1: Distinguishing geochemical characteristics of Group 1 and 2 Tafahi lavas. Some of these features, particularly the LREE concentration, are not mutually exclusive (Figure 4.5). TAF23 has transitional LREE between Group 1 and 2, and TAF45/7 has LREE enrichment, although its other geochemical characteristics suggests it belongs to Group 2. These anomalous samples are marked with an asterisk.

shows that Group 1 lavas also have Nb/Yb ratios (>0.7), which are higher than those of Group 2 (<0.7), but similar to those of PMM (0.76). The two groups are distinguishable on the chondrite-normalised REE patterns (Figure 4.5(f)): Group 1 has LREE-enrichment, whereas Group 2 has LREE-depletion. However, TAF23 has a transitional REE pattern, and TAF45/7 appears to be anomalous as it shows all the characteristics of Group 2 (Table 6.1), but has LREE-enrichment (Figure 4.5(f)). The major elements are not useful for distinguishing between the groups (Figure 4.3), probably because fractionation and/or partial melting overprint the effects of the process or component(s) which caused the differences between them.

These geochemical differences are unlikely to be related to any analytical errors as there were no significant differences between repeated trace element analyses of the same samples (see discussion in Appendix 1). Samples from the two groups were analysed in both of the two isotope runs carried out, and therefore the variations could not be due to either (i) one particular erroneous run, or (ii) sample contamination, or (iii) the data corrections (for isotope fractionation), as both isotopic data sets were corrected in the same way. Also the trace element and isotopic characteristics of the lavas are coherent (apart from the overlap in LREE characteristics). It would be expected that these characteristics would be more random if the variations originated from either the data collection or correction processes.

Figures 5.6 and 5.8 show that the isotopic compositions of the Tafahi lavas are dominated by that of a subduction component derived from altered oceanic crust and Pacific volcanogenic sediments, but an additional end-member component is required (X) to explain the high $^{206}Pb/^{204}Pb$ ratios of the Group 1 lavas. One possibility for end-member X is fluids derived from subducted sediments which have more extreme isotopic compositions than the analysed PVS (from DSDP sites 204 and 595; *Pearce & Hergt, unpubl.*), and may originate from seamounts associated with the Samoan plume (Section 5.5.2). Figures 6.5(a) and (b) highlight the geochemical differences between the two groups of Tafahi lavas and explores another possibility for the origin of end-member X. Figure 6.5(a) shows that end-member X is required in order to explain the isotopic compositions of Group 1 lavas, whereas those of Group 2 (and Niuatoputapu) are a result of mixing between a slab-flux derived from altered oceanic crust (PMM) and PVS.

Mixing curves have been superimposed on Figure 6.5(b) to illustrate possible explanations of the variations in the compositions of the Tafahi lavas. The trajectories of the curves are as shown due to the high Nb/Yb ratios of the residual plume mantle (6.5) relative to the subduction component (<0.1). This diagram shows that the compositions of Group 1 lavas can be explained by mixing between a residual plume end-member (Δ8/4=55; Nb/Yb=6.5) and a hydrous subduction component derived from predominantly end-member X (Δ8/4 between -5 and -15; Nb/Yb<0.1). The mixing curves indicate that these lavas also contain a higher proportion of a residual plume end-member than the Group 2 lavas, but a similar proportion as in those from Niuatoputapu.

Nb is an incompatible element that is a mantle- rather than slab-derived element, due to its immobility in aqueous fluids (Figure 5 of *Pearce & Peate, 1995*). Therefore, unless there is a mechanism that somehow allows it to become more mobile in subduction fluids, it is more likely that the different Nb/Yb ratios of the two groups of

Tafahi lavas are a result of differences in their mantle source characteristics. Figure 6.4 shows that there are no significant differences in either the Zr/Sm ratios, or Zr concentrations between the two groups of lavas from Tafahi. Therefore, Nb is the only HFSE enriched in the Group 1 lavas, which is more likely to be a result of its higher incompatibility compared with Zr in mantle melting (Dsp lhz @ 1200°C Zr=0.04, Nb=0.01; *Pearce & Parkinson, 1993*). This may indicate that the residual plume mantle sources of both the Group 1 Tafahi lavas and also those from Niuatoputapu are less depleted (or more enriched) than those of the Group 2 lavas. The higher slab contribution to the elemental budgets of the highly incompatible slab-derived elements (Sr and Ba) of the Group 2 lavas relative to the Group 1 lavas may be related to the higher degree of source depletion of the former lavas (Figures 4.12 and 4.13). However this is not applicable to the less incompatible slab-derived elements (Th, Ce ± Nd), for which there is a lower slab contribution to elemental budgets in the Group 2 lavas. Therefore, the degree of enrichment of the sources of the Tafahi lavas by the subduction component is not likely to be related to the degree of depletion of their sources.

Another possibility for the origin of end-member X is altered oceanic crust, which is characterised by increasing $^{206}Pb/^{204}Pb$ ratios and decreasing $\Delta 8/4$ values with time. The locus for the average isotopic composition of oceanic crust that has been altered (and subducted) at various times in the past is shown on Figure 6.5(a) to test whether it is a viable option for end-member X. For the calculation of this locus, values for the $^{238}U/^{204}Pb$ ratio and the decay constant (λ) are taken from Table 5.2 and *Steiger & Jäger (1977)* respectively. The value for the $^{238}U/^{204}Pb$ ratio from Table 5.2 is a maximum, using a Pb concentration in altered oceanic crust of 0.69 ppm (*Hart & Staudigel, 1989*). It can be observed from the locus of the isotopic composition of altered oceanic crust, that its composition at 140Ma does not have sufficiently high $\Delta 8/4$ and $^{206}Pb/^{204}Pb$ to be a viable option for end-member X and lies off Figure 6.5(a). This age is approximately the maximum of that of an altered oceanic crustal component (sum of (a) age of subducting slab at the time of dehydration, (b) time for fluid to percolate to the base of the melting column, and (c) time for partial melting and magma ascent; (a)>>(b)+(c)=10-20Ka from U-Th disequilibria; *S. Turner pers. comm.*). Varying the Pb content of the oceanic crust to its lower limit of 0.2 ppm does not vary the locus of its compositions much on this plot, but they are at lower $\Delta 8/4$ and higher $^{206}Pb/^{204}Pb$ for a given age (*Hart & Staudigel, 1989*). Hence, it is unlikely that end-member X is derived from the slab, unless it is composed of plume crust.

Clearly, end-member X has a high Nb/Yb ratio (Figure 6.5(b)), a low $\Delta 8/4$ value and high $^{206}Pb/^{204}Pb$ compared with those of PMM, but does not appear to be enriched in Zr (Figure 6.4(a)). Therefore, it is likely that this component is either

derived from volcanogenic sediments that have a more extreme composition (i.e. higher $^{206}Pb/^{204}Pb$ and lower $^{208}Pb/^{204}Pb$ than those of the field for PVS on Figures 5.8 and 6.5), or it is unidentifiable.

In summary, Figures 6.2-6.5 support the evidence from the isotopes and trace elements (Chapters 4 and 5) that the compositions of the Tafahi lavas are dominated by that of the subduction component, which is derived from altered oceanic crust and Pacific volcanogenic sediments.

6.3 Chapter 6 Summary

• The trace element-isotope variation plots support the models proposed in Chapter 5 for the magma genesis of the lavas from north Tonga. However, data interpretations from them are limited, unless they are used alongside other trace element and isotope diagrams, due to the difficulty in constraining the composition of the subduction component.

The following are summaries of the magma genesis of the suites of lavas from north Tonga:

(i) *The north Tongan boninites* have residual plume mantle sources, which have been variably enriched by a subduction component. However, the boninites from the west, close to the Northern Lau Spreading Centre, are not significantly influenced by a subduction component. The low Ce/Pb ratios are a characteristic signature of a hydrous subduction component, which is enriched in Pb relative to Ce. However, the high $^{208}Pb/^{204}Pb$ and $^{207}Pb/^{204}Pb$ ratios of the north Tongan boninites, which are similar to those of the Samoan plume, may also be attributed to a hydrous subduction component. These fluids may have acquired the isotopic signature of the plume, either from subducting plume crust, or from the mantle wedge as they percolate through it towards the base of the melting column;

(ii) *The lavas from Tafahi* have residual plume mantle sources, which have been enriched by a subduction component. Their low Ce/Pb and high $^{207}Pb/^{204}Pb$ and $^{208}Pb/^{204}Pb$ ratios relative to those of MORB indicate that this subduction component is a mixture of MORB- and sediment-derived fluids. The Pb isotopes show that the composition of this component is dominated by that of PVS.

The lavas from Tafahi form two distinct groups geochemically: Group 1 lavas have $\Delta 8/4 < 0$, Nb/Yb > 0.70, $^{206}Pb/^{204}Pb > 19.2$ and LREE enrichment, whereas Group 2 lavas have $\Delta 8/4 > 0$, Nb/Yb > 0.70 and $^{206}Pb/^{204}Pb < 19.2$ and LREE depletion (except

for TAF23 and TAF45/7 which have transitional characteristics between the two groups). The geochemical differences between the two groups are likely to be the result of both:

(i) *a mantle source characteristic*: the higher Nb/Yb ratios of Group 1 lavas compared with Group 2 ones may indicate that the former were derived from a more enriched source, and,

(ii) *the subduction component*: the high $^{206}Pb/^{204}Pb$ ratios and LREE enrichment of the Group 1 lavas may be the result of a subduction component derived from subducted sediments that have more extreme compositions than those sampled from DSDP sites 204 and 595 (*Pearce & Hergt, unpubl.*).

There are a few discrepancies with this model as it would be expected that the subduction component would have a greater influence on the compositions of lavas whose sources are more depleted (i.e. Group 2 lavas). Group 2 lavas have a higher slab contribution to their Sr and Ba elemental fluxes compared with Group 1 lavas, but a lower one for their Ce and Th (and Nd) elemental fluxes. The slab contribution to the Pb elemental flux is very variable. This suggests that the subduction component enrichment of the sources of the Tafahi lavas is variable depending on the element. Therefore, it is unresolved whether (i) and (ii) are mutually exclusive, or are related in some way;

(iii) **The lavas from Niuatoputapu** have residual plume mantle sources, which have been enriched by a subduction component. Their low Ce/Pb and high $^{207}Pb/^{204}Pb$ and $^{208}Pb/^{204}Pb$ ratios relative to those of MORB indicate that this subduction component is a mixture of MORB- and sediment-derived fluids. However, the Pb isotopes indicate that the isotopic composition of this component is dominated by that of PVS. These lavas have higher Nb/Yb ratios than Group 2 Tafahi lavas and higher Δ8/4 values and lower $^{206}Pb/^{204}Pb$ ratios than Group 1. These suggest that the Niuatoputapu lavas have more enriched sources than Group 2 lavas, and do not contain a subduction component that has been derived from subducted sediments with extremely high $^{206}Pb/^{204}Pb$ ratios;

(iv) **The lavas from the Northern Lau Spreading Centre:** have high Ce/Pb ratios, and Nb/Yb ratios, Δ8/4 and Δ7/4 values which are transitional between those of IMM and the Samoan plume. These indicate that the sources to these lavas are a mixture between Indian MORB- and residual plume mantle, and have had no significant enrichment by a subduction component.

CHAPTER 7

Magma genesis of the north Tongan tholeiites from the eastern dredge section of the 'Kallisto' 1982 cruise

7.1 Introduction

In this chapter the major and trace element, and isotope geochemistry of the north Tongan tholeiites is described. A gabbro, from the cumulates of the ophiolite section associated with the north Tongan tholeiites, is of a similar age to the Eocene volcanics from 'Eua (Section 2.10). Therefore, the geochemistry of the north Tongan tholeiites has been compared to that of the volcanics from 'Eua. Evidence from the K-Ar dating (Section 2.10) suggests that dykes and cumulates from the ophiolite sections form part a basement of Eocene-Miocene age. The trace element geochemistry of the tholeiites is compared with that of the underlying dykes and cumulates to determine whether they are cogenetic. The isotopes and trace elements are then interpreted in terms of end-members and used to determine the relationship between the tholeiites and the initiation of subduction at the Tonga Trench, and whether the Samoan plume influenced the compositions of lavas erupted during early-arc magmatism.

7.2 Major element geochemistry

Figure 7.1 shows plots of SiO_2, Na_2O, K_2O, CaO, FeO^* (total iron as Fe^{II}) and TiO_2 against MgO for the north Tongan tholeiites, the Tofua arc and 'Eua. Several features are observed:

(1) The north Tongan tholeiites have higher MgO contents than the Tofua arc and 'Eua (except for two samples from 'Eua), which shows that any fractional crystallisation that they have undergone involved olivine and pyroxene(s), but plagioclase is not likely to be a fractionating phase (Figures 7.1(b), (d) and (e));

(2) At a given MgO content, both the tholeiites and 'Eua have high Na_2O contents, and low CaO and FeO^* contents, compared with those of the Tofua arc.
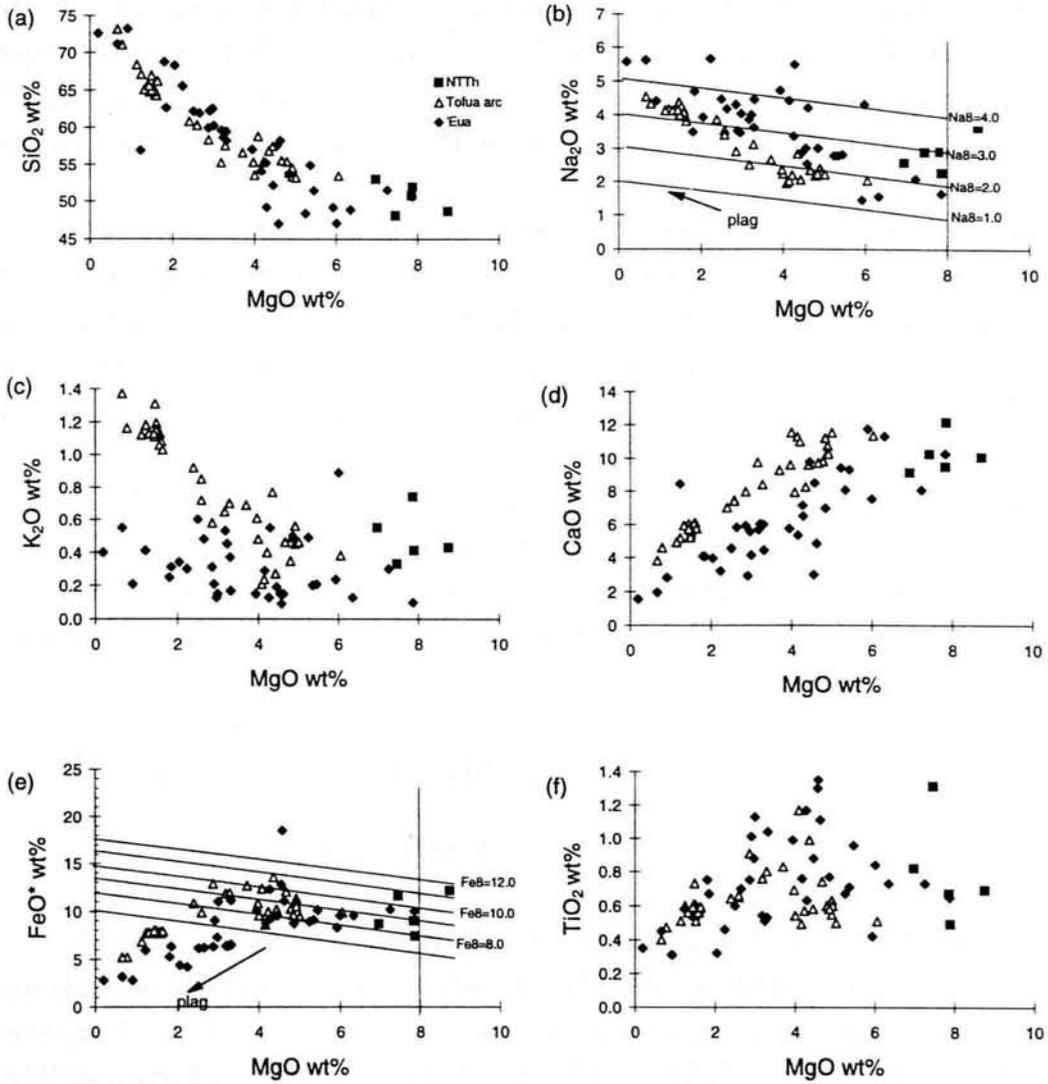
Figure 7.1 : Diagrams showing the major element variations of the north Tongan tholeiites (NTTh), which are compared to those of the central Tofua arc and the Eocene volcanics of 'Eua Island. Liquid lines of descent and vectors for plagioclase fractionation are shown on (b) and (e).

The Na_2O contents of the north Tongan tholeiites, at a given MgO content (for MgO>4wt%), are higher than those of the lavas from 'Eua and the Tofua arc (e.g. Figure 7.6). This is likely to be a result of differences in the compositions of their sources (Sections 7.5.3 and 4.5.6; *Langmuir et al., 1993*).

(3) The CaO-MgO compositions of the north Tongan tholeiites, and the lavas from 'Eua and the Tofua arc form separate trends, which are sub-parallel and have positive gradients (Figure 7.1(d)). The trend formed by the north Tongan tholeiite data is at the lowest CaO content for a given MgO content, whereas the trend of the Tofua arc data is at the highest CaO content for a given MgO content.

(4) The north Tongan tholeiites do not follow the main trend for Fe enrichment of the Tofua arc, but have similar FeO*-MgO compositions to those of the more magnesian lavas from 'Eua (Figure 7.1(e)). This is likely to be a result of their different fractional crystallisation history, which has not involved plagioclase.

7.3 Trace element geochemistry

7.3.1 Trace element variation diagrams

Figures 7.2(a) and (b) show the N-MORB-normalised trace element variation diagram and the chondrite-normalised REE plot for the north Tongan tholeiites. Sample 549-20 from the Eocene volcanics of 'Eua is also shown for comparison. MORB-normalising values are taken from *Sun & McDonough (1989)* and the chondrite-normalising values from *Boynton (1984)*. The trace element variation diagram is flat at 0.6-1.2 x N-MORB values for the REE, but has a negative Ta and Nb anomaly, and an enrichment in LILE relative to the HFSE and REE. The sample from 'Eua has a similar trace element variation pattern at 1-2 x N-MORB values for the REE compared to the north Tongan tholeiites. This sample also has LILE enrichment but not such a great enrichment as the north Tongan tholeiites. It also has a strong depletion in Hf, Zr and the LREE, compared with the north Tongan tholeiites.

The chondrite-normalised REE pattern for the north Tongan tholeiites is flat at 8-17 x chondrite values, but with a slight depletion in LREE. The REE pattern for 'Eua is similar, at 15 x chondrite values, but has a stronger LREE depletion than that of the north Tongan tholeiites.

This shows that the north Tongan tholeiites have different compositions from those of the volcanics from 'Eua, suggesting at least some petrogenetic differences, despite their similar age.

7.3.2 The diabases from the eastern and western ophiolite sections of the 'Kallisto' 1982 cruise: the relationship between the extrusives and the underlying cumulates

The trace element data of three diabases from the western ophiolite section (16-47/26, 16-47/27 and 16-47/29) and one diabase (16-67/8) and two cumulates (16-73/18 and 16-73/29) from the eastern ophiolite section have been used to investigate the relationship between the various units of these sections, especially between the extrusives and their corresponding dykes and cumulates. If the diabases form the feeders to the overlying extrusives then there should be some similarities in their geochemistry.

The trace element and REE data of the diabases are compared with the data of the north Tongan boninites and tholeiites in Figure 7.2(c) and (d). The diabases and cumulates can be divided into three groups:

(1) the diabases from the western ophiolite section (16-47/26, 16-47/27 and 16-47/29) have a flat trace element pattern with a slight Zr and Hf depletion relative to Nd and Sm, and LILE enrichment relative to the HFSE and REE. These samples have a flat chondrite-normalised M-HREE pattern at 10 x chondrite abundances, but with a LREE depletion.

(2) The diabase 16-67/8 from the eastern ophiolite section has a flat REE plot at 7 x chondrite with a slight LREE depletion. This REE pattern is parallel to the pattern of the north Tongan tholeiites. It has a flat REE pattern on the MORB-normalised plot at 0.4 x N-MORB, and has a negative Nb and Ta anomaly and LILE enrichment.

(3) The cumulates 16-73/18 and 16-73/29 from the eastern section have a flat MORB-normalised M-HREE pattern, but a strong depletion in Zr and Hf, extremely low concentrations of Ta and Nb (below the detection limit), and LILE enrichment. These cumulates have a flat M-HREE chondrite-normalised pattern at 2-4 x chondrite abundances with a positive Eu anomaly and a strong LREE depletion. The positive Eu anomaly is likely to be due to plagioclase accumulation during the formation of the cumulates.

The LREE-depleted patterns imply that the diabases from the western ophiolite section have tholeiitic characteristics. If the north Tongan boninites were related to the underlying dykes and cumulates in the corresponding ophiolite section then the boninites and diabases should have similar geochemical characteristics. However, the north Tongan boninites have LREE enrichment (Figure 7.2(d)) and a strong depletion

North Tongan tholeiites (Eocene)
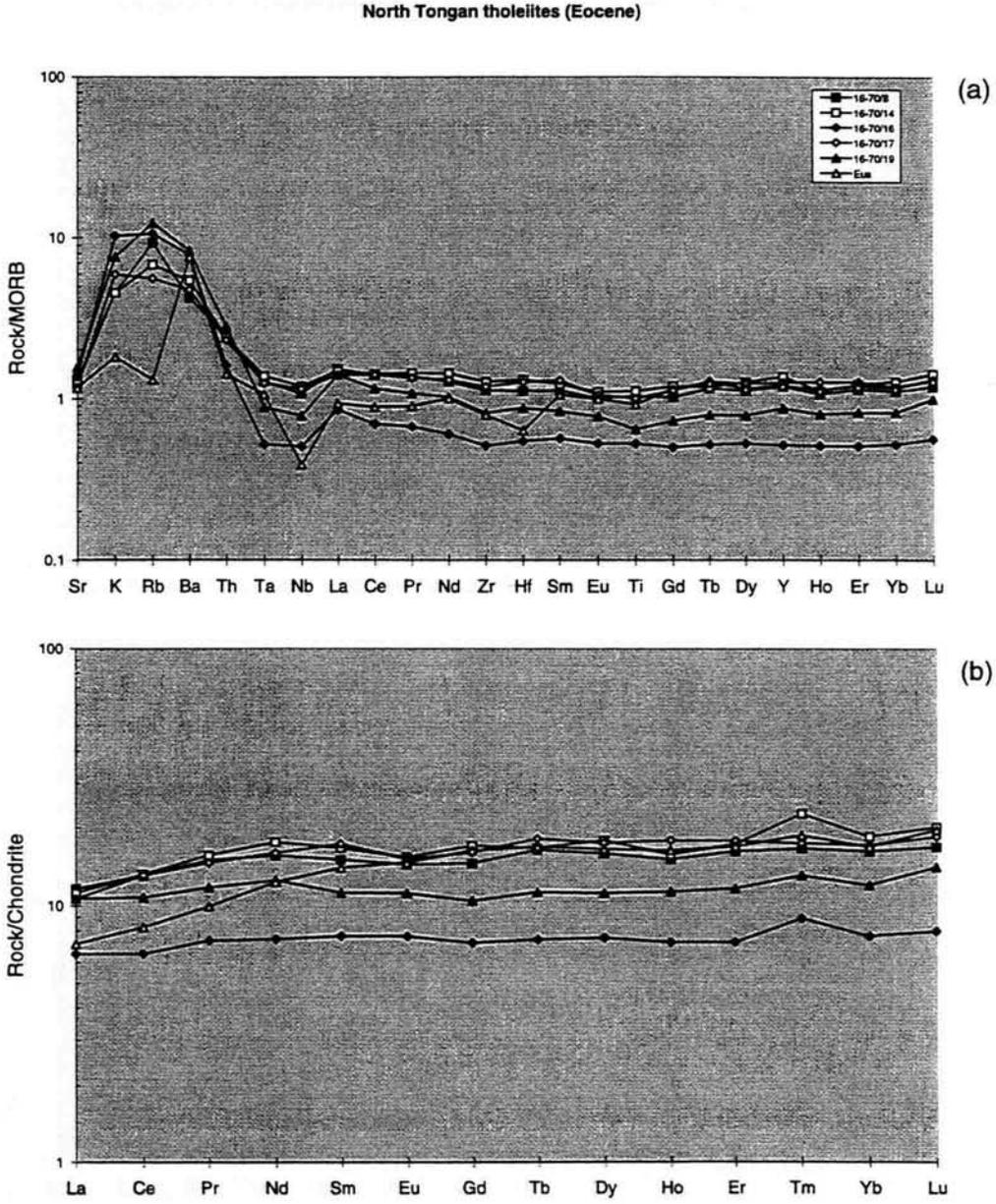
<u>*Figures 7.2(a) and (b)*</u> *:The MORB-normalised trace element variation and chondrite-normalised REE patterns for the north Tongan tholeiites and an Eocene lava from 'Eua. Normalising values are taken from Sun & McDonough (1989) and Boynton (1984), respectively.*

174

Comparison of diabases from the western dredge section and the north Tongan boninites
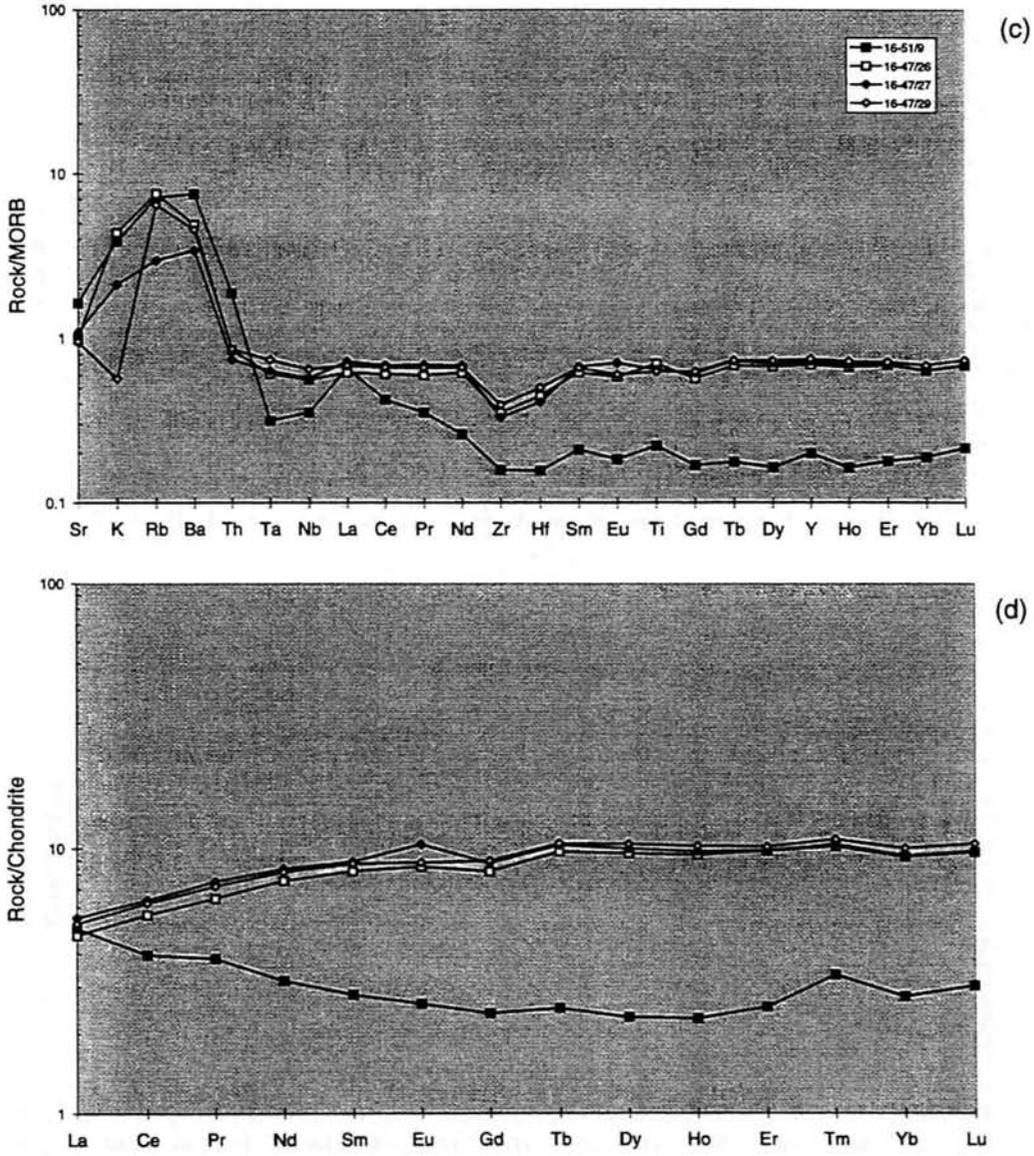
Figures 7.2(c) and (d): *A comparison of the N-MORB-normalised trace element variation and chondrite-normalised REE patterns of the diabases of the western ophiolite section with those of the north Tongan boninites. Normalising values are the same as those used in Figures 6.2(a) and (b).*

175

Comparison of the diabases and cumulates from the eastern section with the north Tongan tholeiites
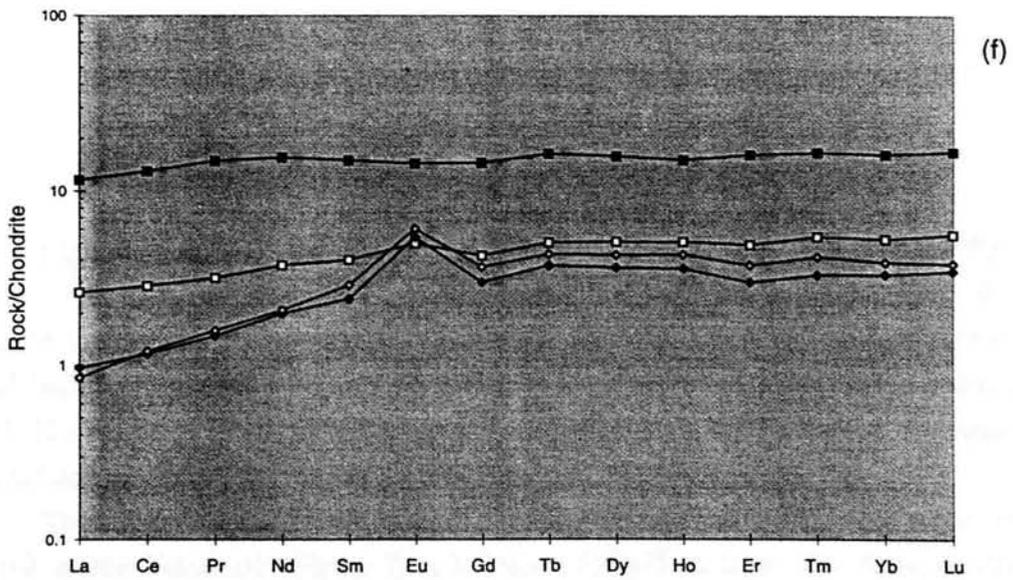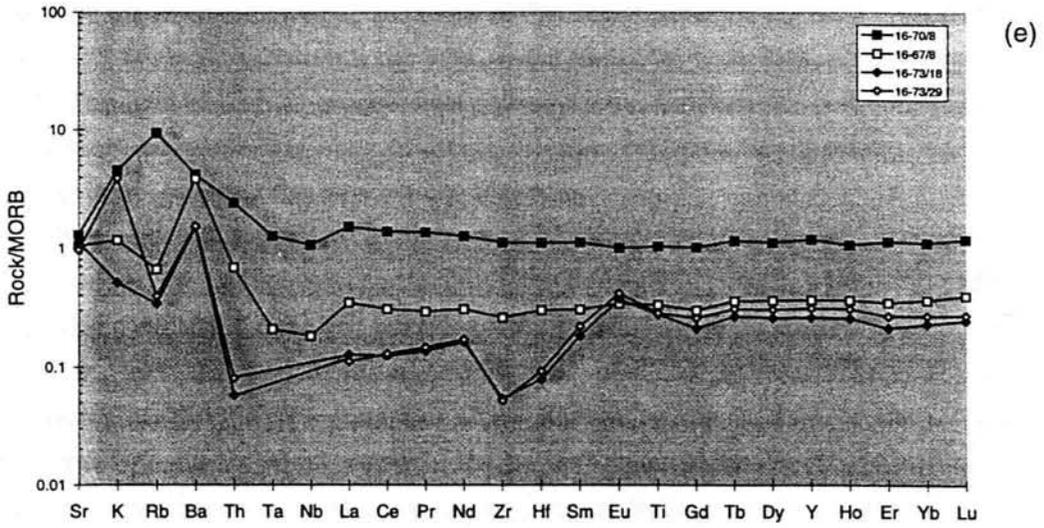
Figures 6.2(e) and (f) : *A comparison of the N-MORB-normalised trace element variation and chondrite-normalised REE patterns of the diabases and cumulates from the eastern ophiolite section with those of the north Tongan tholeiites. Normalising values are the same as those in Figures 6.3(a)-(d).*

in Ta and Nb (Figure 7.2(c)), whereas the diabases from the same section have LREE depletion (Figure 7.2(d)) and a very weak depletion in Ta and Nb (Figure 7.2(c)). A plagiogranite from the plutonic sequence of this ophiolite section gives an older K-Ar age (13±3 Ma) compared with the ages of the boninites (less than 3.5 Ma; Section 2.10). The lack of similar geochemical characteristics between the boninites and the underlying diabases, and the difference in age between the boninites and the plagiogranite, suggests that they are not cogenetic.

The north Tongan tholeiites, by contrast, have similar geochemical characteristics to the diabases, particularly sample 16-67/8, such as a flat REE pattern and a slight depletion in Ta and Nb (Figure 7.2(e)) and LREE depletion (Figure 7.2(f)), which suggests they are likely to be cogenetic with the diabases. Therefore, it is suggested that the diabases form part of the Eocene basement, onto, or from, which the north Tongan tholeiites erupted. The north Tongan boninites erupted at a later stage, between 3.5 and 0.5 Ma, as a result of recent tectonic processes relating to the development of back-arc spreading at the Northern Lau Spreading Centre (Section 2.10).

7.4 Isotope geochemistry

Figures 7.3(a)-(c) are $^{87}Sr/^{86}Sr$-$^{143}Nd/^{144}Nd$, $^{208}Pb/^{204}Pb$- and $^{207}Pb/^{204}Pb$-$^{206}Pb/^{204}Pb$ plots for the north Tongan tholeiites, the Tofua arc and 'Eua. Fields for Pacific and Indian MORB mantle, the Samoan shield and post-erosional volcanics, and Pacific pelagic and volcanogenic sediments are also plotted, as defined in Section 5.3. The Northern Hemisphere Reference Line is shown on the Pb isotope diagrams, as defined by *Hart (1984)* and in Section 5.3.

The north Tongan tholeiites have similar $^{87}Sr/^{86}Sr$ and $^{143}Nd/^{144}Nd$ ratios to those of the Tofua arc (Figure 7.3(a)). Some of the 'Eua lavas also have similar $^{87}Sr/^{86}Sr$ and $^{143}Nd/^{144}Nd$ ratios to those of the Tofua arc. However, three of the 'Eua lavas have higher $^{87}Sr/^{86}Sr$ ratios than those of the Tofua arc. This can be attributed to seawater alteration (Section 5.1).

On the $^{208}Pb/^{204}Pb$-$^{206}Pb/^{204}Pb$ plot (Figure 7.3(b)) the north Tongan tholeiite data form a trend between an end-member with Indian MORB isotopic characteristics and a subduction component (c.f. Figure 5.6(b)). The 'Eua data also form a trend between an end-member with Indian MORB isotopic characteristics, and a subduction component. However, the subduction component of the 'Eua lavas has a higher contribution from Pacific volcanogenic sediments compared with that of the north

7.5 Petrogenesis and the relationship to the initiation of subduction

7.5.1 Enrichment by a subduction component

Plots of La/Yb, Sr/Yb, Zr/Yb and Ba/Yb against Nb/Yb (Figure 7.4) have been made to highlight the LILE and LREE enrichment of the north Tongan tholeiites observed in Figure 7.2. These plots are similar to those in Figure 4.12. Data from 'Eua, the Tofua arc and the Samoan shield, post-erosional volcanics and seamount have been plotted for comparison with the north Tongan tholeiites. On the La/Yb and Ba/Yb versus Nb/Yb diagrams, the north Tongan tholeiites plot above the MORB-plume array, with Nb/Yb ratios close to, and La/Yb and Ba/Yb ratios greater than those of MORB. On the Sr/Yb-Nb/Yb diagram three of the tholeiites have compositions close to those of MORB, whereas the other two lavas have higher Sr/Yb ratios than those of MORB. The tholeiites have lower Sr/Yb and Ba/Yb, higher Nb/Yb and similar La/Yb ratios to those of the Tofua arc. They have similar La/Yb, Sr/Yb and Ba/Yb ratios to 'Eua, but higher Nb/Yb ratios.

On the Zr/Yb-Nb/Yb diagram the north Tongan tholeiites have Zr/Yb and Nb/Yb ratios similar to those of MORB, and therefore their compositions are similar to those of the MORB-plume array. The Tofua arc lavas also have compositions similar to the MORB-plume array.

The high La/Yb, Ba/Yb and Sr/Yb ratios of the north Tongan tholeiites relative to those of MORB are evidence of the enrichment of their sources by a hydrous component derived from the subducting slab. This component contains high concentrations of LILE and LREE due to the incompatibility of these elements in fluids (Section 4.5.2). The degree of this enrichment is not as great as in the Tofua arc lavas, as the Sr/Yb and Ba/Yb ratios of the tholeiites are not as high as those of the Tofua arc. The subduction component for the tholeiites contains very low concentrations of Zr and Nb, as the Zr/Yb and Nb/Yb ratios of the tholeiites are very similar to those of MORB.

The MORB-like Nb/Yb ratios of the tholeiites suggest that their sources have not undergone any depletion relative to those of MORB. This is in contrast to the sources of the Tofua arc and 'Eua lavas which have lower Nb/Yb ratios than MORB, indicating that they have been depleted by previous partial melting episodes (Sections 4.5.2 and 4.5.3). Alternatively, the sources of the tholeiites may have been depleted and then re-enriched by a component that has a high Nb/Yb ratio, such as a small degree silicate melt (e.g. a plume component), thus giving the tholeiites an overall Nb/Yb ratio similar to MORB. However, the Sr, Nd and Pb isotopes (Figure 7.3) do not show evidence that the latter is the case as the Sr and Nd isotopic compositions of
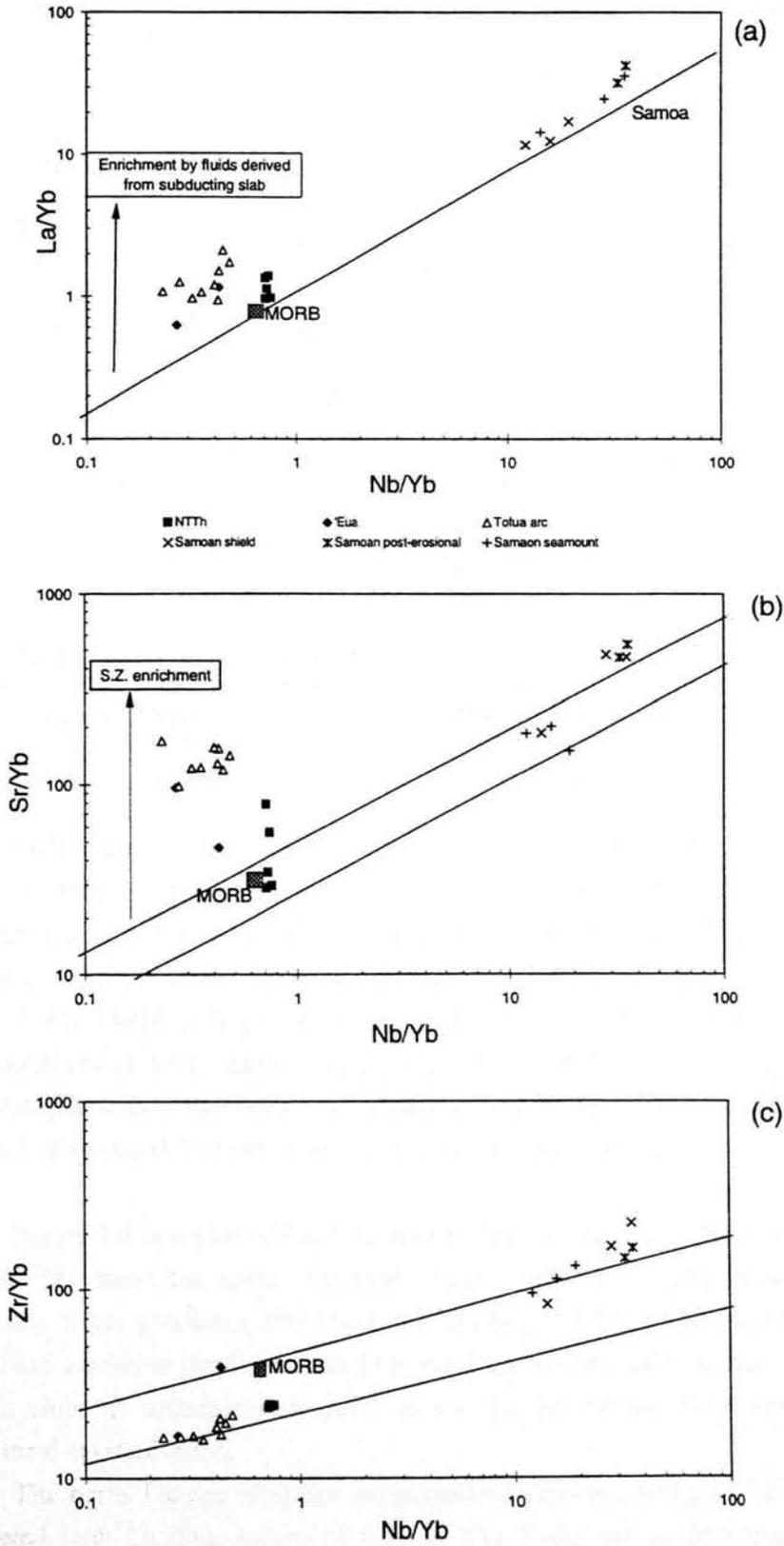
Figures 7.4(a)-(d): Plots of M/Yb vs Nb/Yb, where M=La, Sr, Zr and Ba, for the north Tongan tholeiites (NTTh),
Eua, the Tofua arc and the Samoan shield, post-erosional volcanics and seamount. A point is shown for the average
composition of MORB (Sun & McDonough, 1989) and the MORB-plume array is plotted, as defined in Figure 4.12.
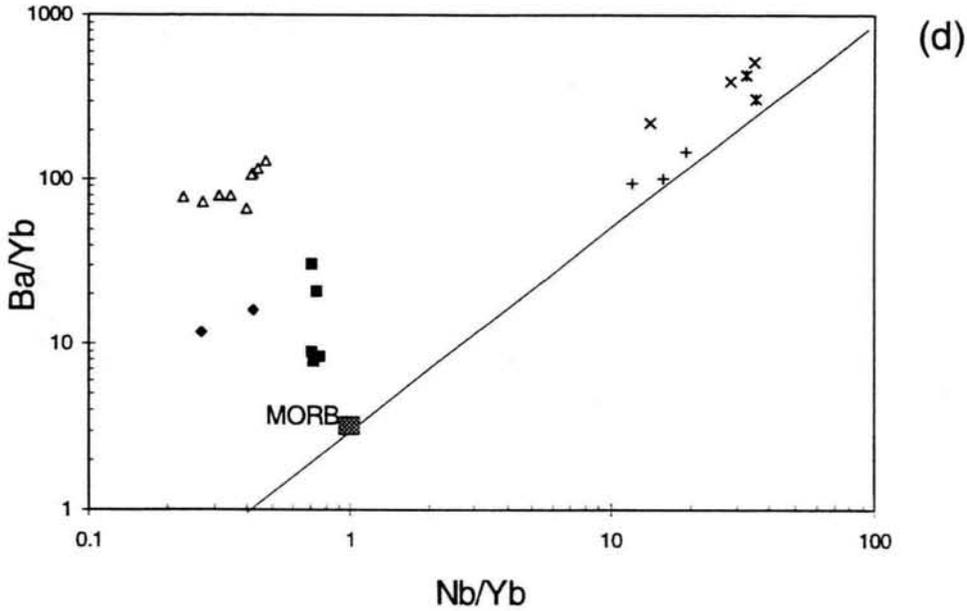
Figure 7.4(d): *Plots of Ba/Yb versus Nb/Yb for the north Tongan tholeiites (NTTh), 'Eua, the Tofua arc and the Samoan shield, post-erosional volcanics and seamount. A point for the composition of N-MORB and the MORB-plume array is plotted on the diagrams. Key as in Figure 7.4(a).*

the tholeiites are similar to those of the Tofua arc, and their Pb isotopic compositions form a trend between an end-member with Indian MORB mantle isotopic characteristics and a subduction component. Therefore, the residual plume mantle under the northern Lau Basin, whose geochemical influence is detected in young lavas from north Tonga (Chapter 4, 5 and 6; *Volpe et al., 1988*), does not affect the compositions of lavas erupted during early-arc magmatism. This suggests that the asthenospheric flow that brings the residual plume mantle from Samoa into the source regions of the north Tongan lavas, is not present in the Eocene.

Figure 7.5 is a plot of La_n/Sm_n against Sm_n (normalising values from *Boynton, 1984*). The trend for source variations and/or dynamic melting is shown on this diagram. These processes affect both the La_n/Sm_n and Sm_n values and therefore this trend has a positive slope. The trend for fractional crystallisation is also shown, which has a slope of approximately zero, as La and Sm behave very similarly during fractional crystallisation.

The north Tongan tholeiites are transitional between being LREE-enriched and depleted with La_n/Sm_n values of 0.7-1.1. The Tofua arc is also transitional with La_n/Sm_n values of 0.6-1.3. 'Eua is LREE-depleted with La_n/Sm_n values of 0.4-0.6.

The La_n/Sm_n values vary very little with Sm_n for the north Tongan tholeiites, the
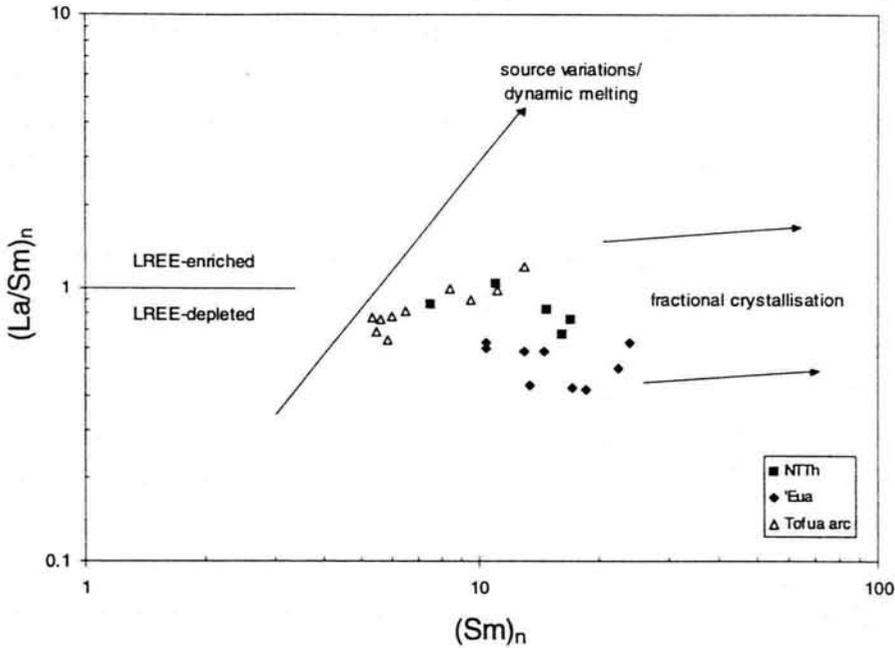
Figure 7.5: Plot of La_n/Sm_n against Sm_n for the north Tonga tholeiites (NTTh), 'Eua and the Tofua arc. The data have been normalised to chondrite values from Boynton (1984). Trends in these values due to source variations and dynamic melting and fractional crystallisation are shown. The diagram also shows whether the samples are LREE-enriched or depleted relative to chondrite.

Tofua arc and 'Eua, suggesting that the variations are due to fractional crystallisation and/or pooled melting. If the variations had been due to either source, or dynamic melting differences, then changes in the Sm_n value would be accompanied by changes in the La_n/Sm_n value.

7.5.2 Nature of the mantle end-member

Pb isotopic data from the Eocene to Miocene volcanics of 'Eua Island, Tonga, which date from the earliest stages of arc magmatism along the Tonga trench, have a large range of Pb isotopic compositions (Figure 7.3(b) and 6.3). *Kempton & Tappin (1995)* explain this in terms of mixing of depleted IMM with a component derived from Pacific crust/mantle ± sediments. Therefore, this suggests that IMM has been present beneath the Tonga arc since the earliest stages of arc magmatism. The data of the north Tongan tholeiites form a mixing trend between an end-member with IMM isotopic characteristics and a subduction component on Figure 7.3(b), which is similar

to that shown by the 'Eua data, although not parallel. However, there is no component derived from Pacific volcanogenic sediments in the Pb isotopic signature of the tholeiites (Figure 7.3(b) and (c)).

The young lavas (less than 6 Ma) from the northern and central Lau Basin also have IMM isotopic signatures (*Loock et al., 1990; Hergt & Hawkesworth, 1994; Pearce et al., 1995b*). These IMM isotopic signatures are only found in the young volcanics from the back-arc spreading centres. This led *Hergt & Hawkesworth (1994)* to propose that IMM has influxed into the Lau Basin since approximately 6 Ma, when back-arc spreading initiated. Spreading is likely to be induced by processes related to slab roll-back (e.g. *Uyeda & Kanamori, 1979*). However, the presence of IMM Pb isotopic signatures in the Eocene volcanics from 'Eua suggest that IMM has, in fact, been present above the Tongan subduction zone since the earliest stages of arc magmatism in the Eocene. This IMM has been contaminated by a subduction component derived from Pacific mantle/crust ± sediments since the Eocene, producing the mixing trends observed in the 'Eua and the north Tongan tholeiite Pb isotope data. Lavas from the early-Lau Basin (pre-6 Ma e.g. Sites 834 and 835 from ODP Leg 135) tap this contaminated mantle as their Pb isotopic signatures are dominated by that of the subduction component (*Hergt & Hawkesworth, 1994*). However, when back-arc spreading initiated at around 6 Ma, uncontaminated IMM mantle was tapped again from greater depths, causing the lavas produced at the spreading centres to have IMM Pb isotopic signatures. Therefore, these signatures in the Eocene volcanics of 'Eua and the north Tongan tholeiites and in the young lavas from the back-arc spreading centres of the Lau Basin, are better explained by IMM having been present above the Tongan subduction zone since the Eocene rather than by it having influxed since 6 Ma, when the Lau Basin began to open, as proposed by *Hergt & Hawkesworth (1994)*.

7.5.3 Comments about the melting processes of the lavas from north Tonga from their major element geochemistry

Values of Na8 and Fe8 for the north Tongan tholeiites, and the lavas from 'Eua which have an Eocene age, and from the Tofua arc, were determined from Figures 7.1(b) and (e) in a similar way as in Section 4.5.6 for the north Tongan boninites and the lavas from Tafahi and Niuatoputapu (*Langmuir et al., 1993; Pearce et al., 1995a*). Na8 and Fe8 are the Na_2O and FeO^* contents of the lavas extrapolated to 8 wt% MgO. Lines for which Na8=1.5, 2, 3 and 4 and Fe8=4, 6, 8 and 10 are drawn on the Na_2O and FeO^* versus MgO plots respectively (Figures 7.1(b) and (e)). Only the lavas with MgO contents greater than 4 wt% were used in determining Na8 and Fe8 values,

as ones with MgO contents less than 4 wt% are likely to have undergone extensive fractionation (see vectors for plagioclase fractionation on Figures 7.1(b) and (e)).
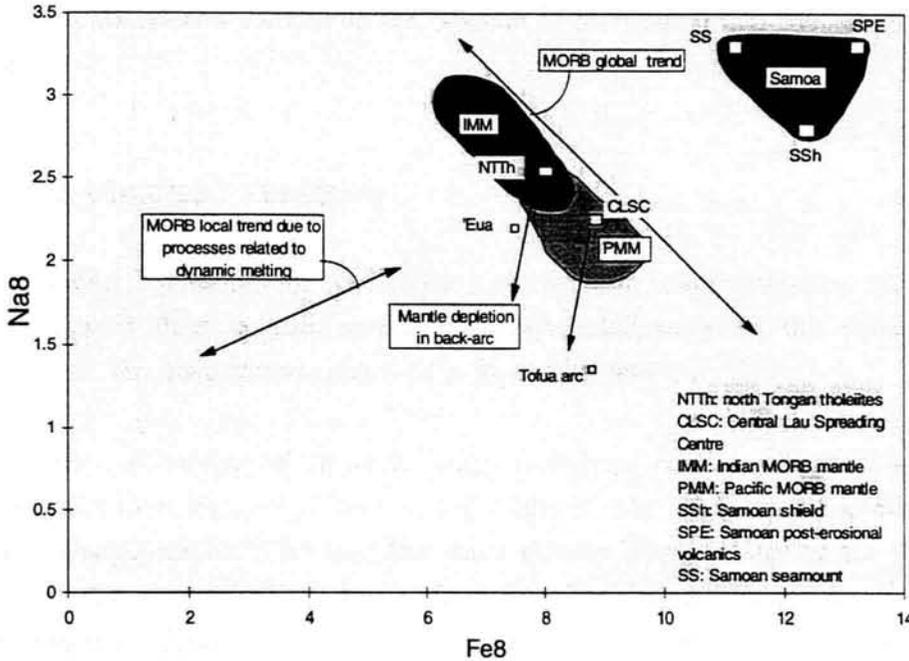
Figure 7.6: *Plot of Fe8 versus Na8 from Langmuir et al. (1993) for the north Tonga tholeiites (NTTh), the Tofua arc and Eocene lavas from 'Eua. Fields for Indian and Pacific MORB and the Samoan plume are superimposed. Double-headed arrows indicate MORB global and local trends (Langmuir et al., 1993). The variation in Na8 and Fe8 between the suites of lavas from Tonga are the result of varying depletion of their mantle sources. The Na8 and Fe8 values of the north Tongan tholeiites are similar to those of MORB suggesting their sources have not been depleted in previous episodes of partial melting. The lavas from 'Eua have lower Na8 values than the north Tongan tholeiites, suggesting that their sources are more depleted. This diagram emphasises that the lavas associated with early-arc magmatism have MORB mantle sources, and their compositions have not been influenced by the plume. The Tofua arc lavas are derived from Lau Basin mantle that has undergone depletion in the back-arc.*

Figure 7.6 is a plot of the Na8 and Fe8 values of the north Tongan tholeiites, the Eocene lavas from 'Eua and the lavas from the modern Tofua arc. The north Tongan tholeiites have a similar Na8 and Fe8 values as those of MORB, whereas 'Eua and the Tofua arc have lower Na8 values than, and similar Fe8 values to, those of MORB. This can be explained if the mantle sources to the 'Eua and Tofua arc lavas had undergone depletion in the back-arc region as a result of melt generation at the spreading centres (*Pearce et al., 1995a;* Section 4.5.6). However, the Na8 and Fe8 values of the north Tongan tholeiites suggest that their sources were similar to those of MORB. The Na8 and Fe8 values of the lavas associated with early-arc magmatism ('Eua and the north Tongan tholeiites) form a distinct mantle depletion trend from

those of the modern Tofua arc on Figure 7.6. This suggests that mantle underlying the region that became the Lau Basin, although it is likely to have had similar isotopic characteristics (Figure 7.3), may not have had similar trace element geochemistry as that under the modern Lau Basin (i.e. sources to the Central Lau Spreading Centre lavas).

7.6 Chapter 7 Summary

Chapter 7 describes the geochemistry of the north Tongan tholeiites and uses it to understand their magma genesis and their relationship to the initiation of subduction. The main features observed in the chapter are:

• The geochemistry of the north Tongan tholeiites (NTTh) is compared with that of volcanics from 'Eua, which have a similar age, in order to determine whether they could be petrogenetically related. The major element geochemistry of the NTTh is similar to the more primitive samples from 'Eua. Both the NTTh and 'Eua have flat REE patterns, a depletion in Nb and LILE enrichment relative to the HFSE and REE on the N-MORB-normalised plot. However, 'Eua has a strong LREE depletion on the chondrite-normalised REE pattern and also depletions in Zr and Hf, whereas the NTTh do not have these depletions. Therefore, this shows that there are variations in composition between the NTTh and 'Eua, suggesting that they have at least some petrogenetic differences, despite their similar age.

• The geochemistry of the diabases from the ophiolite sections has been compared to that of the north Tongan boninites and tholeiites, in order to investigate whether the extrusives are cogenetic with the rest of the dredged ophiolite sections. The diabases from the western (boninitic) ophiolite section have a strong LREE, and weak Nb and Ta depletions compared to the strong LREE enrichment and Nb and Ta depletions of the north Tongan boninites. A plagiogranite from this section has a K-Ar age of 13 ± 3 Ma, whereas the boninites have a K-Ar age of less than 3.5 Ma. The lack of geochemical similarities between the boninites and the underlying diabases, and the differences in age between them and the plagiogranite, suggest that the boninites are not cogenetic with the rest of the ophiolite section.

The NTTh have similar geochemical characteristics to the diabases, such as a flat REE pattern and a slight depletion in the LREE and Ta and Nb. This suggests that they are likely to be cogenetic with the diabases which form part of an Eocene basement. The boninites erupted at a later stage, related to recent tectonic processes in the northern Lau Basin (Section 2.10).

• The NTTh have similar $^{87}Sr/^{86}Sr$ and $^{143}Nd/^{144}Nd$ ratios to the Tofua arc. Their Pb isotope data on the $^{208}Pb/^{204}Pb$-$^{206}Pb/^{204}Pb$ plot form a trend between Indian MORB mantle (IMM) and a subduction component. The Pb isotope data from the Eocene volcanics of 'Eua also form a trend between an end-member with an IMM isotopic signature and a component derived from Pacific altered oceanic crust and sediments, but over a larger range of Pb isotope ratios. The presence of this IMM Pb isotopic signature in these Eocene volcanics is evidence that IMM has been present beneath the Tongan arc since the earliest stages of arc magmatism.

Hergt & Hawkesworth (1994) propose that IMM influxed when the Lau Basin began to open at about 5.5 Ma, and is detected in the Pb isotopes of the young volcanics of the back-arc spreading centres. However, the isotopic data suggest that IMM has been present beneath the Tongan arc since the Eocene, but has been contaminated by a component from Pacific crust ± sediments. Therefore, the IMM Pb isotopic signature is not detected in the Tongan lavas until after the Lau Basin began to open when uncontaminated IMM was tapped again at the back-arc spreading centres, from greater depths

• The NTTh have LILE and LREE enrichment shown by their high La/Yb, Sr/Yb and Ba/Yb ratios compared to MORB. Their Nb/Yb ratios and Pb isotopic composition similar to MORB is evidence that their sources are not residual plume mantle unlike those of the north Tongan boninites and recent north Tongan lavas. This suggests that the flow which brought residual Samoan plume asthenosphere into the northern Lau Basin and the source region of these lavas was not present during early-arc volcanism.

CHAPTER 8

Concluding discussion and implications

8.1 Introduction

In this thesis, a detailed petrologic and geochemical study of some suites of lavas from the northern Lau Basin has been carried out. These lavas are from two ophiolite sections, dredged from the inner wall of the Tonga trench, from the Northern Lau Spreading Centre, the northeastern limb of the King's Triple Junction, and from the volcanic-arc islands of Tafahi and Niuatoputapu.

The ages of the lavas were estimated, using K-Ar dating methods, and therefore, the relationship between the timing of their magma genesis and the tectonic evolution of the region can be constrained.

A petrogenetic model for the northern Lau Basin is developed using evidence from the trace elements, and Sr, Nd and Pb isotopic compositions of the suites of lavas.

The structural and geochemical controls imposed on magma genesis during the tectonic evolution of the region, from an age close to that of the initiation of subduction (c.50 Ma) until after the Lau Basin opened (<6 Ma), are investigated. These controls relate to the extent of the influence of: (i) the Samoan plume; and (ii) along-trench variations in the subduction component, and to the regional tectonics.

8.2 Geochemical characteristics of the lavas from north Tonga

The geochemical characteristics of the lavas from the northern Lau Basin are outlined in the following sections. Evidence from these characteristics has been used to investigate: (i) the derivation of their subduction components; (ii) the degree of depletion or enrichment of their mantle sources; (iii) any processes that may have occurred in the melting column, such as mantle replenishment; and (iv) the nature of any fractional crystallisation.

8.2.1 The north Tongan boninites

Boninitic lavas were dredged from the inner wall of the Tonga trench on the 1982 cruise of the 'Kallisto' vessel. These are associated with the western ophiolite section (Figure 2.6). Boninites were also dredged from close to the Northern Lau Spreading Centre, 40 km west of this ophiolite section. The ophiolite section also contains tectonised harzburgites, cumulate ultramafics and gabbros, diorites, tonalites, trondjemites, diabases. The boninites from the ophiolite sequence have K-Ar ages of 2.54±0.74Ma and 3.09±0.48Ma, whereas those from the west have ages of 0.58± 0.20Ma and 0.89±0.04Ma. These dates suggest that boninite magma genesis was related to the development of back-arc spreading on the Northern Lau Spreading Centre, rather than being associated with the initiation of subduction (c.50Ma), as proposed for the origins of other boninites from the western Pacific (e.g. *Pearce et al., 1992b; Taylor et al., 1994*).

The boninites have low TiO_2, and high MgO and SiO_2 contents (TiO_2 <0.4 wt%, Mg#>0.6 and SiO_2 >56 wt%), and high CaO/Al_2O_3 ratios (>0.75), which satisfy the criteria for high-Ca boninites (*Crawford et al., 1989*). Their major element compositions are similar to those of high-Ca boninites from the Upper Pillow lava Sequence of the Troodos Ophiolite, Cyprus and boninites dredged from Station 21 of the 'Natsushima' 1984 (Figure 8.1; *Falloon & Crawford, 1991*). The variation in their major elements can be explained by the fractionation of olivine, clinopyroxene and orthopyroxene, but plagioclase has not reached the liquidus. The higher MgO contents (>15 wt%), and lower Al_2O_3 (<10 wt%), SiO_2 (<50 wt%) and CaO (<8 wt%) of the boninites dredged from the west compared with those from the ophiolite section, are a result of olivine accumulation.

These boninites have enrichments in LREE relative to MREE, and in LILE and REE relative to HFSE. This has been interpreted as evidence for enrichment of the boninite source by a subduction component. The lack of high Zr/Sm ratios and high Na_2O and Al_2O_3 contents (c.f. those of boninites from Chichijima and the Izu-Bonin fore-arc, *Taylor et al., 1994; Pearce et al., 1992a,b*) indicate that this component is a hydrous fluid derived from the dehydration of the subducting slab ± sediments rather than a partial melt of the slab itself. The low Ce/Pb ratios and high [207]Pb/[204]Pb and [208]Pb/[204]Pb ratios of the boninites may indicate that the subduction component was derived from subducted plume crust.

The depletions in Zr and Hf relative to Sm and Nd, and in Ta and Nb relative to La and Th, of the boninites from the ophiolite section indicate that their sources are highly depleted. However, the boninites from the west are strongly enriched in Nb and Ta and slightly in Zr and Hf, which suggests that they have an enriched source. The

189

Zr/Yb and Nb/Yb ratios of all the boninites form a trend, parallel to, but below, the MORB-plume array (*Pearce & Peate, 1995*). This can be explained if their sources were plume mantle that had undergone a partial melting event in garnet facies at the plume, prior to remelting in spinel facies, during boninite magma genesis. M/Yb-Nb/Yb plots, where M is a slab-derived element (e.g. Sr, Th, Ba, La), also indicate that the residual plume mantle sources of the boninites from the ophiolite section have been enriched by a subduction component. However, these plots show that the sources of the boninites from the west have not had a significant contribution from a subduction component.

All the boninites have high $^{207}Pb/^{204}Pb$ and $^{208}Pb/^{204}Pb$ ratios and high $^{87}Sr/^{86}Sr$ and low $^{143}Nd/^{144}Nd$ ratios similar to those of the Samoan plume.

The temperatures of the boninite primary magmas, which are extrapolated from the temperatures of crystallisation of pyroxenes (from two-pyroxene thermometry), are estimated to be approximately $1230\pm50°C$. This suggests that the boninite sources are either (i) plume mantle that has cooled down from around 1450°C, or (ii) MORB-like mantle. The trace elements suggest that the former is more likely (Figures 4.12 and 5.7).

8.2.2 Tafahi (10-20Ka)

A lava from Tafahi has a K-Ar date of 7Ma, but U-Th disequilibria suggest that the lavas are younger, having ages around 10-20Ka. These dates suggest that either (i) the lavas have been erupting from close to age of opening of the Lau Basin until recently, or (ii) the K-Ar date is inaccurate and the Tafahi lavas are all young, or (iii) the U-Th disequilibria may be inaccurate.

The major element variations of the Tafahi lavas can be explained by the fractionation of olivine, clinopyroxene, orthopyroxene, plagioclase and the Fe-Ti oxides.

The lavas from Tafahi have enrichment in LILE relative to HFSE, and vary from being moderately LREE-enriched to slightly LREE-depleted. They have depletions in Zr and Hf relative to Sm and Nd, and Ta and Nb relative to La and Th. Their enrichment in slab-derived elements relative to MORB is a result of the influence of the subduction component. Their Zr/Yb and Nb/Yb ratios form a trend, similar to that of the north Tongan boninites and lavas from Niuatoputapu, parallel to, but lower than, that of the MORB-plume array. This can be explained if these lavas were derived from residual plume mantle sources.

The Pb isotopic compositions of these lavas are similar to those of Pacific volcanogenic sediments. They have lower $^{143}Nd/^{144}Nd$ ratios than those of average

MORB, and higher $^{87}Sr/^{86}Sr$ ratios than those of the mantle array (incl. average MORB).

8.2.3 Niuatoputapu (<350Ka)

The lavas from Niuatoputapu have K-Ar ages of 1.60-2.10Ma, but U-Th disequilibria dates them at <350Ka (*S. Turner, pers comm.*).

The major element compositions of the lavas from Niuatoputapu lie on the main Tofua arc trend. However, the low CaO and MgO contents of these lavas compared with those of the lavas from Tafahi and the north Tongan boninites suggest they have undergone a larger amount of fractional crystallisation. This fractionation involved olivine, clinopyroxene, orthopyroxene, plagioclase and Fe-Ti oxides.

The lavas from Niuatoputapu have LILE- and a slight LREE-enrichment relative to the HFSE, which is attributed to the influence of a subduction component. They have a pronounced depletion in Ta and Nb relative to Th and La, and in Zr and Hf relative to Nd and Sm.

Their Pb isotopic compositions are similar to those of Pacific volcanogenic sediments. They have lower $^{143}Nd/^{144}Nd$ and higher $^{87}Sr/^{86}Sr$ ratios than those of average MORB, but similar to those of the northern Lau Basin lavas (*Volpe et al., 1988; Loock et al., 1990*). Their lower $^{143}Nd/^{144}Nd$ and high $^{87}Sr/^{86}Sr$ ratios compared with those of MORB are likely to be the result of the influence of the Samoan plume on their magma genesis.

The depletions in HFSE relative to the REE suggest that their sources are more depleted than those of MORB, but their Zr/Yb and Nb/Yb ratios form a similar trend to that of the north Tongan boninites and the lavas from Tafahi, which suggests their sources are also residual plume mantle (Figure 5.7).

8.2.4 The Northern Lau Spreading Centre (< 1.5Ma)

The lavas from the Northern Lau Spreading Centre have a LILE- and weak LREE-enrichments. They do not have an enrichment in slab-derived elements relative to the MORB-plume array (Figure 4.12), suggesting that their compositions are not significantly influenced by a subduction component. Therefore, their LREE and LILE-enrichments relative to MORB are likely to be a result of the influence of the Samoan plume.

Their Pb isotope compositions form a trend between an end-member with an Indian MORB mantle isotopic signature and an end-member with a plume isotopic signature. This suggests that mixing between these end-members has occurred during

the magma genesis of these lavas. This is supported by evidence from their Zr/Yb and Nb/Yb ratios.

8.2.5 The north Tongan tholeiites (c. 50Ma)

Tholeiitic lavas were dredged from the inner wall of the Tonga trench, which form part of an ophiolite sequence (eastern). This sequence also contained cumulate ultramafics and gabbros, diorites, plagiogranites, diabases and tuffs.

These lavas have LILE-enrichment relative to HFSE and REE, a weak LREE-depletion, and Nb and Ta depletions relative to La and Th. These are similar geochemical characteristics to those of the diabases from the eastern ophiolite sequence. This ophiolite sequence has a K-Ar age of 50±9Ma, which is within error of the age of initiation of subduction. Therefore, the tholeiites are likely to have been erupted during early-arc magmatism, as they are cogenetic with the diabases from the ophiolite sequence.

The north Tongan tholeiites have $^{143}Nd/^{144}Nd$ and $^{87}Sr/^{86}Sr$ ratios similar to those of the Tofua arc. Their Pb isotopic compositions form a trend between an end-member with Indian MORB mantle isotopic characteristics and a subduction component derived from subducted Pacific oceanic crust and sediments.

The geochemical signature of the plume is not detected in these lavas, which suggests that the sources of these lavas was MORB-like mantle rather than residual plume mantle. This, therefore, implies that plume mantle was not present under the region during early-arc magmatism (c.50 Ma).

8.3 Petrogenetic model for the northern Lau Basin

The magma genesis of the lavas from the northern Lau Basin is related to the structural and geochemical controls imposed during the tectonic evolution of the region, which are illustrated on Figures 8.1 and 8.3:

8.3.1 The opening of the Lau Basin and its control on the mantle dynamics

Since about 6 Ma, the Lau Basin has been opening (*Parson & Hawkins, 1994*), and the Pacific Plate ripping at the northern termination of the Tonga trench. Figure 8.2 is a diagram illustrating the present-day tectonics at the northern Lau Basin and the effect this has on the regional mantle dynamics (adapted from *Cann, 1994*). The downward force on the subducting plate due to gravity leads to 'roll-back' at the trench. This 'subduction roll-back' causes 'space' to be generated in the mantle

The passive influx of asthenosphere from the west as a result of subduction roll-back at the Tonga trench could also explain the presence of an Indian MORB mantle domain under the central Lau Basin. Its presence has been detected in the isotopic signatures of young lavas from the main back-arc spreading centres (Central and Eastern Lau Spreading Centres), from drillsites located in crust generated at these spreading centres (sites 836 and 837 of ODP Leg 135, Figure 8.1). The mixed plume-IMM isotopic signatures of the lavas from the Northern Lau Spreading Centre can be explained if mixing occurred between the two mantle domains during their magma genesis. Some of the north Tongan tholeiites and Eocene volcanics from 'Eua also have an IMM isotopic signature, which suggests that the Indian MORB reservoir has been present under the region since at least the Eocene. However, lavas from the older parts of the central Lau Basin (sites 834 and 835, Figure 8.1) have isotopic signatures dominated by that of a subduction component, suggesting that the IMM reservoir was contaminated. Therefore, it was not until after back-arc spreading initiated at about 3Ma, that uncontaminated IMM was retapped again from greater depths.

8.3.2 Geochemical controls

The main geochemical controls on magma genesis in the northern Lau Basin are illustrated geographically on Figure 8.1, and in three-dimensions on Figure 8.2. These are related to: (i) the composition of the subduction component, and (ii) mantle source processes.

The subduction component is made up of fluids derived from the subducting slab, which may be altered Pacific oceanic or plume crust, and/or Pacific pelagic and/or volcanogenic sediments. This component contains high concentrations of incompatible, slab-derived elements (e.g. Sr, Ba, Th, K, La and Ce). Therefore, lavas whose compositions have been influenced by a subduction component also contain high concentrations of these elements relative to those of MORB (e.g. *Tatsumi, 1989*). The isotopic composition of the subduction component is hard to constrain as it may vary between the compositions of the three (or four) possible end-members. Isotopic evidence for this component in the lavas from the northern Lau Basin lies in the displacement to high $^{87}Sr/^{86}Sr$ ratios from the mantle array.

The mantle processes that control the compositions of the lavas from the northern Lau Basin, are related to the degree of depletion or enrichment of, and the type of mantle which forms, their sources. The subduction-related lavas from the northern Lau Basin have a plume geochemical signature, indicating that their sources

195

are likely to be *residual plume mantle*. This signature is characterised by high concentrations of (i) LILE, LREE and the more incompatible HFSE (Nb±Zr), and (ii) low ^{143}Nd/^{144}Nd and high ^{87}Sr/^{86}Sr ratios relative to MORB, and in some cases, high ^{207}Pb/^{204}Pb and ^{208}Pb/^{204}Pb ratios relative to the Northern Hemisphere Reference Line and (iii) low Zr/Yb ratios for their Nb/Yb ratios compared to the MORB-plume array (*Pearce et al., 1995a*). Its presence has been recognised in back-arc basin basalts and other boninites dredged from the northern Lau Basin by *Volpe et al. (1988)* and *Falloon & Crawford, (1991)* respectively.

The apparent degree of depletion in incompatible, mantle-derived elements (e.g. HFSE, Ti Y and Yb) of the subduction-related lavas from the northern Lau Basin relative to fertile-MORB mantle is an indication of the extent that their sources have undergone depletion by previous partial melting episodes. The enrichment in very highly incompatible elements relative to highly incompatible elements (both normalised to fertile-MORB mantle) of the north Tongan boninites, Tafahi and Niuatoputapu suggests that their sources were more 'enriched' relative to fertile-MORB mantle, but more 'depleted' than fertile-plume mantle. This is further evidence that the sources of these lavas were residual plume mantle.

Figure 8.3 is a Venn diagram illustrating the magma genesis of the lavas from the northern Lau Basin in terms of combinations of three end-members. The three end-members are Indian MORB- and residual plume-mantle and the subduction component. Indian MORB- and residual plume-mantle are possible end-members for the composition of the mantle wedge. The subduction component may be the result of mixing between three or four end-members (see above), but has been simplified on Figure 8.3. The overlapping regions between the circles represent where two or more of the components are involved in magma genesis. The names of the suites of lavas have been placed into the overlapping region that is representative of all the end-members involved in their magma genesis. The following are comments arising from Figures 8.1 and 8.3:

(1) A mantle domain with the geochemical characteristics of the Samoan plume underlies the northern Lau Basin (shown in red). This has influenced the compositions of all the lavas from north Tonga that have erupted after the opening of the Lau Basin (<6 Ma). This domain does not extend into the central and southern Lau Basin as neither the lavas from the Tofua arc nor those of the Central Lau Spreading Centre contain a plume geochemical signature;

(2) The lavas from the Central Lau Spreading Centre originate from a mantle domain with Indian MORB mantle isotopic characteristics, which is distinct from the one underlying the northern Lau Basin. However, mixing between these two domains

subduction component, whereas those of the boninites from the west have not had this enrichment;

(5) The lavas from the Tofua arc are dominated by the geochemical signature of a subduction component, but their sources are from within the Indian MORB mantle domain;

(6) The plume has *not* influenced the compositions of the Eocene north Tongan tholeiites from the eastern ophiolite section, dredged from the inner wall of the northern Tonga trench ('Kallisto' 1982 cruise). However, their geochemical signatures have originated from a mixture of Indian MORB mantle and a subduction component. This suggests that an Indian MORB mantle domain underlay the region that became the northern Lau Basin (>6Ma) and that the influx of plume asthenosphere did not occur until after the opening of the Lau Basin;

(7) the isotopic composition of the subduction component is strongly controlled by along-trench variations in the compositions of the subducting slab and sediments. In the north, mainly Pacific volcanogenic sediments, which originate from Samoa and its associated seamounts are being subducted. Evidence for this are isotopic compositions of the lavas from Tafahi and Niuatoputapu, which are dominated by those of PVS. However, in the south, dominantly Pacific pelagic sediments are being subducted, which is shown by the isotopic compositions of the Tofua arc, which are explained by mixing between fluids derived from PPS and an altered oceanic crust. In the north, it is also possible that plume crust is being subducted, and therefore, the subduction component may acquire a plume isotopic signature (e.g. the north Tongan boninites).

8.4 Further work

Further work in the area concentrates on collecting more data on existing samples by other, more specialised, geochemical techniques that are out of the scope of this thesis, and acquiring new data and samples to contribute towards making a more extensive data set for the northern Lau Basin. The following are suggestions for this work:

(1) The lavas from Tafahi and Niuatoputapu have U-Th disequilibria indicating that they have ages of <350Ka (*S. Turner, pers. comm.*). A more extensive study of the U-Th disequilibria in other young subduction-related lavas from the northern Lau Basin could be carried out to obtain better estimates of their ages and any short-lived geochemical changes relating to the addition of slab-derived fluids to their sources;

(2) Carrying out Be-B isotopic analyses of the lavas from north Tonga is a better method to trace any recycling of subducted sediments, and could further verify the

nature and presence of any components derived from subducted sediments (*Tera et al., 1986; Morris & Tera, 1989, Morris et al., 1990*). These data along with the Pb isotopes could be used to estimate the relative proportions of sediments and altered oceanic crust contributing to the subduction component (*Ishikawa & Nakamura, 1994*). Other tracers of sediment recycling are $^{18}O/^{16}O$ and a negative anomaly in Ce/Ce* ratios (*Hole et al., 1984*);

(3) Ar-Ar dating would be useful to determine more accurate ages of the lavas from north Tonga, so that the timing of their magma genesis can be better constrained within the tectonic development of the Lau Basin;

(4) collecting further GLORIA sidescan imagery, together with dredge sampling of the northern Lau Basin, particularly in the area of the northern extension of the Northwestern Lau Spreading Centre and west of the King's Triple Junction, in order to have a full tectonic coverage of NLB and to trace the extent of the influence of the Samoan plume on the compositions of the lavas in the west;

(5) Hf isotopic analysis of existing samples to further study the relationships between the different mantle domains in the Lau Basin.

BIBLIOGRAPHY

ARCULUS, R.J. & POWELL, R., 1986. Source component mixing in the regions of arc magma generation. *J. Geophys. Res.*, **91**, 5913-5926.

BECCALUVA, L. & SERRI, G., 1988. Boninitic and low-Ti subduction-related lavas from intraoceanic arc-backarc systems and low-Ti ophiolites: a reappraisal of their petrogenesis and original tectonic setting. *Tectonophysics*, **146**, 291-315.

BEN OTHMAN, D., WHITE, W.M. & PATCHETT, J., 1989. The geochemistry of marine sediments, island arc magma genesis, and crust-mantle recycling. *Earth and Planetary Science Letters*, **94**, 1-21.

BONATTI, E & MICHAEL, P.J., 1989. Mantle peridotites from continental rifts to ocean basins to subduction zones. *Earth and Planetary Science Letters*, **91**, 297-311.

BOYD, F.R., 1973. A Pyroxene geotherm. *Geochimica et Cosmochimica Acta*, **37**, 2533-2546.

BOYNTON, W.V., 1984. Cosmochemistry of the rare earth elements: meteorite studies. *In:* Henderson, P. (ed) *Rare earth element geochemistry*. Elsevier, Amsterdam, 63-114.

BRENAN, J.M., SHAW, H.F. & RYERSON, F.J., 1995. Experimental evidence for the origin of lead enrichment in convergent-margin magmas. *Nature*, **378**, 54-56.

BRIQUEU, L., BOUGAULT, H. & JORON, J.L., 1984. Quantification of Nb, Ta, Ti and V anomalies in magmas associated with subduction zones: petrogenetic implications. *Earth and Planetary Science Letters*, **68**, 297-308.

CAMERON, W.E., 1985. Petrology and origin of primitive lavas from the Troodos ophiolite, Cyprus. *Contributions to Mineralogy and Petrology*, **89**, 239-255.

CANN, M., 1994. A magnetic interpretation of the Lau Basin, Southwest Pacific. M.A. Thesis, University of Durham, unpublished.

COHEN, R.S. & O'NIONS, R. K., 1982. The Lead, Neodynium and Strontium Isotopic Structure of Ocean Ridge Basalts. *Journal of Petrology*, **23**, Part 3, 299-324.

COX, K.G., BELL, J.D. & PANKHURST, R.J., 1979. The Interpretation of Igneous Rocks. (Publ.) George Allen & Unwin, London.

CRAWFORD, A.J., FALLOON, T.J. & GREEN, D.H., 1989. Classification, petrogenesis and tectonic setting of boninites. In CRAWFORD, A.J., (ed.), *Boninites and Related Rocks*, London, (Unwin Hyman), 2-49.

CRAWFORD, A.J., BRIQUEU, L., LAPORTE, C., AND HASENAKA, T., 1995. Coexistence of Indian and Pacific Oceanic upper mantle reservoirs beneath the Central New Hebrides Island Arc. *Active Margins and Marginal Basins of the Western Pacific*, Geophysical Monograph **88**, 199-217.

CUNNINGHAM, J.K. & ANSCOMBE, K.J., 1985. Geology of 'Eua and other islands, Kingdom of Tonga. *In:* Scholl, D.W. and Vallier, T.L. (eds.) *Geology and Offshore Resources of Pacific Island Arcs - Tonga Region*, Texas, 221-258.

DANYUSHEVSKY, L.V., SOBOLEV, A.V. & FALLOON, T.J., 1995. N. Tongan high-Ca boninite petrogenesis: the role of Samoan plume and subducted zone - transform fault transitions. *Journal of Geodynamics*, **20**, No. 3, 219-241.

DAVIES, J.H. & BICKLE, M.J., 1991. A physical model for the volume and composition of melt produced by hydrous fluxing above subduction zones. *Philosophical Transactions of the Royal Society of London*, **335**, 355-364.

DAVIES, J.H. & STEVENSON, D.J., 1992. Physical Model of the Source Region of Subduction Zone Volcanics. *Journal of Geophysical Research*, **97**, 2037-2070.

DICK, H.J.B. & FISHER, R.L., 1984. Mineralogic studies of the residues of mantle melting: abyssal and alpine-type peridotites. *In:* J. Kornprobst, ed., Kimberlites II: The Mantle and Crust-Mantle Relationships (*Developments in Petrology*, Vol. **11B**). Elsevier, Amsterdam.

DUNCAN, R.A. & GREEN D.H., 1980. The role of multistage melting in the formation of oceanic crust. *Geology*, **8**, 22-26.

DUNCAN, R.A. & GREEN, D.H., 1987. The genesis of refractory melts in the formation of oceanic crust. *Contributions to Mineralogy and Petrology*, **96**, 326-342.

EWART, A., 1976. A Petrological Study of the Younger Tongan andesites and dacites and the olivine tholeiites of Niua Fo'ou Island, S.W. Pacific. *Contributions to Mineralogy and Petrology*, **58**, 1-21.

EWART, A. & BRYAN, W.B., 1972. Petrography and Geochemistry of the Igneous Rocks from 'Eua, Tongan Islands. *The Bulletin of the Geological Society of America*, **83**, 3281-3298.

EWART, A. & HAWKESWORTH, C.J., 1987. The Pleistocene-Recent Tonga-Kermadec arc lavas: Interpretation of New Isotopic and Rare Earth Data in terms of a depleted Mantle Source Model. *Journal of Petrology*, **28**, 495-530.

EWART, A., BRYAN, W.B., GILL, J.B.,1973. Mineralogy and Geochemistry of the Younger Volcanic Islands of Tonga, S.W. Pacific, *Journal of Petrology*, **14**, Part 3, 429-465.

EWART, A., BROTHERS, R.N. & MATEEN, A., 1977. An outline of the geology and geochemistry, and the possible petrogenetic evolution of the volcanic rocks of the Tonga-Kermadec-New Zealand Island arc. *Journal of Volcanology and Geothermal Research*, **2**, 205-250.

EWART, A., BRYAN, W.B., CHAPPELL, B.W., RUDNICK, R.L. 1994a. Regional Geochemistry of the Lau-Tonga arc and back-arc systems.*In:* HAWKINS, J., PARSON, L., ALLAN, J., *et. al.*, *Proceedings of the ODP, Sci. Results,* **135**, 385-426.

EWART, A., HERGT, J., HAWKINS, J.W., 1994b. Major, trace element and Pb, Sr and Nd isotope geochemistry of Site 839 basalts and basaltic andesites: Implications for arc magmatism. *In* HAWKINS, J.W., PARSON, L.M., ALLAN, J.F. *et al.*, *Proceedings of the ODP, Sci. Res.,* **135**, College Station, TX (Ocean Drilling Programme), 519-532.

FALLOON, T.J. & CRAWFORD, A.J., 1991. The petrogenesis of high-Ca boninite lavas dredged from the Northern Tong Ridge. *Earth and Planetary Science Letters* **102**, 375-394.

FALLOON, T.J. & GREEN, D.H., 1987. Anhydrous partial melting of MORB pyrolite and other peridotite compositions at 10 kbar: implications for the origin of primitive MORB glasses. *Mineralogy and Petrology*, **37**, 181-219.

FALLOON, T.J., GREEN, D.H. & CRAWFORD, A.J., 1987. Dredged igneous rocks from the northern termination of the Tofua magmatic arc, Tonga and adjacent Lau Basin. *Australian Journal of Earth Science*, **34**, 487-506.

FALLOON, T.J., GREEN, D.H., McCULLOCH, M.T., 1989. Petrogenesis of high-Mg and associated lavas from the north Tonga Trench. In CRAWFORD, A.J., (ed.), *Boninites and Related Rocks*, London, (Unwin Hyman), 2-49.

FALLOON, T.J., MALAHOFF, A., ZONENSHAIN, L.P. & BOGDANOV, Y., 1992. Petrology and Geochemistry of Back-arc Basin Basalts from Lau Basin Spreading Ridges at 15, 18 & 19°S. *Mineralogy and Petrology* **47**, 1-35.

FARLEY, K.A., NATLAND, J.H. & CRAIG, H., 1992. Binary mixing of enriched and undegassed (primitive?) mantle components (He, Sr, Nd, Pb) in Samoan lavas. *Earth and Planetary Science Letters*, **111**, 183-199.

FAURÉ, G., 1986. Principles of Isotope Geology. (Publ.) John Wiley & Sons, Inc., Canada.

GERLACH, D.C., CLIFF, R.A., DAVIES, G.R., NORRY, M. & HODGSON, N., 1988. Magma sources of the Cape Verdes archipelago: Isotopic and trace element constraints. *Geochemica et Cosmochimica Acta*, **52**, 2979-2992.

GÓMEZ, J.M.C., 1990. A program for pyroxene classification and calculation of end-members. *American Mineralogist*, **75**, 1426-1427.

GOVINDARAJU, K., 1989. Compilation of working values and sample description for 272 geostandards. *Geostandards Newsletter*, **13**, 1-113.

GREEN, D.H., 1973. Experimental melting studies on a model upper mantle composition at high pressure under water-saturated and water-unsaturated conditions. *Earth and Planetary Science Letters*, **19**, 37-53.

GREEN, T.H., & PEARSON, N.J., 1987. An experimental study of Nb and Ta partitioning between Ti-rich minerals and silicate liquids at high pressure and temperature. *Geochimica et Cosmochimica Acta*, **51**, 55-62.

HAMBURGER, M.W. & ISAACS, B.L., 1988. Diffuse back-arc deformation in the S.W. Pacific. *Nature*, **332**, 599-604.

HAMELIN, B., DUPRÉ, B. & ALLÈGRE, C.J., 1984. Lead-strontium isotopic variations along the East Pacific Rise and Mid-Atlantic Ridge: a comparative study. *Earth and Planetary Science Letters*, **67**, 340-350.

HAMELIN, B., DUPRÉ, B. AND ALLÈGRE, C.J., 1986. Pb-Sr-Nd isotopic data of Indian Ocean ridges: new evidence of large-scale mapping of mantle heterogeneities. *Earth and Planetary Science Letters*, **76**, 288-298.

HART, S.R., 1969. K, Rb, Cs contents and K/Rb, K/Cs ratios of fresh and altered submarine basalts. *Earth and Planetary Science Letters*, **6**, 295-303.

HART, S.R., 1984. A large scale isotope anomaly in the Southern hemisphere mantle. *Nature*, **309**, 753-757.

HART, S.R., 1988. Heterogeneous mantle domains: signatures, genesis and mixing chronologies. *Earth and Planetary Science Letters*, **90**, 273-296.

HART, S.R. & STAUDIGEL, H., 1982. The control of alkalies and uranium in seawater by ocean crust alteration'. *Earth and Planetary Science Letters*, **58**, 202-212.

HART, S.R. & STAUDIGEL, H., 1989. Isotope characterization and identification of recycled components. *In* HART, S.R. AND GÜLEN, L., (Eds.), *Crust/Mantle Recycling at Convergence Zones*, 15-28. NATO Workshop Vol., Kluwer Academic Publishers, Doredrecht.

HAURI, E.H., NOBUMICHI SIMUZU, DIEU, J.J. & HART, S.R., 1993. Evidence for hotspot-related carbonatite metasomatism in the oceanic upper mantle. *Nature*, **365**, 221-227.

HAWKESWORTH, C.J., HERGT, J.M., MCDERMOTT, F. & ELLAM, R.M., 1991a. Destructive margin magmatism and the contributions from the mantle wedge and subducted crust. *Australian Journal of Earth Sciences*, **38**, 577-594.

HAWKESWORTH, C.J., HERGT, J.M., ELLAM, R.M. & MCDERMOTT, F, 1991b. Element fluxes associated with subduction related magmatism. *Philosophical Transactions, Royal Society of London*, Series A, **335**, 393-405.

HAWKINS, J.W., 1995. Evolution of the Lau Basin - insights from ODP Leg 135. *Active Margins and Marginal Basins of the Western Pacific*, Geophysical Monograph, **88**, 125-173.

HAWKINS, J.W. & MELCHIOR, J.T., 1985. Petrology of Mariana Trough and Lau Basin Basalts. *Journal of Geophysical Research*, **90 B13**, 11431-11468.

HAWKINS, J.W. & NATLAND, J.H., 1975. Nephelinites and basanites of the Samoan linear volcanic chain and their possible tectonic significance. *Earth and Planetary Science Letters*, **24**, 427-439.

HERGT, J.M. & FARLEY, K.N., 1994. Major, trace element and isotope (Pb, Sr and Nd) variations in Site 834 basalts: Implications for the initiation of back-arc opening. *In* HAWKINS, J.W., PARSON, L.M., ALLAN, J.F., *et. al.*, *Proceedings of the ODP, Sci. Res.*, **135**, College Station, TX (Ocean Drilling Programme), 471-486.

HERGT, J.M. & HAWKESWORTH, C.J., 1994. The Pb, Sr and Nd isotopic evolution of the Lau Basin. *In* HAWKINS, J.W., PARSON, L.M., ALLAN, J.F., *et. al.*, *Proceedings of the ODP, Sci. Res.*, **135**, College Station, TX (Ocean Drilling Programme), 505-518.

HICKEY, R & FREY, F., 1982. Geochemical characteristics of boninite series volcanics: implications for their source. *Geochimica et Cosmochimica Acta* **46**, 2099-2115.

HICKEY-VARGAS, R., 1992. A refractory HIMU component in the sources of island-arc magma. *Nature* **360**, 57-59.

HICKEY-VARGAS, R., HERGT, J.M. & SPADEA, P., 1995. The Indian Ocean-Type Isotopic Signature in Wester Pacific marginal basins: origin and significance, *In*

Active Margins and Marginal Basins of the Western Pacific, Geophysical Monograph, **88**, 175-197.

HILDE, T.W.C., UYEDA, S., KROENKE, L., 1977. Evolution of the Western Pacific and its margin. *Tectonophysics*, **38**, 145-165.

HILTON, D.R., HAMMERSCHMIDT, K., LOOCK, G. & FRIEDRICHSEN, H., 1993. Helium and argon isotope systematics of the central Lau Basin and Valu Fa ridge: evidence of crust/mantle interaction in a back-arc basin, *Geochimica et Cosmochemica Acta*, **57**, 2819-2841.

HOFFMAN, A.W., JOCHUM, K.P., SUEFERT, M., & WHITE, W.M., 1986. Nb and Pb in oceanic basalts: new constraints on mantle evolution. *Earth and Planetary Science Letters*, **79**, 33-45.

HOLE, M.J., SAUNDERS, A.D., MARRINER, G.F. & TARNEY, J., 1984. Subduction of pelagic sediments: implications for the origin of Ce-anomalous basalts from the Mariana Islands. *Journal of the Geological Society, London*, **141**, 453-472.

HOLLAND, H.D., 1978. *The Chemistry of the Atmosphere and Oceans*, John Wiley and Sons, New York.

ISHII, T., 1975. The relations between temperature and composition of pigeonite in some lavas and their application to thermometry. *Mineralogical Journal*, **8**, 48-57.

ISHIKAWA, T. & NAKAMURA, E., 1994. Origin of the slab component in arc lavas from across-arc variation of B and Pb isotopes. *Nature*, **370**, 205-208.

ITO, E., WHITE, W.M. AND CÖPEL, C., 1987. The O, Sr, Nd and Pb isotope geochemistry of MORB. *Chemical Geology*, **62**, 157-176.

IWAMORI, H., 1993. A model for disequilibrium mantle melting incorporating melt transport by porous and channel flows. *Nature*, **366**, 734-312.

IWAMORI, H., 1994. ^{238}U-^{230}Th-^{226}Ra and ^{235}U-^{231}Pa disequilibria produced by mantle melting with porous and channel flows. *Earth and Planetary Science Letters*, **125**, 1-16.

IWAMORI, H., MCKENZIE, D., & TAKAHASHI, E., 1995. Melt generation by isentropic mantle upwelling. *Earth and Planetary Science Letters*, **134**, 253-266.

JAQUES, A.L. & GREEN, D.H., 1980. Anhydrous melting of peridotite at 0-15kb pressure and the genesis of tholeiitic basalts. *Contributions to Mineralogy and Petrology*, **73**, 287-310.

JENNER, G.A., 1981. Geochemistry of high-Mg andesites from Cape Vogel, Papua New Guinea. *Chemical Geology*, **33**, 307-332.

KARIG, D.E., 1971. Origin and development of marginal basins in the Western Pacific. *Journal of Geophysical Research*, **76**, No.11, 2542-2561.

KELEMEN, P.B., JOHNSON, K.T.M., KINZLER, R.J. & IRVING, A.J., 1990. High field-strength element depletions in arc basalts due to mantle-magma interactions. *Nature*, **345**, 521-524.

KELEMEN, P.B., SHIMIZU, N. & DUNN, T., 1993. Relative depletion of niobium in some arc magmas and the continental crust: partitioning of K, Nb, La and Ce during melt/rock reaction in the upper mantle. *Earth and Planetary Science Letters*, **120**, 111-134.

KEMPTON, P.D., 1985. An interpretation of contrasting nucleation and growth histories from the petrographic analysis of pillow and dyke chilled margins. Hole 504B Deep Sea Drilling Project Leg 83. *In* ANDERSON, R.N., HONNOREZ, J., BECKER, K. *et.al.*, *Initial Reports on the DSDP*, **83**, Washington, (U.S. Government Printing Office), 165-181.

KEMPTON, P.D., & TAPPIN, D., 1995. Pb- Sr- and Nd-isotope data from 'Eua Island, tonga: Constraints on mantle dynamics in the S.W. Pacific. Abstract, European Union of Geosciences, Strasbourg 9-13 April 1995.

KEMPTON, P.D., HAWKESWORTH, C.J. & FOWLER, M., 1991. Geochemistry and isotopic composition of gabbros from layer 3 of the Indian Ocean crust, hole 735B. *In: Proceedings of the ODP, Sci. Results*, **118**, 127-143.

KEPPLER, H., 1996. Constraints from partitioning experiments on the composition of subduction-zone fluids. *Nature*, **380**, 237-240.

KIMBALL, K.L. & GERLACH, D.C., 1986. Sr isotopic constraints on hydrothermal alteration of ultramafic rocks in two oceanic fracture zones from the South Atlantic Ocean. *Earth and Planetary Science Letters*, **78**, 177-188.

KLEIN, E.M. & LANGMUIR, C.H., 1987. Global correlations of ocean ridge basalt chemistry with axial depth and crustal thickness. *Journal of Geophysical Research*, **92 B8**, 8089-8115.

KLEIN, E.M., LANGMUIR, C.H., ZINDLER, A., STAUDIGEL, H., & HAMELIN, B., 1988. Isotope evidence of a mantle convection boundary at the Australian-Antarctic Discordance. *Nature*, **333**, 623-428.

KNITTEL, V, DEFANT, M.J. & RACZEK, I., 1988. Recent enrichment in the source region of arc magmas from Luzon Islands, Philippines: Sr & Nd isotopic evidence. *Geology*, **16**, 73-76.

KOKELAAR, P., 1986. Magma-water interactions in subaqueous and emergent basaltic volcanism. *Bulletin of Volcanology*, **48**, 275-289.

KRETZ, R., 1982. Transfer and exchange equilibria in a portion of the pyroxene quadrilateral as deduced from natural and experimental data. *Geochimica et Cosmochimica Acta*, **46**, 411-422.

LANGMUIR, C.H., KLEIN, E.M. & PLANK, T., 1993. Petrological systematics of Mid-Ocean Ridge basalts: constraints on melt generation beneath ocean ridges. *In* MORGAN, J.P, BLACKMAN, D.K., & SINTON, J.M. (Eds.), *Mantle Flow and Melt Generation at Mid-Ocean Ridges*, Geophysical Monograph, **71**, 183-280.

LIN, P-N., STERN, R.J. & BLOOMER, S.H., 1989. Shoshonitic volcanism in the Northern Mariana Arc 2: Large-ion-lithophile and rare earth element abundancess, evidence for the source of incompatible element enrichments in intraoceanic arcs. *Journal of Geophysical Research*, **94 B4**, 4497-4514.

LIN, P-N., STERN, R.J. MORRIS, J. & BLOOMER, S.H., 1990. Nd- and Sr- isotopic compositions of lavas from the northern Mariana and southern Volcano arcs:

inplications for the origin of island arc melts. *Contributions to Mineralogy and Petrology*, **105**, 381-392.

LINDSLEY, D.H., 1983. Pyroxene thermometry. *American Mineralogist*, **68**, 477-493.

LINDSLEY, D.H. & ANDERSON, D.J., 1983. A two-pyroxene thermometer. *In:* Proceedings of the 13th Lunar and Planetary Science Conference, Part 2 *Journal of Geophysical Research*, **88**, Supplement, A887-A906.

LOOCK, G., MCDONOUGH, GOLDSIEIN, S.L. & HOFMANN, A.E., 1990. Isotopic compositions of volcanic glasses from the Lau Basin. *Marine Mining*, **9**, 235-245.

MAHONEY, J., NATLAND, J.H., WHITE, W.M., POREDA, R., BOLLOMER, S.H., FISHER, R.L. & BAXTER, A.N., 1989. Isotopic and geochemical provinces of the western Indian Ocean spreading centers, *Journal of Geophysical Research*, **94**, 4033-4052.

MAHONEY, J.A., LEROEX, A.P., PENG, Z., FISHER, R.L. & NETLAND, J.H., 1992. Southwestern limits of Indian Ocean ridge mantle and the origin of low $^{206}Pb/^{204}Pb$ mid-ocean ridge basalt: isotope systematics of the central Southwest Indian Ridge (70°-50°E), *Journal of Geophysical ResearchI*, **97**, 19771-19790.

MCCULLOCH, M.T. & GAMBLE, J.A., 1991. Geochemical and geodynamical constraints on subduction zone magmatism. *Earth and Planetary Science Letters*, **102**, 358-374.

MCDERMOTT, F., DEFANT, M.J., HAWKESWORTH, C.J., MAURY, R.C., & J.L. JORON, 1993. Isotope and trace element evidence for three component mixing in the genesis of hte North Luzon arc lavas (Philippines). *Contributions to Mineralogy and Petrology*, **113**, 9-23.

MCDONOUGH, W.F. & CHAUVEL, C., 1991. Sample contamination explains the Pb isotopic compostion of some Rurutu island and Sasha seamount basalts. *Earth and Planetary Science Letters*, **105**, 397-404.

MCKENZIE, D. & BICKLE, M.J., 1988. The volume and composition of melt generated by extension of the lithosphere. *Journal of Petrology*, **29** Part 3, 625-679.

MERCIER, J.-C., 1976. Single-pyroxene geothermometry and geobarometry. *American Mineralogist*, **61**, 603-615.

MICHARD, A., MONTIGNY, R. & SCHLICH, R., 1986. Geochemistry of the Mantle beneath the Rodriguez Triple Junction and the South-East Indian Ridge. *Earth and Planetary Science Letters*, **78**, 104-114.

MILLER, D.M., GOLDSTEIN, S.L., & LANGMUIR, C.H., 1994. Cerium/lead and lead isotope ratios in arc magmas and the enrichment of lead in the continents. *Nature*, **368**, 514-520.

MITCHELL, J.G., PEATE, D.W., MURTON, B.J., PEARCE, J.A., ARCULUS, R.J., VAN DER LAAN, S., 1992. K-Ar dating of samples from Sites 782 and 786 (Leg 125): the Izu-Bonin forearc region. *In* FRYER, P., PEARCE, J.A., STOCKING, L.B. *et al. Proc. of the ODP, Sci. Res.*, **125**, College Station, TX (Ocean Drilling Program), 203-210.

MORRIS, J. & TERA, F., 1989. ^{10}Be and ^{9}Be in mineral seperates and whole rocks from volcanic arcs: Implications for sediment subduction. *Geochimica et Cosmochimica Acta*, **53**, 3197-3206.

MORRIS, J., LEEMAN, W.P., & TERA, F., 1990. The subducted component in island arc lavas: constraints from Be isotopes and B-Be systematics. *Nature*, **344**, 31-36.

MURTON, B.J., PEATE, D.W., ARCULUS, R.J., PEARCE, J.A., & VAN DER LAAN, S., 1992. Trace element geochemistry of volcanic rocks from Site 786: the Izu-Bonin forearc. *In* FRYER, P., PEARCE, J.A., STOCKING, L.B. *et al. Proc. of the ODP, Sci. Res.*, **125**, College Station, TX (Ocean Drilling Program), 211-236.

NATLAND, J.H., 1980. The progression of volcanism in the Samoan linear chain, *American Journal of Science*, **280A**, 709-735.

NATLAND, J.H., 1982. Crystal morphologies and pyroxene composition in boninites and tholeiitic basalts from Deep Sea Drilling Project Holes 458 and 459B in the Mariana fore-arc region. *Initial reports of the DSDP*, **60**, 681-707.

NAVON, O. & STOLPER, E., 1987. Geochemical consequences of melt percolation: the upper mantle as a chromatographic column. *Journal of Geology*, **95**, 285-307.

OTHMAN, D.B., WHITE, W.M., & PATCHETT, J., 1989. The geochemistry of marine sediments, island arc magma genisis, and crust-mantle recycling. *Earth and Planetary Science Letters*, **94**, 1-21.

PALACZ, Z.A. & SAUNDERS, A.D., 1986. Coupled trace element and isotope enrichment in the Cook-Austral-Samoa Islands, southwest Pacific. *Earth and Planetary Science Letters*, **79**, 270-280.

PARKINSON, I.J., 1993. Geochemistry and Petrogenesis of Forearc Peridotites, ODP Leg 125. PhD Thesis,University of Durham, unpublished.

PARKINSON, I.J., PEARCE, J.A., THIRLWALL, M.F., JOHNSON, K.T.M., & INGRAM, G., 1992. Trace element geochemistry of peridotites from the Izu-Bonin-Mariana forearc, Leg 125. *In* FRYER, P., PEARCE, J.A., STOCKING, L.B., *et al. Proc. of the ODP, Sci. Res.*, **125**, College Station, TX (Ocean Drilling Program), 487-506.

PARSON, L.M. & HAWKINS, J.W., 1994. Successive ridge propagations and the geological history of the Lau backarc Basin. *In* HAWKINS, J.W., PARSON, L.M., ALLAN, J.F., *et. al. Proceedings of the O.D.P, Sci. Res.,* **135**, College Station, TX (Ocean Drilling Programme), 819-828.

PARSON, L.M. & SEARLE, R.C., 1986. Strike-slip fault styles in slow-slipping oceanic transform faults- evidence from GLORIA surveys of Atlantis and Romanche fracture zones. *Journal of the Geological Society of London*, **143**, 757-761.

PARSON, L.M. & TIFFIN, D.L., 1993. The northern Lau Basin: diffuse backarc extension at the leading edge of the Indo-Australian Plate. *Geomarine Letters*, **13**, 107-115.

PARSON, L.M., PEARCE, J.A., MURTON, B.J., & HODKINSON, R.A., 1990. Role of ridge jumps and ridge propagation in the tectonic evolution of the Lau back-arc basin, S.W. Pacific. *Geology*, **18**, 470-473.

PEARCE, J.A., 1975. Basalt geochemistry used to investigate past tectonic environments on Cyprus. *Technophysics*, **25**, 41-67.

PEARCE, J.A., 1982. Trace element characteristics of lavas from destructive plate boundaries. *In* Thorpe, R.S. (Ed.), *Orogenic andesites and related rocks*. Wiley, Chichester, 526-548.

PEARCE, J.A., 1983. Role of the sub-continental lithosphere in magma genesis at active continental margins. *In:* Hawkesworth, C.J. & Norry (eds), *Continental basalts and mantle xenoliths*. Shiva Publishing, Nantwich, U.K., 230-249.

PEARCE, J.A.. & NORRY, M.J., 1979. Petrogenetic implications of Ti, Zr, Y and Nb variations in volcanic rocks. *Contributions to Mineralogy and Petrology*, **69**, 33-47.

PEARCE, J.A. & PARKINSON, I.J.. 1993. Trace element models for mantle melting: application to volcanic arc petrogenesis, *In:* PRICHARD, H.M., *et. al.*, (eds.), *Magmatic Processes and Plate Tectonics, Geological Society of London Special Publication*, **76**, 373-403.

PEARCE, J.A. & PEATE, D.W., 1995. Tectonic implications of the composition of volcanic arc magmas. *Annual Reviews in Earth and Planetary Science*, **23**, 251-85.

PEARCE, J.A., ROGERS, N., TINDLE, A.J., & WATSON, J.S., 1986. Geochemistry and Petrogenesis of basalts from Deep Sea Drilling Project Leg 92, Eastern Pacific. *In*: LEINEN, M., REA, D.K., *et al. Initial Reports of the DSDP*, **42**, Washington (U.S. Government Printing Office), 435-457.

PEARCE, J.A., THIRLWALL, M.F., INGRAM, G., MURTON, B.J., & VAN DER LAAN, S.R., 1992a. Isotopic evidence for the origin of boninites and related rocks drilled in the Izu-Bonin (Ogasawara) forearc, Leg 125. *In* FRYER, P., PEARCE, J.A., STOCKING, L.B., *et al. Proc. of the ODP, Sci. Res.*, **125**, College Station, TX (Ocean Drilling Program), 237-261.

PEARCE, J.A., VAN DER LAAN, S.R., ARCULUS, R.J., MURTON, B.J., ISHII, T., PEATE, D.W. & PARKINSON, I.J., 1992b. Boninite and harzburgite from ODP Leg 125 (Bonin-Mariana fore-arc): A case study of magma genesis during the initial stages of subduction. *In* FRYER, P., PEARCE, J.A., STOCKING, L.B., *et al. Proc. of*

the ODP, Sci. Res., **125**, College Station, TX (Ocean Drilling Program), 623-659.

PEARCE, J.A., ERNEWEIN, M., BLOOMER, S.H., PARSON, L.M., MURTON, B.J., & JOHNSON, L.E., 1995, Geochemistry of Lau Basin volcanic rocks: influence of ridge segmentation and arc proximity. *In:* Smellie, J.L., (ed.) Volcanism Associated with Extension at Consuming Plate margins, *Geological Society of London Special Publication*, **81**, 53-75.

PEARCE, J.A., BAKER, P.E., HARVEY, P.K., & LUFF, I.W., 1995a. Geochemical evidence for subduction fluxes, mantle melting and fractional crystallization beneath the South Sandwich Island Arc. *Journal of Petrology*, **36**, No. 4, 1073-1109.

PEARCE, J.A., ERNEWEIN, M., BLOOMER, S.H., PARSON, L.M., MURTON, B.J., & JOHNSON, L.E., 1995b. Geochemistry of Lau Basin volcanic rocks: influence of ridge segmentation and arc proximity. *In* SMELLIE, J.L. (ed.), *Volcanism Associated with Extension at Consuming Plate Margins, Geological Society Special Publication*, **81**, 53-75.

PIEPGRAS, D.J., WASSERBERG, G.J., & DASCH, E.J., 1979. The isotopic composition of Nd in different ocean masses, *Earth and Planetary Science Letters*, **45**, 223-236.

ROGERS, N.W., MACLEOD, C.J. & MURTON, B.J., 1989. Petrogenesis of boninitic lavas from the Limasol Forest Complex, Cyprus. In CRAWFORD, A.J., (ed.), *Boninites and Related Rocks*, London, (Unwin Hyman), 289-313.

ROSS, M. & HUEBNER, J.S., 1975. A pyroxene thermometer based on temperature-composition relationships of naturally occurring orthopyroxene, pigeonite, and augite (extended abstract). *International Conference on Geothermometry and Geobarometry, Penn. State Univ.*, Oct. 5-10, 1975.

RYERSON, F.J. & WATSON, E.B., 1987. Rutile saturation in magmas: implcations for Ti-Nb-Ta depletions in island arc basalts. *Earth and Planetary Science Letters*, **86**, 225-239.

SAXENA, S.K., 1976. Two-pyroxene geothermometer: A model with an approximate solution. *American Mineralogist*, **61**, 643-652.

SAXENA, S.K. & NEHRU, C.E., 1975. Enstatite-diopside solvus and geothermometry. *Contributions to Mineralogy and Petrology*, **49**, 259-267.

SCHLATER, J.G., HAWKINS, J.W., MAMMERICX, J. & CHASE, C.G., 1972. Crustal extension between the Tonga and Lau Ridges: Petrologic and Geophysical Evidence. *Bulletin of the Geological Society of America*, **83**, 505-518.

SHARASKIN, A.Y., PUSTCHIN, I.K., ZIOLIN, S.K. & KOLESOU, G.M., 1983. Two ophiolite sequences from the basement of the Northern Tonga Arc. *Ofioliti*, **8** No. 3, 411-430.

SHARASKIN, A.Y., KARPENKO, S.F., LJALIKOV, A.V., ZLOBIN, S.K., & BALASHOV, Y.A., 1983. Correlated $^{143}Nd/^{144}Nd$ and $^{87}Sr/^{86}Sr$ data on boninites from the Mariana and Tonga arcs. *Ofioliti*, **8** No. 3, 431-438.

SHAW, D.M., 1970. Trace element fractionation during anatexis. *Geochimica et Cosmochimica Acta*, **34**, 237-243.

SOBOLEV, A.V. & DANYUCHEVSKY, L.V., 1994. Petrology and geochemistry of boninites from the north termination of the Tonga trench: constrains on the generation conditions of primary high-Ca boninite primary magmas. *Journal of Petrology*, **35**, 1183-1211

STAUDIGEL, H., PARK, K.-H., PRINGLE, M., RUBENSTONE, J.L., SMITH, F & ZINDLER, A., 1991. The longevity of the South Pacific isotopic and thermal anomaly, *Earth and Planetary Science Letters*, **102**, 22-44.

STEIGER, R.H., JÄGER, E., 1977. Subcommission of geochronology: Convention on the use of decay constants in geo- and cosmochronology. *Earth and Planetary Science Letters*, **36**, 359-371.

STERN, R.J., MORRIS, J., BLOOMER, S.H. & HAWKINS, J.W., 1991. The source of the subduction component in convergent margin magmas: Trace element and radiogenic isotope evidence from Eocene boninites, Mariana forearc. *Geochimica et Cosmochimica Acta*, **55**, 1467-1481.

STERN, R.J., BLOOMER, S.H., LIN, P-N. & SMOOT, N.C., 1989. Submarine arc volcanism in the southern Mariana arc as an ophiolite analogue. *Tectonophysics,* **168**, 151-170.

SUN, S.-S, 1980. Lead isotopic study of young volcanic rocks from mid-ocean ridges, ocean islands and island arcs. *Philosophical Transactions of the Royal Society of London,* **A 297**, 409-445.

SUN, S-S. & MCDONOUGH, W.F., 1989. Chemical and isotopic systematics of ocean basalts: implications for mantle composition and processes. *In: Saunders, A.D. & Norry, M.J. (Eds.), Magmatism in the Ocean Basins, Geological Society of London Special Publication,* **42**, 313-345.

SUN, S-S., & NESBITT, R.W., 1978. Geochemical regularities and genetic significance of ophiolitic basalts. *Geology,* **6**, 689-93.

SUNKEL, G., 1990. Origin of petrological and geochemical variations of Lau Basin Lavas. *Marine Mining,* **9**, 205-234.

TATSUMI, Y., 1986. Formation of volcanic front in subduction zones. *Geophysical Research Letters,* **13**, 717-720.

TATSUMI, Y., 1989. Migration of fluid phases and genesis of basalt magmas in subduction zones. *Journal of Geophysical Research,* **94**, B4, 4697-4707.

TATSUMI, Y., HAMILTON, D.L., & NESBITT, R.W., 1986. Chemical characteristics of fluid phase released from a subducted lithosphere and origin of arc magmas: evidence from high-pressure experiments and natural rocks. *Journal of Volcanology and Geothermal Research,* **29**, 293-309.

TATSUMI, Y., MURASAKI, M., ARSADI, E.M. & NOHDA, S., 1991. Geochemistry of Quaternary lavas from NE Sulawesi: transfer of subduction components into the mantle wedge. *Contributions to Mineralogy and Petrology,* **107**, 137-149.

TATSUMI, Y., MURASAKI, M. & NOHDA, S., 1992. Across arc variation in the Izu-Bonin Arc: identification of subduction components. *Journal of Volcanology and Geothermal Research,* **49**, 179-190.

TAYLOR, R.N., NESBITT, R.W., VIDAL, P., HARMON, R.S., AUVRAY, B. & GOUDACE, I.W., 1994. Mineralogy, Chemistry and Genesis of the Boninites Series Volcanics, Chichijima, Bonini Islands, Japan. *Journal of Petrology*, **35**, Pt 3, 577-617.

TERA, F., BROWN, L., MORRIS, J., SACKS, I.S, KLEIN, J. & MIDDLETON, R., 1986. Sediment incorporation in island arc magmas: Inferences from Be-10, *Geochimica et Cosmochimica Acta*, **50**, 636-660.

THIRLWALL, M.F., SMITH, T.E., GRAHAM, A.M., THEODOROU, N., HOLLINGS, P., DAVIDSON, J.P., & ARCULUS, R.J., 1994. High field strength element anomalies in arc lavas: source or process? *Journal of Petrology*, **35**, Part 3, 819-838.

THOMPSON, G., 1973. A geochemical study of the low temperature interaction of seawater and oceanic igneous rock, EOS, *Transactions of the American Geophysical Union*, **54**, 1015.

TIFFIN, D.L., 1993. Tectonic and structural features of the Pacific / Indo-Australian plate boundary in the North-Lau Basin regions, southwest Pacific. *Geo-Marine Letters*, **13**, 126-131.

UYEDA, S. & KANAMORI, H., 1979. Back-arc opening and the mode of subduction. *Journal of Geophysical Research*, **84**, B3, 1049-1061.

VAN DER LAAN, S.R., FLOWER, M.F.J. & KOSTER VAN GROOS, A.F., 1989. Experimental evidence for the origin of boninites: near-liquidus phase relations to 7.5 kbar. In CRAWFORD, A.J., (ed.), *Boninites and Related Rocks*, London, (Unwin Hyman), 113-148.

VOLPE, A.M., MACDOUGALL, J.D. & HAWKINS, J.W., 1988. Lau Basin basalts (LBB): Trace element and Sr-Nd isotopic evidence for heterogeneity in back-arc basin mantle. *Earth and Planetary Science Letters*, **90**, 174-186.

VYSOTSKIY, S.V., ACLAND, A.S., PEARCE, J.A. AND ZHITKOV, A.S., 1996. Petrology and geochemistry of a supra-subduction zone ophiolite from the inner trench wall, North Tonga. Part 1. Plutonic and metamorphic rocks. *in press*.

WELLS, P.R.A., 1977. Pyroxene thermometry in simple and complex systems. *Contributions to Mineralogy and Petrology*, **62**, 129-139.

WHARTON, M.R., Unpubl. 1993. Crustal accretion during the earliest stages of intra-oceanic arc volcanism: examples from Fiji and Tonga, SW Pacific. PhD Thesis, Durham University, U.K.

WHELLER, G.E., VARNE, R., FODEN, J.D., & ABBOTT, M.J., 1987. Geochemistry of Quarternary volcanism in the Sunda-Banda Arc, Indonesia, and three-component genesis of island-arc basaltic magmas. *Journal of Volcanology and Geothermal Research*, **32**, 137-160.

WHITE, W.M., HOFMANN, A.W. & PUCHELT, H, 1987. Isotope Geochemistry of Pacific Mid-Ocean Ridge Basalts. *Journal of Geophysical Research*, **92 B6**, 4881-4893.

WILSON, M., 1989. Igneous Petrogenesis, Unwin Hyman, London.

WOOD., B. & BANNO., S., 1973. Garnet-orthopyroxene and orthopyroxene-clinopyroxene relationships in simple and complex systems. *Contributions to Mineralogy and Petrology*, **42**, 109-124.

WOODHEAD, J.D., 1989. Geochemistry of the Mariana arc (western Pacific): Source composition and processes. *Chemical Geology*, **76**, 1-24.

WOODHEAD, J.D. & JOHNSON, R.W., 1993. Isotopic and trace element profiles across the New Britain island arc, Papua New Guinea. *Contributions to Mineralogy and Petrology*, **113**, 479-491.

WOODHEAD, J., EGGINS, S. & GAMBLE, J., 1993. High field strength and transition element systematics in island arc and back-arc basin basalts: evidence for multi-phase melt extraction and a depleted mantle wedge. *Earth and Planetary Science Letters*, **114**, 491-504.

WRIGHT, E. & WHITE, W.M., 1986/87. The origin of Samoa: new evidence from Sr, Nd and Pb isotopes. *Earth and Planetary Science Letters*, **81**, 151-162.

ZINDLER, A. & HART, S., 1986. Chemical geodynamics. *Annual Review of Earth and Planetary Sciences*, **14**, 493-571.

APPENDIX 1

Analytical geochemistry

A1.1 Powdered sample preparation

Bulk rock samples of 0.5-1kg were washed and cleaned using a wire brush to remove any soil or loose material from the samples. Any surficial alteration was removed from the sample using a stainless steel splitting edge linked to a hydraulic press until the sample was reduced to $3cm^2$. It was washed again and dried with a paper towel. The sample was crushed using a Fritsch Pulverisette jaw crusher (type 01-704). The crusher was thoroughly cleaned prior to crushing to avoid contamination from other users' rock powder and also between crushing of different samples. Crushing reduced the sample to a grit of approximately 5mm grain size. Grinding was performed in an agate grinding mill which was run for about 30 minutes to produce a fine powder which was bagged, labelled and stored in dry conditions.

A1.2 XRF analysis

Fusion discs for major element oxide analysis were prepared by mixing a 1:5 mixture of sample and dried lithium tetraborate flux (Spectroflux 100B). The mixture was extensively mixed on a piece of weighing paper with a glass rod before being heated, in platinum crucibles, to 1050°C for 20 minutes. The molten glass was then poured into moulds on a hot-plate set to 250°C before being quenched using a stainless steel plunger. The discs were allowed to cool and bagged and stored in a desiccator prior to analysis.

Pressed powder pellets for trace element analysis were prepared by measuring out about 6g of dry, powdered sample and adding between 6 and 12 drops of Mowiol binding agent. The powder and binding agent were mixed before being compressed for 20 seconds at 10-15 bars. The pellets were then dried in an oven at 100°C prior to analysis.

XRF analysis was carried out on a Philips PW 1500 spectrometer with a Rhodium anode at Durham University. A full range of international standards from

across the compositional range were run as calibration standards. An internal monitor was run over the full study period to monitor between run variations and machine drift. Estimates of analytical accuracy and precision were made by repeated analysis of international reference standards and also internal standards (Table A1.1). Details of the errors are summarised in a 2 sigma form and the recommended values for standards from *Govindaraju (1989)* are shown. Figure A1.1 illustrates comparison plots for the Tafahi and Niuatoputapu XRF and ICP-MS data obtained. Correlation coefficients for these data range from 0.97 to 1.00, indicating the good reproducibility of the two techniques.

Loss-on-ignition values were determined by heating a 2g of powder of the sample in a porcelain crucible at 200°C for 30 minutes to evaporate surficial water (H_2O^-) and then at 900°C for two hours to remove water caught up within the structure of the rock (H_2O^+).

A1.3 ICP-MS analysis

A sub-set of trace elements was analysed by inductively-coupled-plasma-mass spectrometry on a FI Elemental PG2 STE instrument at Silwood Park, Imperial College, Ascot. A powder aliquot of 0.1±0.001g was weighed out and digested with 4ml of Aristar hydrofluoric acid and 1ml of Aristar nitric acid in a savillex beaker for 24 hours. The samples were evaporated to moist residue to remove the hydrofluoric acid and form nitrate salts. To complete this conversion the sample was dissolved in another 1ml of Aristar nitric acid and then the solution was evaporated until a moist residue remained. This last step was repeated. All traces of hydrofluoric acid should be eliminated from the beaker. The samples were then redissolved in 2.5ml of Aristar nitric acid and 10-15ml of deionised water, and the mixture was allowed to boil for 30 minutes. The solutions were left to cool, and then spiked with 1.25ml of 1ppm Rh, Re and Bi solution and made up accurately to 50ml with deionised water. Detection limits for all elements are typically 0.001-0.005 ppm (at 3 sd of background), except for Ce, Gd, Hf (0.01 ppm), Pb (0.09 ppm), Sr (0.86 ppm) and Zr (0.28 ppm). Precision typically ranges from 15% at less than 10 x detection limit (*Murton et al., 1992*), to between 0.5 and 3% at 100 x detection limit.

International standards run as unknowns outside the calibration

	W-2			BIR-1			QLO-1		
	rec	n=3 av	2 s.d.	rec	n=3 av	2 s.d.	rec	n=3 av	2 s.d
SiO2	52.44	52.25	0.27	47.77	47.83	0.08	65.55	65.07	0.67
TiO2	1.06	1.04	0.03	0.96	0.94	0.03	0.62	0.61	0.02
Al2O3	15.35	15.11	0.34	15.35	15.34	0.01	16.18	16.59	0.58
FeO*	9.68	9.69	0.02	10.25	10.00	0.36	3.89	3.94	0.08
MnO	0.16	0.16	0.00	0.17	0.17	0.01	0.09	0.08	0.02
MgO	6.37	6.57	0.28	9.68	9.34	0.48	1.00	0.77	0.33
CaO	10.87	10.85	0.03	13.24	13.16	0.11	3.17	3.16	0.01
Na2O	2.14	2.20	0.09	1.75	1.87	0.17	4.20	4.11	0.12
K2O	0.63	0.62	0.01	0.03	0.04	0.02	3.60	3.56	0.06
P2O5	0.13	0.15	0.03	0.05	0.04	0.01	0.25	0.20	0.07
Rb	20	21.90	2.69	1	0.45	0.78			
Sr	194	192.80	1.70	108	109.25	1.77			
Ba	182	183.30	1.84	7.7	4.55	4.45			
Y	24	23.03	1.37	16	17.60	2.26			
Zr	94	95.93	2.73	22	19.30	3.82			
Nb	8	8.10	0.28	2	2.20	0.28			
Cr	93	92.93	0.09	382	385.40	4.81			
Ni	70	70.17	0.24	166	164.90	1.56			
V	262	265.47	4.90	313	319.05	8.56			
Zn	77	78.13	1.60	71	70.65	0.49			
Cu	103	105.50	3.54	126	125.25	1.06			
Ga	20	19.57	0.61	16	19.45	4.88			
Sc	35	33.17	2.59	44	38.90	7.21			
Co	44	45.00	1.41	51.4	54.70	4.67			

	DNC-1			QUBS3			BOB1		
	rec	n=3 av	2 s.d.	rec	n=3 av	2 s.d.	rec	n=4 av	2 s.d.
Rb	4.5	5.35	1.20	5	5.07	0.10	5	6.43	2.02
Sr	145	148.50	4.95	430	423.40	9.33	200	202.48	11.99
Ba	114	100.05	19.73	140	142.63	3.72	44	40.83	4.48
Y	18	17.40	0.85	23	22.60	0.57	25	26.80	2.55
Zr	41	44.35	4.74	160	163.30	4.67	101	106.60	7.92
Nb	3	3.00	0.00	4	6.67	3.78	4	8.28	6.05
Cr	285	287.30	3.25	511	507.33	5.19	280	274.85	7.28
Ni	247	243.95	4.31	300	272.73	38.57	113	112.25	1.06
V	148	156.05	11.38	302	292.17	13.90	240	243.78	5.34
Zn	66	66.85	1.20	86	88.77	3.92	n.a.	62.08	5.92
Cu	96	90.90	7.21	106	102.10	5.52	n.a.	59.55	5.78
Ga	15	13.55	2.05	20	19.70	0.42	17	17.70	0.99
Sc	31	32.35	1.91	29	29.73	1.03	32	32.38	0.53
Co	54.7	55.50	1.13	72	65.20	9.62	n.a.	53.35	8.54

Table A1.1: International standards run as unknowns outside the XRF machine calibration. Recommended values (rec) are taken from Govindaraju (1989), Potts et al., (1992) and the compilation of J.A.Pearce (BOB-1, pers. comm., 1996).

Figure A1.1 : *Plots to illustrate the comparison between data obtained using the XRF and ICP-MS analytical techniques at Durham. Where the concentration of an element in a sample is close to the detection limit of the XRF machine (e.g. for Rb), then there is a greater scatter in the data.*

A1.4 Electron microprobe analysis

Polished thin-sections prepared by G. Randall at the University of Durham were stored in a desiccator and were carbon-coated at the University of Manchester. Analyses were performed at the University of Manchester on a Cambridge Instruments Geoscan Microprobe fitted with Energy Dispersive Spectrometers (EDS). EDS provides a rapid way of carrying out multi-element oxide analysis. The machine was operated at a beam current of 5nA with an accelerating voltage of 15kV. Each analysis took 100 seconds to process using a Link-290 electronic facility. Spectra of standards are held on hard-disc on the on-line computer. These are compared with the unknown spectra using a cobalt metal standard for the calibration of the unknown metal concentrations. The cobalt standard corrects for any drift in the data, acting as a monitoring sample.

A1.5 Radiogenic isotope analysis

Isotope work was carried out in collaboration with Dr. P. Kempton at the NERC Isotope Geosciences Laboratory, British Geological Survey, Keyworth, Nottingham. Pb, Sr and Nd were extracted on the same dissolution from 200 ± 20mg of rock powder. The samples were leached for 30 minutes using 6N hydrochloric acid in order to remove any alteration effects (Section 5.2). The leachate was removed, evaporated to dryness and prepared for analysis by being converted to nitrate and chloride. The residues were dissolved using approximately 1ml of nitric acid and 3-5ml of hydrofluoric acid. After dissolution, the solution was evaporated to dryness. It was then converted to nitrate by the addition of 1ml of nitric acid, followed by evaporation to dryness. The residue was converted to chloride using hydrochloric acid. 1ml of 1M hydrobromic acid was then added to the final residue. Pb was separated by passing the sample through columns prepared from disposable PVC pipette tips which contained a 2mm diameter polyethylene frit with 5 drops of Dowex 1 x 8, 200-400 mesh resin. A new column was prepared for each sample to minimise the Pb blank.

Sr and Nd were fractions were collected in 2ml of 1M HBr and Pb collected in 1ml of 6N HCl. Sr and Nd were purified using one and two-column cation techniques set up at NIGL. Sr and Pb were run as the metal species on single Ta and single Re filaments, respectively using a Finnegan MAT 262 multicollector mass spectrometer at NIGL. Nd was run as the metal species on triple Re-Ta filament assemblies on a VG354 multicollector mass spectrometer, also at NIGL.

Blanks for Sr, Nd and Pb were less than 500pg, 323pg and 286pg respectively. Reference standards throughout the course of analysis averaged values of $^{87}Sr/^{86}Sr = 0.71021\pm0.00003$ for the NBS987 standard, $^{143}Nd/^{144}Nd = 0.51111\pm0.00003$ for the Johnson Matthey Nd standard. $^{87}Sr/^{86}Sr$ was normalised to $^{86}Sr/^{88}Sr = 0.1194$ and $^{143}Nd/^{144}Nd$ was normalised to a value of $^{146}Nd/^{144}Nd = 0.7219$. Based on repeated runs of NBS981 common Pb standard, the reproducibility is better than 0.1% and the Pb isotopic ratios were corrected relative to the average standard Pb isotopic compositions of *Todt et al. (1984)*. Pb mass fractionation was 0.1% per a.m.u.

APPENDIX 2

Geochemical dataset

This appendix contains the geochemical data collected during the period of this study. The sample localities are found on Figures 2.1, 2.3 and 2.4. The trace element data for the samples analysed by ICP-MS (marked by *) have been normalised to chondrite values from *Boynton (1984)*, and MORB-normalising values from *Sun & McDonough (1989)*.

The abbreviations in the following tables are:

western:	western ophiolite section of the 'Kallisto' 1982 cruise
eastern:	eastern ophiolite section
NTB:	north Tongan boninitic lava
NTB (gabb):	north Tongan boninitic gabbro
otb:	oceanic tholeiitic gabbro
NTTh:	north Tongan island-arc tholeiite
diabase:	diabase dykes
cum:	cumulate gabbro
oib:	ocean island basalts from a seamount associated with the Samoan plume
Taf:	high-Mg basaltic andesitic lavas from Tafahi
Nuia:	andesitic massive *lavas, flows* or agglomeratic *clasts* from Niuatoputapu

n.a. element not analysed by this technique

	TAF1	TAF2	TAF3/1	*TAF3/2	TAF3/3	TAF3/4	TAF4	TAF5/1	TAF5/2	TAF6	TAF7
	Tafahi	Tafahi	Tafahi	Tafahi	Tafahi	Tafahi	Tafahi	Tafahi	Tafahi	Tafahi	Tafahi
	lava	lava	lava	lava	lava	lava	lava	lava	lava	lava	lava
SiO_2	54.33	55.59	53.32	53.29	53.71	53.61	54.24	55.34	55.06	54.95	53.81
TiO_2	0.40	0.41	0.39	0.38	0.38	0.37	0.38	0.40	0.39	0.35	0.37
Al_2O_3	15.30	15.39	16.23	15.83	16.14	16.03	15.90	15.55	15.60	16.27	15.90
Fe_2O_3	11.00	10.67	11.51	11.23	11.20	11.24	11.19	10.82	10.83	10.95	11.25
MnO	0.17	0.17	0.19	0.18	0.18	0.18	0.18	0.17	0.17	0.18	0.17
MgO	5.89	5.12	6.84	6.61	6.61	6.94	6.19	5.54	5.50	6.14	6.60
CaO	12.52	12.14	11.80	12.00	11.85	12.15	11.93	12.08	11.98	11.56	11.80
Na_2O	1.29	1.39	1.17	1.24	1.19	1.16	1.26	1.33	1.36	1.17	1.21
K_2O	0.12	0.17	0.14	0.14	0.12	0.13	0.12	0.18	0.16	0.10	0.15
P_2O_5	0.07	0.06	0.06	0.06	0.08	0.08	0.06	0.06	0.06	0.06	0.10
H_2O-	0.37	0.35	0.50	0.33	0.50	0.32	0.18	0.21	0.23	0.34	0.41
LOI	0.03	-0.06	0.38	0.23	0.41	0.41	0.13	-0.53	0.04	0.08	0.35
Total	101.10	101.10	101.65	100.95	101.47	101.90	101.44	101.48	101.11	101.72	101.36
Sc	43.80	44.60	49.20	49.13	47.40	47.80	49.70	47.30	47.70	49.40	48.20
Ti (ICP)				0.34							
V	324.20	320.30	311.40	305.19	302.90	312.40	302.80	311.40	316.40	310.40	304.30
Cr	47.10	31.80	81.20	86.18	77.00	97.70	59.00	52.20	58.60	96.60	101.80
Mn (ICP)				0.20							
Co	45.00	40.00	47.00	45.38	49.00	50.00	45.00	46.00	46.00	48.00	50.00
Ni	31.00	24.00	41.00	43.04	36.00	40.00	34.00	32.00	32.00	38.00	41.00
Cu	137.00	143.00	127.00	131.40	142.00	150.00	164.00	165.00	171.00	158.00	137.00
Ga	18.00	16.00	21.00	13.36	16.00	13.00	16.00	16.00	18.00	15.00	14.00
Rb	2.60	0.50	2.20	2.17	2.30	2.60	1.20	3.50	3.70	1.30	2.60
Sr	144.00	150.00	130.00	141.62	130.00	127.00	146.00	148.00	148.00	137.00	130.00
Y	8.70	9.70	9.00	8.53	8.10	7.30	8.30	8.70	8.20	8.10	8.00
Zr	13.40	13.00	11.60	13.03	11.40	11.40	12.60	13.40	12.60	12.90	11.00
Nb	0.40	0.60	0.30	0.60	0.70	0.70	0.80	0.60	0.50	1.10	0.20
Cs				0.09							
Ba	47.00	68.30	50.70	43.32	48.30	53.60	71.80	75.80	68.80	50.00	51.30
La	0.29	0.29	1.27	1.30	1.59	1.32	1.53	1.50	0.65	1.32	1.46
Ce	2.18	3.03	3.18	2.57	4.57	3.52	3.96	3.56	2.67	3.54	5.35
Pr				0.39							
Nd	1.31	1.93	1.70	1.97	2.51	2.21	1.62	2.27	0.62	0.27	4.48
Sm				0.70							
Eu				0.31							
Gd				1.00							
Tb				0.19							
Dy				1.35							
Ho				0.29							
Er				0.93							
Tm				0.14							
Yb				0.88							
Lu				0.13							
Hf				0.44							
Ta				0.02							
Pb				1.58							
Th				0.16							
U				0.08							
Chondrite normalised											
La				3.93							
Ce				3.18							
Pr				3.21							
Nd				3.29							
Sm				3.59							
Eu				4.19							
Gd				3.86							
Tb				3.92							
Dy				4.19							
Ho				4.04							
Er				4.42							
Tm				4.17							
Yb				4.23							
Lu				4.17							

	*TAF8	TAF9	TAF10	TAF11	TAF12	TAF13	TAF14/1	TAF14/2	TAF14/4	TAF16	TAF17
	Tafahi	Tafahi	Tafahi	Tafahi	Tafahi	Tafahi	Tafahi	Tafahi	Tafahi	Tafahi	Tafahi
	lava	lava	lava	lava	lava	lava	lava	lava	lava	lava	lava
SiO_2	53.81	53.78	53.16	54.48	53.02	53.00	52.53	54.03	52.78	55.75	52.70
TiO_2	0.37	0.40	0.41	0.39	0.43	0.40	0.41	0.41	0.40	0.40	0.40
Al_2O_3	15.76	15.72	15.32	15.68	15.41	15.29	15.99	15.50	15.81	15.66	15.79
Fe_2O_3	10.98	11.38	11.31	11.11	11.30	11.13	11.32	10.85	10.77	10.62	11.08
MnO	0.18	0.18	0.18	0.18	0.25	0.25	0.22	0.20	0.20	0.18	0.21
MgO	6.67	5.87	5.68	5.94	7.03	7.28	7.83	6.37	7.05	5.35	7.17
CaO	12.23	11.88	12.23	11.90	12.82	13.10	11.99	12.17	12.30	11.94	12.24
Na_2O	1.23	1.31	1.32	1.31	1.44	1.29	1.08	1.24	1.28	1.46	1.28
K_2O	0.14	0.11	0.13	0.17	0.15	0.14	0.15	0.18	0.14	0.21	0.15
P_2O_5	0.06	0.06	0.08	0.07	0.07	0.07	0.06	0.07	0.07	0.06	0.07
H_2O-	0.26	0.70	0.59	0.23	0.25	0.22	0.22	0.18	0.23	0.28	0.35
LOI	0.06	0.32	0.47	0.01	0.08	0.07	0.25	-0.06	0.10	-0.08	-0.08
Total	101.44	100.68	99.81	101.24	101.94	101.95	101.58	101.04	100.80	101.64	101.09
Sc	48.72	45.90	45.40	46.30	45.90	48.70	53.20	46.40	47.70	44.70	51.20
Ti (ICP)	0.34										
V	299.28	314.60	317.80	322.10	314.30	301.00	314.10	309.60	295.20	311.00	321.20
Cr	95.12	54.60	39.80	76.20	61.80	70.50	115.90	64.70	72.20	57.90	101.00
Mn (ICP)	0.19										
Co	44.33	49.00	48.00	49.00	40.30	40.00	45.30	38.30	42.40	34.40	44.00
Ni	35.09	35.00	33.00	38.00	40.20	42.00	47.50	40.10	42.70	37.10	46.80
Cu	120.33	162.00	165.00	151.00	164.70	132.70	161.60	201.70	182.90	128.70	208.40
Ga	12.60	14.00	17.00	14.00	7.80	8.80	17.20	16.40	9.30	11.20	9.70
Rb	1.96	1.80	2.30	4.10	1.70	2.10	3.40	3.40	2.70	4.40	2.00
Sr	143.34	141.00	143.00	142.00	143.60	143.40	128.30	142.10	141.60	148.90	130.30
Y	8.58	8.90	8.60	8.40	8.50	6.50	7.20	7.30	7.60	7.60	7.20
Zr	12.09	12.90	12.40	14.10	16.40	15.50	17.40	17.90	17.30	18.00	15.90
Nb	0.69	0.80	0.20	1.20	1.00	0.70	1.70	1.30	2.30	1.30	1.10
Cs	0.04										
Ba	41.79	56.00	48.30	59.00	39.30	53.50	42.10	41.60	41.80	55.20	44.80
La	1.25	1.95	1.22	0.87	0.03	1.68		0.74		1.33	0.47
Ce	2.75	4.18	4.47	3.80	1.61	4.63	0.83	2.44	0.06	2.59	1.20
Pr	0.40										
Nd	2.08	0.30	2.79	1.95	0.84	3.22	0.44				
Sm	0.76										
Eu	0.29										
Gd	0.93										
Tb	0.19										
Dy	1.34										
Ho	0.31										
Er	0.89										
Tm	0.15										
Yb	0.95										
Lu	0.15										
Hf	0.46										
Ta	0.02										
Pb	1.17										
Th	0.22										
U	0.09										
Chondrite normalised											
La	3.77										
Ce	3.41										
Pr	3.29										
Nd	3.47										
Sm	3.90										
Eu	3.89										
Gd	3.59										
Tb	3.96										
Dy	4.16										
Ho	4.28										
Er	4.26										
Tm	4.57										
Yb	4.52										
Lu	4.53										

	TAF18/1 Tafahi lava	TAF18/2 Tafahi lava	TAF18/4 Tafahi lava	TAF18/5 Tafahi lava	TAF18/7 Tafahi lava	TAF18/8 Tafahi lava	TAF18/9 Tafahi lava	*TAF18/10 Tafahi lava	TAF18/11 Tafahi lava	*TAF18/12 Tafahi lava	TAF18/13 Tafahi lava
SiO_2	54.10	53.70	52.30	51.79	51.10	52.45	53.26	52.12	51.81	53.57	53.09
TiO_2	0.41	0.39	0.41	0.42	0.43	0.41	0.41	0.43	0.42	0.42	0.43
Al_2O_3	15.43	15.31	15.58	15.54	15.15	15.02	14.92	15.44	15.60	15.09	15.30
Fe_2O_3	11.05	10.56	11.61	11.84	12.21	11.43	11.12	12.09	12.07	11.48	11.68
MnO	0.18	0.25	0.29	0.29	0.29	0.26	0.25	0.26	0.26	0.24	0.24
MgO	5.62	5.86	7.44	7.48	7.72	7.05	6.43	7.23	7.52	6.14	6.94
CaO	12.13	12.48	12.63	12.84	13.18	13.34	13.11	12.85	12.77	12.74	12.66
Na_2O	1.61	1.69	1.41	1.35	1.41	1.32	1.42	1.27	1.26	1.38	1.30
K_2O	0.18	0.21	0.20	0.18	0.18	0.18	0.21	0.15	0.14	0.21	0.16
P_2O_5	0.07	0.10	0.07	0.08	0.07	0.08	0.08	0.07	0.08	0.09	0.07
H_2O-	0.42	0.29	0.31	0.32	0.30	0.35	0.36	0.34	0.41	0.50	0.26
LOI	-0.02	-0.11	-0.16	0.10	-0.16	-0.08	-0.04	-0.19	-0.04	0.09	-0.15
Total	100.80	100.53	101.94	101.83	101.73	101.55	101.22	101.91	101.83	101.35	101.88
Sc	48.30	33.50	56.00	50.90	54.80	48.40	45.90	54.64	52.60	47.72	52.50
Ti (ICP)								0.35		0.34	
V	341.80	317.80	346.70	341.20	330.50	326.20	321.50	368.39	372.00	364.66	347.10
Cr	56.10	58.50	126.30	123.40	121.70	60.80	60.60	116.77	121.00	51.88	103.10
Mn (ICP)								0.20		0.18	
Co	47.00	40.00	45.00	49.00	50.00	47.00	46.00	46.90	52.00	42.28	49.00
Ni	34.00	34.00	36.00	42.00	40.00	32.00	31.00	43.34	46.00	29.38	39.00
Cu	130.00	117.00	124.00	146.00	158.00	167.00	174.00	192.34	139.00	167.30	168.00
Ga	18.00	14.00	17.00	14.00	14.00	16.00	14.00	13.60	14.00	13.73	14.00
Rb	2.80	2.80	2.30	2.40	2.50	2.60	3.10	1.68	2.40	2.38	3.30
Sr	152.00	151.00	119.00	120.00	120.00	147.00	143.00	132.29	118.00	158.40	123.00
Y	9.30	8.10	8.20	9.80	11.00	9.30	8.60	8.69	9.60	8.56	9.90
Zr	12.00	12.20	11.40	11.50	11.70	12.20	12.50	11.98	12.90	12.74	12.60
Nb	0.60	0.50	0.70	0.00	0.20	0.50	0.00	0.41	0.00	0.73	0.30
Cs								0.06		0.07	
Ba	66.20	64.20	53.50	54.00	51.70	67.10	63.60	39.45	49.30	55.65	51.80
La	2.59	1.73	1.01	1.03	1.79	1.17	2.21	0.71	0.81	1.44	1.06
Ce	5.56	5.28	3.29	2.88	3.75	2.86	5.20	2.09	2.50	2.93	1.51
Pr								0.34		0.43	
Nd	3.11	3.75	1.77	0.79	1.35	0.20	2.41	1.89	1.14	2.10	
Sm								0.71		0.73	
Eu								0.27		0.30	
Gd								0.91		0.97	
Tb								0.18		0.19	
Dy								1.32		1.33	
Ho								0.29		0.29	
Er								0.96		0.86	
Tm								0.15		0.15	
Yb								0.90		0.88	
Lu								0.16		0.13	
Hf								0.42		0.74	
Ta								0.02		0.02	
Pb								1.47		1.76	
Th								0.10		0.23	
U								0.05		0.08	
Chondrite normalised											
La								2.15		4.36	
Ce								2.59		3.62	
Pr								2.80		3.49	
Nd								3.16		3.50	
Sm								3.63		3.75	
Eu								3.73		4.14	
Gd								3.52		3.73	
Tb								3.78		4.01	
Dy								4.09		4.13	
Ho								4.06		4.10	
Er								4.58		4.08	
Tm								4.66		4.63	
Yb								4.32		4.19	
Lu								4.83		4.07	

	TAF18/14	TAF18/15	TAF20	TAF21	TAF22	*TAF23	TAF26	TAF27	TAF29/1	TAF29/2	TAF29/3
	Tafahi	Tafahi	Tafahi	Tafahi	Tafahi	Tafahi	Tafahi	Tafahi	Tafahi	Tafahi	Tafahi
	lava	lava	lava	lava	lava	lava	lava	lava	lava	lava	lava
SiO_2	52.50	55.21	54.60	54.33	53.72	53.35	53.44	53.56	52.84	51.75	51.85
TiO_2	0.37	0.47	0.40	0.42	0.40	0.44	0.42	0.38	0.42	0.43	0.43
Al_2O_3	15.67	15.09	15.59	15.43	15.73	15.60	15.78	15.73	15.67	15.68	15.66
Fe_2O_3	11.21	10.78	10.62	10.77	10.76	11.35	11.28	11.11	10.39	11.70	11.69
MnO	0.21	0.21	0.23	0.19	0.19	0.20	0.28	0.20	0.24	0.25	0.25
MgO	7.38	5.14	6.30	6.10	6.65	6.37	5.99	6.34	6.58	7.09	7.08
CaO	12.74	12.41	12.20	12.08	12.05	12.13	11.81	11.90	12.23	12.44	12.37
Na_2O	1.20	1.66	1.34	1.24	1.24	1.41	1.61	1.31	1.39	1.31	1.24
K_2O	0.22	0.23	0.27	0.21	0.20	0.11	0.12	0.21	0.15	0.13	0.16
P_2O_5	0.06	0.08	0.07	0.07	0.07	0.07	0.15	0.14	0.09	0.12	0.13
H_2O-	0.31	0.22	0.19	0.25	0.25	0.98	0.81	0.42	0.38	0.62	0.51
LOI	0.18	-0.25	-0.20	-0.19	-0.15	0.47	0.33	0.28	-0.08	0.33	0.33
Total	101.56	101.28	101.60	100.84	101.00	100.96	100.88	100.89	100.99	100.91	100.87
Sc	48.70	41.80	48.30	50.70	45.60	50.72	51.90	48.30	50.10	50.60	52.00
Ti (ICP)						0.35					
V	311.80	378.80	308.10	309.90	304.10	304.83	302.60	299.10	306.90	311.90	309.90
Cr	78.90	48.40	59.80	69.90	72.90	56.95	74.10	74.30	77.30	74.50	77.70
Mn (ICP)						0.19					
Co	48.00	40.00	39.20	39.90	42.10	41.63	42.20	43.40	46.30	46.20	46.80
Ni	41.00	26.00	39.80	42.20	44.00	33.68	41.90	43.50	44.30	46.40	46.60
Cu	153.00	85.00	160.70	79.30	152.10	143.25	153.00	153.40	158.60	146.20	148.00
Ga	16.00	18.00	10.30	14.50	10.10	14.78	12.40	13.90	10.60	15.50	10.90
Rb	5.10	3.70	4.30	2.90	4.40	0.86	1.70	5.10	3.50	4.30	2.50
Sr	138.00	150.00	149.40	150.20	147.30	178.39	144.40	142.50	148.70	154.30	143.60
Y	9.20	10.20	7.70	7.80	7.30	8.17	7.90	8.70	8.60	7.60	8.00
Zr	12.40	16.20	16.70	18.20	16.90	11.79	17.80	17.70	17.60	17.70	17.40
Nb	0.50	0.80	0.60	1.20	1.90	0.48	1.40	0.90	1.30	1.40	0.90
Cs						0.03					
Ba	67.80	66.20	61.80	58.70	52.50	82.30	63.70	56.50	53.40	44.50	56.80
La	0.59	0.04	2.13	2.48	0.25	0.89	1.63	2.04	1.04	2.74	0.78
Ce	2.76	1.15	4.84	4.67	0.55	2.35	4.01	4.94	2.95	6.14	3.27
Pr						0.36					
Nd	1.87		2.14	1.14		1.99	1.27	2.01	0.66	1.95	0.96
Sm						0.60					
Eu						0.29					
Gd						0.90					
Tb						0.18					
Dy						1.24					
Ho						0.28					
Er						0.88					
Tm						0.15					
Yb						0.87					
Lu						0.13					
Hf						0.43					
Ta						0.02					
Pb						1.49					
Th						0.14					
U						0.05					
Chondrite normalised											
La						2.69					
Ce						2.91					
Pr						2.93					
Nd						3.32					
Sm						3.09					
Eu						3.98					
Gd						3.47					
Tb						3.84					
Dy						3.85					
Ho						3.92					
Er						4.20					
Tm						4.61					
Yb						4.18					
Lu						4.12					

	TAF30 Tafahi lava	TAF31/1 Tafahi lava	TAF31/4 Tafahi lava	TAF31/5 Tafahi lava	TAF31/6 Tafahi lava	TAF32/1 Tafahi lava	TAF32/2 Tafahi lava	TAF32/3 Tafahi lava	TAF33 Tafahi lava	TAF34 Tafahi lava	TAF35/1 Tafahi lava
SiO_2	52.39	54.31	51.74	52.24	52.78	50.03	53.38	50.93	53.87	52.54	55.89
TiO_2	0.43	0.47	0.40	0.42	0.43	0.44	0.43	0.45	0.43	0.42	0.36
Al_2O_3	14.98	15.67	15.13	15.14	14.59	14.48	15.06	14.98	15.01	15.20	15.45
Fe_2O_3	11.25	11.12	11.20	11.04	11.15	10.96	10.92	11.03	11.03	11.11	9.73
MnO	0.23	0.22	0.23	0.22	0.22	0.22	0.21	0.20	0.20	0.21	0.19
MgO	6.16	5.32	6.97	7.05	7.07	9.22	6.10	7.91	5.73	6.68	5.39
CaO	12.39	11.47	12.54	13.05	13.39	14.69	12.64	13.59	12.46	12.82	11.92
Na_2O	1.41	1.74	1.56	1.42	1.42	1.37	1.52	1.49	1.45	1.53	1.60
K_2O	0.21	0.25	0.18	0.13	0.17	0.13	0.16	0.14	0.24	0.17	0.23
P_2O_5	0.16	0.09	0.06	0.07	0.07	0.08	0.08	0.07	0.08	0.07	0.08
H_2O-	0.58	0.43	0.24	0.16	0.73	0.47	0.26	0.46	0.20	0.37	0.12
LOI	0.46	-0.09	-0.08	-0.10	-0.04	1.41	-0.17	0.70	-0.19	-0.08	0.00
Total	99.62	100.66	100.00	100.79	101.28	101.61	100.49	100.79	100.50	100.73	100.84
Sc	48.40	44.70	48.80	48.10	46.70	44.30	43.60	45.50	48.20	48.80	39.30
Ti (ICP)											
V	305.20	321.70	308.10	327.60	308.90	315.00	320.70	318.00	323.80	321.90	266.60
Cr	51.00	47.90	76.90	58.90	75.60	58.10	61.30	55.40	52.00	39.00	56.60
Mn (ICP)											
Co	44.00	42.20	43.50	44.50	44.70	42.70	41.60	45.60	43.70	44.30	39.30
Ni	41.20	39.90	44.60	44.20	45.40	42.90	40.90	45.90	39.70	42.40	39.70
Cu	170.10	181.60	120.80	182.30	157.70	160.00	162.60	159.60	171.50	165.70	114.40
Ga	14.10	18.20	16.10	13.20	12.60	16.30	29.10	15.60	28.00	18.30	15.50
Rb	3.10	5.30	3.40	1.20	5.00	2.80	2.60	1.90	5.60	3.50	4.10
Sr	149.50	162.20	136.20	156.80	165.30	168.90	151.30	208.70	153.50	152.50	139.90
Y	8.60	10.00	7.10	8.00	7.80	8.80	7.30	8.30	7.30	7.30	7.00
Zr	17.40	20.10	16.50	17.20	16.60	17.70	16.60	16.10	17.50	16.60	16.10
Nb	1.50	1.60	1.40	0.80	1.30	1.30	1.30	1.40	1.30	1.10	1.00
Cs											
Ba	42.50	71.50	40.00	51.40	46.20	45.70	44.10	36.90	59.50	37.60	51.70
La	2.55	2.01	0.77	0.56	0.53	1.55	1.36	0.88	0.75	2.15	2.10
Ce	6.55	5.68	2.96	2.80	1.42	4.19	4.25	2.55	2.69	5.76	4.76
Pr											
Nd	3.96	2.72	1.69	1.54		1.11	3.00		1.22	3.39	2.90
Sm											
Eu											
Gd											
Tb											
Dy											
Ho											
Er											
Tm											
Yb											
Lu											
Hf											
Ta											
Pb											
Th											
U											

Chondrite normalised
La
Ce
Pr
Nd
Sm
Eu
Gd
Tb
Dy
Ho
Er
Tm
Yb
Lu

	TAF35/2 Tafahi lava	TAF35/3 Tafahi lava	TAF35/4 Tafahi lava	TAF35/5 Tafahi lava	TAF35/6 Tafahi lava	TAF37 Tafahi lava	TAF38/2 Tafahi lava	TAF39 Tafahi lava	*TAF40 Tafahi lava	TAF41/1 Tafahi lava	TAF41/2 Tafahi lava
SiO₂	54.59	56.64	55.02	55.94	56.12	56.18	54.01	56.45	52.99	52.31	51.08
TiO₂	0.39	0.36	0.37	0.37	0.36	0.43	0.47	0.50	0.46	0.44	0.44
Al₂O₃	15.53	15.60	15.73	15.77	15.64	15.26	15.76	15.44	15.57	15.58	15.49
Fe₂O₃	10.37	9.99	10.12	10.08	9.97	10.84	11.57	11.45	11.83	11.85	11.92
MnO	0.20	0.19	0.17	0.20	0.19	0.19	0.19	0.20	0.24	0.23	0.23
MgO	6.08	5.38	6.11	5.36	5.21	5.34	6.13	4.33	6.67	6.97	7.59
CaO	12.32	11.69	11.94	11.92	11.98	11.82	11.53	11.22	12.44	12.67	12.83
Na₂O	1.30	1.55	1.27	1.46	1.49	1.53	1.33	1.69	1.39	1.39	1.50
K₂O	0.22	0.25	0.20	0.22	0.23	0.22	0.19	0.21	0.19	0.16	0.14
P₂O₅	0.08	0.09	0.06	0.13	0.22	0.07	0.06	0.07	0.07	0.06	0.05
H₂O-	0.16	0.16	0.21	0.29	0.28	0.50	0.27	0.23	0.23	0.27	0.41
LOI	-0.07	-0.10	-0.07	0.22	0.26	-0.04	-0.26	-0.24	-0.01	-0.05	0.13
Total	101.08	101.74	101.00	101.44	101.41	101.88	101.25	101.57	101.85	101.66	101.27
Sc	44.20	45.10	44.20	39.10	41.40	45.20	52.70	47.60	48.60	42.00	48.80
Ti (ICP)									0.46		
V	296.10	273.00	281.50	269.80	278.00	322.70	350.80	350.20	35.00	347.70	343.90
Cr	59.30	61.20	68.10	58.90	55.50	55.90	101.20	30.00	362.60	55.70	55.30
Mn (ICP)									0.22		
Co	40.40	36.80	38.50	37.40	35.60	36.00	46.40	35.60	157.00	48.00	49.00
Ni	41.20	38.10	40.50	40.30	35.70	37.00	54.40	30.40	78.00	40.00	31.00
Cu	77.30	128.70	127.30	58.90	97.10	162.10	160.20	172.20	82.90	158.00	159.00
Ga	12.60	19.30	12.20	12.90	13.30	12.10	14.70	17.90	14.00	16.00	16.00
Rb	3.90	3.30	4.80	3.70	4.70	3.40	4.20	3.60	2.45	3.00	2.70
Sr	141.60	140.70	139.20	140.50	151.00	142.60	140.90	153.90	141.93	136.00	137.00
Y	8.20	7.50	7.50	6.80	7.80	6.60	8.60	9.70	8.86	9.40	9.30
Zr	16.90	17.10	16.60	17.30	17.30	16.60	18.60	18.20	10.96	13.00	14.00
Nb	1.20	1.50	1.30	1.70	1.60	0.60	1.60	1.10	0.42	0.60	0.20
Cs									0.10		
Ba	47.90	52.20	40.30	42.60	39.30	46.00	41.70	54.40	40.51	45.00	38.50
La	3.54	2.16	2.40	0.44	1.54	1.17	1.00	1.19	0.78	0.40	2.56
Ce	7.58	5.14	5.72	1.44	4.20	4.23	3.50	3.68	1.94	1.65	5.74
Pr									0.38		
Nd	3.32	2.70	4.89	0.83	2.57	2.21	3.33	1.40	1.78	0.41	2.55
Sm									0.74		
Eu									0.26		
Gd									1.10		
Tb									0.22		
Dy									1.37		
Ho									0.28		
Er									0.91		
Tm									0.14		
Yb									0.98		
Lu									0.16		
Hf									0.47		
Ta									0.05		
Pb									0.64		
Th									0.08		
U									0.05		
Chondrite normalised											
La									2.35		
Ce									2.40		
Pr									3.09		
Nd									2.96		
Sm									3.79		
Eu									3.50		
Gd									4.25		
Tb									4.57		
Dy									4.27		
Ho									3.92		
Er									4.34		
Tm									4.34		
Yb									4.69		
Lu									4.85		

	TAF43/1 Tafahi lava	TAF43/2 Tafahi lava	TAF43/3 Tafahi lava	TAF43/4 Tafahi lava	TAF43/5 Tafahi lava	*TAF43/6 Tafahi lava	TAF43/7 Tafahi lava	TAF43/8 Tafahi lava	TAF43/9 Tafahi lava	TAF43/10 Tafahi lava	TAF43/11 Tafahi lava
SiO_2	53.08	54.82	53.97	54.41	54.14	53.37	53.84	53.51	53.50	54.09	53.02
TiO_2	0.40	0.50	0.50	0.49	0.50	0.41	0.49	0.49	0.41	0.42	0.46
Al_2O_3	15.77	15.32	15.35	15.44	15.49	15.17	15.46	15.46	15.29	15.46	15.40
Fe_2O_3	11.19	11.73	11.87	11.76	11.99	11.72	11.95	11.97	11.57	11.34	12.02
MnO	0.22	0.20	0.21	0.21	0.20	0.21	0.21	0.23	0.21	0.21	0.22
MgO	7.14	5.33	5.72	5.78	5.78	6.95	5.92	6.08	6.49	6.24	6.82
CaO	12.67	11.74	12.03	12.01	11.83	12.40	12.07	12.17	12.72	12.17	12.38
Na_2O	1.27	1.57	1.56	1.46	1.46	1.31	1.52	1.51	1.29	1.44	1.36
K_2O	0.15	0.21	0.22	0.21	0.19	0.15	0.19	0.19	0.16	0.20	0.16
P_2O_5	0.06	0.07	0.08	0.07	0.07	0.06	0.07	0.07	0.07	0.07	0.06
H_2O-	0.33	0.18	0.13	0.16	0.21	0.30	0.25	0.19	0.24	0.25	0.24
LOI	0.08	-0.09	-0.07	-0.09	0.06	-0.08	0.01	-0.15	-0.10	-0.18	-0.08
Total	101.95	101.50	101.50	101.84	101.66	101.76	101.71	101.66	101.72	101.62	101.91
Sc	42.10	47.10	48.70	47.20	46.70	53.94	51.40	45.60	49.40	48.20	47.60
Ti (ICP)						0.33					
V	314.00	320.20	388.10	366.00	375.40	333.78	354.30	378.70	375.90	328.00	325.70
Cr	22.50	67.40	72.20	72.70	74.30	129.91	123.70	60.20	61.10	39.90	77.70
Mn (ICP)						0.19					
Co	40.90	48.00	47.00	46.00	47.00	48.34	52.00	46.00	45.00	45.00	46.00
Ni	37.40	34.00	35.00	30.00	32.00	42.44	43.00	32.00	32.00	29.00	33.00
Cu	174.10	126.00	174.00	181.00	171.00	156.16	167.00	170.00	172.00	119.00	160.00
Ga	14.40	14.00	16.00	15.00	17.00	14.07	16.00	18.00	17.00	17.00	16.00
Rb	5.20	2.90	3.70	4.80	5.20	1.28	2.30	4.70	3.70	3.10	3.70
Sr	163.10	134.00	139.00	141.00	140.00	123.88	118.00	143.00	144.00	136.00	131.00
Y	7.30	9.40	12.00	11.00	11.70	8.13	9.40	11.00	12.00	9.20	8.90
Zr	17.30	13.00	16.00	17.00	17.00	9.88	11.00	17.00	16.00	14.00	15.00
Nb	1.20	0.80	0.70	0.60	0.70	0.39	0.40	0.20	0.40	0.40	0.50
Cs						0.03					
Ba	56.40	45.70	70.90	56.70	64.10	37.08	48.60	55.10	55.80	39.50	46.70
La	1.95	0.91	1.99		0.52	0.55	1.48	2.68	1.96	1.11	1.83
Ce	4.85	2.96	4.85	1.16	2.65	1.80	4.49	5.78	5.15	2.60	3.84
Pr						0.32					
Nd	1.89	0.64	1.88		0.94	1.58	3.27	2.29	3.60	1.77	0.52
Sm						0.62					
Eu						0.26					
Gd						0.88					
Tb						0.16					
Dy						1.19					
Ho						0.29					
Er						0.81					
Tm						0.15					
Yb						0.87					
Lu						0.14					
Hf						0.38					
Ta						0.02					
Pb						0.66					
Th						0.08					
U						0.04					
Chondrite normalised											
La						1.65					
Ce						2.22					
Pr						2.64					
Nd						2.63					
Sm						3.18					
Eu						3.51					
Gd						3.41					
Tb						3.39					
Dy						3.71					
Ho						4.05					
Er						3.83					
Tm						4.63					
Yb						4.17					
Lu						4.48					

	TAF43/12 Tafahi lava	TAF43 Tafahi lava	TAF44/2 Tafahi lava	TAF44/3 Tafahi lava	TAF44/4 Tafahi lava	TAF44/5 Tafahi lava	TAF44/6 Tafahi lava	TAF44/7 Tafahi lava	*TAF44/8 Tafahi lava	TAF44/9 Tafahi lava	TAF45/1 Tafahi lava
SiO_2	53.86	54.95	53.13	53.07	54.65	54.01	54.10	54.03	53.83	54.15	54.16
TiO_2	0.40	0.42	0.42	0.41	0.51	0.43	0.43	0.42	0.42	0.43	0.48
Al_2O_3	15.22	14.45	15.76	15.65	14.95	15.24	15.26	15.42	15.60	15.43	15.70
Fe_2O_3	11.11	10.68	11.56	11.30	11.85	11.02	11.08	10.91	11.02	11.03	12.24
MnO	0.20	0.24	0.24	0.23	0.24	0.22	0.22	0.21	0.21	0.21	0.22
MgO	6.23	5.39	6.75	7.18	5.27	6.32	6.42	6.42	6.68	6.35	5.61
CaO	12.60	13.31	11.99	12.27	12.00	12.11	12.11	12.10	12.13	12.03	11.52
Na_2O	1.38	1.49	1.27	1.25	1.60	1.41	1.34	1.33	1.23	1.34	1.48
K_2O	0.19	0.21	0.17	0.15	0.23	0.17	0.16	0.17	0.18	0.18	0.15
P_2O_5	0.06	0.07	0.07	0.07	0.08	0.06	0.06	0.07	0.07	0.07	0.07
H_2O-	0.26	0.31	0.50	0.30	0.22	0.24	0.32	0.28	0.27	0.26	0.29
LOI	-0.14	-0.21	-0.09	-1.54	-0.22	-0.28	-0.25	-0.17	-1.49	-0.20	0.06
Total	101.24	101.21	101.36	101.59	101.38	100.97	101.16	101.08	101.36	101.18	101.62
Sc	52.10	45.70	54.20	51.50	48.10	49.50	51.80	49.30	49.97	50.70	53.10
Ti (ICP)									0.35		
V	361.40	327.30	320.00	309.10	356.50	331.60	374.80	360.40	320.69	343.80	345.50
Cr	93.00	57.80	63.60	149.40	36.70	86.80	89.00	93.90	96.13	92.60	48.80
Mn (ICP)									0.18		
Co	51.00	47.00	47.50	49.40	44.20	44.60	47.20	46.10	44.44	46.60	48.00
Ni	37.00	27.00	46.50	54.50	37.00	46.50	47.70	48.50	40.07	48.90	24.00
Cu	146.00	173.00	173.80	135.90	173.90	192.90	172.80	153.50	122.98	140.40	156.00
Ga	14.00	15.00	13.00	13.60	11.50	13.80	11.20	17.80	14.13	12.90	12.00
Rb	4.00	4.60	3.30	6.70	4.90	2.50	3.50	2.90	2.60	2.60	2.60
Sr	130.00	146.00	146.00	127.40	159.20	136.50	135.80	134.40	133.31	135.50	145.00
Y	9.80	8.90	7.30	6.90	9.40	6.70	7.50	7.80	8.12	8.70	11.40
Zr	13.00	14.00	16.30	16.30	19.90	16.30	17.10	17.50	10.50	17.00	16.00
Nb	0.00	0.50	0.80	0.80	1.40	1.00	1.40	0.90	0.38	1.50	0.20
Cs									0.08		
Ba	47.20	63.10	41.80	35.50	57.50	49.10	38.30	46.60	38.83	40.00	37.80
La	1.20	1.35	2.28		0.76	1.57		2.08	0.66	0.29	2.20
Ce	4.17	4.38	5.15	0.69	3.25	4.70	1.19	5.88	1.92	2.26	5.50
Pr									0.30		
Nd	3.13	2.89	2.62		1.51	4.36	1.34	5.22	1.66	2.32	3.83
Sm									0.64		
Eu									0.26		
Gd									0.89		
Tb									0.17		
Dy									1.24		
Ho									0.28		
Er									0.82		
Tm									0.14		
Yb									0.83		
Lu									0.13		
Hf									0.67		
Ta									0.02		
Pb									0.82		
Th									0.13		
U									0.05		
Chondrite normalised											
La									2.00		
Ce									2.37		
Pr									2.48		
Nd									2.76		
Sm									3.26		
Eu									3.55		
Gd									3.45		
Tb									3.64		
Dy									3.86		
Ho									3.91		
Er									3.90		
Tm									4.37		
Yb									3.98		
Lu									3.96		

	TAF45/2 Tafahi lava	TAF45/3 Tafahi lava	TAF45/4 Tafahi lava	TAF45/5 Tafahi lava	TAF45/6 Tafahi lava	*TAF45/7 Tafahi lava	TAF45/7/8 Tafahi lava	TAF46 Tafahi lava	TAF47 Tafahi lava	TAF48 Tafahi lava	TAF50 Tafahi lava
SiO$_2$	54.29	55.43	54.55	54.77	55.35	56.04	53.94	53.68	53.27	53.01	53.34
TiO$_2$	0.43	0.47	0.47	0.47	0.47	0.47	0.43	0.39	0.38	0.39	0.39
Al$_2$O$_3$	15.26	15.72	15.56	15.72	15.57	15.53	15.46	15.97	15.70	15.63	15.82
Fe$_2$O$_3$	11.60	11.71	11.85	11.86	11.68	11.16	11.33	11.09	10.93	11.05	10.98
MnO	0.20	0.21	0.20	0.20	0.20	0.18	0.19	0.24	0.21	0.21	0.21
MgO	6.09	5.23	5.43	5.47	5.07	4.50	6.23	6.53	6.89	6.81	6.88
CaO	12.12	11.45	11.55	11.48	11.48	11.52	12.37	12.12	12.07	12.03	12.01
Na$_2$O	1.35	1.41	1.61	1.46	1.51	1.53	1.33	1.36	1.19	1.21	1.15
K$_2$O	0.19	0.21	0.19	0.19	0.21	0.22	0.19	0.18	0.21	0.20	0.18
P$_2$O$_5$	0.06	0.08	0.06	0.06	0.07	0.07	0.06	0.15	0.11	0.11	0.06
H$_2$O-	0.13	0.17	0.30	0.21	0.43	0.25	0.20	0.57	0.33	0.37	0.48
LOI	-0.12	-0.03	-0.14	-0.20	-0.19	-0.10	-0.22	1.23	0.18	0.24	0.23
Total	101.59	101.93	101.48	101.68	101.62	101.22	101.53	101.72	100.95	100.63	101.02
Sc	50.30	51.10	47.70	49.10	43.50	47.54	45.60	50.00	50.40	47.80	48.40
Ti (ICP)						0.41					
V	364.30	370.00	356.70	347.80	347.90	329.53	338.90	314.50	303.10	313.40	309.30
Cr	78.30	49.40	50.10	52.30	44.90	29.55	70.80	54.80	80.60	74.50	86.90
Mn (ICP)						0.18					
Co	48.00	44.00	49.00	47.00	46.00	38.29	46.00	46.80	48.10	45.90	47.70
Ni	30.00	27.00	25.00	24.00	23.00	19.29	29.00	41.70	46.20	48.30	50.50
Cu	160.00	113.00	124.00	170.00	146.00	164.67	144.00	158.70	160.20	152.90	148.90
Ga	15.00	15.00	16.00	13.00	16.00	15.17	17.00	16.40	11.20	16.70	9.80
Rb	2.80	0.90	3.50	3.80	3.70	2.60	3.10	3.00	4.40	4.30	3.80
Sr	134.00	146.00	143.00	142.00	146.00	150.63	141.00	145.60	142.30	143.20	143.70
Y	10.00	13.00	12.00	11.80	11.90	9.71	11.00	8.50	8.40	7.00	7.40
Zr	12.00	15.00	16.00	15.00	15.00	13.99	13.00	19.30	17.40	17.00	16.30
Nb	0.50	0.40	0.70	0.20	1.10	0.50	0.20	1.40	1.30	1.60	1.10
Cs						0.10					
Ba	44.90	55.10	50.40	46.20	44.50	45.88	45.20	48.10	56.10	55.50	54.00
La	0.38	2.29	0.30	0.88	0.32	1.15	0.43	1.61	1.02	2.23	2.35
Ce	1.44	6.40	1.57	3.51	2.66	2.50	0.41	4.20	2.32	5.30	5.90
Pr						0.41					
Nd		4.44	0.84	2.23	1.64	2.16		3.58	0.05	3.88	4.09
Sm						0.74					
Eu						0.34					
Gd						1.07					
Tb						0.21					
Dy						1.47					
Ho						0.32					
Er						1.01					
Tm						0.16					
Yb						1.12					
Lu						0.14					
Hf						0.54					
Ta						0.02					
Pb						1.16					
Th						0.10					
U						0.05					
Chondrite normalised											
La						3.50					
Ce						3.09					
Pr						3.39					
Nd						3.59					
Sm						3.80					
Eu						4.64					
Gd						4.14					
Tb						4.53					
Dy						4.56					
Ho						4.44					
Er						4.79					
Tm						4.84					
Yb						5.36					
Lu						4.49					

	TAF52 Tafahi lava	TAF53/1 Tafahi lava	TAF53/2 Tafahi lava	*TAF54 Tafahi lava	TAF55 Tafahi lava	TAF56 Tafahi lava	NTT3/1 **Niua clast	NTT3/2 **Niua clast	NTT4A **Niua clast	NTT4B **Niua clast	NTT5S **Niua clast
SiO_2	55.44	54.33	53.10	54.55	54.83	53.85	59.97	56.74	57.49	59.41	58.31
TiO_2	0.40	0.41	0.39	0.38	0.38	0.40	0.44	0.42	0.46	0.51	0.44
Al_2O_3	15.73	16.10	16.34	16.05	15.42	15.95	15.09	15.06	14.87	15.20	15.35
Fe_2O_3	10.64	11.07	11.04	10.64	10.53	11.33	11.42	12.61	12.27	12.36	12.08
MnO	0.20	0.21	0.21	0.20	0.19	0.21	0.19	0.20	0.19	0.18	0.18
MgO	5.89	6.26	7.23	6.89	5.79	6.27	2.66	4.12	3.84	2.05	3.26
CaO	11.61	11.44	11.83	11.97	11.96	11.53	9.46	10.93	10.34	8.39	9.29
Na_2O	1.05	1.19	1.08	0.85	1.30	1.23	1.78	1.52	1.61	1.94	1.80
K_2O	0.23	0.22	0.20	0.20	0.19	0.12	0.53	0.30	0.44	0.58	0.43
P_2O_5	0.08	0.06	0.11	0.11	0.07	0.09	0.12	0.07	0.08	0.12	0.08
H_2O-	0.25	0.37	0.46	0.22	0.28	0.60					
LOI	-0.15	-0.02	0.17	0.03	-0.12	0.07					
Total	101.28	101.26	101.51	101.83	100.63	100.98	101.65	101.97	101.58	100.74	101.21
Sc	47.40	50.40	51.70	50.35	45.60	52.70	49.00	53.20	49.10	42.20	46.70
Ti (ICP)				0.32							
V	311.30	314.40	299.70	294.66	287.30	303.80	398.80	464.60	420.90	438.70	367.80
Cr	58.50	87.80	109.20	71.80	51.30	63.00	20.10	51.70	25.70	14.00	36.00
Mn (ICP)				0.19							
Co	38.00	41.70	45.90	41.65	39.50	42.80	37.00	46.00	38.00	37.00	41.00
Ni	38.10	44.50	49.90	39.70	38.30	41.80	12.00	21.00	15.00	15.00	15.00
Cu	34.00	145.20	112.90	32.39	116.10	138.40	58.00	119.00	168.00	140.00	134.00
Ga	13.60	16.40	9.10	13.99	16.70	11.40	15.00	17.00	17.00	13.00	16.00
Rb	3.20	2.70	3.30	2.44	2.90	0.90	7.60	4.90	9.40	9.40	5.70
Sr	147.10	138.30	134.00	137.56	146.90	152.10	213.00	177.00	201.00	208.00	207.00
Y	8.20	8.20	9.10	7.69	7.80	8.60	13.00	10.00	12.00	15.00	13.00
Zr	17.40	17.20	16.90	13.81	16.50	17.50	22.00	15.00	20.00	26.00	22.00
Nb	1.70	1.30	1.10	0.60	1.80	1.20	1.00	0.40	0.40	0.70	0.80
Cs				0.05							
Ba	54.10	46.20	52.50	48.06	49.00	58.00	117.40	76.70	102.70	136.40	99.00
La	1.22	2.08	1.40	1.29		1.17	2.35	0.28	2.23	2.50	1.71
Ce	2.62	5.38	3.80	2.36	2.61	4.20	5.22	2.27	4.82	6.33	5.01
Pr				0.36							
Nd	0.79	2.03	2.87	1.81	3.41	2.36	2.31	2.51	1.61	3.17	3.18
Sm				0.66							
Eu				0.26							
Gd				0.81							
Tb				0.16							
Dy				1.13							
Ho				0.27							
Er				0.78							
Tm				0.12							
Yb				0.80							
Lu				0.14							
Hf				0.48							
Ta				0.03							
Pb				1.13							
Th				0.17							
U				0.08							
Chondrite normalised											
La				3.92							
Ce				2.92							
Pr				2.94							
Nd				3.02							
Sm				3.40							
Eu				3.49							
Gd				3.14							
Tb				3.28							
Dy				3.52							
Ho				3.75							
Er				3.71							
Tm				3.64							
Yb				3.85							
Lu				4.37							

**major elements of clasts from Niuatoputapu obtained from powdered pellets

234

	NTT7E	NTT7	*NTT9	*NTT10	NTT11	NTT12	NTT13	*NTT14	NTT15D	NTT15A	NTT16A
	**Niua clast	**Niua clast	Niua lava	Niua lava	Niua lava	**Niua clast	Niua lava	Niua lava	**Niua clast	**Niua clast	**Niua clast
SiO_2	55.76	59.58	58.66	58.95	58.96	56.73	58.42	58.50	60.01	59.80	56.21
TiO_2	0.31	0.48	0.47	0.51	0.55	0.42	0.55	0.50	0.54	0.54	0.33
Al_2O_3	15.35	15.00	15.53	15.14	14.48	14.95	14.78	14.64	15.05	14.62	15.28
Fe_2O_3	10.80	12.46	12.38	12.56	12.99	12.65	12.95	13.20	12.19	12.46	10.98
MnO	0.17	0.16	0.22	0.20	0.19	0.19	0.20	0.20	0.19	0.20	0.18
MgO	5.61	2.69	3.04	2.50	2.54	4.14	2.71	2.81	1.98	2.23	5.22
CaO	12.16	8.49	8.46	8.56	7.77	10.92	8.09	8.93	8.16	8.36	11.88
Na_2O	1.29	1.71	1.74	1.90	2.00	1.53	2.04	1.82	1.95	1.96	1.40
K_2O	0.26	0.49	0.39	0.43	0.52	0.30	0.37	0.37	0.55	0.55	0.22
P_2O_5	0.07	0.09	0.06	0.10	0.09	0.07	0.11	0.08	0.11	0.11	0.06
H_2O-			2.19	0.19				0.60			
LOI			0.81	0.02				0.25			
Total	101.79	101.16	100.95	100.84	100.08	101.92	100.24	101.06	100.73	100.82	101.76
Sc	45.90	52.10	51.88	47.11	45.40	53.80	42.80	54.88	44.50	44.90	52.20
Ti (ICP)			0.42	0.47				0.46			
V	332.40	393.60	344.99	397.11	376.80	410.90	342.30	432.96	370.90	386.90	331.80
Cr	95.00	27.00	22.01	5.78	6.50	50.90	3.70	10.70	2.70	6.50	75.80
Mn (ICP)			0.22	0.20				0.21			
Co	40.00	36.00	38.87	35.73	36.00	44.00	38.00	36.11	32.00	33.00	39.00
Ni	25.00	10.00	12.09	16.51	8.50	17.00	7.80	12.97	5.10	9.80	21.00
Cu	34.00	155.00	171.27	163.85	202.00	124.00	181.00	175.26	156.00	160.00	90.00
Ga	16.00	13.00	14.12	14.79	14.00	15.00	16.00	14.14	16.00	14.00	13.00
Rb	3.70	9.10	7.49	7.00	11.00	5.50	4.30	6.91	9.60	10.80	5.10
Sr	192.00	202.00	196.94	221.03	217.00	177.00	230.00	201.67	212.00	214.00	193.00
Y	8.90	13.00	8.74	11.56	13.00	10.00	14.00	10.34	15.00	16.00	7.70
Zr	10.00	21.00	17.40	20.81	28.00	15.00	28.00	18.67	30.00	29.00	15.00
Nb	0.20	0.70	1.04	1.06	1.20	0.90	1.60	1.12	2.40	2.10	0.00
Cs			0.18	0.21				0.23			
Ba	70.70	121.80	110.50	110.82	157.30	79.10	153.30	101.64	132.40	125.90	69.90
La	2.06	2.50	2.08	3.05	2.16	1.27	2.97	2.59	2.92	3.65	2.28
Ce	5.15	6.08	5.69	6.58	7.17	4.11	8.88	5.28	6.95	9.08	5.88
Pr			0.71	0.96				0.81			
Nd	2.51	2.43	3.20	4.55	2.28	2.53	6.68	3.68	2.59	4.65	4.35
Sm			1.01	1.34				1.13			
Eu			0.39	0.48				0.43			
Gd			1.17	1.54				1.33			
Tb			0.19	0.30				0.24			
Dy			1.41	1.87				1.68			
Ho			0.30	0.38				0.35			
Er			0.89	1.17				1.09			
Tm			0.15	0.20				0.17			
Yb			1.03	1.32				1.13			
Lu			0.15	0.21				0.19			
Hf			0.62	0.73				1.07			
Ta			0.06	0.07				0.07			
Pb			1.78	2.75				2.02			
Th			0.35	0.45				0.41			
U			0.12	0.13				0.12			
Chondrite normalised											
La			6.31	9.25				7.84			
Ce			7.04	8.15				6.54			
Pr			5.85	7.83				6.62			
Nd			5.33	7.58				6.13			
Sm			5.18	6.85				5.77			
Eu			5.28	6.55				5.83			
Gd			4.50	5.96				5.13			
Tb			4.09	6.24				5.05			
Dy			4.36	5.79				5.22			
Ho			4.18	5.36				4.85			
Er			4.25	5.55				5.21			
Tm			4.75	6.19				5.35			
Yb			4.94	6.30				5.38			
Lu			4.61	6.59				6.03			

	NTT16B	NTT17	NTT18A	NTT18B	NTT19A	NTT20A	NTT20B	NTT21A	NTT21B	NTT22A	NTT23/4
	**Niua	**Niua	**Niua	**Niua	**Niua	**Niua	**Niua	**Niua	**Niua	**Niua	Niua
	clast	clast	clast	clast	clast	clast	clast	clast	clast	clast	flow
SiO_2	56.65	56.75	57.39	58.74	59.73	60.06	63.15	56.74	58.19	58.31	57.04
TiO_2	0.39	0.43	0.45	0.44	0.43	0.44	0.45	0.41	0.43	0.45	0.45
Al_2O_3	15.51	15.40	15.00	15.09	15.74	15.21	15.18	15.26	15.29	15.28	14.71
Fe_2O_3	11.03	11.33	12.68	12.14	10.20	11.57	10.10	11.47	11.89	11.60	13.04
MnO	0.16	0.17	0.20	0.19	0.15	0.18	0.18	0.17	0.19	0.17	0.19
MgO	4.77	4.18	3.62	2.97	2.72	2.45	1.18	5.06	3.28	3.50	3.64
CaO	10.71	10.91	10.32	10.14	9.46	8.85	7.04	10.59	10.61	9.85	9.88
Na_2O	1.63	1.51	1.52	1.64	1.93	1.79	2.10	1.44	1.59	1.66	1.71
K_2O	0.43	0.49	0.42	0.43	0.54	0.50	0.69	0.26	0.35	0.34	0.35
P_2O_5	0.07	0.08	0.07	0.09	0.08	0.10	0.11	0.09	0.08	0.08	0.07
H_2O-											0.58
LOI											-0.01
Total	101.36	101.24	101.67	101.86	100.99	101.16	100.18	101.49	101.92	101.25	101.09
Sc	48.00	44.10	51.60	47.70	35.00	46.30	37.40	45.80	47.20	49.00	57.20
Ti (ICP)											
V	345.80	388.90	379.40	379.50	321.50	346.70	255.40	347.40	364.10	359.60	375.60
Cr	45.70	29.60	18.70	18.40	25.20	10.30	3.80	159.60	15.10	26.20	18.50
Mn (ICP)											
Co	36.00	34.00	39.00	32.00	28.00	31.00	22.00	38.00	38.00	34.00	42.00
Ni	17.00	13.00	6.90	12.00	11.00	9.00	0.90	37.00	14.00	12.00	14.00
Cu	127.00	168.00	148.00	135.00	124.00	103.00	37.00	125.00	72.00	135.00	84.00
Ga	14.00	15.00	15.00	14.00	14.00	13.00	13.00	13.00	12.00	15.00	15.00
Rb	17.40	9.10	8.60	8.00	10.30	6.40	11.80	7.60	6.10	6.60	7.20
Sr	220.00	232.00	207.00	206.00	215.00	209.00	214.00	221.00	189.00	214.00	188.00
Y	11.00	11.00	11.00	12.00	14.00	13.00	17.00	12.00	12.00	12.00	13.00
Zr	19.00	23.00	23.00	22.00	28.00	25.00	32.00	23.00	21.00	25.00	22.00
Nb	0.70	0.90	0.90	0.70	2.20	1.70	2.90	1.60	1.80	1.30	0.80
Cs											
Ba	104.10	131.50	102.30	99.30	130.60	118.00	178.20	72.10	95.80	114.80	96.50
La	2.34	2.40	2.35	1.48	3.51	1.39	3.16	4.01	1.06	2.74	1.48
Ce	5.90	5.47	5.09	3.97	8.82	4.32	7.21	9.13	3.52	4.95	4.46
Pr											
Nd	2.31	3.26	1.49	2.28	4.12	2.04	3.39	5.22	1.22	1.73	1.89
Sm											
Eu											
Gd											
Tb											
Dy											
Ho											
Er											
Tm											
Yb											
Lu											
Hf											
Ta											
Pb											
Th											
U											

Chondrite normalised
La
Ce
Pr
Nd
Sm
Eu
Gd
Tb
Dy
Ho
Er
Tm
Yb
Lu

	NTT23/5 Niua flow	NTT25/1 Niua flow	*NTT25/2 Niua flow	*NTT25/4 Niua flow	NTT25/5 Niua flow	NTT25/6 Niua flow	NTT25/7 Niua flow	NTT25/8 Niua flow	*NTT26/1 Niua flow	NTT26/2 Niua flow	NTT26/3 Niua flow
SiO$_2$	66.90	59.43	59.31	59.77	59.60	59.17	58.82	59.21	56.85	58.47	58.76
TiO$_2$	0.38	0.50	0.50	0.50	0.49	0.49	0.50	0.50	0.52	0.50	0.49
Al$_2$O$_3$	15.13	14.87	15.05	15.04	15.25	15.53	15.59	15.06	15.59	15.60	14.95
Fe$_2$O$_3$	7.23	12.26	12.31	11.97	11.89	12.08	12.49	12.50	13.29	13.01	12.76
MnO	0.11	0.18	0.18	0.18	0.17	0.17	0.19	0.18	0.28	0.20	0.19
MgO	0.26	2.45	2.46	2.40	2.31	2.28	2.39	2.53	2.82	2.65	2.71
CaO	4.01	8.36	8.43	8.30	8.45	8.49	8.34	8.33	9.42	8.62	8.85
Na$_2$O	2.50	2.01	1.95	1.98	1.97	1.97	1.88	1.91	1.83	1.67	1.84
K$_2$O	1.10	0.54	0.54	0.55	0.56	0.57	0.57	0.54	0.53	0.48	0.47
P$_2$O$_5$	0.13	0.11	0.11	0.11	0.11	0.11	0.12	0.10	0.11	0.09	0.09
H$_2$O-	1.03	0.34	0.30	0.35	0.61	0.61	0.73	0.43	0.43	0.54	0.41
LOI	0.08	-0.23	-0.31	-0.21	-0.04	-0.24	-0.16	-0.29	-0.40	-0.05	-0.35
Total	97.77	100.72	100.85	100.80	100.80	100.87	100.88	100.86	101.25	101.28	101.12
Sc	24.10	44.30	49.25	46.53	42.60	44.80	44.70	44.60	52.94	51.50	48.10
Ti (ICP)			0.47	0.46					0.46		
V	7.10	399.60	408.18	401.36	399.80	396.90	404.20	402.70	430.86	431.90	430.50
Cr	-0.50	22.00	14.63	28.42	11.50	12.80	5.80	13.70	8.67	9.00	18.40
Mn (ICP)			0.20	0.19					0.20		
Co	6.30	38.00	31.74	33.28	32.00	34.00	35.00	32.00	33.98	37.00	37.00
Ni	-2.00	9.60	13.47	15.26	11.00	8.90	14.00	8.70	10.23	11.00	8.60
Cu	21.00	142.00	156.60	113.32	169.00	186.00	166.00	123.00	215.01	138.00	113.00
Ga	16.00	13.00	13.63	12.17	18.00	13.00	12.00	13.00	12.98	12.00	10.00
Rb	21.10	9.10	8.20	8.18	9.40	9.20	8.80	11.60	6.28	6.50	7.30
Sr	229.00	211.00	216.97	215.67	212.00	211.00	210.00	210.00	201.96	186.00	194.00
Y	17.00	13.00	11.71	12.00	14.00	16.00	15.00	13.00	10.94	12.00	14.00
Zr	47.00	28.00	20.76	20.97	28.00	28.00	28.00	28.00	18.67	25.00	26.00
Nb	5.40	1.00	1.02	1.07	1.20	1.60	1.30	1.30	1.12	0.90	1.60
Cs			0.14	0.11					0.06		
Ba	263.20	124.30	124.86	127.71	138.00	137.10	135.50	129.10	107.34	106.10	111.90
La	4.13	1.46	3.20	3.61	1.64	1.78	3.02	1.11	2.31	0.90	3.20
Ce	9.26	4.69	5.81	6.18	5.19	7.87	4.06	6.71	5.25	7.81	4.46
Pr			0.88	0.95					0.81		
Nd	3.78	1.02	4.17	4.24	2.19	3.88	1.84	3.05	3.74	3.21	1.61
Sm			1.31	1.35					1.08		
Eu			0.43	0.47					0.41		
Gd			1.40	1.54					1.35		
Tb			0.26	0.26					0.25		
Dy			1.77	1.92					1.72		
Ho			0.41	0.41					0.36		
Er			1.23	1.23					1.13		
Tm			0.21	0.18					0.19		
Yb			1.32	1.35					1.19		
Lu			0.20	0.22					0.20		
Hf			0.74	0.72					0.62		
Ta			0.06	0.07					0.06		
Pb			2.87	3.95					1.75		
Th			0.43	0.43					0.38		
U			0.15	0.14					0.13		
Chondrite normalised											
La			9.71	10.93					7.00		
Ce			7.19	7.65					6.50		
Pr			7.17	7.78					6.62		
Nd			6.94	7.07					6.24		
Sm			6.72	6.91					5.52		
Eu			5.87	6.45					5.59		
Gd			5.39	5.94					5.23		
Tb			5.57	5.53					5.23		
Dy			5.48	5.97					5.36		
Ho			5.71	5.70					4.99		
Er			5.84	5.88					5.40		
Tm			6.51	5.69					5.85		
Yb			6.30	6.44					5.68		
Lu			6.35	6.68					6.18		

	NTT27/2 Niua clast	*NTT28/2 Niua flow	NTT28/4/1 **Niua clast	NTT28/4/2 **Niua clast	NTT28/4/3 **Niua clast	NTT28/4/4 **Niua clast	NTT29/1 Niua flow	NTT29/2 Niua flow	*NTT29/3 Niua flow	NTT29/4 Niua flow	*2218-1 NLSC lava
SiO_2	56.46	58.35	55.54	57.24	57.63	57.23	60.39	59.16	58.64	57.45	51.38
TiO_2	0.38	0.52	0.54	0.53	0.49	0.50	0.52	0.52	0.54	0.56	1.16
Al_2O_3	15.39	15.25	15.85	15.48	15.05	15.86	15.50	16.09	15.52	16.05	15.47
Fe_2O_3	11.03	12.80	12.43	12.52	12.86	12.24	11.87	11.52	11.84	11.81	10.62
MnO	0.17	0.21	0.27	0.26	0.28	0.25	0.18	0.26	0.24	0.27	0.19
MgO	4.71	2.95	3.68	2.74	3.23	2.61	1.84	1.82	1.82	1.84	6.88
CaO	11.77	8.69	9.99	9.63	9.70	9.36	7.94	7.80	8.25	8.07	11.14
Na_2O	1.43	1.78	1.90	2.08	2.00	1.93	2.01	2.31	2.30	2.15	2.81
K_2O	0.20	0.44	0.52	0.54	0.53	0.42	0.57	0.62	0.65	0.69	0.31
P_2O_5	0.06	0.09	0.13	0.12	0.09	0.14	0.11	0.13	0.14	0.16	0.13
H_2O-	0.45	0.18					0.66	0.67	0.59		
LOI	3.30	1.19					-0.41	0.00	-0.07		-0.01
Total	101.61	101.10	100.84	101.14	101.87	100.54	100.93	100.24	99.95	99.05	100.08
Sc	49.50	51.08	46.50	45.00	51.60	44.10	49.00	44.50	44.36	44.20	22.40
Ti (ICP)		0.47							0.53		1.12
V	330.90	363.20	408.10	395.70	378.50	369.90	374.50	386.70	381.00	363.90	300.00
Cr	56.40	14.31	30.80	18.30	23.20	10.90	6.70	4.10	3.00		167.50
Mn (ICP)		0.21							0.19		0.12
Co	40.00	34.30	40.00	36.00	39.00	32.00	31.00	28.00	29.71	29.00	40.00
Ni	21.00	13.10	23.00	9.90	12.00	12.00	1.20	0.00	2.47	1.00	72.90
Cu	77.00	172.68	182.00	168.00	143.00	112.00	230.00	131.00	240.82	145.00	61.00
Ga	17.00	13.52	13.00	15.00	13.00	13.00	13.00	12.00	12.34	14.00	79.00
Rb	3.50	3.95	8.80	9.10	8.50	5.90	8.90	9.40	8.87	10.20	6.38
Sr	197.00	207.70	212.00	219.00	202.00	219.00	207.00	207.00	218.34	207.00	136.02
Y	11.00	10.71	14.00	15.00	13.00	15.00	14.00	14.00	13.43	14.00	29.94
Zr	19.00	19.26	27.00	28.00	27.00	27.00	28.00	28.00	22.95	28.00	75.54
Nb	1.00	1.68	1.00	1.00	1.50	1.20	1.40	1.70	1.28	1.30	2.41
Cs		0.04							0.14		0.13
Ba	72.50	119.65	116.90	122.20	114.60	134.20	129.20	127.60	128.17	136.70	37.78
La	1.29	2.88	2.14	3.43	2.66	3.08	2.28	2.89	3.07	2.98	3.52
Ce	2.87	5.82	6.86	7.76	6.79	8.61	5.30	6.40	6.53	7.34	10.18
Pr		0.93							1.02		1.66
Nd	0.42	4.55	3.86	5.10	4.17	6.64	2.03	2.81	4.53	4.18	8.46
Sm		1.22							1.35		2.87
Eu		0.44							0.48		1.00
Gd		1.55							1.68		3.63
Tb		0.28							0.29		0.71
Dy		1.78							2.05		4.60
Ho		0.38							0.46		0.98
Er		1.14							1.35		2.90
Tm		0.18							0.23		0.45
Yb		1.24							1.50		2.97
Lu		0.20							0.23		0.44
Hf		0.66							1.02		2.46
Ta		0.10							0.11		0.18
Pb		1.57							1.77		0.67
Th		0.37							0.45		0.35
U		0.11							0.15		0.14
Chondrite normalised											
La		8.73							9.30		10.68
Ce		7.20							8.08		12.60
Pr		7.65							8.37		13.58
Nd		7.59							7.54		14.10
Sm		6.27							6.91		14.71
Eu		5.98							6.52		13.56
Gd		5.98							6.49		14.02
Tb		5.97							6.15		14.88
Dy		5.52							6.37		14.28
Ho		5.26							6.45		13.70
Er		5.43							6.44		13.82
Tm		5.67							6.99		13.89
Yb		5.93							7.18		14.21
Lu		6.33							7.08		13.75

	*2218-8	*2218-12	*2212-6
	NLSC	NLSC	NLSC
	lava	lava	lava
SiO_2	50.90	51.89	50.52
TiO_2	1.26	1.55	1.18
Al_2O_3	15.47	15.39	16.14
Fe_2O_3	11.50	12.02	10.57
MnO	0.19	0.20	0.18
MgO	5.99	5.04	5.38
CaO	10.62	9.45	11.45
Na_2O	2.93	3.24	3.09
K_2O	0.37	0.54	0.55
P_2O_5	0.12	0.19	0.18
H_2O-		0.29	
LOI	0.12		0.31
Total	99.47	99.80	99.55
Sc	20.50	16.80	19.50
Ti (ICP)	1.26	1.50	1.16
V	303.10	344.00	314.10
Cr	32.90	21.60	21.20
Mn (ICP)	0.14	0.14	0.14
Co	42.00	37.00	38.00
Ni	37.25	23.85	48.65
Cu	54.00	42.00	78.00
Ga	90.00	109.00	82.00
Rb	7.64	11.13	11.97
Sr	153.95	162.25	210.53
Y	32.04	38.25	30.04
Zr	81.24	102.67	76.82
Nb	3.46	3.84	5.05
Cs	0.13	0.28	0.29
Ba	57.45	68.47	95.82
La	4.41	5.28	6.11
Ce	12.20	14.66	15.47
Pr	1.92	2.32	2.32
Nd	9.86	12.16	11.31
Sm	3.07	3.83	3.26
Eu	1.08	1.34	1.12
Gd	3.92	4.76	3.92
Tb	0.72	0.89	0.72
Dy	4.91	5.89	4.62
Ho	1.07	1.28	1.00
Er	3.11	3.81	2.89
Tm	0.49	0.58	0.46
Yb	3.04	3.73	2.93
Lu	0.46	0.56	0.43
Hf	2.22	2.72	2.04
Ta	0.22	0.26	0.30
Pb	0.88	1.07	0.96
Th	0.43	0.52	0.75
U	0.20	0.23	0.32
Chondrite normalised			
La	13.37	16.00	18.50
Ce	15.11	18.14	19.15
Pr	15.72	18.99	19.05
Nd	16.44	20.27	18.84
Sm	15.76	19.64	16.72
Eu	14.67	18.23	15.30
Gd	15.15	18.38	15.14
Tb	15.20	18.76	15.23
Dy	15.24	18.31	14.35
Ho	14.87	17.89	13.96
Er	14.79	18.16	13.77
Tm	15.14	17.81	14.12
Yb	14.54	17.84	14.00
Lu	14.28	17.27	13.25

section	16-51/8 western bon	16-51/9 western bon	16-51/16 western bon	16-47 western bon gabb	16-55/4 western bon	16-26/1 west bon	16-26/2 west bon	16-70/8 eastern otb	16-70/14 eastern iat	16-70/16 eastern iat	16-70/17 eastern iat	16-70/19 eastern iat
SiO$_2$	48.29	50.74	51.90	54.02	54.63	54.24	47.61	48.02	51.95	50.69	48.58	53.00
TiO$_2$	0.33	0.28	0.24	0.32	0.33	0.25	0.22	1.31	0.49	0.67	0.69	0.82
Al$_2$O$_3$	10.72	10.45	10.86	13.08	12.95	10.82	5.62	15.09	15.56	14.59	14.21	15.18
Fe$_2$O$_3$	12.32	12.17	12.16	10.90	10.82	9.66	10.81	12.81	8.18	9.97	13.48	9.64
MnO	0.14	0.20	0.18	0.16	0.05	0.15	0.18	0.27	0.12	0.16	0.20	0.14
MgO	15.08	14.29	13.36	8.97	9.63	14.10	28.35	7.47	7.89	7.86	8.76	6.98
CaO	8.44	8.48	9.81	10.37	8.48	8.72	4.83	10.25	12.16	9.50	10.06	9.13
Na$_2$O	1.84	1.13	1.36	1.74	1.40	0.53	0.30	2.56	1.86	2.16	3.20	2.02
K$_2$O	0.26	0.28	0.31	0.54	0.65	0.24	0.24	0.33	0.41	0.74	0.43	0.55
P$_2$O$_5$	0.10	0.09	0.05	0.20	0.19	0.07	0.07	0.19	0.15	0.19	0.29	0.17
H$_2$O-	0.58	0.76		0.00				0.58	0.30	0.87	0.20	0.60
LOI	2.52	2.20		1.19	1.59			2.00	1.75	3.08	1.46	1.76
Total	100.62	100.22	99.37	101.49	100.09	100.00	98.86	100.88	100.21	100.48	100.42	99.99
Ti (ICP)	0.22	0.21	0.23	0.32	0.26	0.23	0.23	1.22	1.40	0.60	1.27	0.81
Sc	32.08	47.27		46.89	42.16	34.23	22.73	39.49	41.93	32.42		34.02
Cr	788.76	1165.07	817.50	374.07	399.55	596.19	763.56	251.53		306.87	259.31	196.58
Mn (ICP)	0.17	0.20	0.18	0.17	0.17	0.16	0.16	0.18	0.19	0.18	0.20	0.17
Ni	169.53	160.08	111.97	123.67	120.95	347.57	664.89	62.29	79.32	68.97	73.84	60.70
V	267.75	240.12	278.86	283.76	284.72	197.83	121.44	292.91		234.10	313.13	232.21
Co	47.12	55.53	53.16	41.45	48.52	71.18	115.32	39.83	42.58	32.59	41.38	31.60
Cu	62.18	87.87	114.72	116.21	95.49	103.61	62.38	73.15	89.32	87.96	68.92	77.75
Zn	62.85	79.66	76.82	104.41	58.41	60.69	53.90	81.77	97.01	78.31	93.96	76.67
Rb	1.57	4.00	4.10	9.06	8.01	5.06	5.65	5.23	3.83	5.93	3.14	6.89
Sr	172.85	146.30	149.34	201.46	190.16	102.10	97.39	116.74	110.57	124.85	105.50	139.47
Y	9.10	5.56	6.06	8.56	7.16	6.01	4.76	33.27	38.16	14.53	35.10	24.45
Zr	14.41	11.64	11.82	20.21	19.74	18.30	20.35	83.40	93.75	37.99	87.64	60.71
Nb	1.22	0.83	1.93	1.31	1.78	3.57	4.08	2.50	2.76	1.18	2.68	1.83
Cs	0.09	0.23	0.16	0.40	0.26	0.16	0.08	0.25	0.19	0.18	0.07	0.12
Ba	156.53	47.33	46.89	120.19	109.88	61.70	65.97	26.64	34.46	49.40	30.14	52.50
La	2.87	1.65	1.96	3.00	2.72	2.75	3.76	3.82	3.69	2.14	3.50	3.50
Ce	5.16	3.19	3.93	6.13	5.39	5.52	7.34	10.49	10.63	5.25	10.55	8.67
Pr	0.77	0.47	0.52	0.79	0.71	0.69	0.89	1.82	1.90	0.89	1.78	1.43
Nd	3.52	1.90	2.26	3.58	2.78	2.81	3.58	9.32	10.50	4.44	9.50	7.47
Sm	1.02	0.55	0.64	1.12	0.81	0.68	0.75	2.95	3.24	1.50	3.40	2.21
Eu	0.35	0.19	0.23	0.34	0.28	0.23	0.24	1.03	1.12	0.54	1.08	0.80
Gd	1.01	0.62	0.77	1.11	0.89	0.77	0.78	3.75	4.39	1.85	4.13	2.69
Tb	0.19	0.12	0.15	0.20	0.15	0.13	0.11	0.77	0.79	0.35	0.86	0.53
Dy	1.23	0.74	0.89	1.34	1.04	0.92	0.78	5.09	5.72	2.41	5.60	3.58
Ho	0.27	0.16	0.21	0.29	0.25	0.21	0.17	1.08	1.13	0.52	1.28	0.81
Er	0.94	0.53	0.62	0.92	0.72	0.62	0.43	3.39	3.63	1.52	3.73	2.45
Tm	0.15	0.11	0.11	0.15	0.11	0.09	0.08	0.54	0.74	0.29	0.56	0.42
Yb	0.91	0.58	0.69	1.07	0.78	0.66	0.47	3.38	3.87	1.60	3.58	2.51
Lu	0.17	0.10	0.11	0.17	0.12	0.11	0.08	0.54	0.65	0.26	0.59	0.45
Hf	0.46	0.32	0.38	0.62	0.64	0.56	0.58	2.29	2.69	1.13	2.60	1.81
Ta	0.09	0.04	0.07	0.08	0.12	0.22	0.27	0.17	0.18	0.07	0.16	0.12
Pb	1.53	1.73	4.65	2.41	2.23	8.55	2.60	1.12	0.86	0.90	0.71	1.01
Th	0.34	0.22	0.30	0.54	0.77	0.56	0.70	0.29	0.29	0.19	0.28	0.34
U	0.20	0.12	0.42	0.21	0.25	0.17	0.18	0.18	0.10	0.11	0.09	0.17
chondrite normalised												
La	8.69	5.00	5.94	9.08	8.23	8.35	11.39	11.57	11.17	6.50	10.60	10.62
Ce	6.38	3.95	4.86	7.59	6.66	6.83	9.09	12.98	13.16	6.50	13.06	10.73
Pr	6.30	3.83	4.28	6.46	5.80	5.64	7.32	14.89	15.55	7.32	14.56	11.73
Nd	5.86	3.16	3.76	5.97	4.63	4.68	5.97	15.53	17.50	7.41	15.83	12.46
Sm	5.17	2.80	3.26	5.69	4.16	3.48	3.84	14.95	16.60	7.60	17.23	11.17
Eu	4.87	2.60	3.24	4.74	3.76	3.12	3.20	14.34	15.26	7.57	15.01	11.10
Gd	3.89	2.39	2.96	4.27	3.42	2.98	3.00	14.49	16.95	7.14	15.95	10.40
Tb	4.06	2.49	3.07	4.15	3.23	2.75	2.41	16.33	16.61	7.38	18.05	11.24
Dy	3.81	2.30	2.77	4.15	3.24	2.86	2.41	15.81	17.75	7.47	17.40	11.13
Ho	3.76	2.28	2.88	4.04	3.41	2.90	2.31	15.04	15.69	7.21	17.80	11.27
Er	4.47	2.52	2.98	4.38	3.41	2.95	2.04	16.15	17.26	7.22	17.77	11.65
Tm	4.78	3.33	3.43	4.75	3.46	2.91	2.44	16.59	22.73	8.92	17.41	13.05
Yb	4.34	2.75	3.28	5.14	3.75	3.17	2.25	16.17	18.49	7.64	17.14	11.99
Lu	5.38	3.03	3.54	5.18	3.60	3.54	2.36	16.80	20.13	7.97	18.42	14.08

section	16-47/26 western diabase	16-47/27 western diabase	16-47/29 western diabase	16-67/8 eastern diabase	16-73/18 eastern diabase	16-73/29 eastern diabase	16-94/1 seamount oib	16-95/2 seamount oib	16-95/3 seamount oib
SiO$_2$	51.67	50.92	50.01	51.64	49.09	52.15	46.55	45.35	43.77
TiO$_2$	0.96	0.90	0.37	0.47	0.36	0.86	2.64	3.54	3.72
Al$_2$O$_3$	15.78	16.30	15.96	16.00	15.10	15.83	11.68	12.39	11.61
Fe$_2$O$_3$	11.14	10.59	7.94	8.87	9.29	10.84	12.62	11.94	12.13
MnO	0.21	0.22	0.14	0.14	0.15	0.21	0.17	0.16	0.17
MgO	7.84	8.55	10.81	10.17	12.31	8.12	11.88	10.87	11.34
CaO	8.55	8.68	12.96	10.22	11.82	7.61	7.96	8.98	8.61
Na$_2$O	3.97	3.35	1.67	1.79	1.76	3.97	3.47	1.92	2.83
K$_2$O	0.32	0.15	0.04	0.09	0.04	0.28	1.79	2.52	2.83
P$_2$O$_5$	0.09	0.09	0.01	0.05	0.03	0.10	0.49	0.92	0.68
H$_2$O-	0.57	0.56	0.50	1.08	0.17	0.28	1.18	0.00	0.10
LOI	5.62	3.99	6.04	2.90	0.52	1.06	1.20	1.88	2.48
Total	100.53	99.77	99.92	99.44	99.96	99.98	100.60	99.57	99.45
Ti (ICP)	0.89	0.82	0.80	0.42	0.35	0.36	3.35	2.49	2.87
Sc							32.89	16.44	20.67
Cr	110.49	159.83	172.90	388.51	789.47	736.34			
Mn (ICP)	0.20	0.17	0.19	0.17	0.16	0.16	0.17	0.14	0.13
Ni	36.56	43.14	44.40	101.24	215.56	152.11	327.14	190.21	206.92
V	275.34	246.17	234.89	247.17	140.06	161.27			
Co	40.05	38.64	39.96	37.68	53.65	47.17	57.41	38.02	41.05
Cu	372.78	136.63	249.38	67.62	90.16	97.96	54.93	38.33	44.24
Zn	58.67	103.27	60.43	58.90	168.97	48.20	63.43	42.99	51.02
Rb	4.23	1.65	3.61	0.37	0.19	0.22	36.82	64.86	56.87
Sr	88.81	97.65	86.38	93.82	102.02	87.15	776.98	959.10	816.47
Y	19.41	20.31	20.95	10.23	7.27	8.70	24.85	36.06	27.37
Zr	26.11	24.45	29.31	19.24	4.00	3.84	277.04	470.97	361.02
Nb	1.30	1.33	1.51	0.43	<0.01	<0.01	46.51	74.07	62.11
Cs	0.05	0.04	0.05	<0.01	<0.01	0.01	0.45	1.32	1.22
Ba	30.82	21.48	28.71	24.55	9.55	9.78	653.87	1086.50	977.26
La	1.55	1.81	1.72	0.87	0.32	0.28	40.82	75.47	63.51
Ce	4.55	5.14	5.01	2.31	0.94	0.97	87.72	179.92	142.96
Pr	0.79	0.91	0.88	0.39	0.18	0.19	10.84	21.44	17.06
Nd	4.52	5.01	4.88	2.25	1.20	1.25	43.41	79.40	67.37
Sm	1.64	1.77	1.75	0.80	0.48	0.58	9.17	13.12	13.12
Eu	0.60	0.72	0.62	0.35	0.38	0.42	2.70	3.70	3.46
Gd	2.11	2.27	2.32	1.10	0.78	0.95	9.40	8.59	10.91
Tb	0.46	0.49	0.49	0.24	0.18	0.20	0.96	1.32	1.39
Dy	3.08	3.21	3.33	1.64	1.17	1.37	4.96	6.58	6.42
Ho	0.68	0.70	0.73	0.36	0.26	0.31	0.90	1.20	1.19
Er	2.06	2.06	2.13	1.03	0.63	0.79	2.40	2.93	2.84
Tm	0.33	0.34	0.35	0.18	0.11	0.14	0.32	0.37	0.40
Yb	1.94	1.96	2.09	1.10	0.69	0.82	1.64	2.09	4.38
Lu	0.31	0.31	0.34	0.18	0.11	0.12	0.28	0.39	0.35
Hf	0.92	0.84	1.03	0.61	0.16	0.19	6.31	12.29	11.44
Ta	0.08	0.08	0.10	0.03	0.00	0.00	2.32	5.51	5.10
Pb	1.47	1.01	1.23	0.34	0.10	0.54	5.66	8.22	12.55
Th	0.10	0.09	0.10	0.08	0.01	0.01	4.77	11.49	12.55
U	0.05	0.05	0.05	0.04	0.03	0.02	1.17	3.00	3.60
chondrite normalised									
La	4.69	5.48	5.20	2.63	0.96	0.85	123.69	228.70	192.46
Ce	5.63	6.37	6.21	2.86	1.16	1.21	108.57	222.67	176.93
Pr	6.47	7.48	7.20	3.18	1.48	1.58	88.86	175.70	139.86
Nd	7.54	8.36	8.14	3.75	1.99	2.08	72.35	132.33	112.29
Sm	8.18	8.87	8.73	4.00	2.41	2.88	47.01	67.29	67.26
Eu	8.50	10.31	8.79	4.96	5.39	6.04	36.69	50.28	47.13
Gd	8.14	8.77	8.94	4.24	3.00	3.65	36.28	33.17	42.13
Tb	9.68	10.27	10.39	5.03	3.73	4.32	20.30	27.86	29.28
Dy	9.55	9.96	10.36	5.09	3.63	4.27	15.41	20.43	19.94
Ho	9.44	9.73	10.18	5.08	3.58	4.31	12.56	16.66	16.58
Er	9.79	9.80	10.14	4.90	3.00	3.75	11.43	13.98	13.54
Tm	10.18	10.39	10.81	5.44	3.31	4.19	9.95	11.54	12.31
Yb	9.28	9.37	9.99	5.28	3.32	3.90	7.86	10.00	20.97
Lu	9.68	9.76	10.41	5.60	3.47	3.82	8.83	11.97	10.98

sample	TAF23	TAF23	TAF23	TAF23	TAF23	TAF23	TAF23	TAF23	TAF23	TAF23
locality	rim	core	rim	core	rim	core	rim	core	rim	core
mineral	opx1	opx1	opx2	opx2	opx3	opx3	opx4	opx4	opx5	opx5
SiO_2	54.45	54.88	54.80	55.23	54.69	54.75	53.76	54.58	55.04	54.62
TiO_2	0.18	0.08	0.00	0.12	0.00	0.00	0.12	0.08	0.00	0.00
Cr_2O_3	0.14	0.16	0.20	0.00	0.00	0.18	0.15	0.11	0.11	0.00
Al_2O_3	1.75	1.88	1.20	0.75	1.09	1.03	1.82	1.79	0.99	0.90
FeO	15.34	13.75	13.61	13.67	14.49	13.05	14.85	13.56	13.35	13.37
MnO	0.00	0.00	0.10	0.00	0.25	0.00	0.14	0.00	0.17	0.00
MgO	26.90	28.11	27.61	27.69	27.22	27.91	26.64	27.80	27.68	27.39
CaO	2.11	2.12	1.99	2.06	2.28	1.91	2.26	2.00	2.08	1.97
Na_2O	0.14	0.29	0.20	0.22	0.36	0.22	0.31	0.39	0.36	0.34
K_2O	0.05	0.06	0.00	0.00	0.00	0.00	0.00	0.00	0.00	0.00
total	101.25	101.34	99.70	99.73	100.40	99.05	100.03	100.31	99.78	98.59
Mg#	0.76	0.78	0.78	0.78	0.77	0.79	0.76	0.79	0.79	0.79
Si	1.95	1.94	1.97	1.98	1.96	1.98	1.94	1.95	1.98	1.98
Ti	0.01	0.00	0.00	0.00	0.00	0.00	0.00	0.00	0.00	0.00
Al	0.07	0.08	0.05	0.03	0.05	0.04	0.08	0.08	0.04	0.04
Fe	0.46	0.41	0.41	0.41	0.44	0.39	0.45	0.41	0.40	0.41
Mg	1.43	1.48	1.48	1.48	1.46	1.50	1.43	1.48	1.48	1.48
Ca	0.08	0.08	0.08	0.08	0.09	0.07	0.09	0.08	0.08	0.08
Na	0.02	0.02	0.01	0.02	0.03	0.02	0.02	0.03	0.03	0.02
Cr	0.00	0.00	0.01	0.00	0.00	0.01	0.00	0.00	0.00	0.00
Total	4.02	4.02	4.01	4.01	4.02	4.01	4.02	4.02	4.01	4.01
Wo %	4.37	4.44	4.06	4.10	4.77	3.88	4.86	4.22	4.27	4.03
En %	74.05	77.68	76.21	75.74	76.20	77.12	75.39	77.85	77.04	76.54
Fs %	21.58	17.88	19.73	20.16	19.04	19.00	19.75	17.94	18.70	19.43

sample	TAF23	TAF23	TAF23	TAF23	TAF23	TAF23	TAF23	TAF23	TAF23
locality	core	rim	core	rim	core	rim	core	rim	core
mineral	cpx1	cpx2	cpx2	cpx3	cpx3	cpx4	cpx4	cpx5	cpx5
SiO_2	44.84	47.50	44.00	47.51	45.55	45.06	45.63	44.80	44.90
TiO_2	0.00	0.00	0.00	0.00	0.00	0.00	0.00	0.00	0.00
Cr_2O_3	0.19	0.00	0.00	0.00	0.00	0.10	0.00	0.00	0.00
Al_2O_3	33.93	32.52	35.03	32.95	33.84	34.54	34.42	33.82	33.97
FeO	0.83	0.90	0.60	1.14	0.78	1.04	0.88	0.77	0.86
MnO	0.00	0.00	0.00	0.00	0.00	0.00	0.00	0.00	0.00
MgO	0.35	0.28	0.16	0.33	0.39	0.47	0.30	0.15	0.18
CaO	18.25	17.12	19.53	17.49	18.41	18.71	18.56	18.43	18.70
Na_2O	1.08	1.56	0.51	1.51	1.10	0.79	1.08	0.98	0.80
K_2O	0.00	0.00	0.00	0.00	0.00	0.00	0.00	0.00	0.00
total	99.47	99.88	99.83	100.92	100.06	100.69	100.87	98.95	99.41
Mg#	0.43	0.35	0.32	0.34	0.47	0.45	0.37	0.26	0.27
Si	1.57	1.64	1.53	1.63	1.58	1.56	1.57	1.57	1.57
Ti	0.00	0.00	0.00	0.00	0.00	0.00	0.00	0.00	0.00
Al	1.40	1.33	1.44	1.33	1.38	1.41	1.40	1.40	1.40
Fe	0.02	0.03	0.02	0.03	0.02	0.03	0.03	0.02	0.03
Mg	0.02	0.01	0.01	0.02	0.02	0.02	0.02	0.01	0.01
Ca	0.68	0.63	0.73	0.64	0.68	0.69	0.68	0.69	0.70
Na	0.07	0.10	0.03	0.10	0.07	0.05	0.07	0.07	0.05
Cr	0.01	0.00	0.00	0.00	0.00	0.00	0.00	0.00	0.00
Total	3.77	3.75	3.76	3.75	3.77	3.77	3.77	3.76	3.76
Wo %	53.06	54.82	51.76	54.46	53.37	51.65	53.15	53.25	52.54
En %	20.14	16.12	15.54	15.50	21.98	21.57	17.71	12.05	12.89
Fs %	26.80	29.07	32.70	30.04	24.66	26.78	29.15	34.71	34.57

sample	TAF6	TAF6	TAF6	TAF6	TAF6	TAF6	TAF6	TAF6	TAF6
locality	core	core	core	core	core	core	core	core	rim
mineral	opx1	opx2	opx3	opx4	cpx1	cpx2	cpx3	cpx4	cpx4
SiO₂	54.71	54.21	54.50	55.20	51.99	52.09	53.21	52.50	53.03
TiO₂	0.80	0.11	0.00	0.11	0.14	0.00	0.08	0.10	0.00
Cr₂O₃	0.08	0.00	0.00	0.00	0.29	0.20	0.46	0.09	0.00
Al₂O₃	1.36	1.82	1.31	1.04	2.42	2.44	1.74	2.37	1.75
FeO	14.62	13.18	13.93	16.55	6.49	6.07	3.86	8.67	10.45
MnO	0.34	0.35	0.28	0.10	0.22	0.16	0.15	0.15	0.15
MgO	27.29	27.59	27.48	26.18	16.92	16.67	17.55	16.81	17.14
CaO	2.03	1.96	1.85	2.29	20.41	21.05	22.51	19.26	17.60
Na₂O	0.39	0.31	0.39	0.49	0.32	0.30	0.32	0.46	0.40
K₂O	0.00	0.00	0.00	0.00	0.00	0.00	0.00	0.00	0.00
total	100.89	99.52	99.75	101.95	99.21	98.96	99.91	100.40	100.52
Mg#	0.77	0.79	0.78	0.74	0.82	0.83	0.89	0.78	0.75
Si	1.96	1.95	1.96	1.97	1.93	1.93	1.95	1.93	1.95
Ti	0.00	0.00	0.00	0.00	0.00	0.00	0.00	0.00	0.00
Al	0.06	0.08	0.06	0.04	0.11	0.11	0.08	0.10	0.08
Fe	0.44	0.40	0.42	0.49	0.20	0.19	0.12	0.27	0.32
Mg	1.45	1.48	1.48	1.39	0.94	0.92	0.96	0.92	0.94
Ca	0.08	0.08	0.07	0.09	0.81	0.84	0.88	0.76	0.70
Na	0.03	0.02	0.03	0.03	0.02	0.02	0.02	0.03	0.03
Cr	0.00	0.00	0.00	0.00	0.01	0.01	0.01	0.00	0.00
Total	4.03	4.02	4.02	4.02	4.02	4.02	4.02	4.03	4.02
Wo %	4.15	4.15	3.90	4.76	37.68	38.90	42.02	35.61	33.16
En %	75.26	77.76	77.54	73.08	54.58	53.77	54.58	53.73	52.55
Fs %	20.60	18.10	18.57	22.16	7.75	7.34	3.39	10.66	14.29

sample	TAF44/3	TAF44/3	TAF44/3	TAF44/3	TAF44/3	TAF44/3	TAF44/3	TAF44/3	TAF44/3	TAF44/3
locality	core	core	core	core	core	rim	core	core	core	rim
mineral	opx1	opx2	opx3	cpx1	cpx2	cpx2	cpx3	opx4	cpx4	cpx4
SiO₂	55.21	55.29	55.40	53.20	53.62	52.97	53.68	55.20	52.86	53.21
TiO₂	0.08	0.00	0.12	0.29	0.16	0.12	0.00	0.00	0.28	0.11
Cr₂O₃	0.00	0.00	0.00	0.17	0.27	0.25	0.29	0.00	0.17	0.24
Al₂O₃	0.82	1.29	0.99	2.25	1.91	2.46	1.85	1.06	2.66	2.42
FeO	15.03	14.21	13.85	9.96	8.47	10.08	8.28	14.54	7.74	8.75
MnO	0.13	0.00	0.00	0.17	0.00	0.00	0.00	0.00	0.13	0.12
MgO	27.12	27.18	27.88	16.53	17.54	17.91	18.65	27.10	17.29	17.72
CaO	2.25	2.44	2.14	18.39	19.18	16.59	17.70	2.42	19.68	18.33
Na₂O	0.54	0.50	0.33	0.41	0.30	0.36	0.33	0.47	0.43	0.40
K₂O	0.00	0.00	0.00	0.00	0.00	0.00	0.00	0.00	0.00	0.00
total	101.19	100.90	100.71	101.36	101.45	100.74	100.77	100.80	101.25	101.29
Mg#	0.76	0.77	0.78	0.75	0.79	0.76	0.80	0.77	0.80	0.78
Si	1.97	1.97	1.97	1.94	1.95	1.94	1.95	1.97	1.92	1.94
Ti	0.00	0.00	0.00	0.01	0.00	0.00	0.00	0.00	0.01	0.00
Al	0.03	0.05	0.04	0.10	0.08	0.11	0.08	0.04	0.11	0.10
Fe	0.45	0.42	0.41	0.30	0.26	0.31	0.25	0.43	0.24	0.27
Mg	1.44	1.44	1.48	0.90	0.95	0.98	1.01	1.44	0.94	0.96
Ca	0.09	0.09	0.08	0.72	0.75	0.65	0.69	0.09	0.77	0.71
Na	0.04	0.03	0.02	0.03	0.02	0.03	0.02	0.03	0.03	0.03
Cr	0.00	0.00	0.00	0.00	0.01	0.01	0.01	0.00	0.00	0.01
Total	4.03	4.02	4.01	4.01	4.01	4.02	4.02	4.02	4.02	4.02
Wo %	9.29	4.62	5.06	35.02	35.36	30.51	32.74	9.47	35.97	33.46
En %	72.21	75.45	75.81	50.06	52.53	54.74	55.92	72.01	54.63	54.92
Fs %	18.51	19.93	19.13	14.92	11.82	14.75	11.34	18.52	9.40	11.62

sample	TAF35/3	TAF35/3	TAF35/3	TAF35/3	TAF35/3	TAF35/3	TAF35/3	TAF18/12	TAF18/12	TAF18/12	TAF18/12
locality	core	core	rim	core	core	rim	core	core	rim	core	rim
mineral	opx1	cpx1	cpx1	cpx2	cpx3	cpx3	cpx4	opx1	opx1	opx2	opx2
SiO_2	54.87	52.95	52.61	52.90	53.53	53.36	53.80	53.63	54.02	54.39	54.83
TiO_2	0.11	0.19	0.14	0.21	0.09	0.17	0.15	0.23	0.14	0.00	0.18
Cr_2O_3	0.13	0.11	0.17	0.30	0.17	0.16	0.25	0.00	0.00	0.00	0.00
Al_2O_3	1.38	1.62	2.50	3.05	1.28	1.89	1.04	1.44	1.56	1.26	1.46
FeO	15.24	9.26	8.86	6.13	8.29	8.37	6.84	15.62	14.37	15.77	15.58
MnO	0.10	0.00	0.13	0.13	0.00	0.00	0.13	0.34	0.34	0.42	0.38
MgO	26.81	17.38	17.06	16.66	17.56	17.45	17.56	25.69	26.76	26.61	26.73
CaO	2.17	18.18	19.27	21.72	17.80	19.34	18.61	2.22	2.16	2.26	2.29
Na_2O	0.26	0.31	0.62	0.35	0.00	0.41	0.00	0.30	0.37	0.27	0.20
K_2O	0.00	0.00	0.00	0.00	0.26	0.00	0.24	0.00	0.00	0.00	0.00
total	101.07	99.99	101.34	101.44	98.97	101.14	98.60	99.47	99.72	100.97	101.65
Mg#	0.76	0.77	0.77	0.83	0.79	0.79	0.82	0.75	0.77	0.75	0.75
Si	1.96	1.95	1.92	1.92	1.98	1.94	1.99	1.96	1.95	1.96	1.95
Ti	0.00	0.01	0.00	0.01	0.00	0.00	0.00	0.01	0.00	0.00	0.01
Al	0.06	0.07	0.11	0.13	0.06	0.08	0.05	0.06	0.07	0.05	0.06
Fe	0.46	0.29	0.27	0.19	0.26	0.26	0.21	0.48	0.43	0.47	0.46
Mg	1.43	0.96	0.93	0.90	0.97	0.95	0.97	1.40	1.44	1.43	1.42
Ca	0.08	0.72	0.75	0.84	0.71	0.76	0.74	0.09	0.08	0.09	0.09
Na	0.02	0.02	0.04	0.02	0.00	0.03	0.00	0.02	0.03	0.02	0.01
Cr	0.00	0.00	0.01	0.01	0.00	0.00	0.00	0.00	0.00	0.00	0.00
Total	4.01	4.02	4.04	4.02	3.99	4.02	3.98	4.02	4.02	4.03	4.02
Wo %	7.13	34.75	35.03	39.15	33.08	36.15	34.62		7.60	8.74	8.33
En %	72.01	52.15	55.90	53.36	52.91	53.27	53.65		71.06	72.67	70.24
Fs %	20.86	13.10	9.07	7.49	14.01	10.58	11.73		21.34	18.59	21.43

sample	TAF18/12	TAF18/12	TAF18/12	TAF18/12	TAF18/12	TAF18/12	TAF18/12	TAF18/12	TAF31/1	TAF31/1	TAF31/1
locality	core	rim	core	rim	core	rim	core	rim	core	core	core
mineral	cpx1	cpx1	cpx2	cpx2	cpx3	cpx3	cpx4	cpx4	opx1	opx2	opx3
SiO_2	54.13	54.92	53.67	52.83	52.50	52.83	51.92	52.46	53.35	53.05	53.62
TiO_2	0.15	0.00	0.00	0.17	0.00	0.11	0.26	0.12	0.22	0.21	0.00
Cr_2O_3	0.09	0.00	0.16	0.00	0.33	0.19	0.13	0.15	0.00	0.00	0.00
Al_2O_3	1.01	1.40	1.91	2.03	2.52	1.88	1.86	1.84	1.36	1.60	1.31
FeO	16.02	14.89	8.47	8.92	6.13	10.00	9.68	10.96	19.09	19.11	19.12
MnO	0.29	0.38	0.30	0.11	0.15	0.35	0.30	0.27	0.48	0.45	0.41
MgO	26.33	26.88	17.50	17.40	17.13	18.40	16.35	17.35	24.02	23.73	24.21
CaO	1.93	2.07	19.08	18.63	21.07	15.98	18.49	16.82	2.08	2.15	2.00
Na_2O	0.37	0.25	0.34	0.43	0.34	0.31	0.49	0.31	0.47	0.41	0.49
K_2O	0.00	0.00	0.00	0.00	0.00	0.00	0.00	0.00	0.00	0.00	0.00
total	100.36	100.80	101.42	100.54	100.17	100.03	99.48	100.32	101.08	100.70	101.16
Mg#	0.75	0.76	0.79	0.78	0.83	0.77	0.75	0.74	0.69	0.69	0.69
Si	1.96	1.97	1.95	1.94	1.93	1.95	1.94	1.94	1.95	1.94	1.95
Ti	0.00	0.00	0.00	0.00	0.00	0.00	0.01	0.00	0.01	0.01	0.00
Al	0.04	0.06	0.08	0.09	0.11	0.08	0.08	0.08	0.06	0.07	0.06
Fe	0.49	0.45	0.26	0.27	0.19	0.31	0.30	0.34	0.58	0.59	0.58
Mg	1.42	1.43	0.95	0.95	0.94	1.01	0.91	0.96	1.31	1.30	1.32
Ca	0.08	0.08	0.74	0.73	0.83	0.63	0.74	0.67	0.08	0.08	0.08
Na	0.03	0.02	0.02	0.03	0.02	0.02	0.04	0.02	0.03	0.03	0.03
Cr	0.00	0.00	0.00	0.00	0.01	0.01	0.00	0.00	0.00	0.00	0.00
Total	4.03	4.01	4.02	4.03	4.03	4.02	4.03	4.03	4.03	4.03	4.03
Wo %		7.60	38.01	29.66	31.10	35.46			4.51	4.76	4.51
En %		71.06	55.58	56.26	53.83	52.17			68.95	68.77	68.95
Fs %		21.34	6.41	14.09	15.07	12.38			26.54	26.47	26.54

sample	TAF31/1	TAF31/1	TAF31/1	TAF31/1	TAF31/1	TAF31/1	TAF31/1	TAF31/1	TAF43/6	TAF43/6	TAF43/6
locality	rim	core	core	core	core	rim	coreres	rimres	core	core	core
mineral	opx3	opx4	opx5	opx6	cpx1	cpx1	cpx2	cpx2	opx1	opx2	opx3
SiO₂	53.79	53.05	52.82	54.04	52.13	52.69	52.50	51.90	53.70	53.89	53.77
TiO₂	0.21	0.17	0.00	0.20	0.26	0.20	0.20	0.23	0.14	0.10	0.11
Cr₂O₃	0.00	0.00	0.00	0.00	0.10	0.13	0.09	0.18	0.23	0.17	0.00
Al₂O₃	1.32	1.07	1.62	1.51	2.12	1.68	1.69	1.81	1.58	1.82	1.13
FeO	18.71	17.73	18.53	19.06	10.69	11.01	10.84	12.38	13.52	13.74	14.64
MnO	0.34	0.41	0.40	0.49	0.35	0.35	0.33	0.29	0.00	0.00	0.00
MgO	24.23	23.91	23.58	24.10	16.13	15.95	15.67	15.64	26.87	26.91	25.97
CaO	2.22	2.59	2.10	2.11	18.23	18.43	18.52	17.62	2.12	2.23	2.32
Na₂O	0.55	0.46	0.35	0.39	0.55	0.50	0.46	0.55	0.33	0.25	0.24
K₂O	0.00	0.00	0.00	0.00	0.00	0.00	0.00	0.00	0.00	0.00	0.00
total	101.38	99.40	99.41	101.90	100.57	101.06	100.29	100.64	98.48	99.11	98.18
Mg#	0.70	0.71	0.69	0.69	0.73	0.72	0.72	0.69	0.78	0.78	0.76
Si	1.95	1.96	1.96	1.95	1.93	1.95	1.95	1.94	1.96	1.95	1.97
Ti	0.01	0.00	0.00	0.01	0.01	0.01	0.01	0.01	0.00	0.00	0.00
Al	0.06	0.05	0.07	0.06	0.09	0.07	0.07	0.08	0.07	0.08	0.05
Fe	0.57	0.55	0.57	0.58	0.33	0.34	0.34	0.39	0.41	0.42	0.45
Mg	1.31	1.32	1.30	1.30	0.89	0.88	0.87	0.87	1.46	1.45	1.42
Ca	0.09	0.10	0.08	0.08	0.72	0.73	0.74	0.70	0.08	0.09	0.09
Na	0.04	0.03	0.03	0.03	0.04	0.04	0.03	0.04	0.02	0.02	0.02
Cr	0.00	0.00	0.00	0.00	0.00	0.00	0.00	0.01	0.01	0.00	0.00
Total	4.03	4.03	4.02	4.02	4.03	4.03	4.02	4.04	4.01	4.01	4.01
Wo %	4.80	5.61	4.63	4.54	34.44	35.22	35.99	33.58	7.80	7.08	7.27
En %	69.52	69.26	68.59	68.58	51.91	50.08	48.63	50.03	73.48	73.65	71.17
Fs %	25.68	25.13	26.78	26.88	13.65	14.71	15.38	16.40	18.72	19.27	21.56

sample	TAF43/6	TAF43/6	TAF43/6	TAF43/6	TAF43/6	TAF43/6	TAF43/6	TAF43/6	TAF45/7	TAF45/7	TAF45/7
locality	core	rim	core	rim	coreres	rimres	core	rim	core	core	core
mineral	cpx1	cpx1	cpx2	cpx2	cpx2	cpx2	cpx3	cpx3	opx1	opx2	opx3
SiO₂	53.30	54.44	53.49	52.70	52.85	53.02	52.63	52.63	54.26	53.47	54.47
TiO₂	0.19	0.11	0.18	0.20	0.16	0.18	0.25	0.11	0.12	0.00	0.08
Cr₂O₃	0.12	0.14	0.00	0.22	0.10	0.27	0.16	0.15	0.00	0.00	0.09
Al₂O₃	1.33	1.02	1.60	2.26	1.92	2.73	2.19	1.75	0.87	0.95	1.46
FeO	14.84	13.58	8.74	8.64	10.15	8.52	9.07	9.74	17.01	17.12	16.68
MnO	0.00	0.00	0.16	0.00	0.12	0.18	0.00	0.10	0.18	0.52	0.41
MgO	25.66	27.29	17.67	17.85	16.78	17.20	17.59	17.46	25.61	24.91	25.68
CaO	2.33	2.05	18.03	18.11	18.10	18.92	17.81	17.41	2.01	2.15	2.16
Na₂O	0.33	0.27	0.43	0.30	0.34	0.49	0.37	0.33	0.39	0.43	0.41
K₂O	0.00	0.00	0.00	0.00	0.00	0.00	0.00	0.00	0.00	0.00	0.00
total	98.11	98.89	100.29	100.28	100.52	101.50	100.08	99.67	100.46	99.54	101.42
Mg#	0.76	0.78	0.78	0.79	0.75	0.78	0.78	0.76	0.73	0.72	0.73
Si	1.96	1.97	1.96	1.93	1.95	1.93	1.94	1.95	1.97	1.97	1.96
Ti	0.01	0.00	0.00	0.01	0.00	0.01	0.01	0.00	0.00	0.00	0.00
Al	0.06	0.04	0.07	0.10	0.08	0.12	0.10	0.08	0.04	0.04	0.06
Fe	0.46	0.41	0.27	0.27	0.31	0.26	0.28	0.30	0.52	0.53	0.50
Mg	1.41	1.48	0.97	0.98	0.92	0.93	0.97	0.96	1.39	1.37	1.38
Ca	0.09	0.08	0.71	0.71	0.72	0.74	0.70	0.69	0.08	0.08	0.08
Na	0.02	0.02	0.03	0.02	0.02	0.03	0.03	0.02	0.03	0.03	0.03
Cr	0.00	0.00	0.00	0.01	0.00	0.01	0.00	0.00	0.00	0.00	0.00
Total	4.01	4.01	4.01	4.02	4.02	4.02	4.02	4.02	4.02	4.03	4.02
Wo %	35.07	33.30	34.25	34.59	34.25	34.59	33.43	32.95	4.19	4.61	4.60
En %	52.61	54.97	51.14	54.39	51.14	54.39	54.04	53.37	72.00	71.56	72.63
Fs %	12.32	11.73	14.61	11.02	14.61	11.02	12.54	13.68	23.81	23.83	22.77

sample	TAF45/7	TAF45/7	TAF45/7	TAF45/7	TAF45/7	TAF45/7	TAF45/7	TAF45/7	TAF45/7
locality	core	rim	core	core	rim	core	rim	core	rim
mineral	opx4	opx4	opx5	cpx1	cpx1	cpx2	cpx2	cpx3	cpx3
SiO_2	53.59	53.76	53.72	51.32	52.59	53.01	52.59	52.60	51.89
TiO_2	0.16	0.10	0.14	0.16	0.23	0.11	0.30	0.16	0.15
Cr_2O_3	0.00	0.00	0.00	0.32	0.21	0.14	0.14	0.20	0.19
Al_2O_3	1.52	1.39	1.20	2.94	2.41	1.63	1.86	1.58	2.18
FeO	17.95	17.48	16.75	7.31	10.21	9.84	10.43	9.43	10.11
MnO	0.49	0.43	0.48	0.16	0.20	0.33	0.26	0.18	0.28
MgO	24.44	25.08	25.26	16.34	16.19	17.05	16.30	17.03	16.14
CaO	2.13	2.08	2.19	20.67	18.90	18.04	18.37	18.26	18.45
Na_2O	0.41	0.43	0.42	0.39	0.42	0.45	0.35	0.37	0.46
K_2O	0.00	0.00	0.00	0.00	0.00	0.00	0.00	0.00	0.00
total	100.69	100.74	100.16	99.63	101.38	100.58	100.59	99.80	99.83
Mg#	0.71	0.72	0.73	0.80	0.74	0.76	0.74	0.76	0.74
Si	1.95	1.95	1.96	1.91	1.94	1.95	1.94	1.95	1.93
Ti	0.00	0.00	0.00	0.00	0.01	0.00	0.01	0.00	0.01
Al	0.07	0.06	0.05	0.13	0.08	0.07	0.08	0.07	0.10
Fe	0.55	0.53	0.51	0.23	0.32	0.30	0.32	0.29	0.32
Mg	1.33	1.36	1.37	0.90	0.90	0.94	0.90	0.94	0.90
Ca	0.08	0.08	0.09	0.82	0.73	0.71	0.73	0.73	0.74
Na	0.03	0.03	0.03	0.03	0.02	0.03	0.02	0.03	0.03
Cr	0.00	0.00	0.00	0.01	0.00	0.00	0.00	0.01	0.01
Total	4.02	4.03	4.03	4.04	4.02	4.02	4.02	4.02	4.03
Wo %	4.63	4.51	4.70	37.05	34.95	34.33	35.03	34.86	34.61
En %	70.29	71.85	72.28	55.46	51.11	52.58	50.02	52.38	52.07
Fs %	25.07	23.64	23.02	7.49	13.94	13.09	14.95	12.76	13.33

sample	16-26/1	16-26/1	16-26/2	16-26/2	16-26/2	16-26/2	16-26/2	16-26/2	16-26/2	16-26/2	16-26/2	sample
locality	need	core	core	core	core	core	core	core	core	core	core	locality
mineral	opx1	opx2	opx1	opx2	opx3	opx4	opx5	opx6	opx7	opx8	cpx1	mineral
SiO_2	56.84	57.13	55.70	54.52	55.92	55.25	55.10	55.23	56.26	55.66	53.41	SiO_2
TiO_2	0.00	0.08	0.05	0.09	0.15	0.09	0.00	0.12	0.03	0.13	0.00	TiO_2
Cr_2O_3	0.56	0.37	0.30	0.43	0.34	0.21	0.29	0.28	0.40	0.37	0.55	Cr_2O_3
Al_2O_3	0.58	0.95	1.80	1.50	1.68	1.29	1.11	1.02	0.69	1.03	2.28	Al_2O_3
FeO	7.47	7.88	10.89	10.12	10.22	10.99	10.32	7.13	6.42	6.69	6.18	FeO
MnO	0.00	0.00	0.29	0.43	0.36	0.27	0.29	0.48	0.15	0.26	0.22	MnO
MgO	32.73	32.36	29.36	29.30	29.69	29.03	30.15	31.42	31.85	32.19	17.65	MgO
CaO	1.60	1.65	2.25	2.17	2.32	2.10	2.15	2.25	2.05	2.14	20.66	CaO
Na_2O	0.25	0.38	0.09	0.22	0.34	0.05	0.25	0.46	0.48	0.35	0.17	Na_2O
K_2O	0.00	0.00	0.00	0.00	0.00	0.02	0.00	0.01	0.02	0.02	0.00	K_2O
total	100.04	100.81	100.84	98.79	101.02	99.60	99.91	98.38	98.48	98.91	101.11	total
Mg#	0.89	0.88	0.83	0.84	0.84	0.82	0.84	0.89	0.90	0.90	0.84	Mg#
Si	1.98	1.98	1.96	1.95	1.96	1.97	1.96	1.96	1.99	1.96	1.94	Si
Ti	0.00	0.00	0.00	0.00	0.00	0.00	0.00	0.00	0.00	0.00	0.00	Ti
Al	0.02	0.04	0.07	0.06	0.07	0.05	0.05	0.05	0.03	0.04	0.10	Al
Fe	0.22	0.23	0.32	0.30	0.30	0.33	0.31	0.31	0.19	0.20	0.19	Fe
Mg	1.70	1.67	1.54	1.57	1.55	1.54	1.60	1.60	1.68	1.69	0.95	Mg
Ca	0.06	0.06	0.09	0.08	0.09	0.08	0.08	0.08	0.08	0.08	0.80	Ca
Na	0.06	0.03	0.01	0.02	0.02	0.00	0.02	0.02	0.03	0.02	0.01	Na
Cr	0.02	0.01	0.01	0.01	0.01	0.01	0.01	0.01	0.01	0.01	0.02	Cr
Total	4.01	4.01	4.00	4.01	4.01	4.00	4.03	4.03	4.01	4.02	4.01	Total
Wo %	5.33	3.23	4.50	4.51	4.71	4.19	4.38	4.62	4.09	4.31	37.13	Wo %
En %	85.05	86.52	79.25	81.70	81.21	79.02	82.63	87.41	87.40	88.00	54.35	En %
Fs %	9.63	10.25	16.24	13.79	14.08	16.79	12.99	7.97	8.51	7.69	8.51	Fs %

sample	16-26/2	16-26/2	16-26/2	16-26/2	16-47	16-47	16-47	16-47	16-47	16-47	16-47	sample
locality	core	core	core	core	core	core	core	core	core	core	core	locality
mineral	cpx2	cpx3	cpx4	cpx5	opx1	opx2	opx3	opx4	cpx1	cpx2	cpx3	mineral
SiO_2	52.85	52.61	52.10	53.18	55.83	56.51	56.18	55.61	53.34	54.05	53.19	SiO_2
TiO_2	0.01	0.15	0.09		0.13	0.00	0.07	0.03	0.06	0.11	0.16	TiO_2
Cr_2O_3	0.61	0.54	0.66	0.78	0.25	0.17	0.28	0.18	0.34	0.08	0.30	Cr_2O_3
Al_2O_3	2.53	2.33	1.95	1.37	1.29	1.06	1.55	1.42	1.91	1.87	2.51	Al_2O_3
FeO	6.21	6.09	6.04	4.13	12.01	11.32	10.64	12.23	6.77	6.23	6.35	FeO
MnO	0.06		0.24	0.06	0.23	0.31	0.13	0.22	0.34	0.23	0.21	MnO
MgO	17.47	17.47	17.49	18.25	28.55	29.73	30.28	28.38	17.61	17.47	17.21	MgO
CaO	19.73	20.22	19.41	20.34	2.32	2.14	1.64	2.14	19.83	20.05	20.20	CaO
Na_2O	0.14	0.24	0.23	0.31	0.00	0.11	0.17	0.00	0.10	0.22	0.11	Na_2O
K_2O	0.05				0.00	0.02	0.00	0.06	0.06	0.05	0.08	K_2O
total	99.77	99.84	98.25	98.49	100.77	101.44	100.95	100.29	100.35	100.36	100.43	total
Mg#	0.83	0.84	0.84	0.89	0.81	0.82	0.84	0.81	0.82	0.83	0.83	Mg#
Si	1.94	1.93	1.94	1.96	1.97	1.98	1.98	1.96	1.95	1.97	1.94	Si
Ti	0.00	0.00	0.00	0.00	0.00	0.00	0.00	0.00	0.00	0.00	0.00	Ti
Al	0.11	0.10	0.09	0.06	0.05	0.04	0.04	0.06	0.08	0.08	0.11	Al
Fe	0.19	0.19	0.19	0.13	0.36	0.33	0.33	0.31	0.21	0.19	0.19	Fe
Mg	0.96	0.96	0.97	1.00	1.50	1.55	1.55	1.58	0.96	0.95	0.94	Mg
Ca	0.78	0.80	0.78	0.80	0.09	0.08	0.08	0.06	0.78	0.78	0.79	Ca
Na	0.01	0.02	0.02	0.02		0.01	0.01	0.01	0.01	0.02	0.01	Na
Cr	0.02	0.02	0.02	0.02	0.01	0.01	0.01	0.01	0.01	0.00	0.01	Cr
Total	4.00	4.01	4.01	4.01	3.99	4.00	4.00	4.00	4.01	4.00	4.00	Total
Wo %	35.97	37.35	36.63	39.15	4.59	5.58	3.25	4.26	36.70	37.37	36.95	Wo %
En %	53.57	54.15	54.56	54.93	77.19	78.16	81.31	77.10	52.81	52.19	52.23	En %
Fs %	10.46	8.50	8.80	5.92	18.22	16.25	15.44	18.64	10.49	10.44	10.81	Fs %

16-47	16-51/16	16-51/16	16-51/16	16-51/16	16-51/16	16-51/16	16-51/16	16-51/16	16-51/16	16-51/16
core	core	rim	core	core	rim	core	core	core	rim	core
cpx4	opx1	opx1	opx2	opx3	opx3	opx4	opx5	opx6	opx6	opx7
53.68	56.20	56.66	56.57	56.30	56.29	55.60	56.45	55.64	55.68	56.32
0.13	0.00	0.00	0.13	0.00	0.00	0.00	0.00	0.00	0.00	0.08
0.47	0.50	0.28	0.21	0.50	0.35	0.41	0.32	0.46	0.44	0.32
2.00	1.14	0.75	0.87	1.26	0.87	1.22	0.62	1.31	1.55	0.70
6.29	10.25	10.10	10.23	10.29	10.28	10.30	9.77	10.41	10.28	10.37
0.28	0.20	0.30	0.30	0.18	0.26	0.31	0.21	0.14	0.16	0.31
18.24	30.60	30.67	30.63	30.30	30.14	30.29	30.64	30.18	30.15	30.53
19.45	2.26	2.14	2.18	2.15	2.29	2.24	2.27	2.12	2.30	2.25
0.18	0.34	0.19	0.28	0.29	0.13	0.19	0.26	0.12	0.17	0.40
0.05	0.00	0.00	0.00	0.00	0.00	0.00	0.00	0.00	0.00	0.00
100.77	101.47	101.08	101.39	101.27	100.61	100.57	100.53	100.37	100.72	101.28
0.84	0.84	0.84	0.84	0.84	0.84	0.84	0.85	0.84	0.84	0.84
1.95	1.96	1.98	1.97	1.96	1.98	1.96	1.98	1.96	1.95	1.97
0.00	0.00	0.00	0.00	0.00	0.00	0.00	0.00	0.00	0.00	0.00
0.09	0.05	0.03	0.04	0.05	0.04	0.05	0.03	0.05	0.06	0.03
0.19	0.30	0.29	0.30	0.30	0.30	0.30	0.29	0.31	0.30	0.30
0.99	1.59	1.60	1.59	1.58	1.58	1.59	1.60	1.58	1.58	1.59
0.76	0.08	0.08	0.08	0.08	0.09	0.08	0.09	0.08	0.09	0.08
0.01	0.02	0.01	0.02	0.02	0.01	0.01	0.02	0.01	0.01	0.03
0.01	0.01	0.01	0.02	0.01	0.01	0.01	0.01	0.01	0.01	0.01
4.01	4.02	4.01	4.01	4.01	4.01	4.02	4.01	4.01	4.01	4.02
36.01	4.55	4.20	4.32	4.31	4.50	4.55	4.48	4.26	4.66	4.44
54.36	82.81	82.05	82.42	81.98	80.78	82.43	82.53	81.59	81.74	82.13
9.63	12.65	13.75	13.27	13.72	14.72	13.02	12.99	14.15	13.61	13.44

16-51/16	16-51/16	16-51/16	16-51/16
core	core	core	core
cpx1	cpx2	cpx3	cpx4
53.14	52.36	53.49	53.20
0.00	0.00	0.10	0.09
0.83	0.50	0.67	0.62
2.50	3.07	1.69	1.49
6.47	7.08	5.96	5.92
0.15	0.18	0.11	0.18
18.37	16.76	18.31	18.28
19.34	20.25	19.80	19.52
0.23	0.42	0.34	0.27
0.00	0.00	0.00	0.00
101.03	100.63	100.48	99.57
0.83	0.81	0.85	0.85
1.93	1.92	1.95	1.95
0.00	0.00	0.00	0.00
0.11	0.13	0.07	0.06
0.20	0.22	0.18	0.18
0.99	0.91	0.99	1.00
0.75	0.79	0.77	0.77
0.02	0.03	0.02	0.02
0.02	0.01	0.02	0.02
4.02	4.02	4.02	4.01
34.09	36.20	36.89	36.82
57.47	55.18	55.67	55.26
8.44	8.62	7.44	7.92

sample	16-26/1	16-26/1	16-26/1	16-26/1	16-26/1	16-26/1	16-26/1	16-26/2	16-26/2	16-26/2	16-26/2	16-26/2
locality	core	core	rim	core	core	core	core	core	core	core	core	core
mineral	ol1	ol2	ol2	ol3	ol4	ol5	ol6	ol1	ol2	ol3	ol4	ol5
SiO₂	40.92	41.82	40.78	41.43	40.38	41.72	41.53	41.01	40.34	41.32	40.51	40.38
TiO₂	0.00	0.00	0.00	0.11	0.08	0.00	0.00	0.00	0.00	0.00	0.00	0.07
Cr₂O₃	0.13	0.00	0.00	0.10	0.00	0.00	0.00	0.00	0.05	0.00	0.12	0.08
Al₂O₃	0.00	0.00	0.00	0.25	0.00	0.00	0.00	0.25	0.07	0.21	0.24	0.00
FeO	8.53	9.10	10.63	9.25	8.48	8.92	8.53	9.41	9.63	12.31	9.85	10.02
MnO	0.00	0.00	0.00	0.00	0.00	0.15	0.20	0.17	0.17	0.17	0.06	0.22
MgO	48.92	50.01	48.54	49.45	48.89	50.52	50.02	49.68	47.51	46.20	47.64	48.16
CaO	0.17	0.21	0.21	0.10	0.11	0.18	0.14	0.09	0.15	0.28	0.17	0.14
Na₂O	0.41	0.34	0.32	0.33	0.32	0.42	0.34	0.14	0.19	0.31	0.20	0.70
K₂O	0.00	0.00	0.00	0.00	0.00	0.00	0.00	0.07	0.04	0.00	0.01	0.03
Total	99.08	101.47	100.48	101.00	98.26	101.91	100.70	101.14	98.46	101.13	99.13	100.01
Si	1.01	1.01	1.00	1.00	1.00	1.00	1.00	0.99	1.01	1.01	1.00	1.00
Fe	0.18	0.18	0.22	0.19	0.18	0.18	0.17	0.19	0.20	0.25	0.20	0.21
Mg	1.79	1.79	1.77	1.78	1.81	1.80	1.80	1.79	1.77	1.69	1.76	1.77
Total	3.00	3.00	3.01	3.00	3.00	3.01	3.00	3.01	3.00	2.99	3.00	3.02
Fo%	91.1	90.7	89.1	90.5	91.1	91.0	91.3	90.4	89.8	87.0	89.6	89.5

sample	16-26/2	16-26/2	16-47	16-47	TAF6	TAF23	TAF23	TAF23	TAF43/6	TAF43/6	TAF43/6	TAF43/6
locality	core	core	core	core	core	core	core	core	core	core	core	core
mineral	ol6	ol7	ol1	ol2	ol1	ol1	ol2	ol3	ol1	ol2	ol3	ol4
SiO₂	40.86	40.41	41.19	40.89	39.70	38.96	39.72	38.87	39.67	40.27	39.93	39.20
TiO₂	0.05	0.01	0.03	0.07	0.00	0.00	0.00	0.00	0.00	0.00	0.00	0.00
Cr₂O₃	0.00	0.00	0.04	0.10	0.00	0.00	0.00	0.00	0.00	0.19	0.11	0.00
Al₂O₃	0.13	0.46	0.20	0.28	0.00	0.00	0.00	0.00	0.00	0.00	0.00	0.00
FeO	9.04	10.28	9.19	9.64	16.18	20.47	20.61	22.08	14.22	13.87	17.56	20.20
MnO	0.26	0.29	0.04	0.08	0.25	0.00	0.00	0.00	0.00	0.00	0.00	0.00
MgO	48.18	46.44	49.73	49.69	43.93	40.82	40.96	39.04	44.75	45.11	42.54	40.29
CaO	0.20	0.35	0.00	0.06	0.20	0.26	0.24	0.24	0.22	0.28	0.21	0.25
Na₂O	0.71	0.45	0.54	0.00	0.59	0.46	0.34	0.54	0.36	0.38	0.35	0.46
K₂O	0.00	0.05	0.02	0.00	0.00	0.00	0.00	0.00	0.00	0.00	0.00	0.00
Total	99.42	98.93	101.28	100.90	100.84	100.97	101.87	100.76	99.21	100.10	100.70	100.40
Si	1.01	1.01	1.00	0.99	1.00	1.00	1.00	1.00	1.00	1.01	1.01	1.00
Fe	0.19	0.21	0.19	0.20	0.34	0.44	0.44	0.49	0.30	0.29	0.37	0.43
Mg	1.77	1.72	1.79	1.80	1.64	1.55	1.54	1.50	1.68	1.68	1.60	1.54
Total	3.01	3.00	3.01	3.00	3.02	3.02	3.00	3.01	3.01	3.00	3.00	3.01
Fo%	90.5	89.0	90.6	90.2	82.9	78.0	78.0	75.3	84.9	85.3	81.2	78.0

sample	TAF6	TAF6	TAF6	TAF6	TAF6	TAF6	TAF6	TAF6	TAF44/3	TAF44/3
locality	rim	core	core	rim	core	core	rim	core	core	rim
mineral	plag1	plag1	plag2	plag3	plag3	plag4	plag5	plag5	plag1	plag2
SiO₂	45.37	44.74	44.18	47.14	45.09	44.86	44.48	45.25	44.94	46.49
TiO₂	0.00	0.00	0.00	0.00	0.00	0.00	0.00	0.00	0.00	0.00
Cr₂O₃	0.06	0.00	0.00	0.00	0.00	0.00	0.00	0.00	0.10	0.00
Al₂O₃	32.93	33.66	35.21	33.19	34.58	35.36	34.92	34.80	34.60	33.37
FeO	0.76	0.68	0.72	1.10	0.86	0.60	0.65	0.76	0.87	0.97
MnO	0.00	0.00	0.00	0.00	0.00	0.00	0.00	0.00	0.00	0.00
MgO	0.34	0.43	0.42	0.43	0.34	0.54	0.39	0.41	0.33	0.48
CaO	17.69	18.26	19.29	17.69	18.82	19.43	19.33	18.96	18.89	17.84
Na₂O	1.32	0.95	0.65	1.62	0.81	0.61	0.54	0.89	0.90	1.56
K₂O	0.00	0.00	0.00	0.00	0.00	0.00	0.00	0.00	0.00	0.00
Total	98.50	98.73	100.46	101.16	100.50	101.39	100.31	101.17	100.52	100.70
Si	2.13	2.10	2.04	2.15	2.08	2.05	2.06	2.07	2.07	2.14
Al	1.82	1.86	1.92	1.79	1.88	1.91	1.90	1.88	1.88	1.81
Ca	0.89	0.92	0.96	0.87	0.93	0.95	0.96	0.93	0.93	0.88
Na	0.12	0.09	0.06	0.14	0.07	0.05	0.05	0.08	0.08	0.14
Total	5.02	5.02	5.03	5.02	5.02	5.02	5.02	5.02	5.03	5.03
An%	88.1	91.4	94.3	85.8	92.8	94.6	95.2	92.2	92.1	86.3

sample	TAF44/3	TAF44/3	TAF44/3	TAF44/3	TAF18/12	TAF18/12	TAF18/12	TAF18/12	TAF18/12	TAF18/12
locality	core	core	rim	core	rim	rim	core	gm	gm	core
mineral	plag2	plag3	plag3	plag4	plag1	plag2	plag2	plag3	plag4	plag5
SiO₂	46.17	45.86	46.23	45.97	45.34	45.85	45.37	46.48	45.77	44.84
TiO₂	0.00	0.00	0.00	0.00	0.00	0.00	0.00	0.00	0.00	0.00
Cr₂O₃	0.00	0.13	0.00	0.00	0.00	0.14	0.00	0.11	0.17	0.00
Al₂O₃	34.02	34.06	33.11	33.61	33.18	33.05	33.80	32.91	34.32	34.98
FeO	1.00	0.78	1.10	0.83	0.81	0.83	0.72	1.21	1.00	0.68
MnO	0.00	0.00	0.00	0.00	0.00	0.00	0.00	0.00	0.00	0.00
MgO	0.33	0.46	0.41	0.34	0.22	0.19	0.20	0.30	0.25	0.20
CaO	18.63	18.66	17.71	17.98	18.03	17.86	18.57	17.81	18.50	19.36
Na₂O	1.13	1.07	1.47	1.14	1.12	1.20	0.93	1.27	0.93	0.61
K₂O	0.00	0.00	0.00	0.00	0.00	0.00	0.00	0.00	0.00	0.00
total	101.27	101.02	100.01	99.88	98.70	99.11	99.60	100.09	100.93	100.66
Si	2.11	2.10	2.14	2.13	2.12	2.14	2.11	2.15	2.10	2.07
Al	1.83	1.84	1.81	1.83	1.83	1.82	1.85	1.79	0.86	1.90
Ca	0.91	0.92	0.88	0.89	0.91	0.89	0.92	0.88	0.91	0.96
Na	0.10	0.10	0.13	0.10	0.10	0.11	0.08	0.11	0.08	0.05
Total	5.02	5.02	5.02	5.01	5.01	5.01	5.01	5.01	5.01	5.01
An%	90.1	90.6	87.0	89.7	89.9	89.2	91.7	88.6	91.7	94.6

sample	TAF35/3	TAF43/6	TAF43/6	TAF43/6	TAF43/6	TAF43/6	TAF43/6	TAF43/6	TAF43/6	TAF45/7
locality	gm	core	core	core	rim	core	rim	core	rim	rim
mineral	plag4	plag1	plag2	plag3	plag3	plag4	plag4	plag5	plag5	plag
SiO₂	47.83	45.95	45.74	45.77	45.04	46.84	45.70	45.74	45.30	46.65
TiO₂	0.00	0.00	0.00	0.00	0.00	0.09	0.00	0.00	0.00	0.12
Cr₂O₃	0.17	0.00	0.00	0.00	0.00	0.00	0.09	0.10	0.00	0.00
Al₂O₃	31.08	33.03	33.32	33.34	34.28	31.50	32.97	33.05	33.55	31.52
FeO	1.52	0.83	0.83	0.80	0.76	2.00	1.09	0.82	0.87	1.73
MnO	0.00	0.00	0.13	0.00	0.00	0.00	0.00	0.10	0.00	0.00
MgO	0.00	0.34	0.18	0.25	0.21	0.63	0.27	0.22	0.27	0.58
CaO	16.52	18.02	17.81	18.07	18.72	17.18	18.06	17.72	18.35	16.96
Na₂O	1.70	1.30	1.09	1.13	0.92	1.40	1.21	1.09	1.00	1.41
K₂O	0.27	0.00	0.00	0.00	0.00	0.05	0.00	0.00	0.00	0.03
Total	99.09	99.46	99.10	99.35	99.93	99.80	99.39	98.73	99.34	99.03
Si	2.23	2.14	2.13	2.13	2.09	2.18	2.13	2.14	2.11	2.18
Al	1.71	1.81	1.83	1.83	1.87	1.73	1.81	1.82	1.84	1.74
Ca	0.83	0.90	0.89	0.90	0.93	0.86	0.90	0.89	0.92	0.85
Na	0.15	0.12	0.10	0.10	0.08	0.13	0.11	0.10	0.09	0.13
Total	5.00	5.02	5.00	5.01	5.02	5.02	5.02	5.00	5.01	5.01
An%	84.3	88.4	90.0	89.9	91.8	87.2	89.2	90.0	91.0	86.9

sample	TAF45/7	TAF45/7	TAF45/7	TAF45/7	TAF45/7	TAF45/7	TAF45/7	TAF45/7	TAF45/7	TAF45/7
locality	core	rim	core	rim	core	rim	core	gm	gm	gm
mineral	plag1	plag1	plag2	plag2	plag3	plag3	plag4	plag5	plag6	plag7
SiO₂	44.56	46.65	45.24	45.75	44.81	45.89	46.75	45.12	45.00	45.26
TiO₂	0.00	0.12	0.00	0.00	0.00	0.00	0.06	0.00	0.00	0.07
Cr₂O₃	0.00	0.00	0.00	0.00	0.11	0.00	0.06	0.00	0.00	0.00
Al₂O₃	33.46	31.52	33.92	33.80	33.80	33.41	31.35	33.75	33.49	33.12
FeO	0.83	1.73	0.88	0.94	0.74	1.03	2.24	0.78	0.92	0.88
MnO	0.00	0.00	0.11	0.06	0.00	0.00	0.00	0.07	0.00	0.07
MgO	0.24	0.58	0.27	0.29	0.39	0.21	0.78	0.28	0.30	0.38
CaO	18.27	16.96	18.16	18.07	18.19	18.07	17.15	18.24	18.14	17.86
Na₂O	1.08	1.41	1.10	1.23	1.04	1.28	1.24	1.14	1.12	1.20
K₂O	0.00	0.03	0.00	0.00	0.00	0.00	0.00	0.00	0.00	0.00
total	98.44	99.03	99.68	100.14	99.09	99.89	99.62	99.37	98.97	98.84
Si	2.10	2.18	2.10	2.11	2.09	2.13	2.18	2.10	2.11	2.12
Al	1.86	1.74	1.86	1.84	1.86	1.83	1.72	1.85	1.85	1.83
Ca	0.92	0.85	0.90	0.89	0.91	0.90	0.86	0.91	0.91	0.90
Na	0.10	0.13	0.10	0.11	0.09	0.11	0.11	0.10	0.10	0.11
Total	5.02	5.01	5.02	5.02	5.02	5.02	5.01	5.02	5.02	5.02
An%	90.4	86.9	90.2	89.0	90.6	88.7	88.5	89.8	90.0	89.2

sample	16-47	16-47	16-47	16-47	16-47
locality	core	core	core	core	core
mineral	plag1	plag2	plag3	plag4	plag5
SiO$_2$	48.19	45.70	47.09	47.84	47.29
TiO$_2$	0.01	0.13	0.03	0.00	0.04
Cr$_2$O$_3$	0.03	0.00	0.00	0.01	0.00
Al$_2$O$_3$	31.19	33.76	33.11	31.96	32.74
FeO	0.82	0.52	0.93	1.22	0.75
MnO	0.00	0.00	0.00	0.20	0.01
MgO	0.04	0.00	0.07	0.67	0.02
CaO	16.10	17.80	17.33	17.26	17.04
Na$_2$O	2.01	1.22	1.75	1.28	1.73
K$_2$O	0.07	0.13	0.04	0.14	0.01
Total	98.45	99.31	100.36	100.67	99.62
Si	2.25	2.12	2.17	2.20	2.19
Al	1.71	1.85	1.79	1.73	1.78
Ca	0.80	0.89	0.85	0.85	0.84
Na	0.18	0.11	0.16	0.11	0.16
Total	4.99	5.01	5.01	5.00	5.00
An%	81.5	89.0	84.6	88.2	84.5

Sample	Age (Ma)	$^{87}Sr/^{86}Sr$ (errors are x10^{-6})	$^{143}Nd/^{144}Nd$ (errors are x10^{-6})	$^{206}Pb/^{204}Pb$ (errors are x10^{-3})	$^{207}Pb/^{204}Pb$ (errors are x10^{-3})	$^{208}Pb/^{204}Pb$ (errors are x10^{-3})
North Tongan boninites						
Kallisto Western section						
16-51/8		0.704782±7	0.512807±4	18.822±4	15.608±3	38.728±9
16-51/9	2.54±0.74	0.704707±7	0.512836±4	18.788±2	15.598±2	38.701±5
16-47		0.704622±7	0.512814±4	18.770±1	15.575±1	38.669±2
16-55/4		0.704535±7	0.512793±4	18.839±3	15.600±3	38.756±7
Kallisto site 26						
16-26/1	0.58±0.20	0.704381±7	0.512802±4	18.345±1	15.580±1	38.164±3
16-26/2	0.89±0.04	0.704477±6	0.512733±5	18.684±5	15.609±4	38.560±11
North Tongan tholeiites						
Kallisto Eastern section						
16-70/8		0.703368±7	0.513046±4	18.474±10	15.538±10	38.275±26
16-70/14		0.703561±7	0.512972±4	18.560±3	15.542±3	38.230±7
16-70/16		0.703544±7	0.512992±5	18.727±3	15.539±3	39.372±7
16-70/17		0.703368±7	0.513040±4	18.421±3	15.520±3	38.204±7
16-70/19		0.703494±7	0.513002±3	18.600±1	15.541±1	38.241±3
Tafahi						
TAF 3/2				19.236±2	15.578±2	38.783±5
TAF 8		0.703884±6	0.512931±4	19.303±3	15.590±3	38.856±7
TAF18/10		0.703870±7	0.512948±15	18.991±4	15.564±3	38.587±7
TAF18/12		0.703892±7	0.512935±19	19.322±2	15.603±2	38.910±4
TAF23		0.704303±7	0.512981±47	19.104±5	15.594±4	38.734±10
TAF 31/1	7.00±3.00	0.703863±7	0.512927±6	19.428±3	15.608±2	38.972±6
TAF 40		0.703903±7	0.512942±7	18.986±2	15.578±2	38.601±5
TAF43/6		0.703878±7	0.512929±7	18.978±3	15.559±3	38.560±7
TAF44/8		0.703849±7	0.512935±5	19.025±3	15.584±2	38.638±6
TAF45/7		0.703892±7	0.512957±3	18.938±3	15.583±3	38.580±7
TAF 54				19.252±4	15.587±4	38.824±10
Niuatoputapu						
NTT 9	2.30±0.50	0.703979±6	0.512892±4	18.998±3	15.547±3	38.622±6
NTT10		0.703973±7	0.512881±4	19.024±1	15.578±1	38.708±3
NTT 14		0.703961±7	0.512889±6	19.046±2	15.582±2	38.716±4
NTT25/2	3.00±0.40	0.703968±7	0.512877±5	19.029±1	15.581±1	38.717±2
NTT25/4				19.022±3	15.579±2	38.715±6
NTT26/1	1.60±0.40	0.703975±7	0.512875±10	19.025±2	15.574±2	38.697±4
NTT 28/2		0.703995±7	0.512978±7	19.013±2	15.566±2	38.662±5
NTT29/3		0.703973±7	0.512887±4	18.975±2	15.580±2	38.671±4
Northern Lau Spreading Centre						
2218-1		0.703880±7	0.512834±7	18.579±3	15.578±2	38.621±5
2218-12				18.556±2	15.547±2	38.540±5
2218-8		0.703803±7	0.512862±3	18.530±3	15.544±2	38.516±5
2212-6		0.703820±7	0.512846±4	18.705±3	15.564±3	38.633±7
Samoan seamount						
16-94/1		0.705183±7	0.512480±4	18.319±1	15.617±1	38.422±2
16-95/2		0.705161±7	0.512455±4	18.405±1	15.611±1	38.532±2
16-95/3		0.705183±7	0.512459±5	18.398±1	15.607±1	38.520±3

Leachate data

Sample	$^{87}Sr/^{86}Sr$ (errors are x10^{-6})	$^{143}Nd/^{144}Nd$ (errors are x10^{-6})	$^{206}Pb/^{204}Pb$ (errors are x10^{-3})	$^{207}Pb/^{204}Pb$ (errors are x10^{-3})	$^{208}Pb/^{204}Pb$ (errors are x10^{-3})
North Tongan boninites					
16-51/8	0.705734±7	0.512789±4	18.770±8	15.605±7	38.702±18
16-51/9	0.705425±6	0.512789±4	18.689±2	15.564±2	38.580±4
16-47	0.704654±7	0.512851±8	18.300±2	15.560±2	38.223±4
16-55/4	0.704590±7	0.512757±14	18.203±4	15.572±3	38.234±8
Kallisto site 26					
16-26/1	0.707704±13		17.611±1	15.561±2	37.425±1
16-26/2	0.706347±8		17.841±6	15.616±5	37.794±11
North Tongan tholeiites					
16-70/8	0.704934±57	0.513012±5	18.413±2	15.546±2	38.220±5
16-70/14	0.704029±7	0.513004±17	18.545±3	15.552±3	38.309±6
16-70/16	0.704380±13	0.512996±4	18.524±4	15.544±3	38.265±9
16-70/17	0.705091±7	0.512979±4	18.363±2	15.543±2	38.269±5
16-70/19	0.704278±7	0.512989±3			
Tafahi					
TAF 3/2					
TAF 8					
TAF18/10	0.703885±7	0.512925±4	19.022±3	15.604±2	38.709±6
TAF18/12	0.703963±7	0.512926±4	19.311±2	15.606±2	38.907±4
TAF23	0.705162±7	0.512981±47	19.099±3	15.588±2	38.715±6
TAF 31/1					
TAF 40					
TAF43/6	0.703899±7	0.512958±4	19.035±3	15.621±3	38.740±7
TAF44/8					
TAF45/7	0.703901±6	0.512929±7	18.900±4	15.588±3	38.556±8
TAF 54					
Niuatoputapu					
NTT 9					
NTT10	0.704060±7	0.512886±4	19.012±2	15.582±2	38.699±5
NTT 14					
NTT25/2	0.704045±7	0.512893±5	19.021±2	15.584±1	38.710±3
NTT25/4			18.941±1	15.572±1	38.629±3
NTT26/1	0.704003±7	0.512890±5	19.034±2	15.590±1	38.735±4
NTT 28/2					
NTT29/3	0.704450±7	0.512890±3	18.959±1	15.573±1	38.645±3
Samoan seamount					
16-94/1	0.705496±7	0.512485±10			
16-95/2	0.705178±7	0.512470±4	18.421±1	15.619±1	38.559±2
16-95/3	0.705220±7	0.512474±4			

APPENDIX 3

Petrographic data

This appendix provides a summary of the petrographic information for the north Tongan boninites, the lavas from Tafahi, Niuatoputapu and the Northern Lau Spreading Centre, and the samples from two ophiolite sections, which were dredged from the inner wall of the Tonga trench. This includes the phenocryst and vesicle contents, the texture of the groundmass and any evidence of alteration.

	%Ol	%Opx	%Cpx	%Pl	Gmas	Ves%	Order	Notes
Tafahi lavas								
TAF1		5	7	27	fg, felsitic	3	cpx-pl	Massive lava flow (mlf)
TAF2		<1	2	25	fg, mph agg, alt	1	cpx-(opx)-pl	mlf
TAF3/1		5	5	20	fg, felsitic	5	opx-cpx-pl	mlf
TAF3/2*		3	3	20	fg, mph agg.	7	cpx-opx-pl	mlf
TAF3/3		2	2	20	fg, mph agg.	3	opx-cpx-pl	mlf
TAF3/4		5	<5	20	fg, mph agg.	2	cpx-opx-pl	mlf
TAF4		5	3	25	fg, mph agg.	0	opx-cpx-pl	mlf
TAF5/1		3	2	30	mg, felsitic	0	opx-cpx-pl	mlf
TAF5/2		<1	2	20	fg, mph agg.	7	opx-cpx-pl	mlf
TAF6		7	5	15	fg, mph agg.	2	opx-cpx-pl	mlf
TAF7		2	5	25	fg, mph agg.	2	cpx-opx-pl	mlf
TAF8*	<1	<1	7	20	fg, mph agg.	4	ol-cpx-opx-pl	mlf
TAF9		2	3	20	fg, mph agg.	6	cpx-opx-pl	mlf
TAF10		3	3	20	cg, felsitic	8	opx-(cpx)-pl	mlf
TAF11		5	5	25	mg, felsitic	8	ol-cpx-opx-pl	mlf
TAF12		1	2	20	cg, felsitic	2	opx-cpx-pl	mlf
TAF13		3	5	20	mg, felsitic	5	cpx-opx-pl	mlf
TAF14/1		0	5	30	fg, mph agg, alt	0	cpx-opx-pl	mlf
TAF14/2		2	5	17	fg, mph agg.	1	cpx-opx-pl	mlf
TAF14/4		2	5	20	mg, felsitic	2	cpx-opx-pl	mlf
TAF16		3	12	25	cg, felsitic	3	cpx-opx-pl	mlf
TAF17		3	10	30	cg, felsitic	0	cpx-opx-pl	mlf
TAF18/1		2	2	25	fg, mph agg.	0	opx-cpx-pl	mlf
TAF18/2		1	5	20	fg, mph agg.	0	cpx-opx-pl	mlf
TAF18/4	1	3	5	20	cg, felsitic	0	ol-cpx-opx-pl	mlf
TAF18/5		3	10	30	cg, felsitic	0	cpx-(opx)-pl	mlf
TAF18/7		3	5	20	fg, mph agg.	0	cpx-opx-pl	mlf
TAF18/8		<1	3	25	fg, glassy	0	opx-cpx-pl	mlf
TAF18/9		2	2	20	mg, felsitic	0	opx-cpx-pl	mlf
TAF18/10*	1	2	8	25	fg, glassy, alt.	0	ol-opx-cpx-pl	mlf
TAF18/11	1	3	10	25	fg, mph agg.	0	ol-cpx-opx-pl	mlf
TAF18/12*		2	5	30	fg, mph agg.	0	cpx-opx-pl	mlf
TAF18/13	1	2	5	30	mg, felsitic	0	opx-cpx-pl	mlf
TAF18/14		4	10	30	fg, mph agg.	3	opx-cpx-pl	mlf
TAF18/15		5	13	20	cg, felsitic	2	cpx-(opx)-pl	mlf
TAF20		2	3	25	fg, glassy, alt.	2	opx-cpx-pl	mlf
TAF21		2	3	20	mg, felsitic	0	cpx-opx-pl	mlf
TAF22		2	5	25	mg, felsitic	0	cpx-(opx)-pl	mlf
TAF23*	1	0	<1	25	cg, felsitic	10	ol-cpx-opx-pl	mlf
TAF26		1	1	20	mg, felsitic, alt.	8	cpx-opx-pl	mlf
TAF27		2	3	20	cg, felsitic, alt.	10	cpx-opx-pl	mlf
TAF29/1		1	3	15	mg, felsitic, alt.	10	cpx-opx-pl	mlf
TAF29/2		2	5	15	mg, felsitic, alt.	12	opx-cpx-pl	mlf
TAF29/3		2	3	20	mg, felsitic, alt.	7	cpx-opx-pl	mlf
TAF30		<1	1	20	cg, felsitic, alt.	10	cpx-opx-pl	mlf
TAF31/1		5	5	20	fg, mph agg, alt	8	cpx-opx-pl	mlf
TAF31/4		4	3	20	cg, felsitic	7	cpx-opx-pl	mlf
TAF31/5		2	2	15	cg, felsitic	12	cpx-(opx)-pl	mlf
TAF31/6		1	5	25	cg, felsitic	15	cpx-(opx)-pl	mlf
TAF32/1		1	1	30	mg, felsitic	7	opx-cpx-pl	mlf
TAF32/2		2	1	30	cg, felsitic	3	opx-cpx-pl	mlf
TAF32/3		1	1	20	cg, felsitic	10	cpx-opx-pl	mlf
TAF33		1	1	25	cg, felsitic	0	(cpx)-(opx)-pl	mlf
TAF34		1	<1	20	cg, felsitic	2	opx-(cpx)-pl	pl lathes in gmass
TAF35/1		2	3	30	cg, felsitic	0	cpx-opx-pl	mlf
TAF35/2		1	3	25	cg, felsitic	0	cpx-(opx)-pl	mlf
TAF35/3		<1	3	25	cg, felsitic	0	cpx-(opx)-pl	mlf
TAF35/4		1	5	30	cg, felsitic, alt.	0	cpx-(opx)-pl	mlf
TAF35/5		2	7	30	vcg, felsitic	0	cpx-opx-pl	mlf
TAF35/6		2	2	25	cg, felsitic	0	cpx-(opx)-pl	mlf
TAF37		2	2	30	cg, felsitic	0	opx-cpx-pl	mlf

	%Ol	%Opx	%Cpx	%Pl	Gmas	Ves%	Order	Notes
TAF38/2		1	5	25	mg, felsitic	8	cpx-(opx)-pl	mlf
TAF39		2	1	20	mg, felsitic	0	opx-(cpx)-pl	mlf
TAF40*		5	3	25	cg, felsitic	0	opx-cpx-pl	pl lathes in gmass
TAF41/1		3	2	15	fg, mph agg.	3	opx-cpx-pl	mlf
TAF41/2		3	2	15	cg, felsitic	10	opx-cpx-pl	mlf
TAF43/1		1	2	25	mg, felsitic	5	cpx-(opx)-pl	mlf
TAF43/2		1	1	15	cg, felsitic	1	cpx-(opx)-pl	mlf
TAF43/3		1	2	15	vcg, felsitic	8	cpx-opx-pl	mlf
TAF43/4		1	1	15	cg, felsitic	4	opx-cpx-pl	mlf
TAF43/5		3	7	15	cg, felsitic	1	cpx-opx-pl	mlf
TAF43/6*	1	7	10	27	cg, felsitic	0	ol-opx-cpx-pl	mlf
TAF43/7		5	1	25	fg, mph agg.	4	opx-(cpx)-pl	mlf
TAF43/8		3	2	20	fg, mph agg.	8	cpx-opx-pl	mlf
TAF43/9		2	1	40	fg, mph agg.	10	cpx-opx-pl	mlf
TAF43/10		10	5	25	fg, mph agg.	8	cpx-opx-pl	mlf
TAF43/11		7	<1	18	fg, mph agg.	0	opx-pl	mlf
TAF43/12		1	5	30	fg, mph agg.	0	cpx-opx-pl	mlf
TAF44/2		3	4	25	fg, mph agg.	8	opx-cpx-pl	mlf
TAF44/3		3	10	15	cg, felsitic	8	cpx-opx-pl	
TAF44/4		1	<1	30	fg, mph agg.	0	(opx)-(cpx)-pl	
TAF44/5		2	2	30	cg, felsitic	0	cpx-opx-pl	
TAF44/6		2	5	25	cg, felsitic	10	opx-cpx-pl	
TAF44/7		3	5	25	cg, felsitic	0	opx-cpx-pl	
TAF44/8*		4	7	25	mg, felsitic	0	cpx-opx-pl	
TAF44/9		5	7	20	cg, felsitic	0	opx-cpx-pl	
TAF45/1		1	2	18	fg, mph agg.	8	opx-cpx-pl	
TAF45/2		5	2	15	cg, felsitic	0	cpx-opx-pl	
TAF45/3		8	3	20	fg, mph agg.	0	cpx-opx-pl	pl lathes in gmass
TAF45/4		5	1	30	fg, mph agg.	0	opx-cpx-pl	
TAF45/5		6	2	15	fg, mph agg.	7	opx-cpx-pl	
TAF45/6		4	2	20	fg, mph agg.	4	opx-cpx-pl	
TAF45/7*		2	1	25	fg, mph agg.	3	opx-cpx-pl	
TAF45/7/8		2	2	30	cg, felsitic	0	opx-cpx-pl	
TAF46		2	5	20	fg, mph agg.	7	opx-cpx-pl	
TAF48		4	7	20	cg, felsitic	7	opx-cpx-pl	
TAF50		2	6	20	mg, felsitic	5	cpx-opx-pl	
TAF52		1	7	20	fg, mph agg.	7	opx-cpx-pl	
TAF53/1		3	7	20	fg, mph agg., al	0	cpx-opx-pl	hematite alt. of gmass
TAF53/2		3	5	20	fg, mph agg.	5	cpx-opx-pl	
TAF54*		3	5	20	cg, felsitic	0	ol-opx-cpx-pl	
TAF55	1	2	4	25	mg, felsitic	5	ol-cpx-opx-pl	
TAF56	<1	2	3	25	fg, mph agg.	4	cpx-opx-pl	

Niuatoputapu lavas and clasts

	%Ol	%Opx	%Cpx	%Pl	Gmas	Ves%	Order	Notes
NTT3/1			15		fg, felsitic	7	pl	clast in debris-flow; zeolites
NTT3/2		10	15		fg, felsitic	0	cpx-pl	clast
NTT4A			15		fg, felsitic	0	pl	clast
NTT4B					fg, felsitic	0		clast; clay alt.
NTT5S					fg, felsitic	3		clast; clay alt.
NTT7E		10	15		fg, felsitic	0	cpx-pl	clast
NTT7			7		fg, felsitic	6	pl	clast, alt.
NTT9*					fg, felsitic	0		flow-banded lava (fbl)
NTT10*					fg, felsitic	0		(fbl); vuggy alt.
NTT11					fg, felsitic	0		(fbl)
NTT12		8	10		fg, felsitic	0	cpx-pl	(fbl)
NTT13					fg, felsitic	0		(fbl)
NTT14*					fg, felsitic	0		(fbl)
NTT15D					fg, felsitic	0		clast
NTT15A					fg, felsitic	0		clast
NTT16A		9	13		fg, felsitic	5	cpx-pl	clast
NTT16B		6	10		fg, felsitic	5	cpx-pl	clast
NTT17			17		fg, felsitic	0	pl	clast

	%Ol	%Opx	%Cpx	%Pl	Gmas	Ves%	Order	Notes
NTT18A				10	fg, felsitic	0	pl	clast
NTT18B				8	fg, felsitic	0	pl	clast
NTT19A			5	12	fg, felsitic	6	cpx-pl	clast
NTT20A					fg, felsitic	0		clast
NTT20B					fg, felsitic	0		clast
NTT21A					fg, felsitic	0		clast
NTT21B					fg, felsitic	0		clast
NTT22A					fg, felsitic	0		clast
NTT23/4					fg, felsitic	0		massive lava flow (mlf)
NTT23/5					fg, felsitic	0		(mlf)
NTT25/1					fg, felsitic	0		(mlf)
NTT25/2*					fg, felsitic	0		(mlf)
NTT25/4*					fg, felsitic	0		(mlf)
NTT25/5					fg, felsitic	0		(mlf)
NTT25/6					fg, felsitic	0		(mlf)
NTT25/7					fg, felsitic	0		(mlf)
NTT25/8					fg, felsitic	0		(mlf)
NTT26/1*					fg, felsitic	0		(mlf)
NTT26/2					fg, felsitic	0		(mlf)
NTT26/3					fg, felsitic	0		(mlf)
NTT27/2					fg, felsitic	0		clast
NTT28/2*					fg, felsitic	0		(mlf)
NTT28/4/1					fg, felsitic	0		clast
NTT28/4/2					fg, felsitic	0		clast
NTT28/4/3					fg, felsitic	0		clast
NTT28/4/4					fg, felsitic	0		clast
NTT29/1					fg, felsitic	0		(mlf)
NTT29/2					fg, felsitic	0		(mlf)
NTT29/3*					fg, felsitic	0		(mlf)
NTT29/4					fg, felsitic	0		(mlf)

Northern Lau Spreading Centre

	%Ol	%Opx	%Cpx	%Pl	Gmas	Ves%	Order	Notes
2218-1*		<5	15	10	glassy	0		Gmass devitrified to opaques; mg
2218-8*		<3	10	15	glassy	0		Gmass devitrified to opaques; mg
2218-12*		5	12	12	glassy	0		Gmass devitrified to opaques; mg
2212-6*		7	12	15	glassy	0		Gmass devitrified to opaques; mg

Key to abbreviations

%Ol	% Olivine phenocrysts	**mlf**	Massive lava flow	**ilm**	Ilmenite
%Opx	% Orthopyroxene phenocrysts	**clast**	Clast from volcanic debris-flow	**hem**	hematite
%Cpx	% Clinopyroxene phenocrysts	**fbl**	Flow-banded lava	**alt**	alteration
%Pl	% Plagioclase phenocrysts	**mg**	Microgabbro		
%Qtz	% Quartz phenocryts	**fg**	Fine-grained		
%Alk.fsp.	% Alkali feldspar phenocrysts	**mg**	Medium-grained		
Gmass	Groundmass texture and alteration	**cg**	Coarse-grained		
Ves%	Percentage of vesicles	**ep**	Epidote		
Order	Phenocryst crystallisation order	**chl**	Chlorite		
Notes	Details of deformation or	**serp**	Serpentine		
	alteration and other minerals etc.	**ser**	Sericite		
microcry	microcrystalline	**amph**	Amphibole		
mph	macrophenocrysts	*	Indicates sample analysed by ICP-MS		
agg	agglutinated glomerocrysts				

	%Ol	%Opx	%Cpx	%Pl	%Qtz	%Alk.fsp.	Gmas	Ves%	Order	Notes
Western ophiolite section										
North Tongan boninites										
16-51/8*		10	9				fg, felsitic,alt.		cpx-opx	
16-51/9*		15	8				fg, felsitic,alt.		cpx-opx	
16-51/16*		5	4				fg, felsitic, alt.		cpx-opx	
16-47*	2	2	5	8			fg, felsitic, alt.		ol-cpx-opx-pl	
16-55/4*		8	10	15			fg, felsitic		cpx-opx-pl	
16-26/1*	3	5	10				fg, felsitic		ol-cpx-opx	
16-26/2*	10	6	17				glassy	8	ol-cpx-opx	spherulitic pl-cpx in gmass
Diabases										
16-47/26*							fg, felsitic			(mlf); clay alt., aphyric
16-47/27*							fg, felsitic			(mlf); clay alt., aphyric
16-47/29*							fg, felsitic			(mlf); clay alt., aphyric
Plagiogranite										
16-47/17A				20	5	70	microcry.		pl-alk.fsp-qtz	also 5% calc. & hem.
Tonalites										
16-48/26				10	40	25	granoblastic		amph-pl-alk.fsp-qtz	25% amph.
16-50/40				15	40	20	granoblastic		amph-pl-alk.fsp-qtz	25% amph.
16-50/53				15	30	20	granoblastic		amph-pl-alk.fsp-qtz	10% amph.
16-50/60				25	35	20	granoblastic		amph-pl-alk.fsp-qtz	15% amph.
Cumulate gabbros										
16-48/30			15	35			cumulate		cpx-pl-amph	50% amph (late) from cpx
16-48/36				25			cumulate		pl-amph	15% 1o & 60% 2o amph.
16-48/57			20	45			cumulate		cpx-pl-amph	35% 2o amph.
16-50/49			40	60			70% alt. to clays		cpx-pl	
16-50/55		20	30	25			cumulate		opx-cpx-pl-amph	25% amph.
Cumulate ultramafics										
16-50/8	100						10% serp.			dunite
16-50/35		100					alt. to clays 20%			enstatatite
Tectonised harzburgites										
16-43/2	90	8	<2				alt. to serp.			90% serpentinised
16-46/21	85	12	<3				alt. to serp.			approx 90% serp.
16-48/37	relic	relic					alt. to serp.			100% serpentinised
16-50/4	70	27	<3				alt. to serp.			90% serpentinised
16-50/5	70	28	<2				alt. to serp.			85% serpentinised
16-50/48	65	30	<5				alt. to serp.			80% serpentinised
Eastern ophiolite section										
North Tongan tholeiites										
16-70/8*		<2					alt. to clays			(mlf), fg basalts
16-70/14*							alt. to clays			(mlf); aphyric
16-70/16*							alt. to clays			(mlf); aphyric
16-70/17*							alt. to clays			(mlf), some relic px.
16-70/19*							alt. to clays			(mlf); aphyric
Diabases										
16-67/8*							fg, felsitic			(mlf); clay alt.;aphyric
16-73/29*							fg, felsitic			(mlf); clay alt.;aphyric
Tonalites										
16-73/6				10	45	40			pl-alk.fsp-qtz-ep-ch	4% ep. & 1% chl.; ser. alt.
Cumulate gabbros										
16-73/2	2		40	57					ol-cpx-pl	pxs alt. to amph+clays
16-73/3	15		35	45					opx-cpx-pl	pxs alt. to amph+clays
16-73/12		10	35	55					opx-cpx-pl	cumulate texture
16-73/13	20		25	55					ol-cpx-pl	ol alt to serp.+ilm.
16-73/18*	3		30	70					ol-cpx-pl	cumulate texture

APPENDIX 4

Table of normalising values

Normalising values used in this thesis are of fertile MORB mantle (FMM) from *Pearce & Parkinson (1993)*, C1 chondrite from *Boynton (1984)*, and N-MORB from *Sun & McDonough (1989)*.

FMM		C1 chondrite		N-MORB	
Nb	0.2	La	0.33	Sr	90
Zr	9.2	Ce	0.808	K	600
TiO₂	0.175	Pr	0.122	Rb	0.56
Y	3.9	Nd	0.6	Ba	6.3
Yb	0.42	Sm	0.20	Th	0.12
CaO	3.25	Eu	0.07	Ta	0.132
Al₂O₃	3.75	Gd	0.259	Nb	2.33
Ga	4	Tb	0.0474	La	2.5
V	78	Dy	0.322	Ce	7.5
Sc	15.5	Ho	0.0718	Pr	1.32
MnO	0.13	Er	0.21	Nd	7.3
FeO	8.8	Tm	0.0324	Zr	74
Co	106	Yb	0.209	Hf	2.05
MgO	38.4	Lu	0.0322	Sm	2.63
Cr	2500			Eu	1.02
Ni	2020			Ti	7600.00
				Gd	3.68
				Tb	0.67
				Dy	4.55
				Y	28
				Ho	1.01
				Er	2.97
				Yb	3.05
				Lu	0.455